Order Number 9009739

The influence of surfactants on the motion of spherical fluid particles in an infinite medium and in a tube

He, Zunqing, Ph.D.

City University of New York, 1989

U·M·I
300 N. Zeeb Rd.
Ann Arbor, MI 48106

THE INFLUENCE OF SURFACTANTS ON THE MOTION OF SPHERICAL FLUID PARTICLES IN AN INFINITE MEDIUM AND IN A TUBE

by

Zunqing He

A Dissertation Submitted to the Graduate Faculty in Engineering in Partial Fullfillment of the Requirements for the Degree of Doctor of Philosophy, The City University of New York.

1989

This manuscript has been read and accepted for the Graduate Faculty in Engineering in satisfaction of the dissertation requirement for the degree of Doctor of Philosophy.

June 12, 1989 — Charles Maldarelli

Date — Professor Charles Maldarelli

Chair of Examining Committee

6/12/89 — Jacques E. Benveniste

Date — Professor Jacques E. Benveniste

Executive Officer

Prof. Charles Maldarelli, Chairman

Prof. Zeev Dagan, Co-Chairman

Prof. Andreas Acrivos

Prof. Roberto Mauri

Prof. Sheldon Weinbaum

Prof. Zongyi Yan

(Beijing University, China)

Supervisory Committee

The City University of New York

ABSTRACT

THE INFLUENCE OF SURFACTANTS OF THE MOTION OF SPHERICAL FLUID PARTICLES IN AN INFINITE MEDIUM AND IN A TUBE

by

Zunqing He

Advisors: **Professor Charles Maldarelli**

Professor Zeev Dagan

This thesis studies the influence of surfactant adsorption on the hydrodynamic creeping motion of fluid spheres. Bulk soluble surfactant molecules, present in the continuous phase through which fluid droplets translate, adsorb onto the droplet surface and are convected towards the trailing stagnation pole of the surface. Accumulation at this pole lowers the interfacial tension and creates a Marangoni tension directed towards the leading pole. As this tension opposes the surface flow, the flow is retarded. This retardation is the origin of the surfactant effect on the hydrodynamic motion.

Four problems concerning this physicochemical effect are considered. The first two problems consider the axisymmetric translation of a droplet in an infinite medium. The first one examines the steady motion when the surfactant sorption kinetics is slow in comparison to interfacial convection, and a stagnant cap forms at the trailing stagnation point. A solution for the cap angle, as a function of the physicochemical parameters, has been obtained based on

a nonlinear surface equaton of state, the Frumkin equation, which accounts accurately for the compression of surfactant in the cap.

The second problem studies the unsteady translation of a droplet in an infinite medium due to the transient adsorption of surfactant. Solutions are presented for the unsteady motion for the cases in which the adsorption time is much larger than the characteristic convection time (small Biot number) and when the two time scales are comparable.

The other two problems are concerned with the steady, axisymmetric motion of a spherical drop in a tube. The first problem addresses the case in which the adsorption kinetics is fast relative to surface convection. A first order correction to the Hadamard-Rybczynsky terminal velocity is obtained, which accounts for the influence of surfactants on the droplet motion. The major conclusion of this study is that when a droplet is suspended in Poiseuille flow, the presence of stagnation rings on the droplet surface gives rise to surfactant distributions which can increase the droplet velocity in comparison to that of an uncontaminated droplet.

The fourth problem examines the case in which the sorption kinetics is slow relative to convection, and a stagnant cap forms. Solutions for the terminal velocity of a drop with a cap are calculated as a function of the surfactant physicochemical parameters using the nonlinear Frumkin eqation.

This work is humbly dedicated to my dear parents in China.

Zunqing He

June, 1989

ACKNOWLEDGEMENTS

I wish to thank Professor Charles Maldarelli and Professor Zeev Dagan for their continuous guidance and many contributions in directing this research. I also wish to thank all members of the Supervisory Committee for their help and encouragement.

This research was supported in part by a Department of Energy Grant from Basic Sciences, Grant No. 447861 and a National Science Foundation Grant, Grant No. 8404261, DE-FG02-88ER13820. Their support is gratefully acknowledged.

Table of Contents

List of Tables x

List of Figures xii

Introduction 1

Chapter 1 Physicochemical Hydrodynamic Theory and Literature Review

1.1 The Physicochemical basis for the influence of surfactants on droplet motion 4

1.2 Literature review of the influence of surfactants on the motion of a droplet in an infinite medium 7

1.3 Literature review of the motion of particles in a tube 11

Figure 1 13

Chapter 2 The Size of Stagnant Caps of Bulk Soluble Surfactant on the Interface of Translating Fluid Drops

2.1 Introduction 14

2.2 Formulation 21

2.3 Results and discussion 28

Figures 32

Chapter 3 The Unsteady Translation of a Fluid Droplet Owing to the Adsorption of a Surfactant Monolayer

3.1 Introduction 36

3.2 Mathematical formulation 38

3.3 Solution procedure 46

3.4 Numerical simulations 59

3.5 Conclusions 64

Tables and Figures 66

Chapter 4 The Influence of Surfactant on Droplet Motion Inside a Cylindrical Tube: I. Uniform Retardation Controlled by Sorption Kinetics

4.1 Introduction 79

4.2 Formulation 87

4.3 Solution technique 101

4.4 Clean surface results: Hydrodynamic drag coefficients, terminal velocities and flow fields 114

4.5 Surfactant results 120

4.6 Discussion of significance and conclusions 127

Appendix 133

Tables and Figures 135

Chapter 5 The Influence of Surfactant on Droplet Motion inside a Cylindrical Tube: II. Stagnant Cap Regime

5.1 Introduction 153

5.2 Formulation 155

5.3 Solution technique 156

5.4 Results and discussion 173

Appendix 185

Tables and Figures 193

Chapter 6 Concluding Remarks 213

References 217

LIST OF TABLES

Table		Page
	CHAPTER 3	
1.	Small Marangoni number linear corrections.	66
2.	Comparison of exact results with linear approximation for the small Marangoni number ($\kappa = 0$).	67
3.	Small Biot number linear corrections.	68
4.	Comparison of exact results with linear approximation for the small Biot number ($\kappa = 0$).	69
	CHAPTER 4	
1.	The number of collocation points necessary to achieve the accuracy requirement for the gas bubble (κ=0).	135
2.	Comparison of converged values of drag coefficients λ_u and λ_v with the results of Haberman and Sayre (1958) and Wang and Skalak (1969) for solid particle ($\kappa = 10^8$).	136
3.	Comparison of converged values of drag coefficients λ_u and λ_v with the results of Hyman and Skalak's exact solution (1970) for a fluid droplet.	137
4.	Angular location of upstream stagnation ring (a'/b'=0.5).	138
	CHAPTER 5	
1.	A comparison of λ_u for a gas bubble (κ=0) in an infinite medium with the results from Sadhal-Johnson (1983).	193
2.	A comparison of λ_u and λ_v for a clean gas bubble (ϕ=0,	

κ=0) with the results from Hyman-Skalak (1970). 193

3. A comparison of λ_u and λ_v for a solid sphere (ϕ=180) with the results from Hyman-Skalak (1970). 194

LIST OF FIGURES

Figure Page

Introduction

1. The schematics of surfactant transport processes on the surface of a moving drop. 13

Chapter 2

1. The schematics of surfactant transport processes on the surface of a moving drop. 32
2. The ratio of sorption rates k as functions of cap angle and large Ma numbers for a gas bubble translating in an infinite medium. The solid lines are the numerical results based on the nonlinear equation of state; the dotted lines are the analytical results obtained by Sadhal and Johnson (1983) using the linear surface equation. 33
3. The ratio of sorption rates k as functions of cap angle and small Ma numbers for a gas bubble translating in an infinite medium. The solid lines are the numerical results based on the nonlinear equation of state; the dotted lines are the analytical results obtained by Sadhal and Johnson (1983) using the linear surface equation. 34
4. The surfactant distribution $\Gamma(\theta)$ (nondimensionalized by Γ'_∞) for a gas bubble translating in an infinite medium at Ma=0.5 and Ma=100. The solid lines are the numerical results based on the nonlinear equation of state; the dotted lines are

the analytical results obtained by Sadhal and Johnson (1983) using the linear surface equation. 35

Chapter 3

1. Diagram of a spherical droplet translating in an unbounded medium. 70
2. Nondimensional terminal velocity U computed from Eq.(3.4) as funtion of Bi number (for κ = 0 and different Ma numbers) at steady state. 71
3. Nondimensional terminal velocity U computed from Eq.(3.4) as funtion of Ma number (for κ = 0 and different Bi numbers) at steady state. 72
4. Nondimensional surfactant distribution on the surface of the droplet $\Gamma(\theta)$ computed from Eq.(3.1) as function of the position (for κ = 0, Ma = 1.0 and different Bi numbers) at steady state. 73
5. Nondimensional surfactant distribution $\Gamma(\theta)$ on the surface of the droplet computed from Eq.(3.1) as function of the position (for κ = 0, Bi = 0.5 and different Ma numbers) at steady state. 74
6. Nondimensional terminal velocity U computed from Eq.(3.4) as funtion of κ (for Ma = 0.5 and different Bi numbers) at steady state. 75
7. Nondimensional terminal velocity U computed from Eq.(3.4) as funtion of κ (for Bi = 0.1 and different Ma numbers) at steady state. 76
8. Nondimensional surfactant distribution $\Gamma(\theta)$ on the surface

of the droplet computed from Eq.(3.1) as function of the position (for κ = 0, Bi = 0.1, Ma = 1.0) at unsteady state. 77

9. Nondimensional terminal velocity U computed from Eq.(3.4) as funtion of time (for κ = 0,Bi = 0.1 and different Ma numbers). 78

Chapter 4

1. Definition sketch of the axisymmetric motion in the tube in a frame moving with the spherical fluid particle velocity. The sketch presents the case for motion in an otherwise quiescent medium; for a fluid particle suspended in Poiseuille flow the flow at infinity would be a parabolic profile added to the uniform flow. The presence of surfactants in the continuous phase is indicated by the figures with heads and tails. 139

2. Drag coefficient λ_u for uniform flow past a fixed sphere as a function of the particle to tube ratio a'/b' for different values of the viscosity ratio κ. 140

3. Drag coefficient λ_v for Poiseuille flow past a fixed sphere as a function of the particle to tube ratio a'/b' for different values of the viscosity ratio κ. 141

4. Presentation of the clean surface velocity field for uniform flow κ=0.5 and a'/b'=0.5. 142

5a. Clean surface velocity field for a neutrally bouyant fluid particle in a frame for which the particle is stationary. The magnitude of the velocity vector is normalized by the particle velocity U_0'. This field

is for κ=0.5 and a'/b'=0.5. 143

5b. Enlargement of the upstream pole of the field detailed in Fig. 5a showing the recirculation in the continuous phase and the location of the stagnation ring on the surface. 144

6. Velocity field for Poiseuille flow past a fixed fluid particle. The velocity vector is normalized by V'; the centerline velocity of the Poiseuille flow. 145

7. First order velocity distribution due to the Marangoni surface force derived from the zeroth order uniform flow. The velocity vector is normalized by U_0', and the distribution is for κ=0.5 and a'/b'=0.5. 146

8. First order velocity distribution due to the Marangoni surface force derived from the zeroth order Poiseuille flow. The velocity vector is normalized by V'; and the distribution is for κ=0.5 and a'/b'=0.5. 147

9. First order drag coefficient correction $\lambda_{u(1)}$ for the surface Marangoni force corresponding to the uniform zeroth order flow as a function of a'/b' for different values of κ. 148

10. First order drag coefficient correction $\lambda_{v(1)}$ for the surface Marangoni force corresponding to the zeroth order Poiseuille flow as a function of a'/b' for different values of κ. 149

11. The first order velocity correction for a surfactant-laden droplet moving under bouyancy in a tube filled with a quiesent fluid as a function of a'/b' for different values of κ. 150

12. The first order correction for the surfactant distribution for bouyancy driven motion in a quiesent liquid for a neutrally bouyant particle suspended in Poiseuille flow. (κ=0.5, a'/b'=0.5). 151

13. The first order velocity for a neutrally bouyant surfactant-laden droplet moving in a tube as a function of a'/b' and κ. 152

CHAPTER 5

1. Definition sketch of the axisymmetric motion in the tube in a frame moving with the spherical fluid particle (with a cap) velocity. The sketch presents the case for motion in an otherwise quiescent medium; for suspension in Poiseuille flow the flow at infinity would be a parabolic profile added to the uniform flow. The presence of surfactants in the continuous phase is indicated by the figures with heads and tails. 195

2. Drag coefficient λ_u for uniform flow past a fixed sphere with a cap as a function of the particle to tube ratio a'/b' for different values of the cap angle ϕ at the viscosity ratios a)κ=0, b)κ=0.5, c)κ=2.0. 196

3. Drag coefficient λ_v for Poiseuille flow past a fixed sphere with a cap as a function of the particle to tube ratio a'/b' for different values of the cap angle ϕ at the viscosity ratios a)κ=0, b)κ=0.5, c)κ=2.0. 199

4. Presentation of the velocity field for uniform flow past a fixed sphere with a surfactant stagnant cap at a)ϕ=30, b)ϕ=90, c)ϕ=150. The magnitude of the velocity vector is

normalized by the uniform speed at infinity. This field is for κ=0.5 and a'/b'=0.5. 202

5. Velocity distribution for Poiseuille flow past a fixed fluid particle with a surfactant stagnant cap at a)ϕ=30, b)ϕ=90, c)ϕ=150. The magnitude of the velocity vector is normalized by the centerline velocity V' of the Poiseuille flow. This field is for κ=0.5 and a'/b'=0.5. 205

6. Presentation of the test for the accuracy of the computation. The comparison is made for the results of the total amount surfactant on a gas bubble between Sadhal and Johnson (1983) exact solution and present collocation solution. 206

7. Ratio k of the sorption rates as function of cap angles and the diameter ratio a'/b' at Ma(U'_{H-R})=100 and κ=0.0. 207

8. Ratio k of the sorption rates as function of cap angles and Ma(U'_0) numbers at κ=0.0 and a)a'/b'= 0.2, b)a'/b'=0.4, a'/b'=0.6. 208

Introduction

Surfactants are molecules which preferentially adsorb onto fluid-fluid interfaces, and lower the interfacial tension in the region of adsorption. In nonequilibrium flow circumstances, convection of adsorbed surfactant molecules towards converging surface stagnation points creates gradients of interfacial tension which exert tangential tractions (Marangoni stresses) along the surface. These stresses of physicochemical origin significantly influence the hydrodynamics of the flow.

This dissertation outlines a research program to study the influence of surfactant adsorption and Marangoni stresses on the creeping motion of spherical fluid particles moving in an unbounded liquid medium or axisymmetrically in a tube. Such problems find important applications in many areas of chemical engineering practice, as for example, in mass transfer in dropwise extraction, foam flows and fluid-fluid displacements in porous media and suspension rheology. The study of the motion of fluid particles in tubes is also applicable to hemodynamic problems of the human microcirculation as for example the motion of gas bubbles dissolved in the blood after too rapid decompression in deep sea divers.

Four problems connected with the influence of surfactants on the creeping motion of a droplet are addressed. In each of these the droplet is taken as spherical. This will be the case as long as the capillary number, the ratio of the distending action of the viscous flow to the restoring force of interfacial tension, is small. In addition, in each of those problems, the surfactant distribution is assumed to be determined by interfacial convection and sorption

kinetics, i.e. the exchange of surfactant between the surface and the bulk sublayer immediately adjacent to the surface. It is assumed that the flow circumstances are such that the surfactant concentration in the bulk is effectively uniform and bulk diffusion does not therefore contribute. The individual problems addressed are outlined below.

The first problem studies the steady motion of a droplet in an infinite medium under conditions in which the surfactant sorption kinetics is slow in comparison to interfacial convection and a stagnant cap forms at the trailing droplet edge. The mixed boundary value problem of zero velocity in the cap region and continuity of tangential stress in the surfactant free region has been solved exactly by Sadhal & Johnson (1983) for the terminal velocity as a function of ϕ, the cap angle. Attempts by these authors at obtaining expressions for ϕ as a function of the physicochemical parameters of the surfactant were confined to a linear equation of state, and this assumption can underpredict the cap angle as compressive stresses in the cap region due to accumulation of surfactant are underestimated. In this study, a solution for ϕ is presented for a nonlinear equaton of state, the Frumkin equation, which accounts more accurately for the compression of surfactant in the cap.

The second problem studies the unsteady translation of a droplet in an infinite medium due to the transient adsorption of a surfactant. This is a new area of research, since all other studies have been restricted to steady motion. In the present study, solutions are presented for the unsteady motion for the cases in which the adsorption is slow with respect to convection (i.e. the growth of a stagnant cap) and of a comparable order.

The third and fourth problems concern the steady, axisymmetric motion of a spherical drop in a tube. The first problem addresses the case in which the adsorption kinetics is fast relative to surface convection, and hence the terminal velocity is expressed as the sum of the clean value plus a small correction. The major conclusion of this study is that when the droplet is suspended in Poiseuille flow, the presence of stagnation rings on the droplet surface gives rise to surfactant distributions which can accelerate the droplet relative to the clean surface value.

The fourth problem concerns the opposite case where the sorption kinetics is slow relative to convection, and a stagnant cap forms. Solutions for the terminal velocity of a drop with a cap are calculated as a function of the surfactant physicochemical parameters using the nonlinear Frumkin eqation, as was done in the first problem.

This dissertation is divided into six chapters. Chapter 1 gives a brief discussion of the physicochemical hydrodynamic theory necessary to understand the influence of surfactants on droplet motion, and it also presents a literature review. Each of the next four chapters is devoted to one of the four problems stated above. The dissertation ends with a concluding chapter which summerizes the research and outlines some areas of future work suggested by this theoretical study.

Chapter 1

Physicochemical Hydrodynamic Theory and Literature Review

1.1 The Physicochemical Basis For the Influence of Surfactants on Droplet Motion

The slow hydrodynamic movement of fluid droplets in an immiscible fluid medium is significantly influenced by the presence of adsorbing surfactants dissolved either in the droplet or the continuous bulk phases. The physicochemical basis of this effect was first outlined by Levich (Frumkin and Levich (1947) and Levich (1962)). Levich proposed that the clean surface of a freshly formed droplet which begins to translate becomes populated with surfactant molecules because of the adsorption of these molecules from the bulk adjoining phase. This adsorption depletes the molecular concentration in the vicinity of the interface, and molecules from the bulk begin to diffuse towards the droplet interface. Surfactant which is adsorbed is convected towards the trailing pole. Interfacial convection creates a gradient of surfactant along the interface, with the trailing pole having a much higher concentration. Surfactant collecting at this pole begins to desorb, and these molecules then subsequently diffuse away from the droplet. Surface diffusion also serves to reduce the concentration at the trailing pole. Eventually a steady state is reached wherein the uptake of surfactant onto the surface at the leading edge by adsorption and bulk diffusion towards the drop is balanced by the loss at the trailing edge via desorption, diffusion away from the drop and surface diffusion towards the leading edge. A

schematic of the transport mechanisms is given in Fig. 1 for the case of a droplet in an infinite medium. The surface concentration gradient of surfactant which develops as the surfactant distribution evolves towards steady state causes the interfacial tension to be larger away from the rear pole. Since the tension decreases with the surface concentration. The interface experiences a stress opposite to the flow, and the surface velocity and consequently the terminal velocity of the drop are reduced.

In an effort to simplify the analysis, previous studies of the infinite medium problem have identified at steady state three limiting cases. These are discussed below so as to provide a background for the literature review which is presented in section 1.2 and 1.3.

The first case pertains to the regime where the following two conditions are governing: First, the transport of surfactant molecules by surface diffusion is very slow in comparison to convective transport. (The nondimensional ratio of the convection to surface diffusion is the Peclet number defined as the product of the droplet velocity multipied by the droplet radius and divided by the surface diffusivity.) Second, either sorption kinetics is slow relative to convection or the diffusion rate of surfactant molecules in the adsorption depth layer is slow in comparison to convection in that layer. The adsorption depth layer is the depth underneath the surface for which, per unit area of surface, there is as much surfactant at equilibrium as on the surface. Under nonequilibrium flow conditions, surfactant exchanged from the bulk to the surface lies primarily in this layer, and therefore the adsorption depth thickness provides a convenient length scale for the estimation of bulk diffusive and convective transport effects. The proper nondimensional measure of the

ratio of the rates of diffusion and convection in this layer is a Peclet number based on the adsorption depth. In the asymptotic limit in which the surface and adsorption depth Peclet numbers tend to infinity, surfactant on the surface collects in zones located around the stagnation points since convection towards these points dominates the dispersing mechanisms of surface diffusion and desorption coupled with diffusion back into the bulk. This case is referred to as the "stagnant cap" regime. The regime is usually realized in systems in which the flow is fast enough so that the Peclet numbers are large.

In the second case either the transport by surface diffusion is very fast in comparison to convection, or the series processes of surface to bulk kinetic exchange and bulk diffusion are fast in comparison to convective transport. For this case the surfactant distribution on the surface of the droplet deviates only slightly from the value which would be realized for the surface concentration under equilibrium (zero-flow) conditions. This case is termed the "uniformly retarded" regime because the small deviation of the surface concentration from the equilibrium value along the surface creates a distributed Marangoni tension which retards uniformally the convection on the surface. Uniform retardation may be realized if the flow is extremely slow so that surface Peclet numbers are small and surface diffusion, acting as the dominant transport mechanism, forces the concentration to be nearly uniform. Alternatively, if the surface Peclet number is of order one, this case occurs if the kinetic transport between the bulk and the surface is fast compared to convection, and if the rate of diffusion in the adsorption depth layer is fast relative to convection in that layer (adsorption depth Peclet number much less than one).

The final case is the regime in which one (or possibly two) of the nonconvective surfactant transport mechanisms - either surface or bulk diffusion or kinetic exchange - is slow relative to convective transport, and the rest are fast. A solution is obtained with the rate limiting mechanism solved exactly, and the fast transport mechanisms regarded as in equilibrium in a quasistatic sense. The primary example of this case is the treatment of the kinetic exchange as infinitely fast (and thereby regarded as in equilibrium) and the bulk diffusion in the adsorption depth layer as rate limiting.

1.2 Literature Review of the Influence of Surfactants on the Motion of A Droplet in an Infinite Medium

As mentioned above, research efforts on the influence of surfactants on the motion of a droplet in an infinite medium have examined three regimes: the stagnant regime, the uniform retardation regime and the diffusion limiting regime. The literature review of investigations of these three cases are given separately below.

1.2.1 The Stagnant Cap Regime

The stagnant cap regime was first studied theoretically and experimentally by Savic in 1953. The mixed boundary value problem resulting from the assumption of a stagnant cap was solved approximately by truncating the Gegenbauer series solution for the stream function to six terms, and a resulting expression for the drag coefficient as a function of the cap angle was obtained. The size of the cap angle was calculated by assuming the interfacial tension at

the pole in the stagnation region to be equal to zero. Experimentally, photographs were obtained of water drops falling in castor oil which revealed that the streamlines were not symmetric about the equator, an observation consistent with the presence of a stagnant cap. Further experimental evidence for cap formation was provided by Horton, Fritsch and Kintner (1965) who observed a shift in the recirculation vortex in the drop interior away from the cap in the presence of surface adsorption. Additional studies by Garner and Skelland (1955), Elzinga and Banchero (1961), Huang and Kintner (1969) and Beitel and Heideger (1971) connected with the influence of surfactant adsorption on mass transfer from the droplet also observed a stagnant cap of surfactant.

Griffith (1962) pointed out that in contrast to Savic's formulation, the interfacial tension at the pole in the cap is not zero, but should be calculated through an equation of state for the interfacial tension as a function of the surface concentration. Assuming a linear equation, he obtained an expression for the cap angle as a function of the difference between the equilibrium surface tension (i.e. the tension corresponding to the bulk concentration of surfactant) and the clean value. Griffith also undertook experiments in which the terminal velocity was measured for ethylene-glycol drops translating in mineral oil as a function of bulk surfactant concentration. He found that his approach of calculating the cap pole tension resulted in correlating formulae which worked well for some surfactants, but not others.

Unlike Griffith's approach of using a linear constitutive relation to compute the size of the cap angle, Davis and Acrivos(1966) assumed that the interfacial tension at the pole in the stagnant cap

was equal to the monolayer collapse tension. These authors then computed the cap angle as a function of the difference between the collapse and the clean interfacial tensions. Further progress in the computation of the drag coefficient as a function of the cap angle was made by Harper (1973) and Sadhal and Jonson (1982). Harper derived analytic expression for the drag as a function of the cap angle for small cap angles. Finally, Sadhal and Jonson (1982) obtained an exact closed form solution for arbitrary stagnant cap size by inverting the dual series equations which come from the mixed boundary conditions at the interface. Their results refine the numerical calculations of Savic and Davis and Acrivos and agree at small cap angle with Harper's expansion.

1.2.2 The Uniform Retardation Regime

In the uniform retardation regime, the distribution of surfactant is assumed to deviate only slightly from the equilibrium value. As explained in 1.1, this regime is realized when surface diffusion is fast relative to surface convection (surface Peclet number small) or the series processes of bulk diffusion and sorption kinetic exchange are fast relative convection. Frumkin and Levich (1947) and Levich (1962) examined individually the cases in which the sorption kinetics, the bulk diffusion or the surface diffusion are fast but limiting. These expressions were unified by Newman (1966), and generalized by Schechter and Farley (1963) who obtained expressions for the drag coefficient for a general distribution of interfacial tension. Agrawal and Wasan (1979) included surface viscosity, an effect not present in a stagnant cap where no surface motion is present. The

influence of surface viscosity was formulated in a more general way by Levan (1981).

1.2.3 Diffusion Limiting Regime

Several studies have attempted to obtain expressions for the drag coefficient in the intermediate limit in which mass transfer from the bulk is not infinitely fast relative to convection, and therefore the surface concentration is not a small perturbation from the equilibrium value and not infinitely slow so a stagnant cap is realized. The initial effort was the perturbation study of Wasserman and Slattery (1969), who analyzed the case of a small bulk concentration of surfactant. A first order correction to the drag on a clean droplet was obtained assuming sorption equilibium and neglecting surface diffusion. If the bulk Peclet number is large, then boundary layer theory may be used to obtain asymptotic expression for the diffusion of surfactant to the surface. Efforts in this direction by Saville (1973) and Harper (1974) were complicated by a divergence of the asymptotic solution at the trailing pole. This singularity was removed by Harper (1982). Numerical solutions were undertaken by Levan and Newman (1976), and are essentially in agreement with Harper (1982). Additional numerical solutions were obtained by Levan and Holbrook (1983). The studies of Saville (1973), Harper (1974, 1982) and Levan and Newman (1976) all assumed infinite sorption kinetics. The inclusion of finite sorption kinetics was undertaken by Levan and Holbrook (1983) for the case in which bulk diffusion is fast and the bulk concentration is uniform.

1.3 Literature Review of the Motion of Particles in Tube

Most of the previous investigations of the motion of particles in a tube were concerned with spherical solid particles. Studies by Ladenburg (1907), Faxen(1922), Burgers(1940), Happer and Byrne (1954, 1965), Wakiya (1953), Kynch (1959), Bohlin (1960), Greenstein and Happel (1970) etc. were based on the method of both reflection and used the point force technique to solve for the axisymmetry motion of a single solid sphere in a tube. Those results showed that these methods are good for small sphere-tube diameter ratio. Haberman and Sayre (1958) were the first to obtain the exact solution for the solid sphere translating by solving the system of linear algebraic equations for the constants which arise from a series expansion for the stream function. Wang and Skalak (1969) studied a line of rigid spheres inside a cylinder; the drag coefficient and the pressure drop were obtained by superposing periodic functions for the steamlines in spherical coordinates. Skalak et al (1970) used the finite-element method to treat space periodic solid particles. Leichtberg, Pfeffer and Weinbaum, (1976) presented the solution for the drag coefficient for the Stokes flow past finite rigid spheres inside a cylinder by solving the fundamental governing equations. After Fourier transforming to eliminate the spherical disturbance, the boundary conditions on the tube wall are satisfied exactly and multipole truncation is used to satisfy the boundary conditions on the spheres at discrete points. Other works which confirm the accuracy of Haberman and Sayre's results for the rigid sphere are Coutanceau (1971), Paine and Sherr (1975) and Tozeren (1983); in an experimental investigation, verification of the numerical results was obtained by

Ambari, Gauthier-Manuel and Guyon (1985) using a magnetic sphere rheometer.

Haberman and Sayre (1958) also calculated approximately the drag exerted on the translating fluid spheres for both stationary and moving fluids inside an infinitely long cylinder by approximately solving the first two of the linear simultaneous equations. The method is valid for droplet-cylinder diameter ratio up to 0.6. Brenner (1970, 1971) worked out the solution for small neutrally-buoyant droplets without necessarily satisfying the boundary conditions explicitly on the tube wall. The numerically exact solution for a periodic train fluid spheres was obtained by Hyman and Skalak (1969,1970) for sphere to tube diameter ratio of 0.8 and different values for the spaces between the spheres. The largest intersphere distance calculated was 40 cylinder radii, and the results may be taken to be valid for single particles.

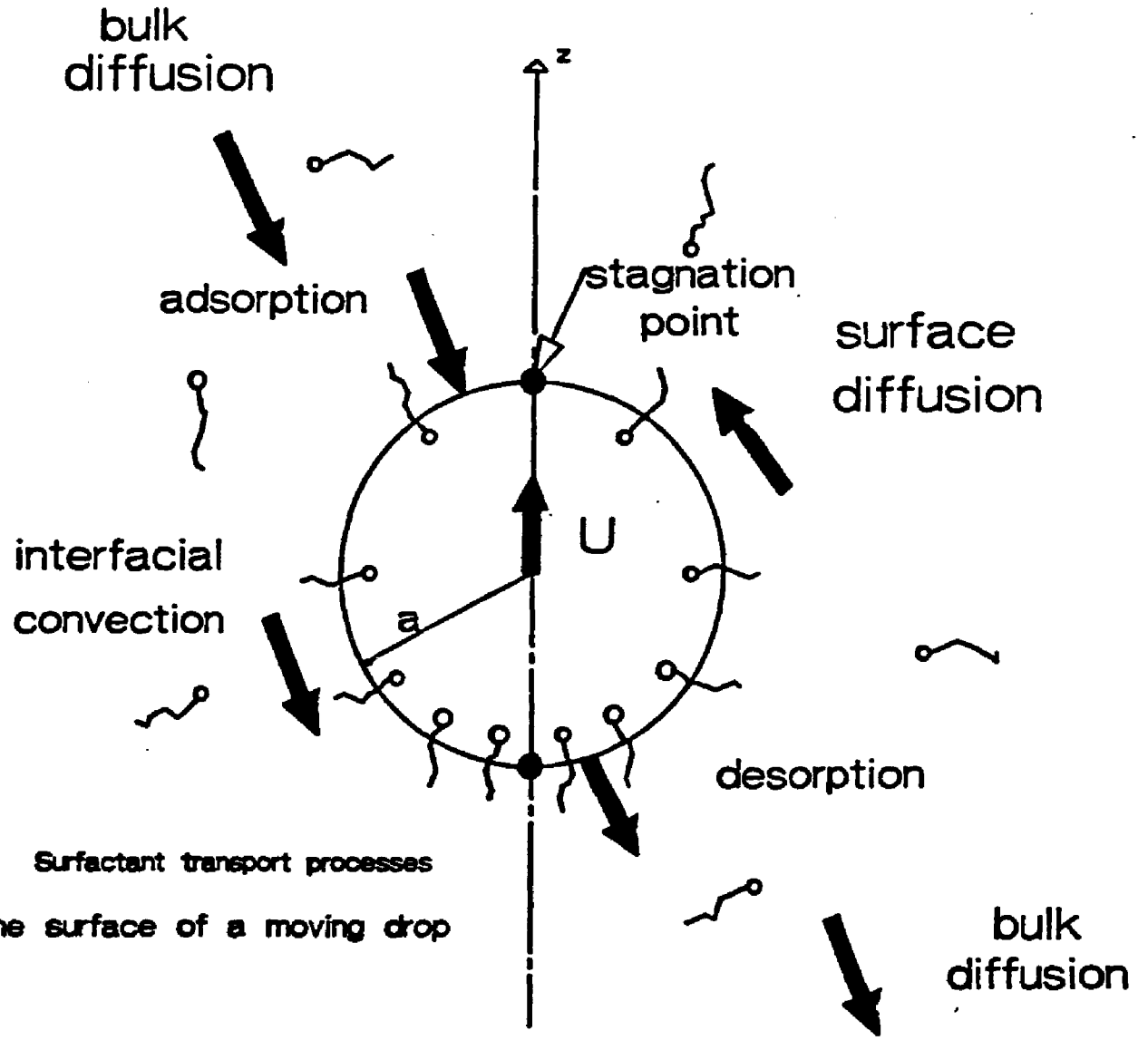

Fig.1 Surfactant transport processes on the surface of a moving drop

Chapter 2

The Size of Stagnant Caps of Bulk Soluble Surfactant on the Interface of Translating Fluid Droplets

2.1 Introduction

The presence of surfactant molecules in the continuous phase through which a fluid droplet translates reduces the terminal velocity of the droplet. The mechanism for this physicochemical effect was first suggested by Frumkin and Levich (1947). When a fluid droplet moves through a continuous liquid phase that contains a bulk soluble surfactant, the surfactant molecules adsorb onto the interface of the droplet. Once adsorbed, they are convected to the trailing or rear pole of the droplet where they accumulate in the vicinity of that pole. This accumulation eventually causes desorption of the molecules into the sublayer of liquid immediately adjacent to the rear part of the interface. The desorption locally elevates the bulk concentration of surfactant relative to the concentration far from the drop, and the surfactant diffuses away into the bulk. The convection of surfactant to the rear lowers the surface concentration near the leading pole and leads to both a surface diffusive flux from the rear to the leading pole, and additional adsorption from the adjoining liquid sublayer at the droplet front. The sublayer concentration, depleted by this adsorption, is replenished by diffusion as the concentration of surfactant in this sublayer is lower than that far from the drop. These surfactant transport mechanisms are pictured schematically in Figure 1.

The accumulation of surfactant at the rear of the drop by convection lowers the interfacial tension in this region relative to the front end because the surfactant molecules which are compressed at the rear by the accumulating action of the convection exert an outward force (the surface pressure). This difference in interfacial tension causes the surface to be tugged towards the front pole and since this action (a Marangoni tension) is opposite to the direction of surface convection, the surface flow is retarded. The reduction in the surface flow increases the drag exerted by the continuous phase on the droplet, causing the droplet to decelerate. The surface flow retardation also lowers the rate of convective clearance of surfactant at the front end and accumulation at the rear and therefore allows the bulk diffusion and sorption kinetic rates to become commensurate with the rate of surface convective transport. Eventually a steady state is reached where the rate at which surfactant diffuses towards and becomes adsorbed onto the front end is balanced by desorption and diffusion back to the bulk at the rear. This steady state is one of diminished terminal velocity relative to the value for the surfactant-free surface conditions.

The surfactant gradient which develops at steady state determines the Marangoni tension and hence the magnitude of the terminal velocity reduction. The gradient which evolves is a function of the relative rates with which the surfactant transport processes take place. Two regimes provide bounds on the retardation. If the rate of surface convection is much slower than either the rate of surface diffusion, or the rates of the series mechanisms of adsorption and desorption and bulk diffusion, then the surface concentration is asymptotically close to Γ_0', the value which is realized under equilibrium (zero-flow)

conditions. In this case, the concentration at the rear of the drop is only slightly larger than Γ'_0, and that at the front end is just less than Γ'_0. This is the regime of uniform retardation, referred to as such because the small deviation of the surface concentration from Γ'_0 creates a distributed Marangoni tension which uniformally retards the surface velocity. The regime has been studied theoretically by Frumkin and Levich (1947), Levich (1962), Newman (1966), Schechter and Farley (1963) and Agrawal and Wasan (1979). Since in uniform retardation the surfactant gradient and corresponding Marangoni tension are small, this regime results in the least retardation, and the drop moves with nearly the clean surface value. Alternatively if the rate of surface convection is both fast with respect to the rate of surface diffusion and fast when compared to either the rate of bulk diffusion or the rates of adsorption and desorption, then the surfactant is swept into a cap region where the surface velocity is equal to zero. For a given bulk concentration of surfactant, this regime results in the greatest retardation. Obviously, if enough surfactant is present in the continuous phase the stagnant cap angle can stretch across the entire surface of the droplet resulting in a completely immobile interface and a terminal velocity characteristic of a solid particle. The stagnant cap regime has been examined theoretically by Savic (1983), Griffith (1962), Davis and Acrivos (1966), Harper (1972, 1973, 1974 and 1982), and Sadhal and Johnson (1982).

Clearly, the rate at which surfactant is transported by convection relative to the rate of transport by surface or bulk diffusion is characterized by the values of the bulk and surface Peclet numbers, defined as U'_0D'/a' and $U'_0D'_s/a'$, respectively, where a'

and U_0' are the droplet radius and terminal velocity for a clean surface and D' and D_s' are the bulk and surface diffusion coefficents. In drop flows Peclet numbers are usually very large because of the small values of the diffusion coefficients of surfactants in liquids, and therefore the stagnant cap regime is potentially the most common physically realizable regime. Several experimental investigations at high Peclet and small Reynolds numbers have provided indirect evidence for the existence of a stagnant cap. Savic (1953) noted that the streamlines surrounding a falling drop of water in castor oil were not symmetric about the droplet equator. Horton et al. (1965) observed that in the presence of surfactants in the continuous phase, the center of the recirculation vortex in the drop interior shifted away from the leading pole. Additional studies by Garner and Skelland (1955), Elzinga and Banchero (1961), Huang and Kintner (1969) and Beitel and Heideger (1971) connected with the influence of surfactant adsorption on mass transfer from a falling droplet also observed the vortex shift and the asymmetric streamline pattern around the drop equator. The vortex shift and streamline asymmetry are inconsistent with uniform retardation since in this regime the velocity is uniformally reduced along the length of the drop and the streamlines remain symmetric about the drop equator as they are in the clean surface Hadammard-Rybczynski solution. However, a cap wherein the surface velocity is zero breaks this symmetry, and the interior vortex moves away from the cap to reduce the viscous drag on the cap side facing the interior.

In this chapter, we study the stagnant cap regime because it can be realized in the physically common circumstance of high Peclet numbers. We consider the case of a single droplet translating in an

infinite medium in steady, axisymmetric creeping flow with the interfacial tension large enough so that viscous tractions do not distend the droplet from sphericity. Thus both the Reynolds and capillary numbers are each assumed to be much smaller than one, where the Reynolds number is defined as $\rho' U_0' a' / \mu'^{(2)}$ and the capillary number as $\mu'^{(2)} U_0' / \sigma'$. (Here σ' denotes the interfacial tension and $\mu'^{(2)}$ the viscosity of the continuous phase; in what follows droplet variables are denoted by a superscript (1) and continuous phase variables by a superscript (2).) As a purely hydrodynamic problem, the velocity field due to a stagnant cap at the rear of a translating drop can be solved for exactly (Sadhal and Johnson (1982) in terms of an infinite series of Gegenbauer polynomials with constants which are a function of the cap angle ϕ. From this series, a closed form solution for the drag exerted on the drop can be obtained as a function of ϕ, and from this function the terminal velocity may be computed once the external force on the drop is resolved.

The cap angle, as yet undetermined, is obtained by computing the surfactant distribution in the cap region. This is obtained by first equating the difference in viscous shear stresses exerted on the surface by the adjoining bulk phases (as computed from the hydrodynamic solution) to the interfacial tension gradient. This gradient, which represents the surface pressure exerted by the surfactant molecules as they are compressed in the cap, can be rewritten as a surfactant concentration gradient once an equation of state relating the surface concentration (Γ') to the interfacial tension σ' is specified. The balance of Marangoni and viscous stresses, reformulated in term of σ', is integrated to obtain the

surfactant distribution and yields σ' as a function of ϕ and a dimensionless group (the Marangoni number, Ma) characterizing the ratio of the surface pressure which the surfactant molecules exert when they are compressed to the viscous forces tending to concentrate the surfactant. Once obtained, the surfactant distribution is integrated over the cap region to obtain the total amount on the surface, M. The variable M is also computed independently from the surfactant conservation equations; equating the two expressions yields ϕ. Once ϕ is specified, the problem is closed as the drag coefficent and terminal velocity may be computed.

The above procedure was first introduced by Griffith (1962) whose study is incomplete since he did not have the proper hydrodynamic solution, and later by Sadahal and Johnson (1982) in their exact solution of the problem. Each of these authors assumed that the surface pressure exerted by the surfactant compressed in the stagnant cap may be represented by the gaseous expression:

$$\sigma_0' - \sigma' = R'T'\Gamma', \tag{1.1}$$

where R' and T' denote, respectively, the gas constant and temperature. The use of this constitutive equation for all flow regimes is seriously flawed because gaseous behavior is only realized when the surface coverage is low. When the surfactant density becomes large, strong repulsions between surfactant molecules yield surface pressures that vary much more strongly than linearly with the surface concentration. The concentration of surfactant in the stagnant cap will depend principally on the amount adsorbed, and the degree of compression exerted by the viscous forces. If these forces are large

enough, they can compress the surfactant to a density high enough so that (1.1) does not apply. In such a flow circumstance, the surface pressure which the surfactant exerts will be much larger than (1.1) because of the stronger repulsions occuring at the higher density, and this extra surface pressure above the gaseous value must be described by a nonlinear equation. Since the use of a gaseous constitutive equation underpredicts the surface pressure, Sadhal and Johnson's results underpredict the cap angle and consequently the drag coefficent. The aim in this chapter is to obtain a more realistic value for the cap angle by allowing for nonlinear interactions.

In this study, to formulate an expression for a nonlinear surface pressure, the Langmuir isotherm is used in conjunction with the Gibbs-Duhem equation. In this isotherm, the surface concentration Γ_0' in equilibrium with the uniform bulk concentration C_∞' is given by:

$$\Gamma_0' = \Gamma_\infty' \frac{k}{1+k} \tag{1.2}$$

where Γ_∞' is the maximum packing density of the surfactant and k is the nondimensional measure of the bulk concentration given by $k = \beta' C_\infty'/\alpha'$. In the definition of k, β' and α' are the adsorption and desorption rate constants, with the net sorption given for a sublayer concentration C_s' by $Q'(\Gamma', C_s') = \beta' C_s'(\Gamma_\infty' - \Gamma') - \alpha'\Gamma'$. Assuming that the bulk concentration of surfactant is small enough so that activities may be replaced by concentrations in the expression for the chemical potential, $\Gamma' = -R'T'\frac{\partial \sigma'}{\partial \ell n(C')}$. Integrating this isotherm results in Frumkin's constitutive equation:

$$\sigma_0' - \sigma' = -R'T'\ell n(1-\Gamma'/\Gamma_\infty') \qquad (1.3)$$

Note that this relation reduces to gaseous beavior for low surface coverage compared to the maximum packing density ($\Gamma'/\Gamma_\infty' \ll 1$). Frumkin's equation also retains the physics we seek in that the surface pressure varies much more strongly than Γ' for high surface coverages. The Frumkin equation does, however, have its limitations in that the surface pressure diverges as Γ' approaches the maximum packing density and clearly the Frumkin equation overcompensates for the repulsive interactions. Therefore the results obtained herein using this equation may be regarded as giving an upper bound on the cap angle for a particular flow circumstance.

This chapter is organized as follows. In the next section the surfactant conservation equations are formulated, and the numerical technique for obtaining the cap angle using the nonlinear isotherm is described. The following section presents and gives a discussion of the results.

2.2 Formulation

The surfactant conservation equations on the droplet interface balance the diffusive flux of surfactant between the bulk and the surface with clearance due to convection and diffusion on the surface, and balance the bulk to surface diffusive flux with the exchange due to the sorption process. To formulate these equations nondimensionally, scales of U_0', C_∞' and Γ_∞' are chosen for velocity and bulk and surface concentrations, respectively. In the context of these

scales, it is clear that convection and diffusion are of order $C'_\infty U'_0/a'$ and $C'_\infty D'_s/a'^2$, respectively and adsorption and desorption scale as $\beta' C'_\infty \Gamma'_\infty$ and $\alpha' \Gamma'_\infty$, respectively. Scaling the diffusive flux is more involved. At large Peclet numbers, surfactant is transported to the surface through a boundary layer. The size of the boundary layer thickness, δ', is dependent upon the surface mobility. Elementary boundary layer arguments (Levich (1962)) indicate that for a mobile surface $\delta'/a' = O(Pe^{-1/2})$, while for a stagnant interface $\delta'/a' = O(Pe^{-1/3})$. With surfactant adsorbed onto the surface the mobility on average is intermediate, and therefore the boundary layer thickness is taken here as $\delta'/a' = O(Pe^{-\eta})$, $1/3 \le \eta \le 1/2$. Thus the diffusive flux scales as $C'_\infty D' Pe^{-\eta}/a'$. With these nondimensionalizations, the mass conservation equations become:

$$\frac{1}{\sin\theta}\frac{\partial}{\partial\theta}(V_s(\theta)\Gamma\sin\theta) + Pe_s^{-1}\left(\frac{1}{\sin\theta}\frac{\partial}{\partial\theta}\left(\sin\theta\frac{\partial\Gamma}{\partial\theta}\right)\right) = \Phi^{-1}\frac{\partial C}{\partial r}_{|r=0} \qquad (2.1)$$

$$\Phi^{-1}\frac{\partial C}{\partial r}_{|r=0} = Bi[C_s(\theta)(1-\Gamma) - k^{-1}\Gamma] \qquad (2.2)$$

These equations are formulated with respect to a spherical coordinate system (r',θ,ϕ) fixed with respect to the droplet and with the angle θ measured from the front stagnation point. The functions $V_s(\theta)$ and $C_s(\theta)$ denote the dimensionless tangential surface velocity and the sublayer concentration. The nondimensional radial coordinate in the normal flux, r, is defined by $(r'-a')/\delta'$. The bulk (Pe) and surface

(Pe_s) Peclet numbers and the parameter k which appear in these equations have been defined in the Introduction. Finally, in (2.1) and (2.2), $Bi = \beta' C'_\infty/(U'_0/a')$, and characterizes the ratio of the rate of adsorption of surfactant to the rate of surface convection and $\Phi = Pe^{1-\eta}(\Gamma'_\infty/a'C'_\infty)$, and characterizes the surface convective rate to the bulk diffusive rate. (Φ is termed the surface activity parameter as introduced and discussed by Deryagin et al. (1960) and Harper (1972 and 1974)).

Stagnant cap behavior follows in the limits $Pe_s \to \infty$ and either $Bi \to 0$ or $\Phi \to \infty$ since in these limits the surface conservation equation reduces to

$$\frac{1}{\sin\theta}\frac{\partial}{\partial\theta}(V_s(\theta)\Gamma\sin\theta) = 0 \qquad (2.3)$$

As the general solution of (2.3) is $V_s(\theta)\Gamma = \chi/\sin\theta$, χ a constant, there are no nontrivial continuous solutions for both $\Gamma(\theta)$ and $V_s(\theta)$ which are bounded and valid everwhere in the domain ($0 \le \theta \le \pi$). Hence solutions are constructed which are piecewise continuous. The simplest construction consistent with the unidirectional nature of the surface convection pattern is to assume $\Gamma(\theta)$ to be nonzero in a region only along the rear of the droplet, i.e. $\pi - \phi < \theta \le \pi$. Since this region includes the pole $\theta = \pi$, $\chi = 0$, and since $\Gamma(\theta)$ is nonzero, $V_s(\theta) = 0$ and the sector is stagnant. In this region, the difference in shear stresses exerted by the bulk phases on the surface (defined as $\tau^{(2)}_{r\theta(s)} - \tau^{(1)}_{r\theta(s)}$) is equated to the Marangoni stess. For the leading part of the drop

$0 \le \theta < \pi - \phi$, $\Gamma(\theta) = 0$ and this satisfies (2.3). In this front region $V_s(\theta)$ is left unconstrained and the shear stresses exerted by the bulk phases on the surface are required to be equal. Summarizing, the following boundary prescription satisfies the conservation equation:

$$\Gamma(\theta) = 0 \qquad (2.4a)$$

$$(0 \le \theta < \pi - \phi)$$

$$\tau^{(2)}_{r\theta(s)} - \tau^{(1)}_{r\theta(s)} = 0 \qquad (2.4b)$$

$$V_s(\theta) = 0 \qquad (2.5a)$$

$$(\pi - \phi < \theta \le \pi)$$

$$\tau^{(2)}_{r\theta(s)} - \tau^{(1)}_{r\theta(s)} = \frac{1}{U'_0 \mu'(2)} \frac{\partial \sigma'}{\partial \theta} \qquad (2.5b)$$

Other constructions in which surfactant is organized in belts are consistent with (2.3), but are not relevant here since the clean surface flow is unidirectional. However, if the surfactant-free convection pattern contained stagnation rings, as is the case for certain slug and droplet creeping flows regimes in tubes, then surfactant will partition itself in domains about these rings, and more complicated constructions would be required.

The hydrodynamic problem consisting of the Stokes field equations and the interface boundary conditions of continuity of velocity along the entire surface and (2.4b) and (2.5a) is well-posed (for unknown ϕ), and an exact solution was obtained by Sadhal and Johnson (1982). The cap angle is determined by computing the amount of surfactant which it is necessary to adsorb to cause a surface pressure that

balances the compression due to the viscous shear on a cap of angle ϕ, and then comparing this value to the amount adsorbed as computed from the conservation equation.

Sadhal and Johnson give the following equation for the difference in shear stresses exerted by the surrounding phases on the interface in the cap region:

$$(\tau^{(2)}_{r\theta(s)} - \tau^{(1)}_{r\theta(s)}) = -h(\theta,\phi)/\lambda = \frac{1}{\pi(1+\kappa)} \tan(\theta/2)\{\frac{(1+\cos\phi)^{3/2}}{(\cos\theta - \cos\phi)^{1/2}} + \frac{3}{2}(1+\cos\theta)[\arcsin(\frac{(\cos\theta - \cos\phi)}{1-\cos\theta})^{1/2} + \frac{(\cos\theta - \cos\phi)^{1/2}(1+\cos\phi)^{1/2}}{(1+\cos\theta)}]\} \tag{2.6}$$

where κ is the ratio of the droplet to the continuous phase viscosity $(\mu'^{(1)}/\mu'^{(2)})$ and λ is the drag coefficent defined by:

$$\lambda = \{[2\phi + \sin\phi - \sin 2\phi - \tfrac{1}{3}\sin 3\phi]/2 + \pi(2+3\kappa)\}/2\pi(1+\kappa)$$

The dimensional drag F'_D exerted by the continuous phase on the droplet is given by $F'_D = 2\pi\mu'^{(2)}a'[(2+3\kappa)/(1+\kappa)]U'$, where U' is the terminal velocity.

From the Frumkin constitutive equation (1.3) and the Marangoni stress balance (2.5b), a differential equation for the surfactant distribution may be obtained:

$$\frac{Ma}{(1-\Gamma)} \frac{\partial\Gamma}{\partial\theta} = -h(\theta,\phi)/\lambda \tag{2.7}$$

where Ma identifies the Marangoni number, and is defined as $Ma = R'T'\Gamma'_\infty/(\mu'^{(2)}U'_0)$. The Marangoni number characterizes the ratio of the linear surface pressure force to the compressive force due to the viscous shear. The surfactant distribution $\Gamma(\theta)$ is obtained by integrating (2.7) from $\pi-\phi$ to an angular position θ in the cap; from a second integration the total amount on the surface is obtained. Thus:

$$\Gamma(\theta) = 1 - \exp\left(-\frac{1}{Ma}\int_{\pi-\phi}^{\theta} h(\theta',\phi)/\lambda d\theta'\right) \tag{2.8}$$

$$M(\phi)/2\pi = \int_{\pi-\phi}^{\pi} \sin\theta\left(1 - \exp\left(-\frac{1}{Ma}\int_{\pi-\phi}^{\theta} \lambda h(\theta',\phi)d\theta'\right)\right)d\theta \tag{2.9}$$

In obtaining (2.8) the condition $\Gamma(\pi-\phi) = 0$ has been used.

A second relation for the total amount adsorbed is obtained by multiplying the conservation equations (2.1) and (2.2) by $\sin\theta$ and integrating from 0 to π. Using this procedure (2.1) demonstrates that the net diffusive flux is equal to zero,

$$\int_0^{\pi} \sin\theta \left.\frac{\partial C}{\partial r}\right|_{r=0} d\theta = 0 \tag{2.10}$$

while (2.2) results in an equation for $M(\phi)$:

$$M(\phi)/2\pi = \int_0^{\pi} \sin\theta\ [kC_s(\theta)(1-\Gamma(\theta))]d\theta \tag{2.11}$$

Note that although (2.10) and (2.11) are true for all Bi and Φ, they do not yield a definitive value for $M(\phi)$ without complete resolution of the surface and sublayer concentration fields. To realize stagnant cap behavior, either $Bi \to 0$ or $\Phi \to \infty$. Three possibilities exist with regard to these asymptotes: (i) $Bi \to 0$, $Bi\Phi \to 0$, (ii) $\Phi \to \infty$, $Bi\Phi \to \infty$ and (iii) $Bi \to 0$, $\Phi \to \infty$, $Bi\Phi = O(1)$. In the first, sorption kinetics is slower than bulk diffusion, and to leading order, from (2.2), $\left.\frac{\partial C}{\partial r}\right|_{r=0} = 0$. Therefore the concentration of surfactant in the bulk, and particularly in the sublayer, remains equal to one. From (2.11) with $C_s(\theta)=1$, a simple equation for $M(\phi)$ is obtained:

$$M(\phi)/2\pi = \frac{2k}{(1+k)} \tag{2.12}$$

In the second possibility ($\Phi \to \infty$, $Bi\Phi \to \infty$), bulk diffusion is slower than sorption kinetics. From (2.2) in the limits $\Phi \to \infty$ and $Bi\Phi \to \infty$ the sublayer and surface are found to be in local equilibrium $\Gamma(\theta) = kC_s(\theta)/(1+kC_s(\theta))$. However, $M(\phi)$ cannot be found explicitly until $C_s(\theta)$ is obtained as the solution of a boundary layer problem with surface conditions $C_s(\theta)=0$, $0<\theta<\pi-\phi$, and $C_s(\theta)$ given by the solution of (2.8) and the local equilibrium constraint for $\pi-\phi<\theta<\pi$. In the last possibility ($Bi \to 0$, $\Phi \to \infty$, $Bi\Phi = O(1)$), bulk diffusion and sorption kinetics are of the same order. The bulk and sublayer concentration fields and ultimately $M(\phi)$ are obtained from the simultaneous solution of the boundary layer equation and (2.2) and (2.8).

Here the first possibility Bi→0, BiΦ→0 will be addressed. For this case, combining (2.9) and (2.12) results in the following implicit equation for ϕ:

$$\frac{k}{(1+k)} = \frac{1}{2}\int_{\pi-\phi}^{\pi} \sin\theta[1 - \exp(-\frac{1}{Ma}\int_{\pi-\phi}^{\theta} h(\theta',\phi)/\lambda d\theta')]d\theta \qquad (2.13)$$

As the inner integral in (2.13) can be evaluated analytically, solutions for ϕ as a function of k and Ma may be obtained by fixing Ma and ϕ and numerically evaluating the outer integral so as to solve for k. The results obtained are presented in the next section.

2.3 Results and Discussion

Consider first the case in which Ma is very large (>10), and therefore the characteristic linear surface pressure forces are much larger than the compressive viscous shear forces. Because of this disparity, the adsorbed monolayer cannot be compressed very much by the viscous forces, and the cap size ϕ increases dramatically with small increases in the bulk concentration. This expected trend is exhibited by the solid lines in Fig. (2) which are the solution of (2.13) for $k(\phi)$ with Ma as a parameter equal to 10, 100 and 1000 and κ=0. In the limit of large Marangoni number, an expansion in inverse Ma can be constructed for $k(Ma,\phi)$ of the form: $k(Ma,\phi) = \frac{1}{Ma} S(\phi) + O(Ma^{-2})$, where $S(\phi)$ satisfies (for κ=0) the relation

$$S(\phi) = \int_{\pi-\phi}^{\pi} (\sin\theta \int_{\pi-\phi}^{\theta} h(\theta',\phi)d\theta')d\theta \qquad (3.1)$$

$$S(\phi) = (2\phi - 4\phi\cos\phi - \sin 2\phi + 4\sin\phi)/4\pi \qquad (3.2)$$

The second line follows from analytic integration. The approximate relation $k \approx S(\phi)/(Ma)$ is plotted in Fig. 2 as the dotted lines, and the excellent agreement with the numerical solution is clearly evident. Recasting the asymptotic relation in the form $S(\phi) \approx k\lambda \cdot Ma$, and noting that for small k, $M \approx 4\pi k$, $S(\phi) \approx (M/4\pi)Ma = R'T'\Gamma_0'/(\mu'^{(2)}U')$. These latter equations also follow from the assumption of linear kinetics ($Q'(\Gamma',C_s')=\beta' C_s' \Gamma_\infty' - \alpha\Gamma'$; isotherm $\Gamma_0'=k$) and a gaseous equation of state ($\sigma_0' - \sigma' = R'T'\Gamma$), and were obtained by Sadhal and Johnson.

When the Marangoni number is small, the viscous compression forces far exceed the linear surface pressure, and surfactant is compressed considerably so that nonlinear repulsions provide the added surface pressure necessary to balance the viscous action. As a result of the significant compression, relatively high bulk concentrations of surfactant (compared to the large Marangoni regime) are required to achieve significant cap angles. These results are shown in Fig. 3, again for $\kappa=0$. For small Ma, we do not expect the gaseous equation to give accurate results because of the significant viscous compression. For this case, $k(\phi,Ma)$ is obtained by expanding the right hand side of (2.13) to obtain:

$$\frac{k}{1+k} = 2S(\phi)/(3Ma) \qquad (3.3)$$

This equation is plotted as the dotted line in Fig. 3, and it is clear that the use of the linear equation of state allows the monolayer to be too compressible, and thus severely underpredicts the cap angle. More importantly, for values of Ma<1, it can easily be shown that the right hand side of (3.3) reaches 1 for $\phi<\pi$, and therefore for Ma < 1, as k increases, the cap angle asymptotes to a fixed value. Thus the monolayer is so compressible that an infinite amount of surfactant can be contained in a finite sized cap if Ma is small enough. The surfactant distributions for Ma=0.5 is pictured in Fig. 4 for the linear and nonlinear isotherm. for the same value of k (0.218; $\phi=60^{o}$ for the nonlinear and 45.6^{o} for the linear). The figure clearly indicates that the use of the linear isotherm yields a surfactant concentration at the rear pole which is a factor of 1.5 larger than the maximum packing density. A representative distribution for large Ma is also provided (Ma=100, k= $1.8\text{x}10^{-3}$, $\phi = 59.9^{o}$), and the agreement between the linear and nonlinear, and the small values of Γ' in relation to Γ'_{∞} are clearly evident.

Consider the limit of ϕ(k,Ma) as Ma→0 for fixed k. If a gaseous equation is assumed, $\phi\rightarrow 0$ (cf. (3.3)) and all the surfactant is compressed into the rear pole. However, when the nonlinear Frumkin equation is used, when Ma→0 and the viscous compressive stresses become infinite, surfactant is compressed to the extent that $\Gamma\rightarrow 1$ and the surface pressure forces become singular in order to balance the infinite viscous forces. Surfactant is packed with a density Γ'_{∞} into a cap of a particular size obtained by taking the limit of (2.13) as Ma→0. The result is:

$$\frac{k}{1+k} = \frac{1}{2}(1-\cos\phi) \qquad (3.4)$$

The above function, plotted in Figure 3, provides an envelope below which the value of k for a particular cap angle at finite Marangoni number may be found.

Thus we conclude that the use of a gaseous equation of state, as has been undertaken exclusively in the literature, is only valid for large Marangoni numbers (Ma>10), and that the extension to regimes of small Ma significantly underpredicts the cap angle. The numerical solutions given in Fig.3 which use the Frumkin equation to describe the interfacial tension constitutive equation provide a more accurate computation of the cap angle for the regime of Ma<10. Together with $\lambda(\phi)$, Fig. 3 allows for the direct determination of the translational velocity of the droplet in terms of the bulk concentration and the Langmuir constants of the surfactant.

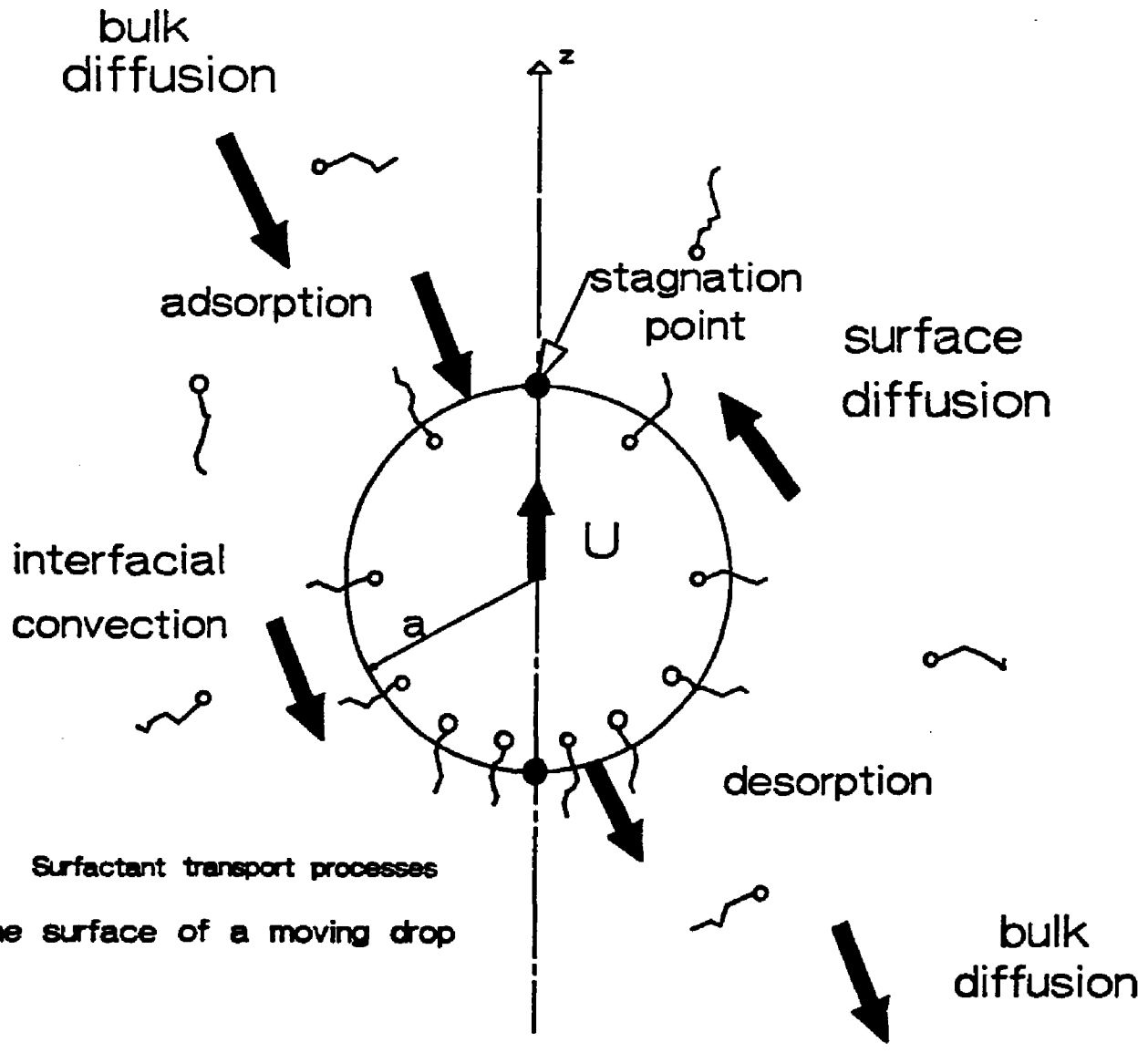

Fig.1 Surfactant transport processes on the surface of a moving drop

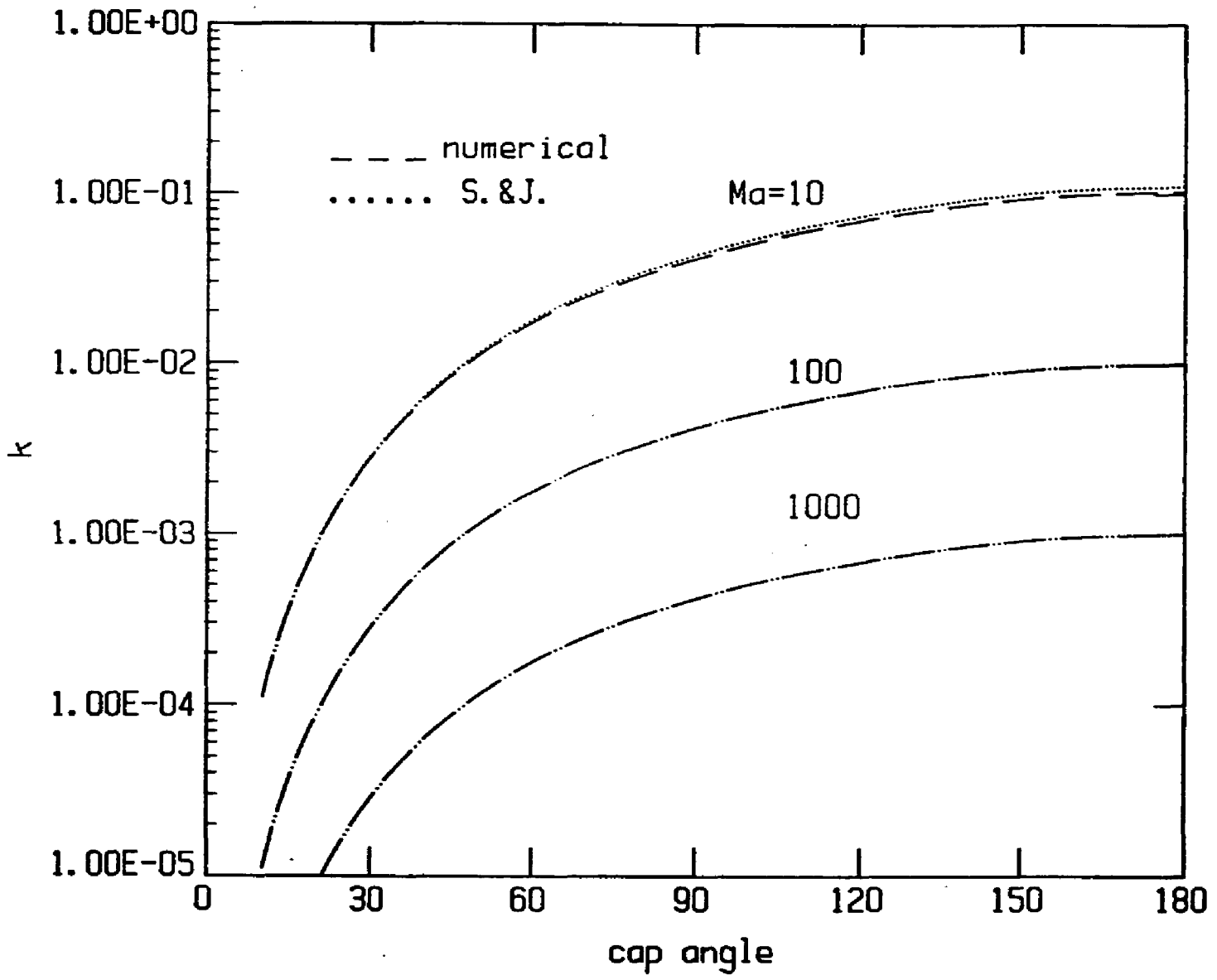
1.00E+00
1.00E-01
1.00E-02
1.00E-03
1.00E-04
1.00E-05
K
0
30
60
90
120
150
180
cap angle
numerical
S.&J.
Ma=10
100
1000

Figure 2

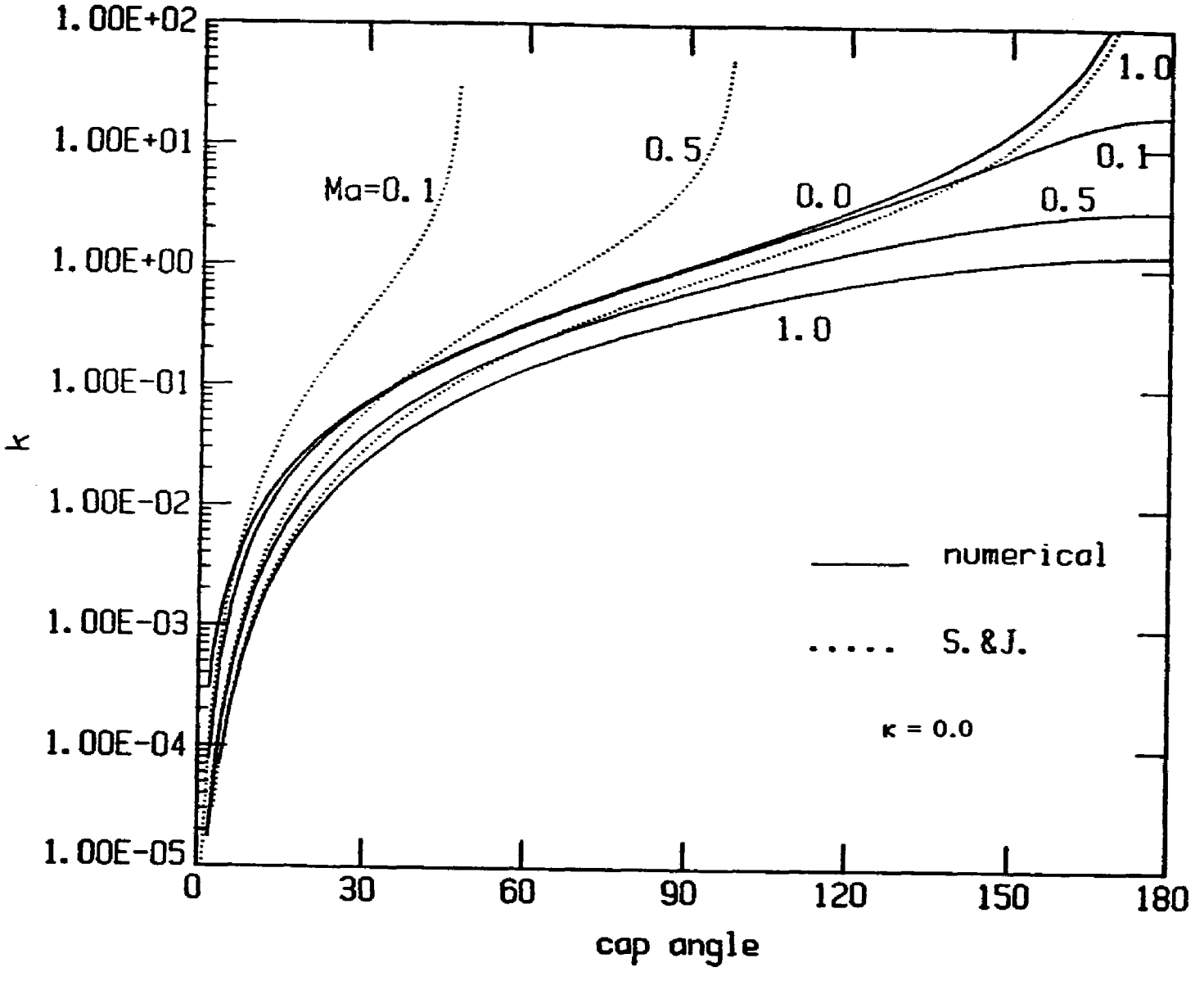
1.00E+02
1.00E+01
1.00E+00
1.00E-01
1.00E-02
1.00E-03
1.00E-04
1.00E-05
K
0
30
60
90
120
150
180
cap angle
Ma=0.1
0.5
1.0
0.0
0.1
0.5
1.0
numerical
S.&J.
κ = 0.0

Figure 3

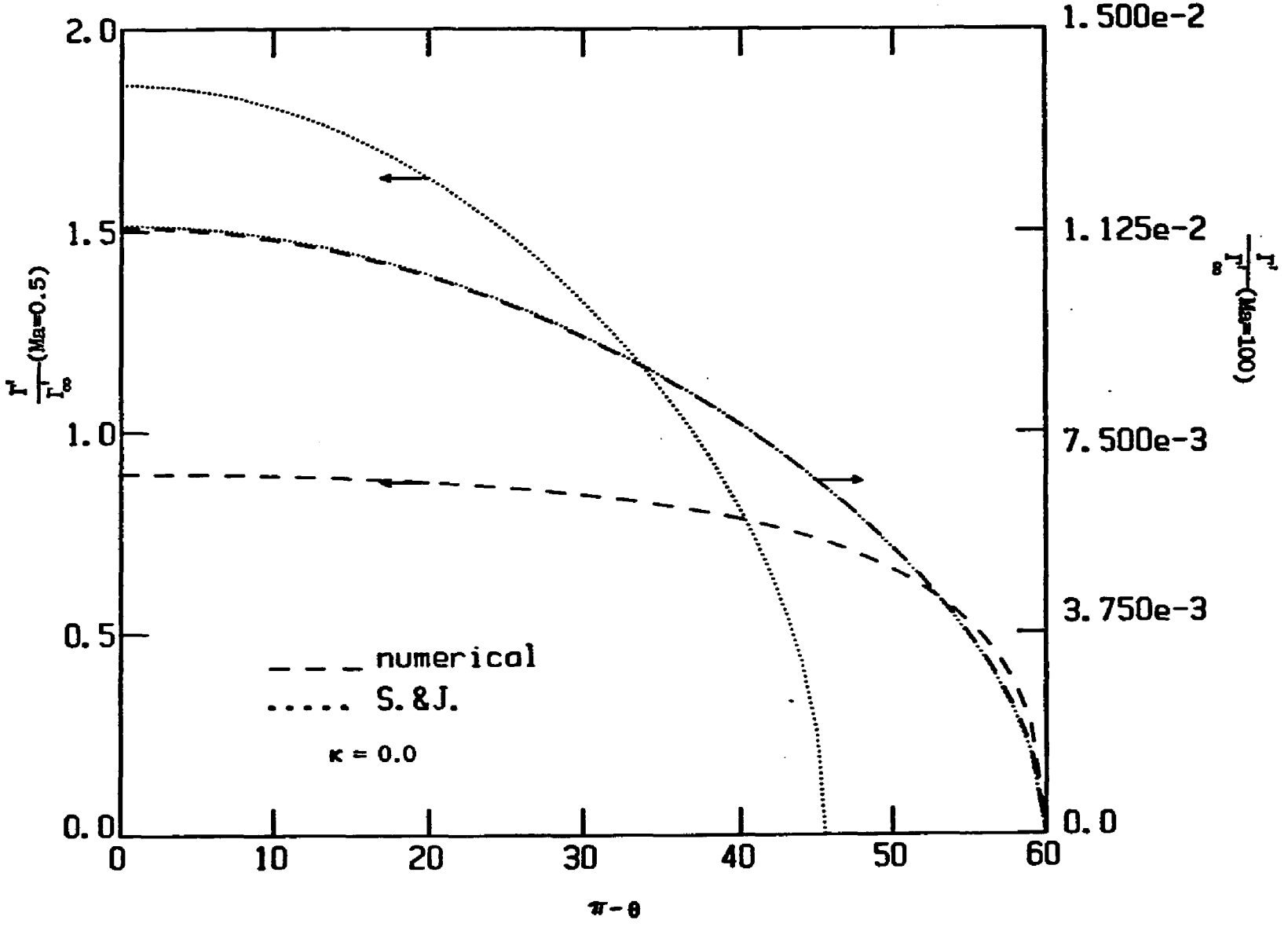
2.0
1.5
1.0
0.5
0.0
1.500e-2
1.125e-2
7.500e-3
3.750e-3
0.0
0
10
20
30
40
50
60
numerical
S.&J.
κ = 0.0
π-θ

Figure 4

Chapter 3

The Unsteady Translation of a Fluid Droplet Owing to the Adsorption of a Surfactant Monolayer

3.1 Introduction

The hydrodynamic movement of a fluid droplet in an unbounded continuous liquid phase is significantly retarded by the presence of strongly adsorbing surfactants dissolved in the droplet or continuous bulk phases. The physicochemical basis of this retardation was first outlined by Levich (Frumkin and Levich (1947) and Levich (1962)). Levich proposed that the clean surface of a freshly formed droplet which begins to translate becomes populated with surfactant molecules because of adsorption of these molecules from the bulk adjoining phases. This adsorption depletes the molecular concentration in the vicinity of the interface, and molecules from the bulk begin to diffuse towards the droplet interface. Surfactant which has adsorbed is convected towards the trailing pole. The interfacial convection creates a gradient of surfactant along the interface, with the trailing pole having a much higher concentration. Surfactant collecting at this pole begins to desorb, and these molecules subsequently diffuse away from the droplet. Eventually a steady state is reached wherein the uptake of surfactant onto the surface at the leading edge by adsorption and bulk diffusion towards the drop is balanced by the loss at the trailing edge via desorption and diffusion away from the drop. The surface gradient of surfactant which develops as the surfactant distribution evolves towards steady state causes a

gradient in interfacial tension, and therefore a tangential stress, which opposes the shear stress applied to the droplet by the continuous phase. The result is a gradual retardation of the droplet terminal velocity.

The extent of the retardation is a function of the severity of the surfactant gradient which develops. The gradient is primarily a function of the time scales which characterize the interfacial convection, bulk diffusion and adsorption-desorption of surfactant. When the time scale for convection is much faster than both those of bulk diffusion and adsorption-desorption, the surfactant concentration at the trailing edge is very high compared to elsewhere on the drop interface and the retardation is large. In the further limit in which the latter two time scales become infinite, the leading pole of the drop is swept completely clean, and surfactant collects in a stagnant cap at the trailing pole. This circumstance of stagnant cap formation results in the largest retardation. When the rates of adsorption-desorption and surfactant diffusion are very fast in comparison to the rate of surface convection, then the surfactant gradients are reduced since the rapid exchange from the bulk minimizes the sweeping effect of interfacial convection. The result is a small retardation.

Levich's model has been the basis of several theoretical studies. The hydrodynamics of the stagnant cap has been investigated numerically by Davis and Acrivos (1966), and analytically by Harper (1973, 1982) for small caps and Sadhal and Johnson (1983) for arbitrary cap sizes. The opposite limiting case of rapid exchange from the bulk was originally studied by Levich (1962), who considered the mechanisms of diffusion and adsorption-desorption separately, and later Newman (1966) who treated both transport mechanisms

simultaneously. An understanding of the problem for the intermediate case in which the adsorption-desorption and diffusion rates are slow, but not infinitely slow so as to form a stagnant cap, were undertaken by Levan (1982) and Holbrook and Levan (1983a, 1983b), who obtained numerical solutions for the translational velocity.

The previous studies have been concerned solely with the calculation of the steady translational velocity. No attention has been focused on the study of the unsteady hyrodynamics of gradual droplet retardation with the adsorption of surfactant. The aim of this chapter is to detail these unsteady hydrodynamics.

3.2 Mathematical Formulation

The system under consideration is a spherical viscous incompressible droplet of radius a' moving unsteadily and axisymmetrically at the instantaneous translational velocity U' through an unbounded Newtonian fluid which is immiscible with the droplet fluid. It is assumed that the surface tension of the droplet is large enough that the droplet retains its spherical shape as it is moving. The surfactant is assumed to be uniformly present in the continuous phase and adsorbs on the surface of the droplet.

The origin of the coordinate system is located at the center of the droplet. The angle θ is measured from the front stagnation point (Fig.1). Droplet variables are denoted with the superscript 1 and continuous phase variables are demarcated with the superscript 2. The variables in the formulation are nondimensionlized in the following way: (Dimensional quantities are marked by a prime, and dimensionless quantities are unprimed throughout the analysis.)

$$r = \frac{r'}{a'} \qquad t = \frac{t'U_0'}{a'} \qquad U = \frac{U'}{U_0'} \qquad V_j^{(i)} = \frac{V_j'^{(i)}}{U_0'}$$

$$\tau_{ij} = \frac{\tau_{ij}' a'}{\mu'^{(2)} U_0'} \qquad \kappa = \frac{\mu'^{(1)}}{\mu'^{(2)}} \qquad \Gamma = \frac{\Gamma'}{\Gamma_0'} \tag{2.0a}$$

in the above t' is the time, μ' is the viscosity, τ_{ij}' is the stress tensor, and Γ_0' is the equilibrium surface concentration. U_0' is the steady velocity of the droplet in the absence of the surfactant, i.e., the Hadmard-Rybczynski velocity given by

$$U_0' = \frac{2(1+\kappa)}{3\kappa+2} \frac{(\rho'^{(1)} - \rho'^{(2)}) a'^2 g'}{3\mu'^{(2)}} \tag{2.0b}$$

where ρ' is the density and g' is the gravitational constant. Finally in equation (2.0a) $V_j'^{(i)}$ are the components of the velocity.

Owing to the assumption of axisymmetry, the components of the velocity may be expressed in terms of the stream function ψ, that is

$$V_r^{(i)} = -\frac{1}{r^2 \sin\theta} \frac{\partial \psi^{(i)}}{\partial \theta} \tag{2.1a}$$

$$V_\theta^{(i)} = \frac{1}{r \sin\theta} \frac{\partial \psi^{(i)}}{\partial r} \tag{2.1b}$$

and the dimensionless form of the function ψ is

$$\psi = \frac{\psi'}{a'^2 U_0'} \tag{2.1c}$$

Note in the above, the time is scaled by the convective time scale, $\frac{a'}{U_0'}$.

Assuming the Reynolds number for the drop is small, the Navier-Stokes equations in terms of the stream function become

$$E^2(E^2\psi^{(i)}) = 0 \tag{2.2}$$

The E^2 operator is the axisymmetric stream function operator in spherical coordinates, which is defined below:

$$E^2 = \frac{\partial^2}{\partial r^2} + \frac{\sin\theta}{r^2}\frac{\partial}{\partial\theta}\left(\frac{1}{\sin\theta}\frac{\partial}{\partial\theta}\right) \tag{2.2a}$$

The hydrodynamic boundary conditions are as follows:

(1) Far from the droplet, the velocity field is uniform:

$$\lim_{r\to\infty} \psi^{(2)} = \frac{U}{2} r^2 \sin^2\theta \tag{2.3a}$$

(2) The velocity components must remain finite at all points within the droplet.

(3) Since there is no slip between fluids at their interface, the tangential interfacial velocity components must be continuous, i.e.

$$v_\theta^{(1)} = v_\theta^{(2)} \qquad r=1 \qquad (2.3b)$$

(4) The normal components of the inner and outer fluid velocities are continuous and zero since the interface is not moving; thus

$$v_r^{(1)} = v_r^{(2)} = 0 \qquad r=1 \qquad (2.3c)$$

(5) Because the drop has been assumed to remain spherical, the use of the normal stress balance is precluded, and the instantaneous translational velocity in the gravitational field is determined by an integral force balance in the direction of the motion. Thus

$$\int_0^\pi \left((-P^{(2)} + \tau_{rr}^{(2)})\cos\theta - \tau_{r\theta}^{(2)}\sin\theta\right) \sin\theta \, d\theta = \frac{2(\rho'^{(1)} - \rho'^{(2)})g'}{3\mu'^{(2)}U_0'} \qquad r=1 \qquad (2.3d)$$

(6) The tangential stress is balanced by the gradient of the surface concentration of the surfactant:

$$\tau_{r\theta}^{(2)} - \tau_{r\theta}^{(1)} = \frac{1}{\mu'^{(2)} U_0'} \frac{\partial \sigma'}{\partial \theta} = \frac{\Gamma_0}{\mu'^{(2)} U_0'} \frac{\partial \sigma'}{\partial \Gamma'} \frac{\partial \Gamma}{\partial \theta} \quad r=1 \qquad (2.3e)$$

where σ' is the surface tension and is a function of the distribution of the surfactant on the surface.

As is evdent from the above formulation, in order to solve the problem completely the surfactant distribution must be determined. This distribution is computed from the equation which represents conservation of surfactant at the interface of the droplet. The equation giving the surfactant balance on the interface can be written in spherical coordinate as follows:

$$\frac{\partial \Gamma}{\partial t} + \frac{1}{\sin\theta} \frac{\partial}{\partial \theta}(\sin\theta \Gamma V_\theta) = \frac{1}{Pe_s \sin\theta} \frac{\partial}{\partial \theta} (\sin\theta \frac{\partial \Gamma}{\partial \theta}) + Q(\Gamma, C_s) \qquad (2.4)$$

where V_s is the surface velocity ($V_s = V_\theta^{(i)}(\theta, r=1)$), and Pe_s is the surface Peclet number ($Pe_s = \frac{a' U_0'}{D_s'}$, D_s' is the surface diffusion coefficient). The function $Q(\Gamma, C_s)$ in (2.4) describes the adsorption-desorption kinetics (C_s is the surfactant sublayer concentration and nondimensionalized by C_∞', $C_s = C(r=1, \theta)$). Here the Langmuir formulation for the kinetics is adopted (Davies and Rideal 1963); thus in dimensional form

$$Q'(\Gamma', C_s') = -\alpha' \Gamma' - \beta' C_s' (\Gamma' - \Gamma_\infty') \qquad (2.5)$$

where α' and β' are kinetic constants of desorption and adsorption respectively, Γ'_∞ is the maximum packing desity of the surfactant. From (2.5), the concentration Γ'_0 which is in equilibrium with the maximum sublayer surfactant concentration C'_∞ can easily be obtained from $Q'(\Gamma'_0, C'_\infty)=0$; thus

$$\frac{\Gamma'_0}{\Gamma'_\infty} = \frac{k}{1+k} \tag{2.6}$$

where $k = \beta' C'_\infty/\alpha'$ and is the ratio of adsorption to desorption rates. Nondimensionalization of (2.5) by $U'_0\Gamma'_0/a'$ yields after some manipulation the surfactant mass equation

$$\frac{\partial \Gamma}{\partial t} + \frac{1}{\sin\theta}\frac{\partial}{\partial \theta}(\sin\theta \Gamma V_s) = \frac{1}{Pe_s \sin\theta}\frac{\partial}{\partial \theta}\left(\sin\theta \frac{\partial \Gamma}{\partial \theta}\right) - \tag{2.7}$$

$$Bi^*\left[C_s(\Gamma - 1) + \frac{1}{k}(\Gamma - C_s)\right]$$

where Bi^* is called Biot number and is in the form:

$$Bi^* = \frac{\beta' C'_\infty}{(U'_0/a')}$$

Two disparate regimes are described by the Biot number. When the convective time scale $\frac{a'}{U'_0}$ is much less than the adsorption time $\frac{1}{\beta' C'_\infty}$ the Biot number is small compared to unity. With this regime surfactant accumulates at the rear pole exerting a drag resisting the

flow. On the other hand, when the Biot number is large, the solution approaches the equilibrium condition whereby the interfacial concentration is uniform and equal to the equilibium value Γ'_0.

The sublayer concentration, C_s, is solved as follows. Formally, C_s can be obtained by solving the steady convective-diffusion equation in the continuous phase, i.e.

$$Pe\vec{V}\cdot\vec{\nabla}C = \nabla^2 C \tag{2.8}$$

where ∇^2 is the Laplacian operator, Peclet number is $U'_0 a'/D'$, D' is the bulk diffusivity of the surfactant and C is the bulk concentration. The boundary conditions on the bulk concentration are:

$$\frac{\partial C}{\partial r}\Big|_{r=1} = \frac{\delta'}{a'} Pe\ Bi^*[C_s(\Gamma - 1) + \frac{1}{k}(\Gamma - C_s)] \tag{2.9}$$

and

$$\lim_{|z|\to\infty} C(z,\rho) = 1 \tag{2.10}$$

$$\frac{\partial C}{\partial \rho}\Big|_{\rho=b} = 0 \tag{2.11}$$

where δ' is the adsorption depth of the surfactant, Γ'_0/C'_∞. Assume $\frac{\delta'}{a'}\frac{1}{Pe}Bi^* \ll 1$, Eqn.(2.9) is reduced to $\frac{\partial C}{\partial r}\Big|_{r=1} \to 0$, therefore C_s is a constant which is equal to 1. Eqn.(2.7) is in the form

$$\frac{\partial \Gamma}{\partial t} + \frac{1}{\sin\theta}\frac{\partial}{\partial \theta}(\sin\theta \Gamma V_s) = \frac{1}{Pe_s \sin\theta}\frac{\partial}{\partial \theta}(\sin\theta \frac{\partial \Gamma}{\partial \theta}) - Bi(\Gamma - 1) \tag{2.12}$$

where Bi is called modified Biot number and equal to $Bi^{*}\frac{1+k}{k} = \frac{a'(1+k)}{U_0'/a'}$.

With the Langmuir choice of the adsorption isotherm (Eqn.(2.5)), the dependence of the surface tension on the surfactant surface concentration ($\sigma'(\Gamma')$) may be formulated from the Frumkin equation

$$\frac{\partial \sigma'}{\partial \Gamma'} = - \frac{R'T'}{(1 - \Gamma'/\Gamma_\infty')} \tag{2.13}$$

Substituting Eq.(2.13) into Eq.(2.3e) yields the following equation:

$$\tau_{r\theta}^{(2)} - \tau_{r\theta}^{(1)} = - Ma \frac{1}{(1-\Gamma\frac{k}{1+k})} \frac{\partial \Gamma}{\partial \theta} \qquad r=1 \tag{2.3f}$$

where

$$Ma = \frac{R'T'\Gamma_0'}{\mu'^{(2)}U_0'}$$

Although this problem should be solved using the nonlinear form Eqn.(2.3f), we assume here that k is small enough so $\Gamma\frac{k}{1+k}$ is negligible compare to 1. Therefore the linear condition of the tangential stress

$$\tau_{r\theta}^{(2)} - \tau_{r\theta}^{(1)} = - Ma \frac{\partial \Gamma}{\partial \theta} \qquad r=1 \tag{2.3g}$$

is valid for both larger and small Marangoni numbers (cf. Chapter 2).

3.3 Solution Procedure

The surfactant concentration $\Gamma(t,\theta)$ can be expressed in a Legendre series

$$\Gamma(t,\theta) = \sum_{m=0}^{\infty} a_m(t)P_m(\cos\theta) \tag{3.1}$$

where $P_m(\cos\theta)$ is the Legendre polynomial of order m and $a_m(t)$ is a set of unknown time dependent coefficients.

The solution of Eq.(2.2) can be obtained by a separation of variables. The solution for the droplet and exterior phases which is bounded at the poles is:

$$\psi^{(i)} = \sum_{n=0}^{\infty} (A_n^{(i)} r^n + B_n^{(i)} r^{-n+1} + C_n^{(i)} r^{n+2} + D_n^{(i)} r^{-n+3}) C_n^{-1/2}(\cos\theta) \tag{3.2}$$

for i=1, 2 respectively. In Eq. (3.2) $C_n^{-1/2}(\cos\theta)$ is the Gegenbauer polynomial of order n and degree -1/2.

The boundary conditions (2.3) are applied to the above expansions in a straight forward manner. Consequently, the stream function can then be rewritten in terms of the unknown $a_n(t)$ coefficients:

$$\psi^{(1)} = \frac{1}{1+\kappa} \sum_{n=2}^{\infty} [\frac{1}{2}U\delta_{2} + \frac{n(n-1)Ma}{2(2n-1)} a_{n-1}(t)] r^n(r^2 - 1) C_n^{-1/2}(\cos\theta) \tag{3.3a}$$

$$\psi^{(2)} = \sum_{n=2}^{\infty} [U(r^2 - \frac{2+3\kappa}{2(1+\kappa)} r + \frac{\kappa}{2(1+\kappa)} \frac{1}{r}) \delta_{n2}$$

$$+ \frac{n(n-1)}{2(2n-1)} \frac{Ma}{(1+\kappa)} a_{n-1}(t)\, r^{-n+1}(r^1-1)] C_n^{-1/2}(\cos\theta) \tag{3.3b}$$

After using the boundary condition (2.3d) the dimensionless droplet translational velocity is given by:

$$U = 1 + \frac{Ma}{3(1+\frac{3}{2}\kappa)}\, a_1(t) \tag{3.4}$$

Note that U depends, therefore, on the first unknown coefficient in the expansion of the surfactant concentration $\Gamma(t,\theta)$. Furthermore, the terminal droplet velocity can be obtained from Eq. (3.4) in the limit as $t\to\infty$. Numerically, it depends only on the convergence of a(t) for large value of t.

In order to determine a(t), it is necessary to introduce the expansion of the tangential interfacial velocity into equation (2.12). This velocity is obtained directly from (3.3b) together with the definition (2.1b) at r=1, that is:

$$V_\theta(1,\theta) = \frac{1}{\sin(1+\kappa)} \sum_{n=2}^{\infty} \{[1 + \frac{Ma}{3(1+\frac{3}{2}\kappa)}\, a_1]\delta_{n2} + \frac{n(n-1)Ma}{2n-1}\, a_{n-1}\}\, C_n^{-1/2} \tag{3.5}$$

Substitution of Eq. (3.5) and the expansion (3.1) into the surfactant balance equation (2.12) results in a non-linear equation in the time dependent coefficients $a_n(t)$:

$$\sum_{m=0}^{\infty} \dot{a}_m(t) P_m(\cos\theta) = \frac{1}{1+\kappa} \sum_{n=2}^{\infty} \sum_{m=0}^{\infty} [U\delta_{n2} + \frac{n(n-1)Ma}{2n-1}\, a_{n-1}(t)\,]$$

$$[m(m+1)a_m(t)\, \frac{C_n^{-1/2}(\cos\theta) C_{m+1}^{-1/2}(\cos\theta)}{\sin^2\theta} - a_m(t) P_m(\cos\theta) P_{n-1}(\cos\theta)] \cdot$$

$$\frac{1}{Pe}\sum_{m=1}^{\infty} m(m+1)a_m(t)P_m(\cos\theta) - Bi\left[\sum_{m=0}^{\infty} a_m(t)P_m(\cos\theta) - 1\right] \qquad (3.6)$$

where $\dot{a}_m$ represents the time derivative of a_m and U is given by equation (3.4) in terms of a_1.

The first coefficient $a_0(t)$ can be solved independently and exactly, providing the leading term in the surfactant concentration series representation. Since

$$\dot{a}_0 + Bia_0 = Bi \qquad (3.7)$$

with the initial zero concentration on the droplet interface condition, i.e.

$$a_m(0) = 0 \qquad \text{for all m} \qquad (3.8)$$

Eq (3.7) is then solved in the form

$$a_0(t) = 1 - e^{-Bit} \qquad (3.9)$$

Note that since

$$a_0(t) = \frac{1}{2}\int_0^{\pi} \Gamma\sin\theta d\theta \qquad (3.10)$$

$4\pi a^2 a_0(t)\Gamma_0$ represents the total amount of surfactant instantaneously adsorbed on the droplet surface. When $t \to \infty$, $\lim_{t\to\infty} a_0(t) = 1$, and thus the steady amount on the surface is simply $4\pi a^2\Gamma_0$.

The solution of Eq.(3.6) for other coefficients will be described in the following subsections for three different cases: (i) non-linear solution for arbitrary Marangoni and Biot number, (ii) solution for small values of Ma, and (iii) solution for small values of Bi.

3.3.1 Solution for Arbitrary Ma and Bi Number

Eq. (3.6) can be solved by the numerical Galerkin technique. The expansions in Eq. (3.6) are truncated after N terms. Thus

$$\sum_{m=0}^{N} \dot{a}_m(t)P_m(\cos\theta) - \frac{1}{1+\kappa}\sum_{n=2}^{N+1}\sum_{m=0}^{N}\left[U\delta_{n2} + \frac{n(n-1)Ma}{2n-1}\,a_{n-1}(t)\right]$$

$$\left[m(m+1)a_m(t)\,\frac{C_n^{-1/2}(\cos\theta)C_{m+1}^{-1/2}(\cos\theta)}{\sin^2\theta} - a_m(t)P_m(\cos\theta)P_{n-1}(\cos\theta)\right]+$$

$$\frac{1}{Pe}\sum_{m=1}^{N} m(m+1)a_m(t)P_m(\cos\theta) + Bi\left[\sum_{m=0}^{N} a_m(t)P_m(\cos\theta) - 1\right] = R_N(t,\theta) \tag{3.11}$$

In Eq. (3.11), $R_N(t,\theta)$ is the residual. The residual is made orthogonal to Legendre function $P_\ell(\cos\theta)$ for $\ell = 0$ to N on the interval $\theta = 0$ to π with respect to the weighting function $\sin\theta$. The result is the series of N+1 differential equations in time for $a_0(t)$ ... $a_N(t)$. These equations are of the form:

$$\dot{a}_\ell(t) + \frac{\ell(\ell+1)}{Pe}\, a_\ell(t) + Bi[a_\ell(t) - \delta_{\ell 0}] \qquad (\ell = 1,2,\ldots,N)$$

$$- \frac{2\ell+1}{2(1+\kappa)} \sum_{n=2}^{N+1} \sum_{m=0}^{N} a_m(t)[U\delta_{n2} + \frac{n(n-1)Ma}{2n-1}\, a_{n-1}(t)]\, I(m,n,\ell+1) \qquad (3.12)$$

where $I(m,n,\ell+1)$ is an integral defined by

$$I(m,n,\ell+1) = \int_0^\pi P_m(\cos\theta) C_n^{-1/2}(\cos\theta) C_{\ell+1}^{-1/2}(\cos\theta) \frac{1}{\sin\theta}\, d\theta \qquad (3.13)$$

The above integral can be solved analytically by using the results given by Hsu (1938).

The solution of equation (3.12) for $\ell \neq 0$ can be obtained by forward integration using a standard Runge-Kutta procedure with the initial conditions (3.8).

The calculations based on above procedure are effective for intermediate to large values of the Marangoni and Biot number. Convergence was determined based on the following two criteria. First, a sufficiently large value of N was determined so that the relative change between the N and N+1 terms of the steady translational velocity (i.e. $a_1(t)$) was less than 10^{-5}, i.e.

$$\frac{a_1^{(N)}(\infty) - a_1^{(N-1)}(\infty)}{a_1^{(N)}(\infty)} < 10^{-5} \qquad (3.14)$$

Next, N was increased until the steady Γ distribution converged to within $5.0 \cup 10^{-3}$ at each of 37 equally spaced positions (every 5°) on the surface of the sphere.

The above procedure works well for all cases except when both the Ma and Bi number are very small. For the latter cases excessive number of terms are required to obtain the convergence. In order to facilitate solutions in low Ma and Bi regimes, asymptotic methods were employed. These are described in the next two subsections.

3.3.2 Solution for Small Marangoni Number

When the Marangoni number is small the behavior of the droplet will not depart greatly from the solution for an uncontaminated droplet (i.e., the Hadamard-Rybczynksi result). This departure can be examined in terms of an asymptotic expansion in the small parameter ϵ = Ma. In this pertubation scheme, the functions $a_m(t,Pe,Ma,Bi)$ are expanded regularly in Ma. Thus

$$a_m(t,Pe,\epsilon,Bi) = a_{m(0)} + \epsilon a_{m(1)} + \epsilon^2 a_{m(2)} + O(\epsilon^3) \qquad (3.15a)$$

$$U = U_{(0)} + \epsilon U_{(1)} + \epsilon^2 U_{(2)} + O(\epsilon^3) \qquad (3.15b)$$

The relationship between $U_{(j)}$ and $a_{m(j)}$ is given by Eq. (3.4):

$$U_{(0)} = 1 \qquad (3.16a)$$

$$U_{(j)} = -\frac{a_{1(j-1)}}{3(1+\frac{3}{2}\kappa)} \qquad (3.16b)$$

Thus the $U_{(j)}$'s (j = 1,2,...) represent the corrections to the surfactant free droplet terminal velocity (the Hadamard-Rybczynski formula), and account for the influence of Marangoni stresses.

Substituting expansions (3.15a) and (3.15b) into Eq.(3.12) yields the following equations for $a_{\ell(0)}$:

$$\dot{a}_{\ell(0)} + [\frac{\ell(\ell+1)}{Pe} + Bi]\, a_{\ell(0)} = \frac{2\ell+1}{2(1+\kappa)} \sum_{m=0}^{N} a_{m(0)}\, I(m,2,\ell+1) \qquad (3.17)$$

$$(\ell = 1,2,\ldots,N)$$

and the first order correction for U follows from Eq.(3.16b), thus

$$U = 1 + \frac{Ma}{3(1+3\kappa/2)}\, a_{1(0)}(t) + O(\epsilon^2) \qquad (3.18)$$

3.3.3 Solution for Small Biot Number

The small Biot number limit corresponds to a slow rate of exchange surfactant between the surface of the droplet and the continuous phase sublayer beneath the surface. Unlike the limit of small Marangoni numbers, Eq.(3.12) can not be expanded in a regular asymptotic expansion in the Biot number for Bi → 0. The reason lies in the presence of a long time scale for reaching steady state when Bi → 0. This scale becomes evident from the exact equation for the total amount of the surfactant on the surface as the function of time (Eq.(3.9), Eq.(3.10)):

$$4\pi a^2\Gamma_0 a_0(t) = 4\pi a^2\Gamma_0(1 - e^{-Bit}) = 2\pi a^2\Gamma_0\int_0^{\pi} \Gamma \sin\theta d\theta \qquad (3.19)$$

A regular expansion of the above in powers of Bi would not be uniform in t as $t \to \infty$. To remove this nonuniformty an extended time scale τ which is equal to $Bi\theta t$ is introduced into the formulation to replace t. Variables, now considered as function of τ instead of t, are expanded regularly in the parameter ϵ for $\epsilon = Bi$. As will be shown below, this scaled expansion has a stagnant cap as its zeroth order state. The latter possesses an exact solution (Sadhal & Johnson 1983) and consequently it is more useful to formulate the asymptotic analysis in terms of the original variables rather than the Legendre solution given by Eq.(3.6).

In order to be agreement with the result given by Sadhal & Johnson (1983), the coordinates of the problem are taken to be the same as those used in their study, i.e. the angle θ is measured from the back stagnation point.

The variables $\Gamma(\tau,Ma,\epsilon,\theta)$ and $\psi(\tau,Ma,\epsilon,\theta,r)$ are expressed as expansion about $\epsilon = 0$. Thus

$$\Gamma(\tau,Ma,\epsilon,\theta) = \Gamma_{(0)}(\tau,Ma,\theta) + \epsilon\Gamma_{(1)}(\tau,Ma,\theta) + O(\epsilon^2) \qquad (3.20)$$

$$\psi^i(\tau,Ma,\epsilon,\theta,r) = \psi^i_{(0)}(\tau,Ma,\theta,r) + \epsilon\psi^i_{(1)}(\tau,Ma,\theta,r) + O(\epsilon^2) \qquad (3.21)$$

$$U = U_{(0)} + \epsilon U_{(1)} + O(\epsilon^2) \qquad (3.22)$$

The field equations become

$$E^2(E^2\psi^i_{(j)}) = 0 \tag{3.23}$$

for each order j. The boundary conditions (2.3a-d) for each order j remain unchanged except that all the variables are subscripted by the order j. The zeroth and first order of mass balances are

$$\frac{\partial}{\partial\theta}\,[V_{\theta(0)}(1,\theta)\;\Gamma_{(0)}\sin\theta] = 0 \tag{3.24}$$

$$\frac{\partial\Gamma_{(0)}}{\partial\tau} + \frac{1}{\sin\theta}\,\frac{\partial}{\partial\theta}[(\Gamma_{(0)}V_{\theta(1)} + \Gamma_{(1)}V_{\theta(0)})\sin\theta] + (\Gamma_{(0)}-1) = 0 \tag{3.25}$$

where surface diffusion has been neglected.

The singular scaling of t yields, therefore, a quasi-steady zeroth order equation (3.24) which represents the behaviour of insoluble surfactants on the droplet surface. This problem admits a stagnant cap solution, whereby for $0\le\theta\le\phi$ the droplet surface is immobile due to the presence of surfactants, while on the remaining surface $\phi<\theta\le\pi$ the surfactant concentration is zero. The exact solution for this case has been obtained by Sadhal and Johnson (1983). The cap angle is a function of the total amount of surfactant to order zero on the surface. From Eq.(3.19)

$$2(1 - e^{-\tau}) = \int_0^{\pi}\Gamma_{(0)}\sin\theta\,d\theta$$

The relationship between the cap angle and the total amount of the surfactant on the surface can be obtained from equations detailed in

Sadhal & Johnson. After nondimensionalizing as given in Eq.(2.0a) and using the above integration the following formulas are obtained:

$$\Gamma_{(0)}(\theta) = -\frac{2(1+\kappa)}{Ma}\sum_{k=1}^{\infty}\frac{2k+1}{k(k+1)}C_k[P_k(\cos\theta)-P_k(\cos\phi)] \tag{3.26}$$

$$(1-e^{-\tau})4\pi\ Ma\ \frac{C_{s1}}{C_s} = 2\phi - 4\phi\cos\phi + 4\sin\phi - \sin 2\phi \tag{3.27}$$

where

$$C_k = \frac{1}{4\pi(1+\kappa)}\{\sin(k+2)\phi - \sin k\phi + \sin(k+1)\phi - \sin(k-1)\phi -$$

$$2[\frac{\sin(k+2)\phi}{k+2} + \frac{\sin(k-1)\phi}{k-1}]\}\frac{C_s}{C_{s1}} \qquad k\geq 2 \tag{3.28a}$$

$$C_1 = -\frac{1}{4\pi(1+\kappa)}[2\phi+\sin\phi-\sin 2\phi-\tfrac{1}{3}\sin 3\phi]\frac{C_s}{C_{s1}} \tag{3.28b}$$

$$C_s = -\frac{3\kappa+2}{2(1+\kappa)} \tag{3.28c}$$

$$C_{s1} = -\frac{1}{4\pi(1+\kappa)}[\,2\phi + \sin\phi - \sin 2\phi - \sin 3\phi/3\,] + C_s \tag{3.28d}$$

Eq.(3.27) is used to determine the cap angle [$\phi(\tau)$] as a function of the Marangoni number (Ma) and the the total amount instantaneously on the surface. Eq. (3.26) and (3.27) assumed that $\Gamma_0(\phi) = 0$ in order that forces be balanced along the ring $\theta = \phi$. When the total amount adsorbed is large enough so that ϕ approaches π, Eq.(3.27) must be

modified because material begins to accumulate at π. The modified equations which incorporate $\Gamma(\pi)$ are:

$$\Gamma_{(0)} = -\frac{2(1+\kappa)}{Ma}\sum_{k=1}^{\infty}\frac{2k+1}{k(k+1)}C_k[P_k(\cos\theta)-P_k(\cos\pi)] + \Gamma(\pi) \qquad (3.29)$$

and $\Gamma(\pi)$ can be computed from Eq.(3.19) thus

$$\Gamma(\pi) = (1 - e^{-\tau}) - \frac{1 + 3\kappa/2}{Ma(1 + \kappa)} \qquad (3.30)$$

The corresponding interfacial velocity is

$$V_{\theta(0)} = -\frac{1}{\sin\theta}\left[3C_2^{-1/2}(\cos\theta) + 2\sum_{k=1}^{\infty}C_k^{*}\,C_{k+1}^{-1/2}(\cos\theta)\right] \qquad (3.31)$$

with

$$C_n^{*} = C_n, \qquad C_1^{*} = C_s \qquad (3.32a,b)$$

The zeroth order terminal velocity $U_{(0)}$ is given by

$$U_{(0)} = \frac{1}{1 + \dfrac{2\phi + \sin\phi - \sin2\phi - \sin3\phi/3}{2\pi(3\kappa + 2)}} \qquad (3.33)$$

where ϕ is the cap angle given by Eq.(3.27).

The first order solution is now sought by introducing the Legendre series representation for $\Gamma_{(1)}$ [$\Gamma_{(1)} = \sum_{m=0}^{\infty} a_{m(1)}(\tau)P(\cos\theta)$] and solving the first order hydrodynamic equations which are of the

form of equation (3.23) and boundary conditions (2.3). The first order interfacial velocity is obtained by

$$V_{\theta(1)}(1,\theta) = \frac{Ma}{\sin\theta}\left[\frac{2}{3\kappa+2}\, a_{1(1)}\, C_2^{-1/2}(\cos\theta)\right.$$

$$\left. + \frac{1}{(1+\kappa)} \sum_{n=3}^{\infty} \frac{n(n-1)}{2n-1}\, a_{n-1(1)}\, C_n^{-1/2}(\cos\theta)\right] \qquad (3.34)$$

A set of equations for $a_{m(1)}$ can be derived from the mass balance equation (3.25) according to the Galerkin procedure, i.e. substitute Eq.(3.26), (3.34), and (3.31) for $\Gamma_{(0)}$, $V_{\theta(1)}$ and $V_{\theta(0)}$ respectively in Eq.(3.25). Truncating the series of N terms and making the residual orthogonal to $P_1(\cos\theta)$ ... $P_N(\cos\theta)$ over the integral $\theta = 0$ to π yields the equations in the linear form, that is:

$$\sum_{m=1}^{N} G_{\ell m} a_{m(1)} = -D_{\ell} \qquad (\ell = 1,2,\ldots,N) \qquad (3.35)$$

where $G_{\ell m}$ is the element in the N by N matrix and it has the following form

$$G_{\ell m} = \frac{(1+\kappa)}{3\kappa+2}\left[\frac{\ell\, C_{\ell+1}}{(\ell+2)(2\ell+1)} - \frac{(\ell+1)C_{\ell-1}}{(\ell-1)(2\ell+1)}(1-\delta_{\ell 1}) + \right.$$

$$\frac{2}{3}\sum_{k=1}^{\infty}\frac{2k+1}{k(k+1)}\, C_k P_k(\cos\phi)\delta_{\ell 1}]\delta_{1m} - \frac{3\ell(\ell+1)}{4(2\ell+1)(2\ell-1)}\,\delta_{(\ell-1)m} +$$

$$\frac{\ell(\ell+1)}{(2\ell+1)^2}\sum_{k=1}^{\infty}\frac{2k+1}{k(k+1)}\, C_k P_k(\cos\phi)\,\delta_{\ell m}(1-\delta_{\ell 1}) + \qquad (3.36)$$

$$\frac{3\ell(\ell+1)}{4(2\ell+1)(2\ell+3)}\,\delta_{(\ell+1)m} + \frac{1}{2}\left[\sum_{k=1}^{\infty} C_k^{*}\, I(m,k+1,\ell+1) + \right.$$

$$\left.\frac{m(m+1)}{2m+1}\sum_{k=1}^{\infty}\frac{2k+1}{k(k+1)}\,C_k\, I(k,m+1,\ell+1)(1-\delta_{\ell 1})\right]$$

and D_ℓ is the colum vector in the form

$$D_\ell = \frac{4(1+\kappa)}{Ma\ell(\ell+1)}\,\dot{\phi}\,\frac{\partial C_\ell}{\partial \phi} + \frac{(1+\kappa)}{\ell(\ell+1)}\,\frac{C_\ell}{Ma} \tag{3.37}$$

In the above formula, $\frac{\partial C_\ell}{\partial \phi}$ can be obtained from Eq.(3.28), $\dot{\phi} = \frac{\partial \phi}{\partial \tau}$ and it can be obtained from Eq.(3.27), thus

$$\dot{\phi} = \frac{4\pi Mae^{-\tau}\,\frac{C_{s1}}{C_s}}{1 + 2\phi\sin\phi - \cos 2\phi + (e^{-\tau}-1)\,\frac{Ma}{2C_s}\,(2+\cos\phi - 2\cos 2\phi\,\cos 3\phi)} \tag{3.38}$$

Finally, the translational velocity of the droplet is obtained from the integral force balance. The first order correction can be written in terms of $a_{1(1)}$. Thus

$$U = U_{(0)} - Bi\,\frac{2Ma}{3(3\kappa+2)}\,a_{1(1)} + O(\epsilon^2) \tag{3.39}$$

where $a_{1(1)}$ is the numerical coefficient obtained from the solution of (3.35) and $U_{(0)}$ is the solution given by Eq.(3.33). Equation (3.39) provides a practical correction to the Sadhal and Johnson terminal velocity for a droplet exposed to slow adsorption regardless of the

magnitude of the Marangoni number. Furthermore, it can be useful in experimental studies in which adsorption rates can be calculated from simple velocity measurements.

3.4 Numerical Simulations

3.4.1 Arbitrary Values for the Marangoni and Biot Numbers

As explained in Sec. 3.1, numerical results for the unsteady translational velocity and surfactant distribution are obtained by integrating the set of ordinary differential equations (3.12). In these results, the value of the surface Peclet number, Pe, is equal to 10^5, and, therefore, the influence of surface diffusion is negligible. The main purpose of these calculations is to examine the effect of the rate of exchange of surfactant and the Marangoni stress on the unsteady and terminal droplet velocity.

Consider first the case of a gas bubble ($\kappa = 0$). Fig.2 and Fig.3 show respectively the terminal velocity U as a function of the Biot and Marangoni numbers. It is clear from Fig.2 that U increases as the Bi number increases for fixed values of the Ma number. For each fixed value of the Marangoni number all the curves asymptotically approach 1 as $Bi \to \infty$. As the Bi number becomes large, the rate of exchange of the surfactant becomes large in comparison to the rate of convective sweeping. Thus a uniform distribution of the surfactant develops, the Marangoni force tends to zero and $U \to 1$. In the opposite limit as $Bi \to 0$, the exchange becomes so slow that a stagnant cap develops and retards the terminal velocity. Fig.4 shows the development of the stagnant

cap distribution at decreasing values of the Biot number. The low Bi limit will be discussed further in section 4.2.

Fig.3 establishes that at a fixed exchange rate, increasing the Marangoni number decreases the terminal velocity. This can be understood in the following way. As Ma→∞, surfactant gradients disappear. Since from Eq.(2.3d) it is clear that in order for the difference in shear stress to remain bounded as Ma→∞, $\frac{\partial \Gamma(\theta)}{\partial \theta}$ must become zero. This behaviour is also shown numerically in Fig.5. As $\Gamma(\theta)$ becomes uniform the balance (2.4) indicates that $V_\theta(1,\theta)$ must tend to zero. Therefore, the terminal velocity tends to the Stokes value. For $\kappa = 0$, $U_{stokes} = \frac{2}{3}$ and therefore all the curves of Fig.3 approach 2/3 asymptotically to $\frac{2}{3}$ as Ma→∞. In the opposite limit, as Ma → 0, the surfactant distribution has no effect on the shear stress, and the velocity tends to the Hadamard-Rybczynski value. Fig.3 also indicates that there is a sensitive region in which the terminal velocity changes rapidly as a function of the Marangoni number between the asymptotic values of $\frac{2}{3}$ and 1. This region extends approximately from 0.2 and 2 in the Marangoni number.

The influence of κ on the terminal velocity is shown in Fig.6 and Fig.7. Both figures indicate that at fixed values of Bi and Ma, as $\kappa \to \infty$, U→1. This limit is realized because as $\kappa \to \infty$ the surface velocity becomes uniformly smaller and eventually approaches zero. The terminal velocity U approaches the Stokes value as does the Hadmard-Rybczynski value (2.0b). Thus the nondimensionalized velocity approaches 1. Note also that as κ becomes large ($\kappa > 0.75$), the

terminal velocities are less sensitive functions of the Biot and Marangoni numbers.

The unsteady regimes are described by Fig.8 and Fig.9. Fig.8 shows the accumulation of surfactant on the clean droplet surface as function of time. Initialy, an approximatly uniform surfactant profile is present on the surface; with time surface convection sweeps the adsorbed surfactant to one end, forming the cap . (The cap will not be exactly stagnant because of the small influence of surface diffusion, as Pe = 10^{-5} in the simulation.) Fig.9 illustrates the dependents for a gas bubble (κ = 0) of the unsteady terminal velocity on the Marangoni number for a fixed Biot number (Bi = 0.1). The curves indicate that steady state is reached earlier at large values of the Ma number. This is due to the fact that for the large Ma numbers, the surfactant distribution is nearly uniform (2.3d). In the surfactant balance (2.4) there are only three terms; the convection term ($\frac{1}{\sin\theta}\frac{\partial}{\partial\theta}(\sin\theta V_\theta \Gamma)$, the unsteady term ($\frac{\partial\Gamma}{\partial t}$) and the exchange rate term [Bi(Γ - 1)]. Since the latter two are proportional to the Biot number and the Bi number is small, these two terms are also small. Thus

$$0 = \frac{1}{\sin\theta}\frac{\partial}{\partial\theta}(\sin\theta V_\theta \Gamma) \approx \frac{\Gamma}{\sin\theta}\frac{\partial}{\partial\theta}(\sin\theta V_\theta) \qquad (4.1)$$

and therefore $V_\theta(1,\theta)$ tends to zero. Hence for large Ma and small Bi numbers, the Stokes velocity is approached when any amount of surfactant is absorbed. For the case of large Biot numbers, obviously, the steady state is reached very quickly.

These nonlinear results can only be obtained to good accuracy up to Ma < 1 and Bi = 0.5. For lower values, roundoff errors contribute and thus in these regions asymptotic expressions are necessary. These asymptotic expressions are presented below.

3.4.2 Asymtotic Results for small Marangoni and Biot Numbers

Asymtotic results for Marangoni and Biot number tending to zero were only obtained at steady state. Consider first the case of a small Marangoni number. The regular perturbation procedure is described in Sec.(3.2). For steady state conditions, the equations which determin the zeroth order Legendre coefficients $[a_{\ell(0)}]$ are given by Eq.(3.17) with $\dot{a}_{\ell(0)} = 0$. Rewriting this equation in matrix-vector form yields:

$$\sum_{m=1}^{N} B_{\ell m}\, a_{m(0)}(\infty) = E_{\ell} \qquad (\ell = 1,2,\ldots N) \tag{4.2}$$

where

$$B_{\ell m} = \left(\frac{\ell(\ell+1)}{Pe} + Bi\right)\delta_{\ell m} - \frac{2\ell+1}{2(1+\kappa)}\, I(m,2,\ell+1) \tag{4.4}$$

$$E_{\ell} = \frac{2\ell+1}{2(1+\kappa)}\, I(0,2,\ell+1) \tag{4.3}$$

The N*N matrix $B_{\ell m}$ was inverted to obtain vector $a_{m(0)}$ for particular values of the viscosity ratio κ and the Bi number. Since the first order correction to the terminal velocity is given by $a_{1(0)}(\infty)$ (cf.Eq. 3.18), sufficiently large values of N were used so that $a_{1(0)}$

converged to within 10^{-3}. The results for $\kappa = 0$, $\kappa = 0.1$ and $\kappa = 1.0$ and Bi = 0.2, Bi = 0.5 and Bi = 1.0 are listed in table I for $a_{1(0)}(\infty)$. Recall from Eq.(3.18) that $a_{1(0)}(\infty) / 3(1 + 3\kappa/2)$ is equal to the first order correction for U in the small Marangoni number. In table II, a comparison is given of the numerical values for U as given by Eq.(3.18) and Eq.(3.4).(i.e., the nonlinear Eq. for $\kappa = 0$.) The results indicate that for Ma value less than 0.1 the agreement is within 1%. Similar conclusions were reached for $\kappa = 0.1$ and $\kappa = 1.0$. In resolving $a_{1(0)}$ to an accuracy of 10^{-3} for $\kappa = 0$, N = 275 for Bi = 0.2, N = 69 for Bi = 0.5 and N = 17 for Bi = 1.0. For $\kappa > 0$, less terms were required for each particular value of the Biot number.

Consider next the regime of small Biot numbers. As described in the Sec.3.3, the correction to the droplet velocity is given in terms of the first coefficient in the Legendre expansion of the first order correction for the surfactant distribution. This coefficient is obtained in a manner similar to the computation of $a_{1(0)}$ for the case of small Marangoni numbers. Again attention is restricted to the steady state. Thus the equation for solving $a_{\ell(1)}$ can be written in the same form as Eq.(3.35) but D_ℓ defined as follows:

$$D_\ell = \frac{(1 + \kappa)}{\ell(\ell + 1)} \frac{C_\ell}{Ma} \tag{4.4}$$

because the first term is equal to zero for a quasi-time independent assumption. Note that some of the terms $G_{\ell m}$ contain an infinite series; these terms arise from the stagnant cap solution (Sadhal and

Johnson 1983) which is the zeroth order state in the asymtotic solution. Values of $a_{1(1)}$ were obtained in the following manner: First the value of N was fixed and sufficient terms in the stagnant cap series were taken until $a_{1(1)}$converged to 10^{-2}. Next N was increased by 1, the procedure was repeated and the resulting value of $a_{1(1)}$ was compared to the value for N - 1. The results are given in table III for κ = 0, 0.1 and 1.0. Also tabulated in table III are the values of the cap angle as obtained from the Eq.(3.27) with $\tau \to \infty$. In Table IV is given the results from a linear approximation (3.39) and the solution of the nonlinear equations (3.4 and 3.11) for κ = 0. Comparison of the indicates that the values of Bi number less than or equal 0.1, the linear approximation is within 1.5% of the exact results.

3.5 Conclusions

This study has examined the influence of surfactant adsorption-desorption kinetics on the unsteady retardation of droplet motion in a continuous liquid phase. Linear adsorption-desorption kinetics is assumed in the study. The mathematical formulation indicated that the effect of finite linear kinetics on the translational velocity was described by a Biot number representing the ratio of the linear exchange coefficient, $\beta' C'_\infty$ to the convective scale U_0/a. Two numerical solutions were developed. In the first, the unsteady equations were solved for arbitrary values of the Biot number, and profiles of the unsteady terminal velocity and surfactant distribution on the drop surface were obtained. The simulations showed the expected trend that

as the Biot number is sucessively decreased, the time necessary for the steady velocity to be achieved is increased. The simulations also indicated that this time can diminish as the Marangoni number is increased. As explained in the text, this result follows from the fact at a fixed value of the Bi number, increasing the Marangoni number forces the surfactant distribution to be fairly uniform at each instant in time. The enforced uniform velocity lowers the translational velocity of the droplet toward the asymptotic value.

Sufficiently converged solutions could not be obtained for $Bi < 0.05$ without the expense of extended computer time. For the regime of $Bi \to 0$ an asympotic analysis was undertaken. The zeroth order solution in the perturbation scheme was found to be a stagnant cap solution in which the size of the cap grew with time. A first order correction in Bi was obtained for the steady terminal velocity; this correction was accurate to less than one percent when compared to the numerically obtained non-linear solution for $Bi < 0.1$.

TABLE I

Small Marangoni Number Linear Corrections

	Bi	$\frac{a_{1(0)}^{(\infty)}}{3(1 + 3\kappa/2)}$
$\kappa = 0.0$		
	0.2	-0.8109
	0.5	-0.4652
	1.0	-0.2892
$\kappa = 0.1$		
	0.2	-0.5883
	0.5	-0.3842
	1.0	-0.2336
$\kappa = 1.0$		
	0.2	-0.2113
	0.5	-0.1159
	1.0	-0.06378

TABLE II

Comparison of Exact Results with Linear Approximation for the Small Marangoni Number ($\kappa = 0$)

	Ma	Linrear U	Nonlinear U
Bi = 0.2			
	0.1	0.9302	0.9378
	0.2	0.8605	0.8879
	0.5	0.6511	0.7920
Bi = 0.5			
	0.1	0.9533	0.9576
	0.2	0.9066	0.9224
	0.5	0.7664	0.8483
Bi = 1.0			
	0.1	0.9710	0.9730
	0.2	0.9420	0.9495
	0.5	0.8551	0.8948

TABLE III

Small Biot Number Linear Corrections

	Ma	Cap Angle	$\frac{a_{1(1)}^{(\infty)}}{3(1 + 3\kappa/2)}$
$\kappa = 0.0$			
	0.1	47.58°	-1.2522
	0.5	99.07°	-0.7161
	1.0	180.00°	-0.0333
$\kappa = 0.1$			
	0.1	47.37°	-1.4321
	0.5	97.03°	-0.7063
	1.0	159.15°	-0.3521
$\kappa = 1.0$			
	0.1	46.64°	-1.4214
	0.5	90.22°	-0.6199
	1.0	133.88°	-0.3793

TABLE IV

Comparison of Exact Results with Linear Approximation for the Small Biot Number (κ = 0)

	Bi	Linear U	Nonlinear U
Ma = 0.1			
	0.1	0.9254	0.9265
	0.2	0.9379	0.9378
	0.5	0.9754	0.9576
Ma = 0.5			
	0.1	0.7490	0.7608
	0.2	0.7848	0.7920
	0.5	0.8922	0.8483
Ma = 1.0			
	0.1	0.7000	0.7035
	0.2	0.7333	0.7300
	0.5	0.8333	0.7846

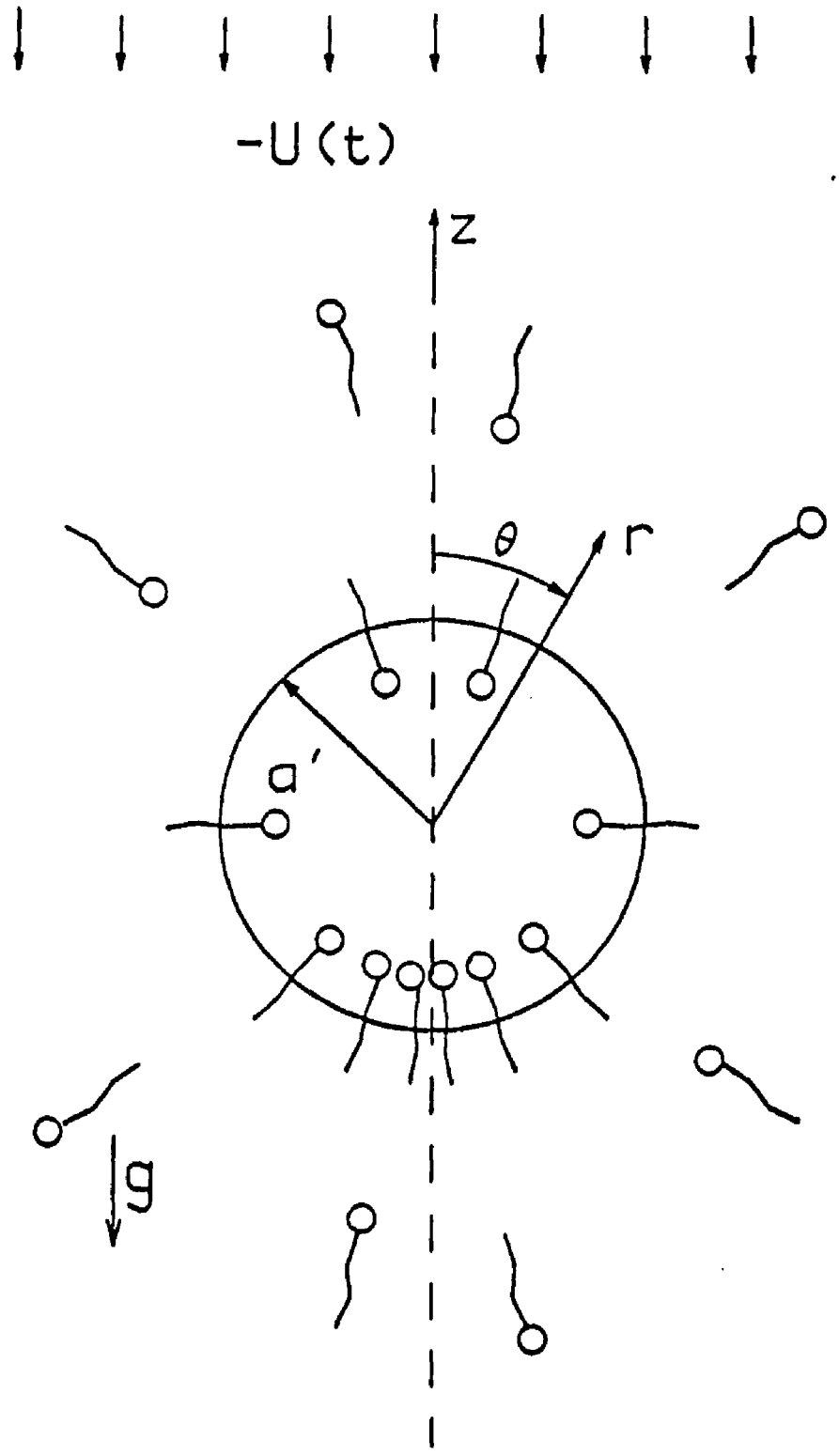

Figure 1

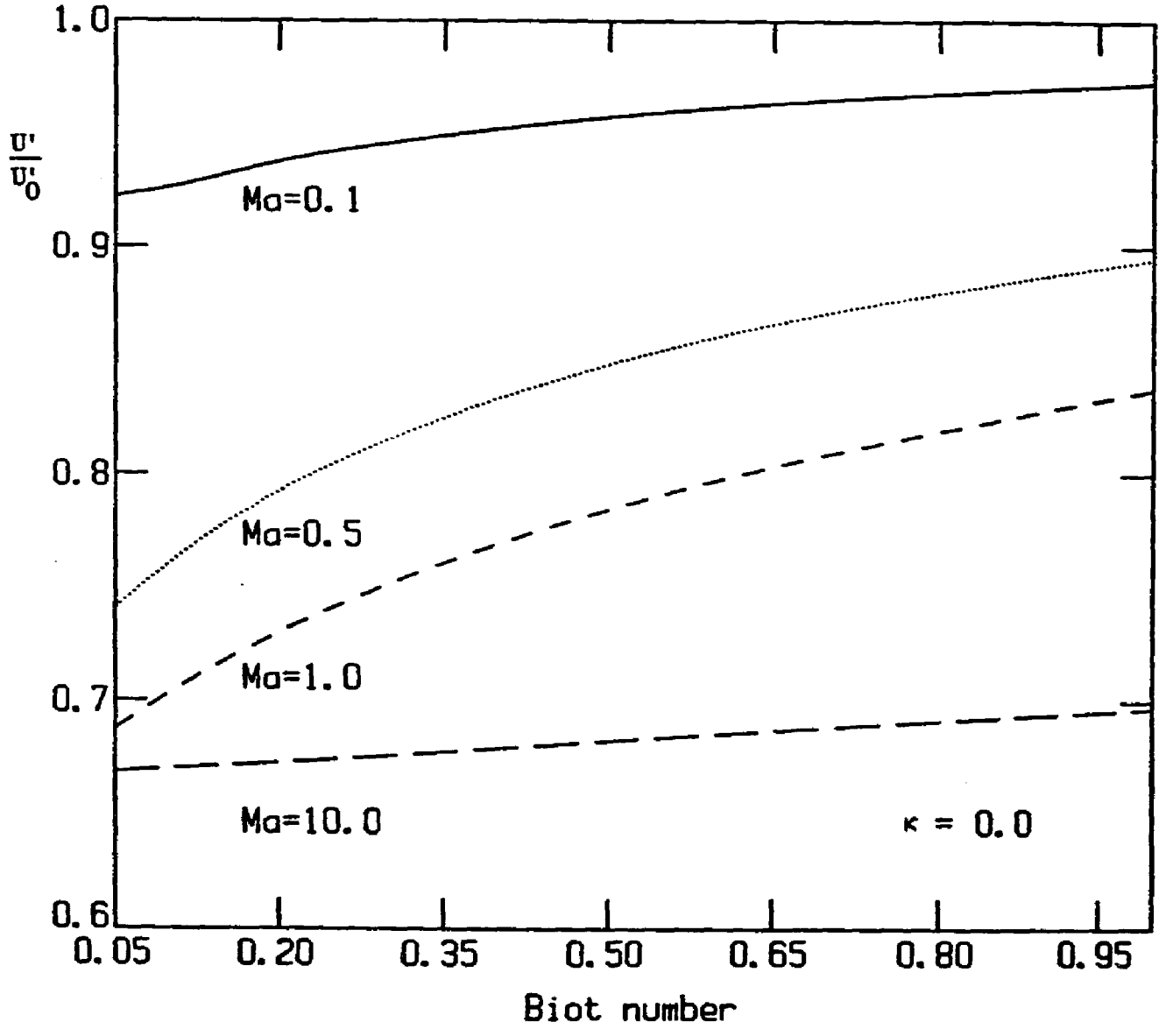
1.0
0.9
0.8
0.7
0.6
$\frac{U'}{U'_0}$
Ma=0.1
Ma=0.5
Ma=1.0
Ma=10.0
κ = 0.0
0.05
0.20
0.35
0.50
0.65
0.80
0.95
Biot number

Figure 2

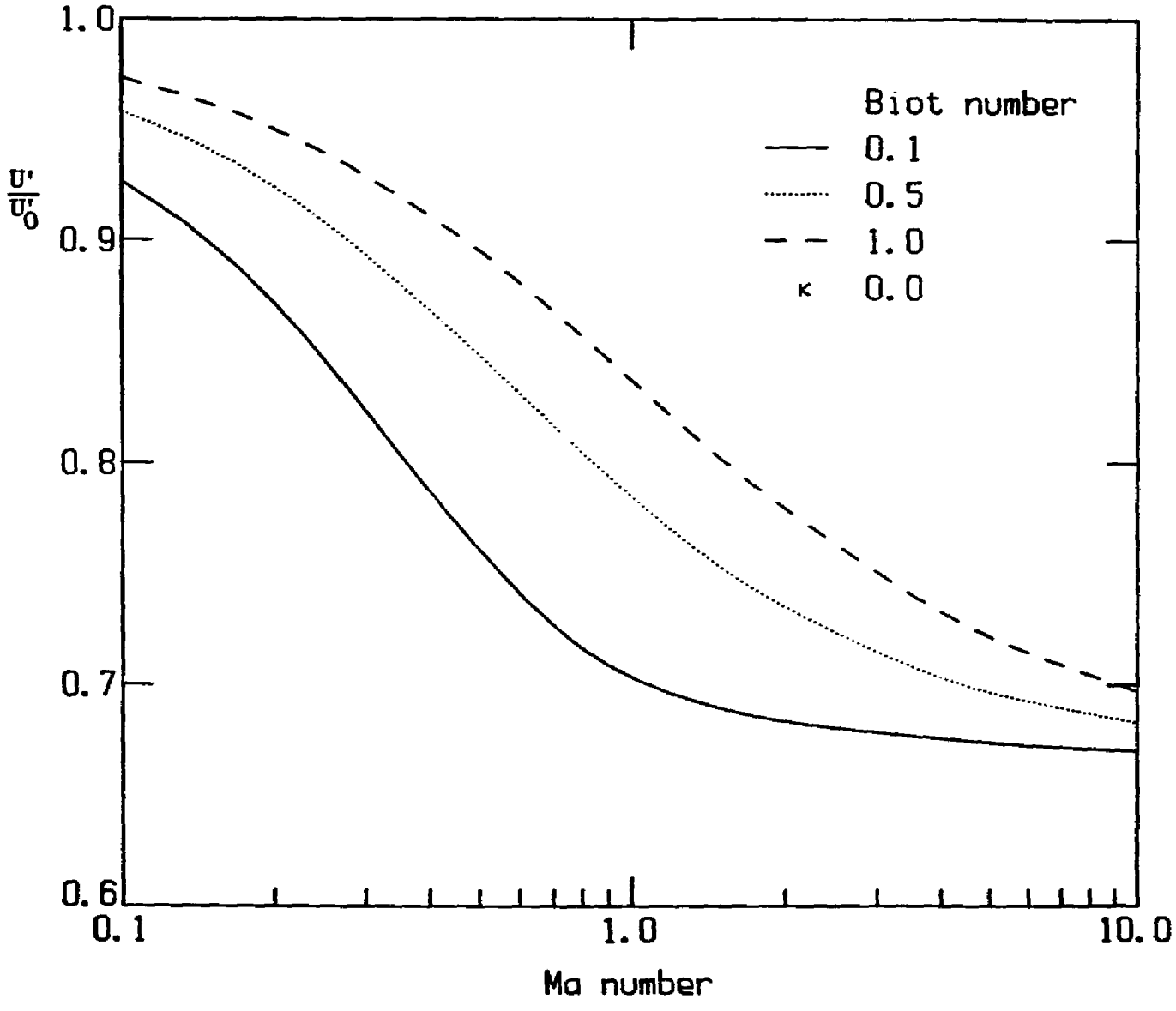

Figure 3

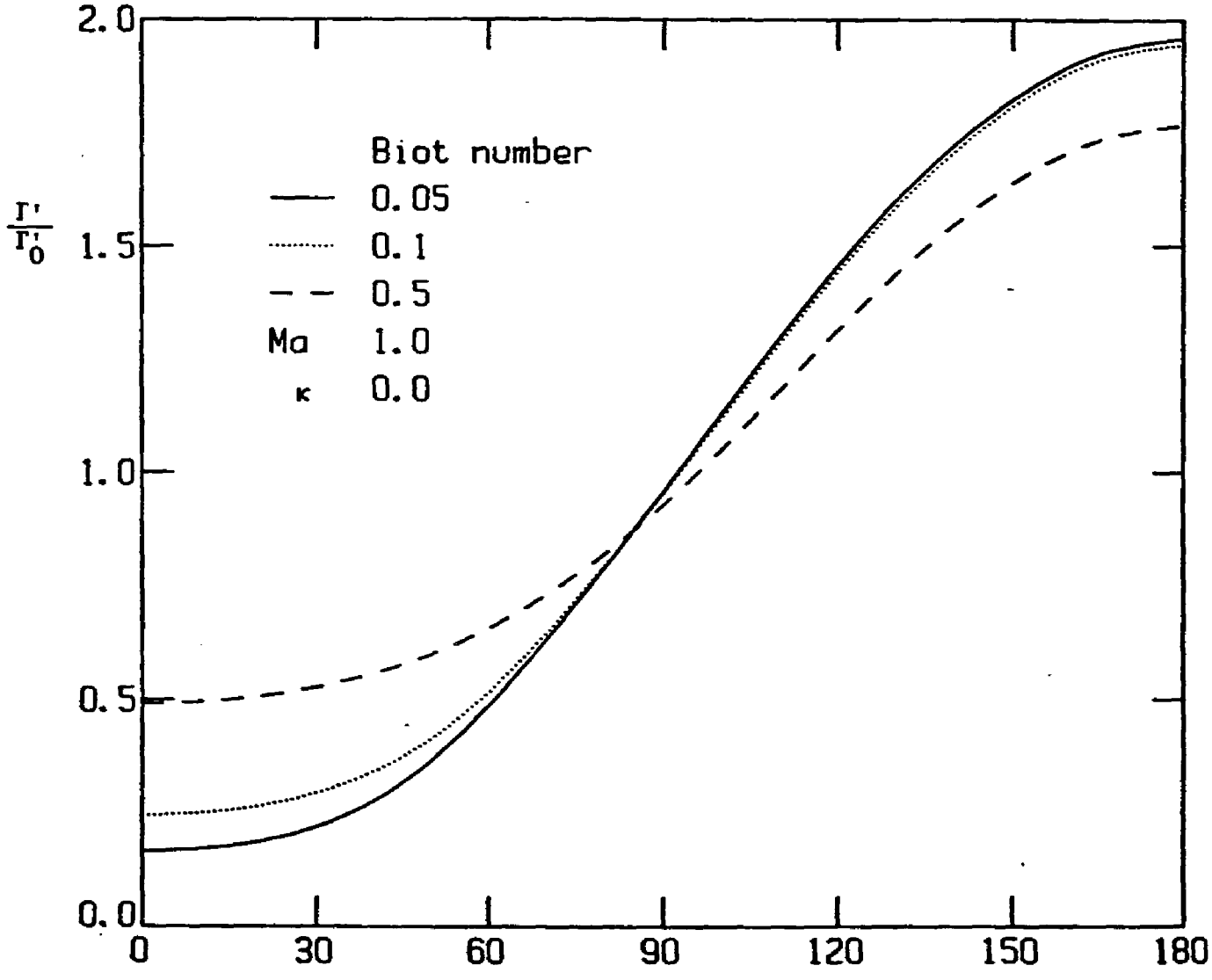
2.0
1.5
1.0
0.5
0.0
$\frac{\Gamma'}{\Gamma'_0}$
Biot number
0.05
0.1
0.5
Ma 1.0
κ 0.0
0
30
60
90
120
150
180
θ

Figure 4

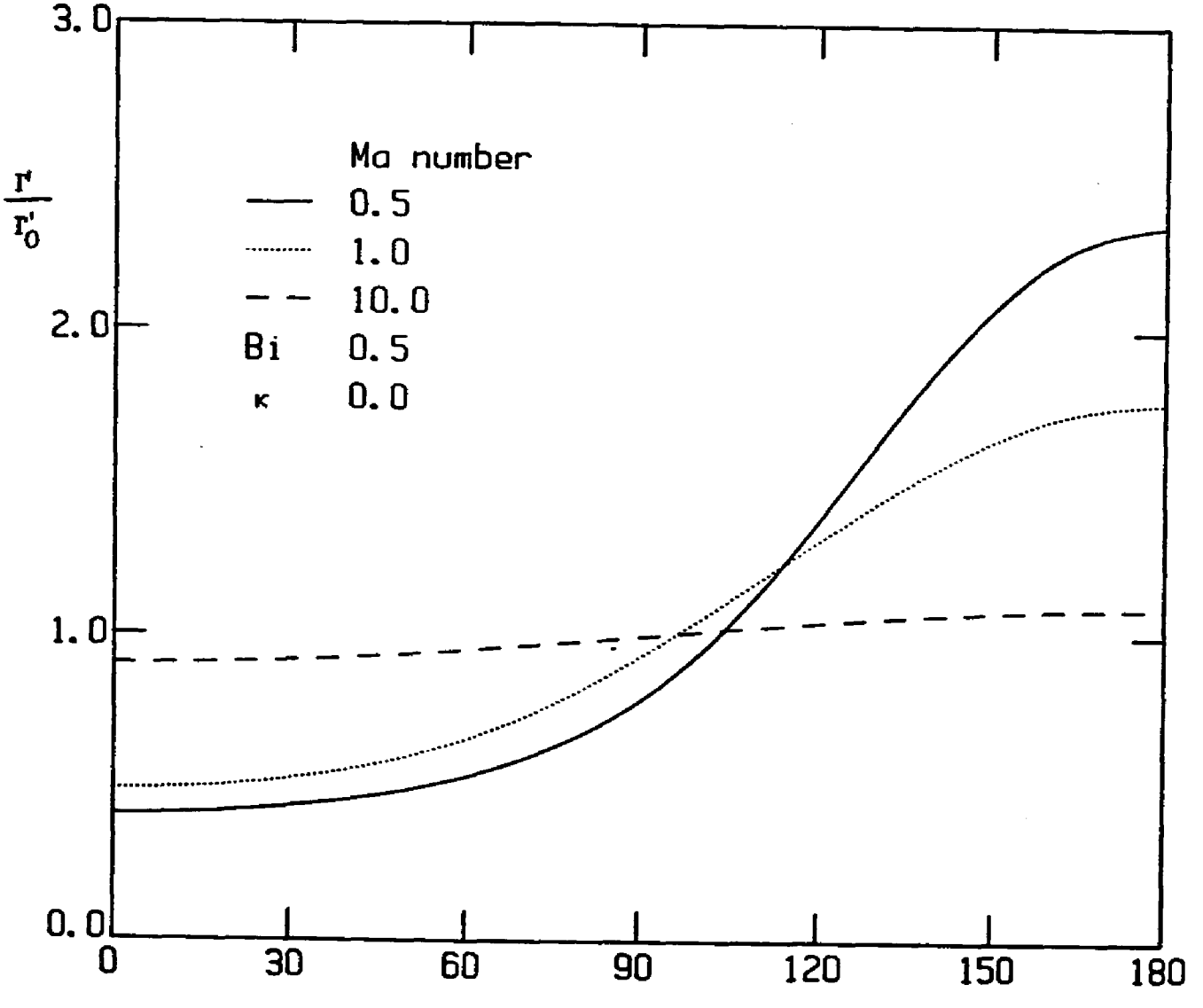
3.0
2.0
1.0
0.0
r'/r'0
Ma number
0.5
1.0
10.0
Bi 0.5
κ 0.0
0
30
60
90
120
150
180
θ

Figure 5

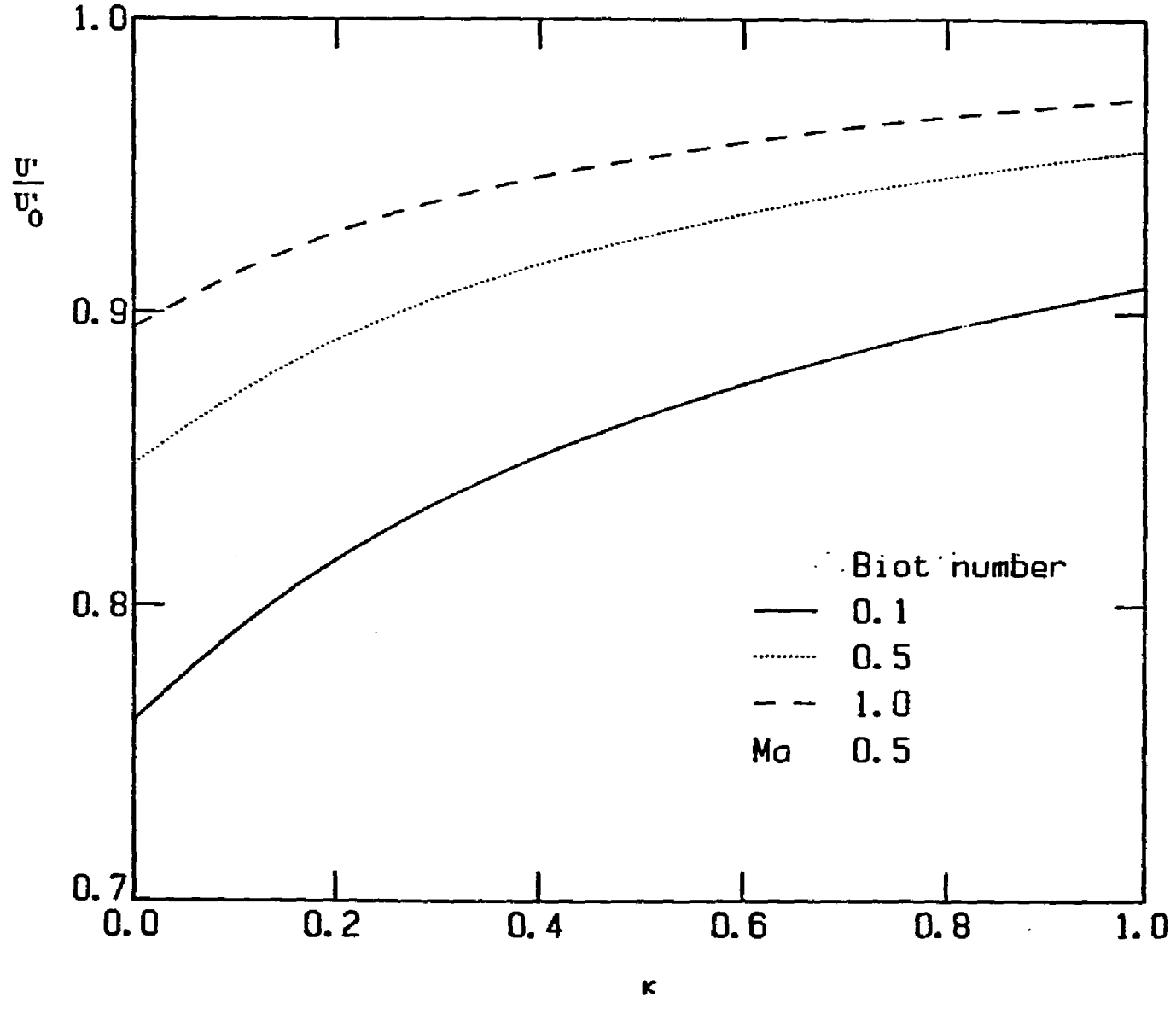

Figure 6

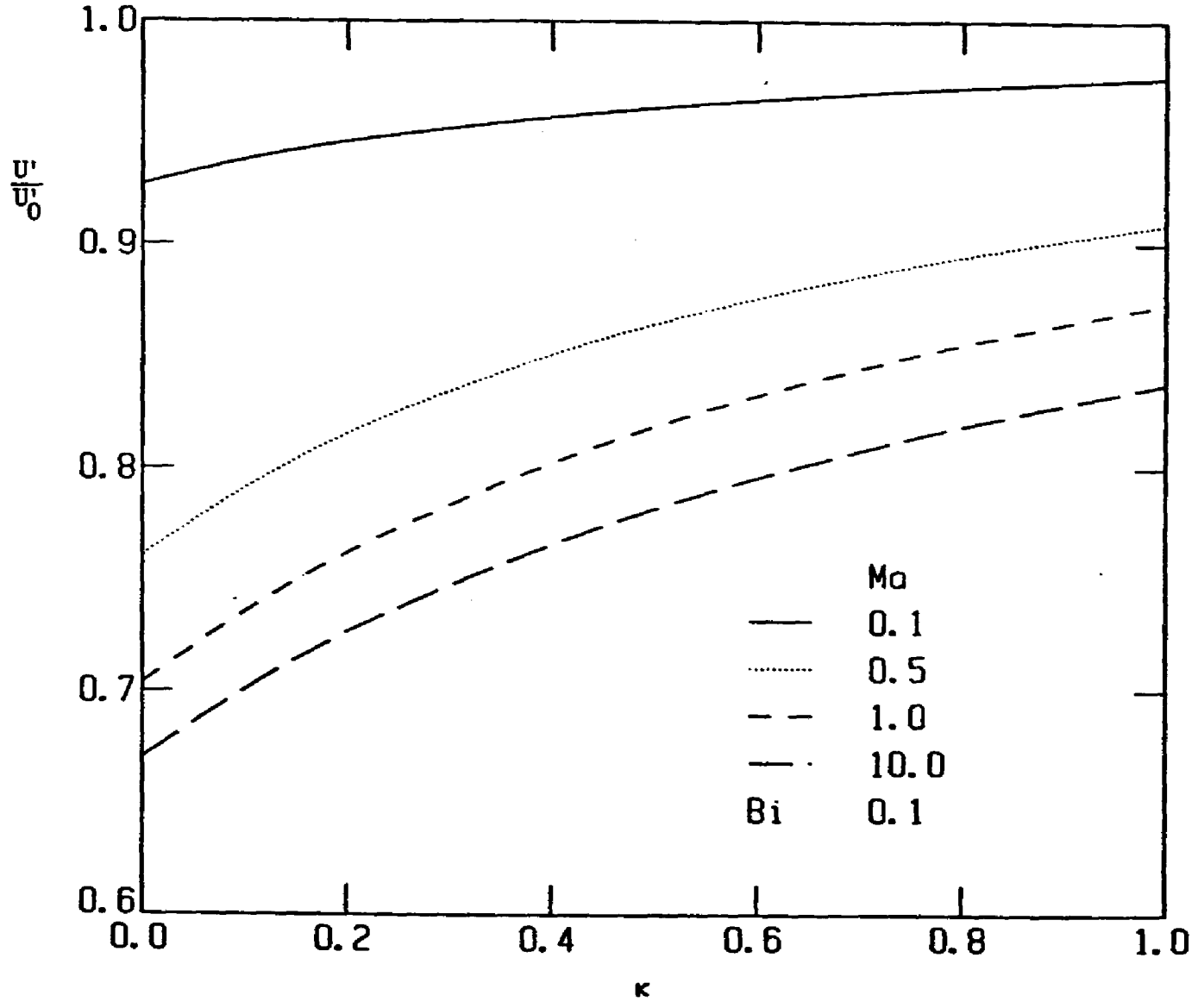

Figure 7

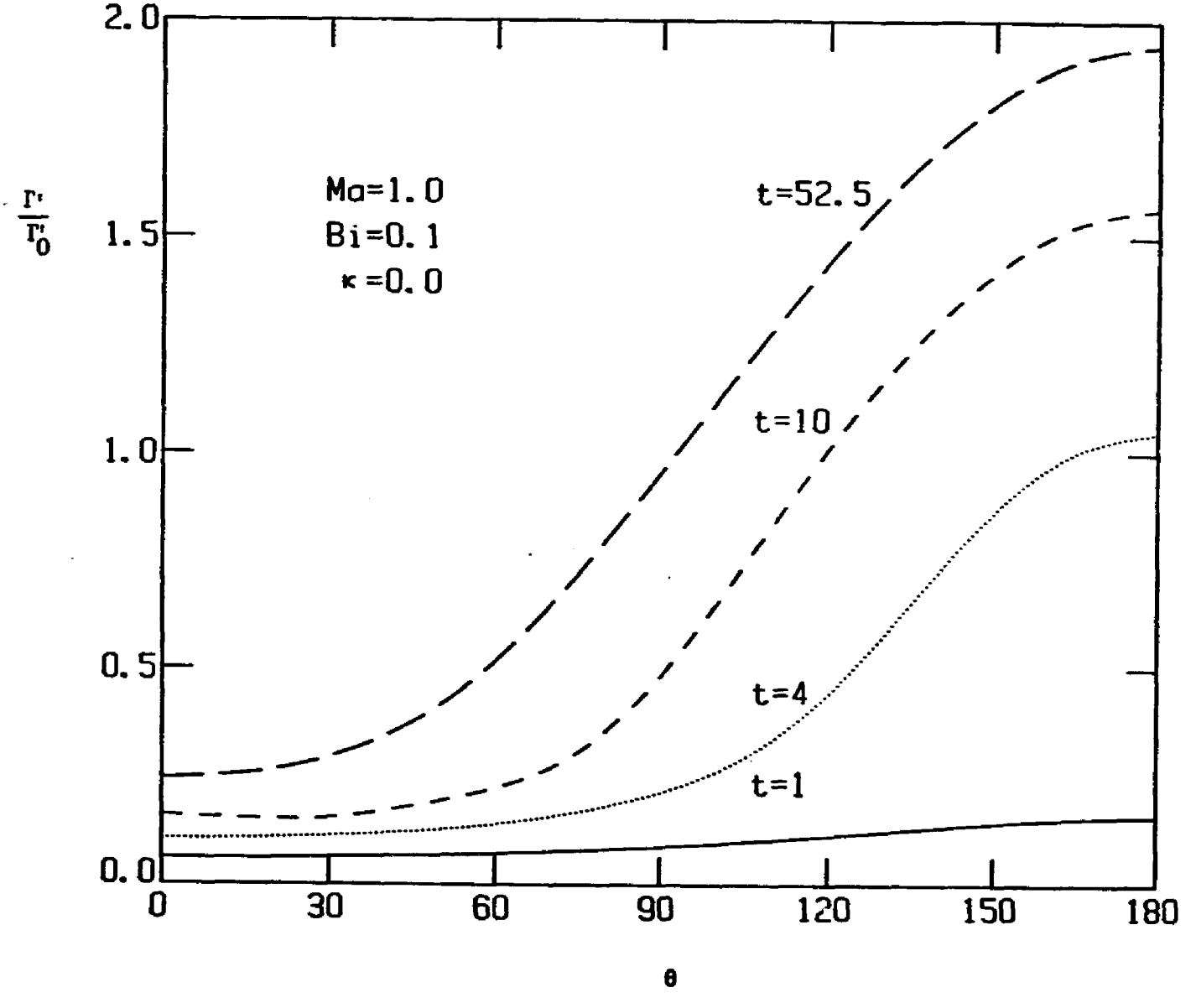
2.0
1.5
1.0
0.5
0.0
$\frac{r}{r_0}$
Ma=1.0
Bi=0.1
κ=0.0
t=52.5
t=10
t=4
t=1
0
30
60
90
120
150
180
θ

Figure 8

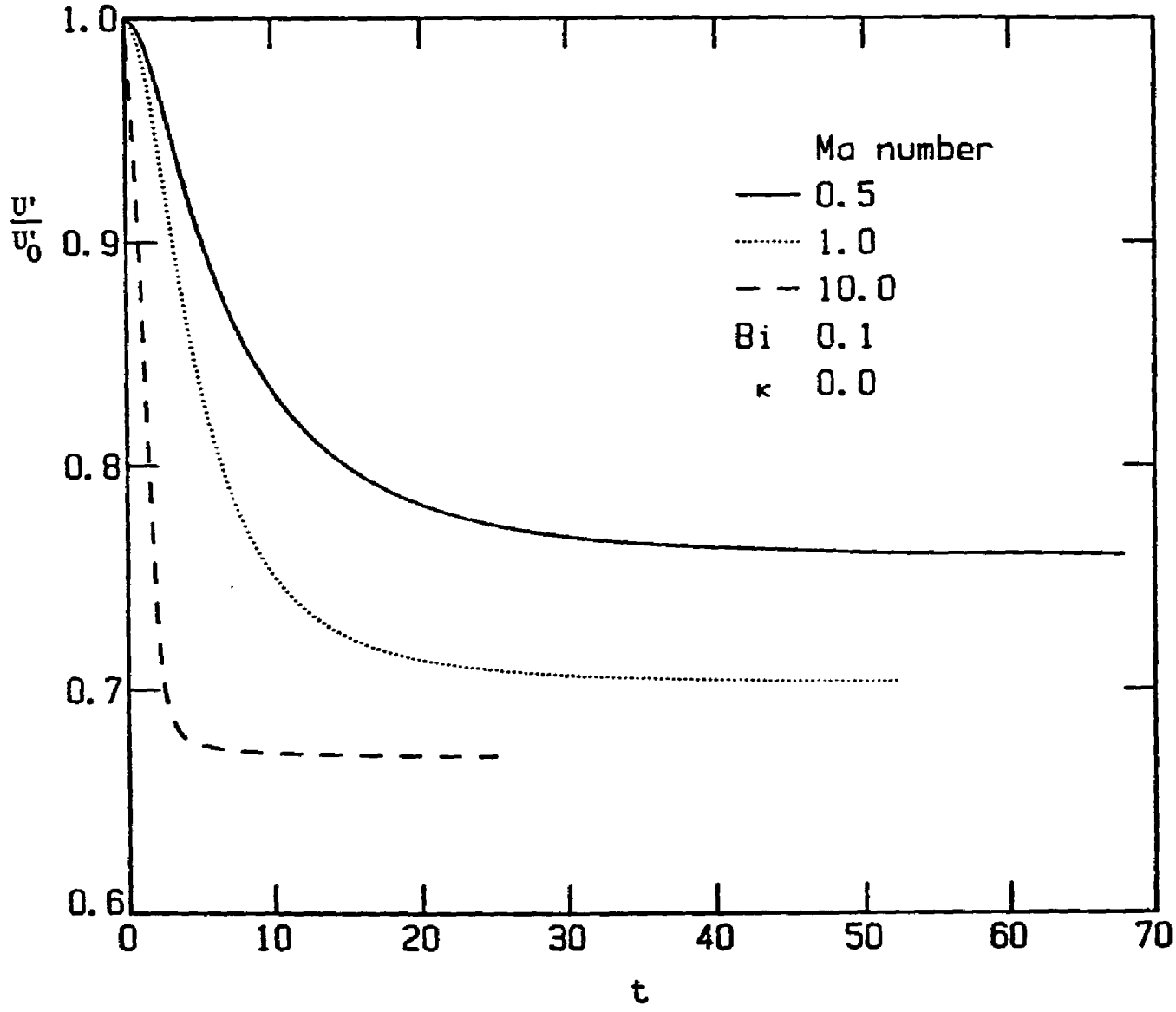
1.0
0.9
0.8
0.7
0.6
$\frac{v'}{v'_0}$
0
10
20
30
40
50
60
70
t
Ma number
0.5
1.0
10.0
Bi 0.1
κ 0.0

Figure 9

Chapter 4

The Influence of Surfactant on Droplet Motion Inside a Cylindrical Tube
I. Uniform Retardation Controlled by Sorption Kinetics

4.1 Introduction

The slow movement of fluid droplets in liquid filled channels is a hydrodynamic flow with important and obvious applications in the study of foam transport and liquid-liquid displacements in porous media (cf., for example, Mast (1972), Bikerman (1973), Lawson and Hirasaki (1985) and Ginley and Radke (1988)), and cell and gas bubble motion in blood vessels (Evans and Skalak (1979) and D. Biesel et al.(1986)). A logical starting point for the investigation of the channel flows of fluid particles is the consideration of the fundamental problem of the translation of a single fluid droplet in a long cylindrical tube. In this paper, fully converged numerical solutions of the Navier-Stokes equations for the single droplet problem are constructed for spherical fluid particles in steady, axisymmetric creeping flow. Clearly, the geometrical constraint of sphericity restricts the analysis to situations in which the interfacial tension of the droplet is large enough to resist the distending action exerted by the viscous tractions of the surrounding liquid phase.

The analysis presented herein addresses two separate problems in the motion of a fluid particle in a tube. In the first problem, the particle fluid and the liquid filling the tube (the continuous phase) are both assumed to be free of surfactant contamination and therefore

the fluid-fluid interface of the droplet is clean, and completely mobile.

The steady, axisymmetric, creeping motion of an interfacially mobile spherical fluid particle in a tube has not been studied in much detail in the literature. The early efforts on problems of this type concerned solid spheres: Ladenburg (1907), Faxen (1923), Wakiya (1953), Happel and Byrne (1954) and Bohlin (1960) used the method of reflections (cf. Happel and Brenner (1962)) to obtain approximate values for the hydrodynamic drag exerted on a translating solid sphere. Because of the fact that only a few reflections were calculated, these results were estimated to be only valid for sphere to tube diameter ratios of approximately 0.6 and less. Numerically exact values of the drag for arbitrary sphere to tube diameter ratios were first obtained by Haberman and Sayre (1958) using a matching of cylindrical and spherical solutions of the creeping flow equations. The numerically exact results established that the few term reflection calculations were only valid up to 0.6, as estimated. Later exact solution investigations by Wang and Skalak (1969), Coutanceau (1971), Paine and Sherr (1975), Leichtberg et al. (1976) and Tozeren (1983) confirmed the accuracy of Haberman and Sayre's calculations; experimental verifications of the numerical results were obtained as well by Ambari, Gauthier-Manuel and Guyon (1985) using a magnetic sphere rheometer.

For fluid spheres, the first theoretical effort was the investigation of Haberman and Sayre (1958). These authors computed an approximate expression for the drag exerted on a spherical fluid particle in tube flow using the cylindrical-spherical solution matching procedure which they employed in the exact solution of the

solid sphere problem. However, they truncated the procedure after a two constant matching, and thereby obtained only approximate results in the form of an analytical expression. Based on a similar truncation for a solid sphere and the comparison with the exact results, Haberman and Sayre estimated that their approximate formula is valid for sphere to tube diameter ratios of 0.6 and less. An exact numerical computation of the drag was obtained by Hyman and Skalak (1969 and 1970). Hyman and Skalak considered the problem of an infinite periodic chain of fluid spherical particles which are arbitrarily spaced. Periodic, infinite series solutions of the creeping flow equations which contained constants were developed, and the series was truncated so that the constants could be obtained numerically by satisfaction of the boundary conditions. The results for the hydrodynamic drag for a particle spacing of 40 tube radii were found to coincide within a few percent to the approximate formulae of Haberman and Sayre for all values of the ratio of droplet to continuous phase viscosity and for sphere to tube diameters of 0.6 and less. Brenner (1970 and 1971) obtained approximate values for the drag of a single particle in axisymmetric flow by an expansion in the ratio of the particle to tube diameter. The values for the drag, correct to the fifth power in this ratio, were in agreement with Hyman and Skalak and Haberman and Sayre's approximate expression for sphere to tube diameter ratios of 0.6 or less, regardless of the viscosity ratio.

From this review of the completed studies on the axisymmetric motion of a clean fluid sphere in a tube, it is clear that, unlike the case of the solid sphere, the only exact results for the drag are those of Hyman and Skalak, and these have only been checked, by

asymptotic procedures, for sphere to tube diameter ratios of 0.6 and less. Therefore, with respect to the motion of clean fluid particles, it is the aim of this investigation to verify Hyman and Skalak's results for sphere to tube diameter ratios of 0.6 and larger. In addition it is the intention of this study to provide fully converged velocity fields for the clean surface flows, and to identify stagnation points on the fluid particle surface. These hydrodynamic details were not provided by Hyman and Skalak, but they are especially important in understanding how surfactants influence this tube flow. The effect of surfactants is the second and major problem addressed in this investigation, and the scope of the study which will be undertaken with regards to this effect is described below.

In the second problem, the continuous phase is assumed to contain a bulk soluble surfactant. When the droplet is placed in the continuous phase and begins to move, surfactant molecules diffuse towards and adsorb onto the surface of the fluid particle. Once adsorbed, these molecules are convected towards surface stagnation points where they may collect, desorb or diffuse away along the surface. At steady state a surfactant distribution evolves on the surface which represents the balance of the competing effects of bulk and surface diffusion and convection, and surface to bulk kinetic adsorption and desorption.

Of key importance is the fact that the surfactant distribution gives rise to interfacial tension gradients on the surface which create tangential tractions (Marangoni stresses). Because the surfactant congregates at the surface stagnation points, areas in the vicinity of these points are at lower interfacial tension than regions with less surfactant. As a result, the Marangoni stress is directed

opposite to the that of convection, and thus retards the flow towards the stagnation points.

The existing literature has not examined the influence of surfactants on the movement of fluid particles in tubes, although the corresponding problem of their influence on the motion of spherical fluid particles in an infinite medium has been studied thoroughly. Owing to the complexity of the surfactant mass transfer and the Marangoni coupling, it is difficult, even for the infinite medium, to solve the entire hydrodynamic and mass transfer problem for the most general case in which all transport mechanisms are important. In an effort to simplify the analysis, previous studies of the infinite medium problem have identified at steady state three limiting cases. These are discussed below so as to provide a background for how the influence of surfactants in the confined geometry of the tube will be treated.

The first case pertains to the regime where the following two conditions are governing: First, the transport of surfactant molecules by surface diffusion is very slow in comparison to convective transport. (The nondimensional ratio of the convection to surface diffusion is the Peclet number defined as the product of the droplet velocity multiplied by the droplet radius and divided by the surface diffusivity.) Second, either sorption kinetics is slow relative to convection or the diffusion rate of surfactant molecules in the adsorption depth layer is slow in comparison to convection in that layer. The adsorption depth layer is the depth underneath the surface for which, per unit area of surface, there is as much surfactant at equilibrium as on the surface. Under nonequilibrium flow conditions, surfactant exchanged from the bulk to the surface

lies primarily in this layer, and therefore the adsorption depth thickness provides a convenient length scale for the estimation of bulk diffusive and convective transport effects. The proper nondimensional measure of the ratio of the rates of diffusion and convection in this layer is a Peclet number based on the adsorption depth. In the asymptotic limit in which the surface Peclet Number tends to infinity and either the sorption kinetic exchange tends to zero or the adsorption depth Peclet numbers tend to infinity, surfactant on the surface collects in zones located around the stagnation points since convection towards these points dominates the dispersing mechanisms of surface diffusion and desorption coupled with diffusion back into the bulk. This case is referred to as the "stagnant cap" regime. The regime is usually realized in systems in which the flow is fast enough so that the Peclet numbers are large. The movement of a fluid sphere in an infinite medium for the stagnant cap regime has been studied by Savic (1953), Davis and Acrivos (1966), Harper (1973, 1982), Sadhal and Johnson (1982) and Holbrook and Levan (1983a).

In the second case either the transport by surface diffusion is very fast in comparison to convection, or the series processes of surface to bulk kinetic exchange and bulk diffusion are fast in comparison to convective transport. For this case the surfactant distribution on the surface of the droplet deviates only slightly from the value which would be realized for the surface concentration under equilibrium (zero-flow) conditions. This case is termed the "uniformly retarded" regime because the small deviation of the surface concentration from the equilibrium value along the surface creates a distributed Marangoni tension which retards uniformly the convection

on the surface. Uniform retardation may be realized if the flow is extremely slow so that surface Peclet numbers are small and surface diffusion, acting as the dominant transport mechanism, forces the concentration to be nearly uniform. Alternatively, if the surface Peclet number is of order one, this case occurs if the kinetic transport between the bulk and the surface is fast compared to convection, and if the rate of diffusion in the adsorption depth layer is fast relative to convection in that layer (adsorption depth Peclet number much less than one). The case of uniform retardation was introduced by Levich (1962) in his study of the influence of surfactants on the motion of a drop in an infinite medium, and was later studied, for the same problem, by Schechter and Farley (1963), Newman (1967) and Holbrook and Levan (1983a).

The final case is the regime in which one of the nonconvective surfactant transport mechanisms - either bulk diffusion or kinetic exchange - is slow relative to convective transport and the other is fast. A solution is obtained with the rate limiting mechanism solved exactly, and the fast transport mechanisms regarded as being in equilibrium in a quasistatic sense. The primary example of this case is the treatment of the kinetic exchange as infinitely fast (and thereby regarded as in equilibrium) and the bulk diffusion in the adsorption depth layer as rate limiting. This case was treated by Levich (1962) and later Saville (1973) using a boundary layer technique. Wasserman and Slattery (1969) and Levan and Newman (1976) studied this case in the limit of zero solubility of the surfactant by a regular perturbation, and finally Holbrook and Levan (1983b) solved numerically the convective-diffusion equation for the surfactant mass

transfer. The alternative case in which sorption kinetics is rate-limiting and bulk diffusion is fast was treated by Holbrook and Levan (1983b) and He et al. (1988). In all of these studies the surface Peclet number was either very large or infinite.

This study examines the regime of uniform retardation controlled by kinetic exchange. Since surface Peclet numbers in fluid flows are seldom very small and only caused to be such under special circumstances, uniform retardation is practically realized when the series processes of kinetic exchange and bulk diffusion are fast relative to convection. As remarked above, these processes are fast when the kinetic exchange is fast (relative to convection) and the Peclet number based on the adsorption depth is small. To describe uniform retardation precisely, a regular perturbation approach is adopted in which the inverse ratio of the time scale for kinetic exchange to the scale for convection is set equal to a small parameter. To focus solely on the influence of kinetic exchange, the adsorption depth Peclet number is equated to the square of this parameter, thus relegating bulk diffusive effects to higher than first order. This is a sensible approach because even at low bulk concentrations of surfactant adsorption depths are usually of the order of tenths of millimeters or less (cf. the discussion in the review article by Harper (1972)). Furthermore, the adsorption depth becomes vanishingly small as the bulk concentration approaches and exceeds the critical micelle concentration of the surfactant. Note finally that in this perturbative scheme, the zeroth order solution will have an uniform concentration of surfactant on the surface and thus will be identical to the clean solution since Marangoni stresses are equal to zero.

This chapter is organized into six major sections. Section 2 details the exact governing equations and boundary conditions (§2.1) and outlines the perturbation scheme which describes the regime of kinetically controlled uniform retardation (§2.2). Section 3 outlines the collocation technique which is used to obtain numerical solutions. The technique involves exact satisfication of the wall hydrodynamic conditions (§3.1) and a pointwise satisfication of the kinematic and surfactant mass transfer conditions at the spherical particle interface (§3.2). Convergence criteria and a verification of the method by comparison to solid sphere results are presented in §3.3. The results are detailed in §4 for the case of a clean droplet and §5 for the surfactant contaminated case. The results are presented in tabulations of hydrodynamic drag coefficients, the calculation of terminal velocities and the presentation of velocity fields. The chapter ends with a conclusion section (§6).

4.2 Formulation

4.2.1 Governing Equations and Boundary Conditions

The problem under examination is that of a fluid droplet moving steadily and axisymmetrically through a continuous liquid in an infinitely long cylindrical tube. Both the droplet and continuous phases are assumed to be incompressible and Newtonian. Far away from the droplet, the continuous fluid flow is either stationary or Poiseuillian. The Reynolds and capillary numbers are assumed to be small enough so that inertia is negligible and the droplet retains a spherical shape. A bulk soluble surfactant is present in the

continuous phase and is adsorbed on the surface of the droplet. The concentration of surfactant far from the droplet is assumed to be uniform. In the solution technique which will be used both cylindrical (ρ,ω,z) and spherical coordinates (r,θ,ϕ) are needed. The origin of both systems is located at the center of the moving droplet, and therefore in these systems the tube wall is moving in the axial direction (see Fig.1). The velocity of the droplet in absence of the surfactants is denoted as U_0'. (Dimensional quantities are marked by a prime, and dimensionless quantities are unprimed throughout the analysis.) U_0' is taken as positive when the drop is moving in the positive z direction, and therefore, in the droplet frame, the wall is moving in -z direction when U_0' is greater than zero. The center line velocity in the Poiseuille flow is denoted as V' and is taken as positive when Poiseuille flow is in the +z direction. The angle θ is measured from the front stagnation point and the gravitational force is acting in the -z direction.

In formulating the hydrodynamic equations for the droplet motion, droplet and continuous phase variables are denoted by superscripts (1) and (2) respectively. The tube and the droplet radiis are denoted by b' and a' respectively. Coordinates are nondimensionalized by the droplet radius a'. The kinematic variables (of both phases) are scaled as follows: velocities by the steady translational velocity of the droplet in the absence of the surfactant in the tube, U_0', and shear stress tensors τ_{ij}' and pressure P' by $\mu'^{(2)}U_0'$, where $\mu'^{(2)}$ is the viscosity of the exterior fluid. The surfactant concentration Γ' is nondimensionalized by Γ_0' which is the

surfactant concentration in equilibrium with the uniform bulk concentration C'_∞ and κ is the viscosity ratio $\mu'^{(1)}/\mu'^{(2)}$. Since the flow is axisymmetric and incompressible, velocities may be represented by a stream function ψ' which is nondimensionalized by $a'^2U'_0$.

The Navier-Stokes equation for steady axisymmetric creeping flow can be written in terms of the stream function $\psi^{(i)}$ (Happel and Brenner (1970)) as:

$$E^2(E^2\psi^{(i)}) = 0 \qquad (i = 1, 2) \qquad (2.1)$$

where E^2 is the axisymmetric stream function operator. In spherical coordinates, E^2 is denoted by E_s^2 and is

$$E_s^2\psi^{(i)} = \frac{\partial^2\psi^{(i)}}{\partial r^2} + \frac{\sin\theta}{r^2}\frac{\partial}{\partial\theta}\left(\frac{1}{\sin\theta}\frac{\partial\psi^{(i)}}{\partial\theta}\right) \qquad (2.2)$$

while in cylindrical coordinates, it has the form

$$E_c^2\psi^{(i)} = \frac{\partial^2\psi^{(i)}}{\partial z^2} + \frac{\partial^2\psi^{(i)}}{\partial\rho^2} - \frac{1}{\rho}\frac{\partial\psi^{(i)}}{\partial\rho} \qquad (2.3)$$

The velocity components can be expressed in terms of the stream function:

$$v_r^{(i)} = -\frac{1}{r^2\sin\theta}\frac{\partial\psi^{(i)}}{\partial\theta}, \qquad v_\theta^{(i)} = \frac{1}{r\sin\theta}\frac{\partial\psi^{(i)}}{\partial r},$$

(2.4)

$$v_z^{(i)} = -\frac{1}{\rho}\frac{\partial \psi^{(i)}}{\partial \rho}, \qquad v_\rho^{(i)} = \frac{1}{\rho}\frac{\partial \psi^{(i)}}{\partial z}.$$

The boundary conditions are formulated at the center of the droplet, the tube wall, the droplet surface and far from the droplet. These are:

(1) At the droplet center $\lim_{r\to 0} v_r^{(1)}$ and $\lim_{r\to 0} v_\theta^{(1)}$ exist.

(2) Far from the droplet, the velocity field is either uniform

$$\lim_{|z|\to\infty} v_z^{(2)} = -U \tag{2.5}$$

or of Poiseuille type

$$\lim_{|z|\to\infty} v_z^{(2)} = V\left(1 - \frac{\rho^2}{b^2}\right) - U \tag{2.6}$$

where U is the velocity of the droplet and V is the center line velocity of the Poiseuille flow at infinity (nondimensionalized by U_0').

(3) At the tube wall, ρ=b (b=b'/a')

$$v_z^{(2)} = -U, \quad v_\rho^{(2)} = 0 \tag{2.7}$$

(4) At the surface of the droplet, r=1 (r=r'/a'=1)

$$v_r^{(1)} = v_r^{(2)} = 0 \tag{2.8}$$

$$v_\theta^{(1)} = v_\theta^{(2)} \tag{2.9}$$

$$\tau_{r\theta}^{(2)} - \tau_{r\theta}^{(1)} = \frac{1}{\mu'^{(2)} U_0'} \frac{\partial \sigma'}{\partial \theta} = - Ma \frac{\partial \Gamma}{\partial \theta} \tag{2.10}$$

where σ' is the surface tension and Ma is the Marangoni number defined by

$$Ma = - \frac{\Gamma_0'}{\mu'^{(2)} U_0'} \frac{\partial \sigma'}{\partial \Gamma'}$$

Due to the assumption that the droplet retains its spherical shape, the normal stress balance on the interface is replaced by an integrated force balance:

$$F_z' = 2\pi \mu'^{(2)} U_0' a'^2 \int_0^\pi \{(- P^{(2)} + \tau_{rr}^{(2)}) \cos\theta - \tau_{r\theta}^{(2)} \sin\theta\} \sin\theta d\theta$$

$$= \frac{4}{3} \pi a'^3 (\rho'^{(1)} - \rho'^{(2)}) g' \tag{2.11a}$$

where F_z' is the hydrodynamic drag exerted by the exterior fluid on the drop, $\rho'^{(i)}$ is the density of phase i and g' is the gravitational

acceleration. Equation (2.11a) will be used to determine the droplet terminal velocities. Writing the normal ($\tau_{rr}^{(2)}$) and shear ($\tau_{r\theta}^{(2)}$) stresses in terms of the stream function in spherical coordinates, (2.11a) may be expressed in the form

$$F_z' = a'U_0'\mu'^{(2)}\pi\int_0^{\pi} r'^3\sin^3\theta\ \frac{\partial}{\partial r'}\left[\ \frac{E^2\psi^{(2)}}{r'^2\sin^2\theta}\ \right]d\theta \qquad (2.11b)$$

The appearance of the Marangoni stress term in (2.10) indicates that the surfactant distribution on the surface of the droplet, $\Gamma(\theta)$, must be determined in order to obtain the velocity field. This distribution is established from the solution of the equation of surfactant conservation at the interface of the droplet; at steady state this relation is in the form

$$\frac{1}{\sin\theta}\frac{\partial}{\partial\theta}(\sin\theta\Gamma V_s) = \frac{1}{Pe_s\sin\theta}\frac{\partial}{\partial\theta}(\sin\theta\frac{\partial\Gamma}{\partial\theta}) + Q(\Gamma,C_s) \qquad (2.12)$$

where V_s is the surface velocity (V_s=$V_\theta^{(i)}(\theta,r=1)$), and Pe_s is the surface Peclet number (Pe_s= $\frac{a'U_0'}{D_s'}$, where D_s' is the surface diffusion coefficient). The function $Q(\Gamma,C_s)$ in (2.12) describes the adsorption-desorption kinetics (C_s is the surfactant sublayer concentration and nondimensionalized by C_∞', C_s=$C(r=1,\theta)$). Here the Langmuir formulation for the kinetics is adopted (Davies and Rideal 1963); thus in dimensional form

$$Q'(\Gamma',C_s') = -\alpha'\Gamma' - \beta' C_s'(\Gamma' - \Gamma_\infty') \tag{2.13}$$

where α' and β' are kinetic constants of desorption and adsorption respectively and Γ_∞' is the maximum surfactant concentration at the surface. From (2.13), the equilibrium concentration Γ_0' can easily be obtained from $Q'(\Gamma_0',C_\infty')=0$; thus

$$\frac{\Gamma_0'}{\Gamma_\infty'} = \frac{k}{1+k} \tag{2.14}$$

where $k = \beta' C_\infty'/\alpha'$ and is the ratio of adsorption to desorption rates. Nondimensionalization of (2.13) by $U_0'\Gamma_0'/a'$ yields after some manipulation and combination with (2.12) the surfactant mass equation

$$\frac{1}{\sin\theta}\frac{\partial}{\partial\theta}(\sin\theta\Gamma V_s) = \frac{1}{Pe_s\sin\theta}\frac{\partial}{\partial\theta}\left(\sin\theta\frac{\partial\Gamma}{\partial\theta}\right) - Bi\left[C_s(\Gamma - 1) + \frac{1}{k}(\Gamma - C_s)\right] \tag{2.15}$$

where

$$Bi = \frac{\beta' C_\infty'}{(U_0'/a')}$$

and is the nondimensional ratio of the rate of adsorption of surfactant onto the surface to the rate at which surfactant is convected from one end of the droplet to the other.

With the above choice of the adsorption isotherm, the dependence of the surface tension on the surfactant surface concentration ($\sigma'(\Gamma')$) may be formulated from the Gibbs adsorption equation,

$$\frac{d\sigma'}{d\mu'} = - \Gamma' \tag{2.16}$$

where μ' is the chemical potential. The bulk concentration is assumed to be dilute enough so as to be ideal, $\mu' = \mu'_0(T', p') + R'T'\ell n(C')$, where T' denotes the temperature, p' is the thermodynamic pressure and R' is the gas constant. Integrating (2.16) gives

$$\sigma' = \sigma'_0 - R'T'\Gamma'_\infty \ell n(1/(1 - \Gamma'/\Gamma'_\infty)) \tag{2.17}$$

where σ'_0 is surface tension of the clean interface. Consequently, from (2.17) $\frac{\partial \sigma'}{\partial \Gamma'}$ is calculated to be

$$\frac{\partial \sigma'}{\partial \Gamma'} = - \frac{R'T'}{(1 - \Gamma'/\Gamma'_\infty)} \tag{2.18}$$

and

$$Ma = \frac{R'T'\Gamma'_\infty}{\mu'(2)U'_0} \left(\frac{k}{1 + k - k\Gamma} \right) \tag{2.19}$$

The problem is not fully determined until C_s, the sublayer concentration, is solved for. Formally, C_s can be obtained by solving the steady convective-diffusion equation in the continuous phase, i.e.

$$Pe\vec{V}\cdot\vec{\nabla}C = \nabla^2 C \tag{2.20}$$

where ∇^2 is the Laplacian operator, $Pe=U_0'a'/D'$, D' is the bulk diffusivity of the surfactant and C is the bulk concentration. the boundary conditions on the bulk concentration are:

$$\frac{1}{Pe_A}\frac{\partial C}{\partial r}\Big|_{r=1} = Bi[C_s(\Gamma - 1) + \frac{1}{k}(\Gamma - C_s)] \tag{2.21}$$

and

$$\lim_{|z|\to\infty} C(z,\rho) = 1 \tag{2.22}$$

$$\frac{\partial C}{\partial \rho}\Big|_{\rho=b} = 0 \tag{2.23}$$

In (2.21), $Pe_A = \frac{U_0'\delta'}{D'}$ where δ' is the adsorption depth of the surfactant, Γ_0'/C_∞'. This completes the formulation.

4.2.2 Perturbation Scheme Describing the Surfactant Influence

In the absence of dissolved surfactants in the continuous phase, the governing equations are given by (2.1) and the boundary conditions are equations (2.5)-(2.11) with the Marangoni stress equated to zero. As remarked in the Introduction, to describe the influence of surfactant adsorption, the limiting case in which sublayer-surface kinetic exchange is fast but rate determining is considered. To describe this case perturbatively, the ratio of the adsorption rate to the rate at which the surfactant is convected ($\beta' C_\infty'/U_0'/a' = Bi$) is set equal to $1/\epsilon$, and k, the ratio of adsorption to desorption, is taken

to be of order 1. The Peclet numbers, Pe_s and Pe are both taken to be of order 1. This relegates the influence of surface diffusion to second order and above. With this scaling, however, bulk diffusion would be rate determing to zeroth order. To remove this effect to second order and higher, Pe_A is taken to be of order ϵ^2, a reasonable ordering since adsorption depth δ' is usually much small than one (Harper 1973), and becomes vanishingly small at high surfactant concentrations. The ordering scheme is summarized below:

$$\begin{aligned} Pe_A &= O(\epsilon^2) \\ Pe_s &= O(1) \\ k &= O(1) \\ Bi &= O(\epsilon^{-1}) \end{aligned} \qquad (2.24)$$

The stream function, terminal velocity and surface and bulk concentration of surfactant are expanded in an asymptotic series in powers of ϵ as follows:

$$\begin{aligned} \psi &= \psi_{(0)} + \epsilon\psi_{(1)} + O(\epsilon^2) \\ U &= U_{(0)} + \epsilon U_{(1)} + O(\epsilon^2) \\ \Gamma &= \Gamma_{(0)} + \epsilon\Gamma_{(1)} + O(\epsilon^2) \end{aligned} \qquad (2.25)$$

$$C = C_{(0)} + \epsilon C_{(1)} + O(\epsilon^2)$$

where the subscripts indicate the asymptotic order of the variables. For each order of ϵ, the stream function equation is given by

$$E^2(E^2\psi^{(i)}_{(\ell)}) = 0 \qquad (\ell = 0,1,2,\cdots) \tag{2.26}$$

Also, for each order of ϵ, the velocity boundary conditions at $r = 1$ are:

$$V^{(1)}_{r(\ell)} = V^{(2)}_{r(\ell)} = 0 \quad \text{and} \quad V^{(1)}_{\theta(\ell)} = V^{(2)}_{\theta(\ell)} \tag{2.27a,b,c}$$

while at $\rho = b$

$$V^{(2)}_{z(\ell)} = - U_{(\ell)} \qquad \text{and} \quad V^{(2)}_{\rho(\ell)} = 0 \tag{2.28a,b}$$

Far away from the droplet, for uniform flow, the perturbation condition is

$$\lim_{|z|\to\infty} V^{(2)}_{z(\ell)} = - U_{(\ell)} \tag{2.29}$$

For Poiseuille flow, the zeroth order condition is different from the higher order conditions. Thus

$$\lim_{|z|\to\infty} v^{(2)}_{z(0)} = V\left(1 - \frac{\rho^2}{b^2}\right) - U_{(0)} \tag{2.30}$$

and

$$\lim_{|z|\to\infty} v^{(2)}_{z(\ell)} = - U_{(\ell)} \qquad (\ell = 1,2,\cdots) \tag{2.31}$$

The forms for the tangential stress and integrated force balance are also different. For the zeroth order, they are

$$\tau^{(2)}_{r\theta(0)} - \tau^{(1)}_{r\theta(0)} = - Ma(\Gamma_{(0)})\frac{\partial \Gamma_{(0)}}{\partial \theta} \tag{2.32}$$

and

$$\int_0^{\pi} \{(- P^{(2)}_{(0)} + \tau^{(2)}_{rr(0)})\cos\theta - \tau^{(2)}_{r\theta(0)}\sin\theta\} \sin\theta d\theta = \frac{2a'(\rho'^{(1)} - \rho'^{(2)})g'}{3\mu'^{(2)}U'_0} \tag{2.33}$$

where $Ma(\Gamma)$ is given by (2.19). For higher orders, the perturbation condition for the integrated force balance is:

$$\int_0^{\pi} \{(- P^{(2)}_{(\ell)} + \tau^{(2)}_{rr(\ell)})\cos\theta - \tau^{(2)}_{r\theta(\ell)}\sin\theta\} \sin\theta d\theta = 0 \tag{2.34}$$

$$(\ell = 1,2,\cdots)$$

For the tangential balance, a simple form for the higher orders is not possible since the Marangoni number must be expanded. Still, since the problem will only be solved to first order, only the order ϵ tangential balance is detailed.

$$\tau^{(2)}_{r\theta(1)}(r=1) - \tau^{(1)}_{r\theta(1)}(r=1) = - \left[Ma(\Gamma=\Gamma_{(0)})\frac{\partial \Gamma_{(1)}}{\partial \theta} + \frac{\partial Ma}{\partial \Gamma}\Big|_{\Gamma=\Gamma_{(0)}} \Gamma_{(1)}\frac{\partial \Gamma_{(0)}}{\partial \theta}\right] \tag{2.35}$$

To zeroth order, the surfactant conservation equations (2.15), (2.20-2.23) become, (note the scalings (2.24))

$$C_{s(0)}(\Gamma_{(0)} - 1) + \frac{1}{k}(\Gamma_{(0)} - C_{s(0)}) = 0 \tag{2.36}$$

$$Pe\vec{V}_{(0)}\cdot\vec{\nabla}C_{(0)} = \nabla^2 C_{(0)} \tag{2.37}$$

$$\frac{\partial C_{(0)}}{\partial r}\Big|_{r=1} = 0 \tag{2.38}$$

$$\lim_{|z|\to\infty} C_{(0)}(z,\rho) = 1 \tag{2.39}$$

$$\frac{\partial C_{(0)}}{\partial \rho}\Big|_{\rho=b} = 0 \tag{2.40}$$

From the last four relations it is clear that $C_{(0)}(z,\rho)=1$ and thus $C_{s(0)}=1$. Since $C_{s(0)}=1$, from equation (2.36), $\Gamma_{(0)}=1$, and the zeroth order tangential balance becomes

$$\tau^{(2)}_{r\theta(0)} - \tau^{(1)}_{r\theta(0)} = 0 \tag{2.41}$$

Thus the zeroth order solution is just the solution for the hydrodynamic field in the absence of surfactants and $U_{(0)}=1$.

For the first order, the surfactant balances become:

$$\frac{1}{\sin\theta}\frac{\partial}{\partial\theta}(\sin\theta\Gamma_{(0)}V_{s(0)}) = -Bi^{*}(1+\frac{1}{k})\Gamma_{(1)} + \frac{Bi^{*}}{k}C_{s(1)} \qquad (2.42)$$

where $Bi = \frac{Bi^{*}}{\epsilon}$ and

$$Pe\vec{V}_{(0)}\cdot\vec{\nabla}C_{(1)} = \nabla^{2}C_{(1)} \qquad (2.43)$$

$$\frac{\partial C_{(1)}}{\partial r}\Big|_{r=1} = 0 \qquad (2.44)$$

$$\lim_{|z|\to\infty} C_{(1)}(z,\rho) = 0 \qquad (2.45)$$

$$\frac{\partial C_{(1)}}{\partial \rho}\Big|_{\rho=b} = 0 \qquad (2.46)$$

The last four equations determine that $C_{(1)} = 0$. Hence, Eqn.(2.42) becomes an explicit equation for $\Gamma_{(1)}$ in terms of the zeroth order dilation of the surface. This expression for $\Gamma_{(1)}$ can be combined with the first order tangential balance to yield

$$\tau^{(2)}_{r\theta(1)}(r=1) - \tau^{(1)}_{r\theta(1)}(r=1) = \phi\frac{\partial}{\partial\theta}(\frac{1}{\sin\theta}\frac{\partial}{\partial\theta}\sin\theta V_{s(0)}) \qquad (2.47)$$

where $\phi = \frac{Ma(\Gamma-1)}{Bi^{*}(1+1/k)}$ and

$$Ma(\Gamma-1) = \frac{R'T'\Gamma'_\infty}{\mu'^{(2)}U'_0}\, k.$$

Solution of (2.26), (2.27a,b,c),(2.28a,b), (2.29) (or (2.31)), (2.34), (2.47) determines the first order velocity $U_{(1)}$. These equations are identical to the zeroth order (surfactant-free) equation except for the term representing the gradient of the surface dilation in the tangential stress balance (2.47). Thus an identical numerical technique can be used for the zeroth and first order. This technique is outlined in the next section. Note finally that in principle corrections to U of all orders can be calculated, but the effort here is confined to the first order.

4.3 Solution Technique

The effort involved in solving the zeroth and first order equations can be reduced if advantage is taken of the symmetry in z. The governing equations and boundary conditions are in terms of ρ, z, θ, and r where $\theta(\rho,z)=\text{Arctan}(\rho/z)$ $(0\leq\theta<\pi)$ and $r=(\rho^2+z^2)^{1/2}$. Consider the transformation to coordinates $\rho"$, z", $\theta"$ and r" where $\rho"=\rho$, $z"=-z$, $\theta"=\pi-\theta$ and $r"=r$. Note that in the double prime system, the functional transformations $\theta"(\rho",z")$ and $r"(\rho",z")$ are identical in form to the unprimed system. If the field equation in terms of ρ and z, and boundary conditions of the zero and first order (i.e. (2.26), (2.27a,b,c)), (2.28a,b), (2.29), or (2.30) and (2.31), and (2.41)and (2.47)) are written in terms of $\rho"$, z", $\theta"$, and r" they would be identical in form. Thus, if the solution for the stream function in

the cylindrical system is $\psi(\rho,z)$, the solution in the double prime system is identical in form and is given by $\psi''(\rho'',z'')=\psi(\rho'',z'')$. But from the definition of the transformation, $\psi''(\rho'',z'')=\psi(\rho'',-z)$. Hence

$$\psi(\rho'',z'') = \psi(\rho'',-z'')$$

and the symmetry in z is proved. Note that since

$\Gamma_{(1)}(\theta)=-\frac{1}{Bi^*(1+1/k)}\frac{1}{\sin\theta}\frac{\partial}{\partial\theta}(\sin\theta V_{\theta(0)})$, and ψ is symmetric in z, $\Gamma_{(1)}(\pi-\theta)=-\Gamma_{(1)}(\theta)$, i.e. $\Gamma_{(1)}$ is antisymmetric.

In cylindrical and spherical coordinates, the solution of (2.26) may be obtained by the method of separation of variables. For the droplet interior, only the solution in spherical coordinates is needed. The form for $\psi^{(1)}_{(\ell)}(r,\theta)$ which admits bounded solutions as $r\to 0$ for $V^{(1)}_{r(\ell)}$ and $V^{(1)}_{\theta(\ell)}$ (as given by (2.4)) and which is symmetric in z is:

$$\psi^{(1)}_{(\ell)} = \sum_{n=2}^{\infty}(E^{(1)}_n r^n + F^{(1)}_n r^{n+2})C_n^{-1/2}(\cos\theta) \qquad n\text{-even} \qquad (3.1)$$

where $C_n^{-1/2}(\cos\theta)$ is the Gegenbauer polynomial of order n and degree -1/2.

For the continuous fluid, the cylindrical coordinate solution of (2.26) which is symmetric in z and bounded as $|z|\to\infty$ (necessary for compatibility with (2.29) or (2.30) and (2.31)) is

$$\psi^{(2)}_{(\ell)}(\rho,z) = \psi^{\infty}_{(\ell)}(\rho) + \int_0^{\infty} dk\{A_{(\ell)}(k)\rho I_1(k\rho) + B_{(\ell)}(k)\rho^2 I_0(k\rho)\}\cos(kz)$$

$$+ \int_0^{\infty} dk\{C_{(\ell)}(k)\rho K_1(k\rho) + D_{(\ell)}(k)\rho^2 K_0(k\rho)\}\cos(kz) \qquad (3.2)$$

where

$$\psi^{\infty}_{(0)}(\rho) = \begin{cases} \frac{1}{2}\rho^2 & \text{(Uniform)} \\ -Vb^2[\frac{1}{2}(\frac{\rho}{b})^2 - \frac{1}{4}(\frac{\rho}{b})^4] + \frac{1}{2}\rho^2 & \text{(Poisuelle)} \end{cases}$$

and

$$\psi^{\infty}_{(\ell)}(\rho) = \frac{U_{(\ell)}}{2}\rho^2 \qquad (\ell=1,2,\cdots)$$

where I_0, I_1, K_0, and K_1 are the modified Bessel functions of the first and second kind. The above form for $\psi^{(2)}_{(\ell)}(\rho,z)$ is subject to the condition that $V^{(2)}_{z(\ell)}$ and $V^{(2)}_{\rho(\ell)}$ be bounded as $\rho \to 0$ along the rays $z>1$ and $z<-1$. This condition is difficult to apply. The second integral in (3.2) gives unbounded values for $V^{(2)}_{z(\ell)}$ as $\rho \to 0$ for all z; elimination of this integral is too restrictive since boundedness is only required for $|z|>1$.

To circumvent this difficulty, the second integral can be replaced by the Gagenbauer expansion solution of $E_s^4\psi=0$, which yields bounded velocities at infinity. Thus

$$\psi^{(2)}_{(\ell)}(\rho,z,r,\theta) = \psi^{\infty}_{(\ell)}(\rho) + \int_0^{\infty} dk\{A_{(\ell)}(k)\rho I_1(k\rho)$$

$$+ B_{(\ell)}(k)\rho^2 I_0(k\rho)\}\cos(kz) \qquad n\text{=even}$$

$$(3.3)$$

$$+ \sum_{n=2}^{\infty}\{E_n^{(2)} r^{-n+1} + F_n^{(2)} r^{-n+3}\}C_n^{-1/2}(\cos\theta)$$

The above form constitutes a sufficiently general solution (Leichtberg et al,(1976)).

The technique used to obtain the constants and the k functions in Eq.(3.1) and (3.3) is outlined as follows. First, the boundary conditions on the tube wall are satisfied exactly, by using the Fourier inverse cosine integral to solve for the unknown coefficients A(k) and B(k) in (3.3). Second, the stream function is rewritten in a compact form in terms of r,θ and the unknown constants $E_n^{(2)}$ and $F_n^{(2)}$. Finally, a collocation technique is used to satisfy the boundary conditions on the surface of the droplet. In the following subsection §3.1, the first two steps are detailed. The collocation satisfaction of the r=1 boundary conditions is described in §3.2. In §3.1 and §3.2 the solution technique is described for the zeroth order in ℓ, and therefore the subscript is dropped in the notation. The solution for ℓ=1 is similar, and is described at the end of §3.2. Finally, in §3.3 the convergence criteria is formulated, and a verification of the method is presented.

4.3.1 Exact Solution of the Wall Boundary Conditions

Using Eq.(3.3), the boundary conditions (2.28a) becomes

$$\int_0^{\infty} dk\{A(k)kI_0(bk)+B(k)[bkI_1(bk) + 2I_0(bk)]\}\cos(kz) =$$

(3.4)

$$- \sum_{n=2}^{\infty}[E_n^{(2)}G_n^1(z) + F_n^{(2)}G_n^2(z)]$$

Instead of using $V_\rho^{(2)}(\rho=b)=0$ (2.28b), the equivalent condition $\psi^{(2)}(\rho=b)=\psi^{\infty}(b)$ is applied for convenience. That is

$$\int_0^{\infty} dk\{A(k)bI_1(bk)+B(k)b^2I_0(bk)\}\cos(kz) = - \sum_{n=2}^{\infty}[E_n^{(2)}G_n^3(z) + F_n^{(2)}G_n^4(z)]$$

(3.5)

where, for i=1,2,3,4, $G_n^i(z)$ are of the form as:

$$G_n^1(z) = (b^2 + z^2)^{-(n+1)/2}P_n[\frac{z}{(b^2 + z^2)^{1/2}}]$$

$$G_n^2(z) = (b^2 + z^2)^{-(n-1)/2}\{P_n[\frac{z}{(b^2 + z^2)^{1/2}}] + 2C_n^{-1/2}[\frac{z}{(b^2 + z^2)^{1/2}}]\}$$

(3.6)

$$G_n^3(z) = (b^2 + z^2)^{-(n-1)/2}C_n^{-1/2}[\frac{z}{(b^2 + z^2)^{1/2}}]$$

$$G_n^4(z) = (b^2 + z^2)^{-(n-3)/2}C_n^{-1/2}[\frac{z}{(b^2 + z^2)^{1/2}}]$$

In the above, spherical coordinates (r,θ) have been transformed into cylindrical coordinates (ρ,z). The boundary conditions (3.4) and

(3.5) can be inverted by the inverse Fourier cosine transform so as to solve for A(k) and B(k). Integrating the inverse integrals yields:

$$A(k)kI_0(bk) + B(k)[bkI_1(bk) + 2I_0(bk)] = -\sum_{n=2}^{\infty}[E_n^{(2)}H_n^1(k) + F_n^{(2)}H_n^2(k)]$$

$$A(k)bI_1(bk) + B(k)b^2I_0(bk) = -\sum_{n=2}^{\infty}[E_n^{(2)}H_n^3(k) + F_n^{(2)}H_n^4(k)] \tag{3.7}$$

where, $H_n^i(k)$, i=1,2,3,4, are given as (Leichtberg et al,(1976)):

$$H_n^1(k) = (-1)^{n/2}\frac{2}{\pi n!}k^nK_0(bk)$$

$$H_n^2(k) = -(-1)^{n/2}\frac{2}{\pi n!}k^{n-2}[n(n-1)K_0(bk) - (2n-3)bkK_1(bk)]$$

$$H_n^3(k) = -(-1)^{n/2}\frac{2}{\pi n!}\,bk^{n-1}K_1(bk) \tag{3.8}$$

$$H_n^4(k) = -(-1)^{n/2}\frac{2}{\pi n!}\,bk^{n-3}[(2n-3)bkK_0(bk) - (n-2)(n-3)K_1(bk)]$$

A(k) and B(k) can be solved in terms of the unknown constants $E_n^{(2)}$ and $F_n^{(2)}$. Substituting this solution into Eq.(3.3), the stream function can be written in a new compact form in spherical coordinates as follows:

$$\psi^{(2)}(\theta,r) = \psi^{\infty}(r,\theta) + \sum_{n=2}^{\infty}[E_n^{(2)}S_n^1(r,\theta) + F_n^{(2)}S_n^2(r,\theta)] \tag{3.9}$$

In the above

$$S_n^1(r,\theta) = r^{-n+1}C_n^{-1/2}(\cos\theta) + \int_0^\infty dk\ \cos(kr\cos\theta)\{T_n^1(k)r\sin\theta I_1(kr\sin\theta) + T_n^3(k)(r\sin\theta)^2 I_0(kr\sin\theta)\}$$

$$S_n^2(r,\theta) = r^{-n+3}C_n^{-1/2}(\cos\theta) + \int_0^\infty dk\ \cos(kr\cos\theta)\{T_n^2(k)r\sin\theta I_1(kr\sin\theta) + T_n^4(k)(r\sin\theta)^2 I_0(kr\sin\theta)\} \qquad (3.10)$$

The $T_n^i(k)$'s (i=1,2,3,4) functions appearing in (3.10) are defined as

$$T_n^1(k) = [(2 + bk\Omega)H_n^3(k) - b^2H_n^1(k)]/\Delta$$

$$T_n^2(k) = [(2 + bk\Omega)H_n^4(k) - b^2H_n^2(k)]/\Delta$$

$$T_n^3(k) = [b\Omega H_n^1(k) - kH_n^3(k)]/\Delta \qquad (3.11)$$

$$T_n^4(k) = [b\Omega H_n^2(k) - kH_n^4(k)]/\Delta$$

where Ω and Δ are defined below

$$\Omega = \frac{I_1(kb)}{I_0(kb)} \quad \text{and} \quad \Delta = b^2 k I_0(bk) - 2bI_1(bk) - b^2 k I_1(bk)\Omega$$

The integrals in (3.10) must be evaluated numerically.

4.3.2 Collocation Solution of Droplet Surface Boundary Conditions

The boundary condition $V_r^{(1)}(r=1,\theta)=0$ (2.27a) can be applied directly to (3.1) to eliminate $F_n^{(1)}$. Thus the inner solution becomes

$$\psi^{(1)}(r,\theta) = \sum_{n=2}^{\infty} E_n^{(1)}(r^n - r^{n+2})C_n^{-1/2}(\cos\theta) \qquad (3.12)$$

If the other boundary conditions at r=1 ((2.27b,c) and (2.41; ℓ=0) or (2.47 ℓ=1)) are applied to the solution (3.9) and (3.12), three simultaneous equations in the form of infinite series are obtained. In the collocation technique, the three boundary conditions are satisfied at m discrete points along the surface of the sphere, and the series (3.9) and (3.12) is truncated into a finite form which includes a total of 3m terms. A set of 3m simultaneous linear algebraic equation is therefore generated and can be solved using any standard matrix reduction technique to obtain the 3m unknown constants $E_n^{(1)}$, $E_n^{(2)}$, and $F_n^{(2)}$.

When the boundary conditions on the surface of the sphere are applied by the collocation technique described above, the 3m truncated equations from boundary conditions (2.27b,c) and (2.41) are given as:

$$V\cos\theta_i[1 - (\sin\theta_i / b)^2] - \cos\theta_i = \sum_{n=2}^{2m} [E_n^{(2)} S_n^3(1,\theta_i) + F_n^{(2)} S_n^4(1,\theta_i)] \tag{3.13}$$

$$V\sin\theta_i[1 - (\sin\theta_i / b)^2] - \sin\theta_i = \sum_{n=2}^{2m} [E_n^{(2)} S_n^5(1,\theta_i) + F_n^{(2)} S_n^6(1,\theta_i) + \frac{2}{\sin\theta_i} E_n^{(1)} C_n^{-1/2}(\cos\theta_i)] \tag{3.14}$$

$$V\sin\theta_i[1 + (\sin\theta_i / b)^2] - \sin\theta_i = \sum_{n=2}^{2m} [E_n^{(2)} S_n^7(1,\theta_i) + F_n^{(2)} S_n^8(1,\theta_i) - \frac{2(2n-1)\kappa}{\sin\theta_i} E_n^{(1)} C_n^{-1/2}(\cos\theta_i)] \tag{3.15}$$

where i denotes the collocation point (i=1,2,$\cdots$,m) and the $S_n^q(1,\theta_i)$ are given in Appendix A. The above equations are valid for Poisueille flow at infinity. The equations valid for uniform flow may be obtained from these by letting V=0.

The first order solution follows the same procedure of solving unknown coefficients as the zeroth order except that the Marangoni stress term of (2.47) must be included. Writing $V_{s(0)}(\theta)$ up to order 2m as

$$V_{s(0)}(\theta) = - V\sin\theta[1 - (\sin\theta/b)^2] + \sin\theta + \sum_{n=2}^{2m} [E_{n(0)}^{(2)} S_n^5(1,\theta) + F_{n(0)}^{(2)} S_n^6(1,\theta)] \tag{3.16}$$

where the $E^{(2)}_{n(0)}$ and $F^{(2)}_{n(0)}$ are obtained from Eqs.(3.13)-(3.15), and using the above expression for $V_{s(0)}(\theta)$, the equations which determine the first order coefficients $E^{(2)}_{n(1)}$, $F^{(2)}_{n(1)}$ and $E^{(1)}_{n(1)}$ are:

$$- U_{(1)}\cos\theta_i = \sum_{n=2}^{2p} [E^{(2)}_{n(1)} S^3_n(1,\theta_i) + F^{(2)}_{n(1)} S^4_n(1,\theta_i)] \tag{3.17}$$

$$- U_{(1)}\sin\theta_i = \sum_{n=2}^{2p} [E^{(2)}_{n(1)} S^5_n(1,\theta_i) + F^{(2)}_{n(1)} S^6_n(1,\theta_i) + \frac{2}{\sin\theta_i} E^{(1)}_{n(1)} C_n^{-1/2}(\cos\theta_i)] \tag{3.18}$$

$$- U_{(1)}\sin\theta_i + \phi \frac{\partial}{\partial\theta} (\frac{1}{\sin\theta} \frac{\partial}{\partial\theta} \sin\theta(- V\sin\theta[1 - (\sin\theta/b)^2] + \sin\theta + \sum_{n=2}^{2m} [E^{(2)}_{n(0)} S^5_n(1,\theta) + F^{(2)}_{n(0)} S^6_n(1,\theta)]))_{|\theta-\theta_i} \tag{3.19}$$

$$- \sum_{n=2}^{2p} [E^{(2)}_{n(1)} S^7_n(1,\theta_i) + F^{(2)}_{n(1)} S^8_n(1,\theta_i) - \frac{2(2n-1)\kappa}{\sin\theta_i} E^{(1)}_{n(1)} C_n^{-1/2}(\cos\theta_i)]$$

where 2p is the order of the first order field. Again, the above equations are valid for Poisueille flow. Those valid for uniform flow may be obtained by setting V=0 in (3.19).

An important question arises as to how to choose the location of discrete points on the surface of the droplet to obtain a prescribed accuracy and how to formulate a convergence criteria. Due to the symmetry in z, collocation points need only be located from $0 \le \theta \le \pi/2$.

Furthermore, since the droplet is moving in a bounded domain, a hydrodynamic influence of the wall on the moving droplet can be significant. This influence is largest at the equator of the droplet and decreases as θ varies from $\frac{\pi}{2}$ to 0. The points chosen are thus more dense near the equator and less dense near the pole in order to take into account the effect of the wall.

4.3.3 Convergence Criteria and Verification of Method

As explained in the Introduction, the aim of this study is to compute the hydrodynamic drag on the droplet, and therefore convergence criteria are based on the accurate computation of F_z'. Inserting (3.9) into (2.11b) shows that the drag is determined solely by $F_2^{(2)}$.

$$F_z' = - 4\pi a' \mu'^{(2)} U_0' F_2^{(2)}$$

Hydrodynamic drags are usually expressed in terms of drag coefficients λ. Consider first the zeroth order $F_{2(0)}^{(2)}$. For uniform flow, $F_{2(0)}^{(2)}$ is obtained from the solution of (3.13)-(3.15) with V=0. The drag coefficient for uniform flow with no surfactant is denoted by λ_u and is defined as the ratio of F_z' to the force exerted on a droplet moving at U_0' in an infinite medium. The latter is the Hadamard-Rybczynski value $4\pi' a' \mu'^{(2)} U_0' (\frac{1+3\kappa/2}{1+\kappa})$. Thus

$$\lambda_u = F^{(2)}_{2(0)} \frac{1 + \kappa}{1 + 3\kappa/2} \tag{3.20}$$

For Poiseuille flow, (3.13)-(3.15) indicate that $F^{(2)}_{2(0)}$ is the sum of two contributions, one $F^{(2)}_{2u(0)}$ from the uniform flow terms (identical to the previous case) and one from the Poiseuille terms ($F^{(2)}_{2v(0)}$) and which is linear in $V=V'/U'_0$. The contribution due to the Poiseuille terms gives rise to a drag $4\pi a'\mu'^{(2)}V'F^{(2)}_{2v(0)}$. A drag coefficient, λ_v is defined as this contribution divided by the Hadamard-Rybczynski drag for a sphere moving with velocity V'. Thus

$$\lambda_v = F^{(2)}_{2v(0)} \frac{1 + \kappa}{1 + 3\kappa/2} \tag{3.21}$$

and the total zeroth order drag in terms of drag coefficients is

$$F'_{z(0)} = - 4\pi a'\mu'^{(2)}\left(\frac{1 + 3\kappa/2}{1 + \kappa}\right) [U'_0\lambda_u - V'\lambda_v] \tag{3.22}$$

This decomposition reflects the linearity of the zeroth order problem: The total zeroth order drag can be thought of has the sum of drags from two flow idealizations, one the uniform flow past a fixed sphere and the second Poiseuille flow past a fixed sphere.

For the first order, it is evident from (2.34) and (3.17)-(3.19) that $F^{(2)}_{2(1)}$ is a sum of three contributions and the sum is equal to zero. The first is $F^{(2)}_{2u(1)}$, and is due to (and linear in) the $U_{(1)}$

terms. This is identical to $F^{(2)}_{2u(0)}$. The second, $F^{(2)}_{2u(1)}$ is due to the uniform flow terms in (3.16). A drag coefficient $\lambda_{u(1)}$ may be defined as

$$\lambda_{u(1)} = F^{(2)}_{2u(1)} \ (\phi=1)\left(\frac{1 + \kappa}{1 + 3\kappa/2}\right) \tag{3.23}$$

Note that since (3.19) is linear in ϕ, the problem is solved for the normalized case $\phi=1$, and then ϕ is reintroduced in the drag expression (3.25) (see below). Finally the third contribution $F^{(2)}_{2v(1)}$ is due to the Poiseuille terms in (3.16) and is linear in V; a drag coefficient similar to λ_v may be defined by:

$$\lambda_{v(1)} = \frac{U'_0}{V'} F^{(2)}_{2v(1)}(\phi=1)\left(\frac{1 + \kappa}{1 + 3\kappa/2}\right) \tag{3.24}$$

Thus the complete first order drag is

$$F'_{z(1)} = - 4\pi a'\mu'^{(2)}\left(\frac{1 + 3\kappa/2}{1 + \kappa}\right) \{U'_{(1)}\lambda_u + \phi(U'_0 \lambda_{u(1)} - V'\lambda_{v(1)})\}=0 \tag{3.25}$$

The decomposition of $F'_{z(1)}$ results from the linearity of the first order: The first order drag can be thought of as the sum of drags from three flow idealizations. The first is the uniform flow (with magnitude $U'_{(1)}$) past a fixed sphere. The second and third are the flows due to the Marangoni surface force term on the left hand side of (3.19), with $V_{s(0)}$ given by the uniform flow contribution U'_0 in one

idealization and by the Poiseuille contribution (i.e. the terms linear in V) in the other idealization.

For the zeroth order, λ_u and λ_v are computed until the difference for successive values of m divided by the previous value is less than 10^{-5}. For $\lambda_{u(1)}$ and $\lambda_{v(1)}$, the same preocedure is followed in p with m held fixed, and then m is varied until a precision of 10^{-5} is reached. Table I illustrates the number of points necessary to achieve this described accuracy for κ=0 and for λ_u, λ_v, $\lambda_{u(1)}$ and $\lambda_{v(1)}$. Interestingly, as Table I indicates, for convergence of the first order drag coefficients, less collocation points were necessary for the determination of the zeroth order surface velocity than were needed for the convergence of the zeroth order drag coefficients (m for convergence of λ_u and λ_v are larger than m for convergence of $\lambda_{u(1)}$ and $\lambda_{v(1)}$).

This section concludes with a verification of the method. Previous studies by Haberman-Sayre (1958) and Wang and Skalak (1969) have computed λ_u and λ_v for a solid sphere. These values are compared in Table II with values obtained from this method for κ=10^8. The fact that the deviations are all less than 1% lends confidence to the method. Further verification will be obtained when the clean fluid particle drag coefficients are compared to those of Hyman and Skalak (1969 and 1970). This comparison is detailed in the next section (§4).

4.4 Clean Surface Results: Hydrodynamic Drag Coefficients, Terminal Velocities and Flow Fields

The zeroth order hydrodynamic drag, $F'_{z(0)}$, is the sum of two terms and these terms may be thought of as the drags from two flow idealizations. The first is the uniform flow with magnitude U'_0 past a fixed sphere. The dimensional drag for this idealization is $-\xi'\lambda_u U'_0$, where $\xi'=4\pi a'\mu'^{(2)}(1+3\kappa/2)/(1+\kappa)$. The second idealization is the Poiseuille flow with centerline velocity V' past a fixed sphere; the drag for this idealization is $\xi'\lambda_v V'$. Converged values for λ_u and λ_v are detailed graphically in Figs. 2 and 3, respectively, for κ = 0, 0.5, 1.0, 2.0 and 10^8 (solid sphere), and for a range of a'/b' between 0 and 1. The values are also listed in Table III for κ = 0 and 1, and compared with the results of Hyman and Skalak's numerically exact solution. The fact that the agreement is within 0.1 percent for all values of a'/b' between 0.1 and 0.8 (the range considered by Hyman and Skalak) supports the accuracy of the calculations presented in this paper.

Figures 2 and 3 exhibit several interesting features. It is clear from these figures that, for fixed κ, both λ_u and λ_v increase as a'/b' increases. Since the drag in each idealization is the coefficient multiplied by the factor $\xi'U'_0$ (or $\xi'V'$), and ξ' is not a function of a'/b', it is clear that for fixed values of U'_0 and V', the drag increases as a'/b' increases. This is to be expected because as the gap between the sphere perimeter and the tube wall decreases, the shear rate in the gap in the vicinity of the sphere increases. This results in a higher shear stress being applied to the sphere by the fluid, and the drag consequently increases. A second common characteristic of Figs. 2 and 3 is the fact that λ_u and λ_v increase

with κ at fixed a'/b'. For fixed U_0' or V', the drag also increases because ξ' is a monotonically increasing function of κ varying from 1 to 3/2. Similar reasoning explains this increase: As the ratio of the droplet to continuous phase viscosity increases, the droplet surface velocity decreases. This reduction in the surface velocity causes the shear rate in the vicinity of the drop to increase, and thus the drag coefficient becomes larger. Finally, the results show that for fixed κ and a'/b', λ_u is always larger than λ_v, and this difference is more pronounced at larger values of a'/b' and κ. From the definitions given in §3.3, it is clear that the drag coefficent for uniform flow is equal (apart from the factor ξ') to the drag for unit velocity at infinity (unit terminal velocity), while the drag coefficient for Poiseuille flow is directly proportional to the drag for a unit centerline velocity. Thus the flow rate of fluid in the gap between the sphere and tube is, for the case of uniform flow, twice that of Poisuelle flow. This increased flow rate gives rise to a higher shear rate near the sphere, and thus a larger drag. Note that when the gap is very thin (a'/b' large) or the surface velocity is reduced (κ large) this effect is proportionately higher, and it explains the larger differences between λ_u and λ_v as either a'/b' or κ is increased.

With the hydrodynamic drag determined, terminal velocities for different circumstances can be computed. Three cases are considered here: (i) the motion of a drop in a vertical tube due only to gravity, (ii) the motion of a neutrally-bouyant drop suspended in Poiseuille flow and (iii) the motion of a drop in a vertical tube due to gravity

and Poiseuille flow. These are considered separately in the following three paragraphs.

The first case is that of the motion of a droplet, in a vertical tube, due to gravity with the fluid at rest far away from the drop. In this case the force exerted on the drop is equal to $\frac{4}{3}\pi a'^3(\rho'^{(1)} - \rho'^{(2)})g'$. Equating this force to the hydrodynamic drag as given in (3.22) with V'=0 yields:

$$- U_0'\lambda_u\xi' - \frac{4}{3}\pi a'^3(\rho'^{(1)} - \rho'^{(2)})g' = 0 \qquad (4.1)$$

In Eq.(4.1) the sign on each term denotes the direction of the force. From (4.1) the following equation for U_0' is obtained:

$$\frac{U_0'}{U_{H-R}'} = \frac{1}{\lambda_u} \qquad (4.2)$$

where U_{H-R}' denotes the Hadamard-Rybczynski gravitational terminal velocity in an infinite medium and is given below.

$$U_{H-R}' = - \frac{a'^2(\rho'^{(1)} - \rho'^{(2)})g'}{3\,\mu'^{(2)}}\left(\frac{1+\kappa}{1+3/2\kappa}\right) \qquad (4.3)$$

An illustration of the velocity field for this case for a'/b'=0.5 and κ=0.5 is given in Fig. 4 in the reference frame in which the sphere is stationary and the wall and the fluid at infinity are moving with velocity U_0'. At each point the magnitude of the velocity in this

illustration is nondimensionalized by U_0'. This field and others which follow are computed in the following manner: A portion of the flow field in the tube is divided into a grid. At each of the grid points the velocity is computed from the expressions for the stream function given in Eqs. (3.9) and (3.12). This is undertaken at a particular value of m, and m is then increased until a one percent convergence is obtained at all the grid points. Figure 4 shows clearly the circulation inside the drop owing to the shear stress exerted by the exterior fluid and the presence of a maximum in the magnitude of the velocity in the gap between the sphere and the tube wall.

The second case is the motion of a neutrally bouyant sphere in Poiseuille flow. In this case no force is exerted on the drop, and the hydrodynamic drag is equal to zero. Setting $F'_{z(0)}=0$ in (3.22) yields the relationship between U_0', the steady droplet velocity, and V', the centerline velocity of the Poiseuille flow:

$$\frac{U_0'}{V'} = \frac{\lambda_v}{\lambda_u} \tag{4.4}$$

Note that since $\lambda_v<\lambda_u$, the terminal velocity U_0' is always less than the centerline velocity V'. Note that λ_v/λ_u is a decreasing function of κ and a'/b' since as discussed above the disparity between λ_v and λ_u increases as either a'/b' or κ is increased. Thus the terminal velocity of a fluid droplet suspended in a Poiseuille flow will decrease relative to the Poiseuille centerline velocity V' as either κ or a'/b' is increased. Illustrations of the flow field for this case

are given in Figs. 5a and 5b for κ=0.5 and a'/b'=0.5 in the frame in which the drop is stationary and the wall is moving at U_0'. In these illustrations, as in Fig. 4, the magnitude of the velocity vector at each point is nondimensionalized by U_0'.

The flow fields of Figs. 5a and 5b show the recirculation of the continuous phase in the front and back of the drop due to the fact that the terminal velocity is less than the centerline velocity. The stagnation rings on the surface of the sphere which are caused by the recirculation are shown clearly in the inset schematic (5b). For decreasing values of U_0'/V' (for example due to increasing κ), the rings move towards the equator ($\theta=\pi/2$) as the recirculation becomes more pronounced. This trend is shown in Table IV where the location of the upstream stagnation ring is detailed as a function of κ for a'/b'=0.5.

The last case is a droplet moving in a vertical tube due to gravity with Poiseuille flow at infinity. The zeroth order force balance is:

$$(V'\lambda_v - U_0' \lambda_u)\xi' - \frac{4}{3}\pi a'^3(\rho'^{(1)} - \rho'^{(2)})g' = 0 \qquad (4.5)$$

from which the terminal velocity U_0' may be computed in terms of the centerline Poiseuille velocity and the gravitational force. Thus:

$$\frac{U_0'}{V'} = \frac{1}{\lambda_u}\frac{U'_{H-R}}{V'} + \frac{\lambda_v}{\lambda_u} \qquad (4.6)$$

It is clear from (4.6) that U_0'/V' may take on any value depending on the ratio U_{H-R}'/V'. As U_{H-R}'/V' decreases from zero and tends to $-\lambda_v$ (the value that arrests the sphere) U_0'/V' decreases from the neutrally bouyant value (λ_v/λ_u) towards zero. The stagnation ring moves from the neutrally bouyant location towards the equator ($\theta=\pi/2$). This behavior is detailed in Table IV for $\kappa=0.5$ and $a'/b' = 0.5$.

The centerline velocity for which the sphere remains suspended in the gravitational field of the vertical tube is obtained from (4.6) by setting $U_0' = 0$. The result is V' equal to $-U_{H-R}'/\lambda_v$. The velocity field around the arrested sphere is illustrated in Fig. 6, again for $a'/b'=0.5$ and $\kappa=0.5$. In this illustration the magnitude of the velocity vector is nondimensionalized by the centerline velocity V'. The flow field is similar to that of Fig. 4.

4.5 Surfactant Results

4.5.1 Hydrodynamic Drag Coefficients

As explained in §3.3, the first order hydrodynamic drag, $F_{z(1)}'$, is composed of three terms. Because of the linearity of the first order equations, these terms may be interpreted as the drags exerted on the droplet from three separate flow idealizations. The first idealization is the uniform flow, with magnitude $U_{(1)}'$, past a fixed sphere. This drag is dimensionally equal to $-\xi'\lambda_u U_{(1)}'$. The second and third idealizations are the flows caused by the surface force $\phi\frac{\partial}{\partial\theta}$

$(\frac{1}{\sin\theta}\frac{\partial}{\partial\theta}\sin\theta V_{s(0)})$, where $V_{s(0)}$ is equal to the zeroth order surface velocity resulting from uniform or Poiseuille flow. In these idealizations the wall and the fluid at infinity are motionless. The surface velocity is the sum of two contributions. The first is the surface velocity which results from uniform flow (with magnitude U_0') past a fixed sphere. The second is the surface velocity which results from Poiseuille flow, with centerline velocity V', past the fixed sphere. For the uniform flow contribution, when $U_0'>0$, surfactant is convected to the negative z pole, and therefore a Marangoni stress is directed from the negative z to the positive z pole. This traction causes the fluid to move in the positive z direction, and a balancing hydrodynamic drag in the negative z direction develops. The dimensional magnitude of this drag is equal to $-\xi'\phi\lambda_{u(1)}U_0'$. The flow pattern for $U_0'=1$ is shown in Fig. 7. The figure indicates that the magnitude of the fluid velocity is largest at the droplet surface. This high surface velocity is due to the fact that the driving force is being exerted on the surface. Also note from the figure that a recirculation develops in the gap between the sphere and the tube wall since the flow at infinity is equal to zero. For the second contribution, when V'>0, the zeroth order flow convects surfactant to the positive z pole and therefore a Marangoni stress is created which is directed from the positive to the negative pole. This causes fluid to move in the minus z direction, and an equalizing hydrodynamic drag develops in the positive z direction. The magnitude of this drag is equal to $\xi'\phi\lambda_{v(1)}V'$. The flow pattern for the Poiseuille induced surface force is given in Fig. 8 for V'=1. The structure is similar

to the field induced by the uniform flow, but the magnitude of the velocities is uniformly smaller. This can be explained as follows. As remarked in §4, for unit magnitudes of U_0' and V', the flow rate in the gap between the sphere and the tube wall for uniform flow is twice as large as that for Poiseuille flow. Since the flow rate is larger the change in the average velocity between the entrance and exit to the gap, and the gap center, is much larger for uniform flow than for Poisueille flow. Therefore the surface gradient of velocity and thus the dilatation is larger. Since the dilatation is proportional to the surface force it too is larger for the uniform flow and thus the velocities arising from the surface force for this case are larger.

The converged results for $\lambda_{u(1)}$ and $\lambda_{v(1)}$ are given, respectively, in Figs. 9 and 10 for κ=0, 0.5, 1 and 2 and the gap ratio a'/b' in the range 0.1 to 0.7. From these figures it is clear that $\lambda_{u(1)}$ and $\lambda_{v(1)}$ are, for fixed κ, increasing functions of a'/b'. This behavior is identical to the dependency of the zeroth order drags λ_u and λ_v on a'/b', and the reason is the same: At decreasing gap thicknesses, large shear rates develop around the particle and these high rates cause increased viscous shear stresses to be exerted on the drop. However, the dependency on the viscosity ratio for fixed a'/b' is different for the first order drag coefficients in that they decrease rather than increase with increasing κ. Note that when $\lambda_{u(1)}$ and $\lambda_{v(1)}$ are multiplied by ξ' which increases monotonically with κ, $\xi'\lambda_{u(1)}U'$ and $\xi'\lambda_{u(1)}V'$ and thus the actual drag still decreases with κ with $U_0'\phi$ and $V'\phi$ held constant. This phenomenon can be explained as follows. As the ratio of the droplet to the continuous phase

viscosity increases, the circulation within the droplet is diminished and the surface dilatation $\frac{\partial}{\partial\theta}\left(\frac{1}{\sin\theta}\frac{\partial}{\partial\theta}\sin\theta V_{s(0)}\right)$ is reduced. The reduction in the dilatation causes a decrease in the surface force which drives the flows in the two idealizations with respect to which $\lambda_{u(1)}$ and $\lambda_{v(1)}$ are defined. From Figures 9 and 10, it is clear that this decrease in drag due to the reduction in the surface force is not compensated by the increase in drag due to the increase in viscosity of the continuous fluid. Finally note from Figs. 7 and 8 that as a'/b' tends to zero, $\lambda_{u(1)}$ approaches $\lambda_{v(1)}$. This is to be expected since as $a'/b'\to 0$, the zeroeth order surface velocities for uniform and Poiseuille flow become equal. (Recall that in this limit, λ_u approaches λ_v).

As remarked in the Introduction, there have been no attempts in the literature to examine the hydrodynamic drag exerted on fluid particles in tubes for the case in which surfactants are adsorbed onto the fluid particle surfaces. However, the influence of surfactants on the drag exerted on particles in an infinite medium has been studied extensively and these studies may be used to verify the present results. In particular, for the case described in §2.2 in which sublayer-surface kinetic exchange is fast, but rate limiting, Levich (1962) derived the following expression for $\lambda_{u(1)}$:

$$\lambda_{u(1)} = \frac{\left(2 - \frac{1 + 2\kappa}{1 + \kappa}\right)}{3(1 + 3\kappa/2)}$$

Values from Levich's expression should agree with the converged values of $\lambda_{u(1)}$ as given in Fig. 9 as a'/b' tends to zero since in this limit the hydrodynamic effect of the wall on the drag becomes negligible. The values from Levich's expression for κ=0, 0.5, 1 and 2 are, respectively, 0.333, 0.127, 0.0667, and 0.0278. These values agree with the asymptotes in the figure, and this agreement provides a check of the first order results.

5.2 First order terminal velocities

In this subsection, the three flow circumstances which were examined previously in §4 are re-evaluated in order to compute the first order terminal velocities for each of these flows. The first flow is the motion, due to gravity, of a droplet in a vertical tube filled with a quiescent liquid. The zeroeth order velocity is given by equation (4.2), $U'_0=U'_{H\text{-}R}/\lambda_u$. Since the first order force exerted on the drop is equal to zero for the gravity driven motion, $F'_{z(1)}=0$, and Eq. (3.25) with V'=0 becomes:

$$-U'_{(1)}\lambda_u - \phi U'_0\lambda_{u(1)} = 0 \qquad (5.1)$$

From Eq. (5.1) $U'_{(1)}$ may be obtained. Thus

$$\frac{U'_{(1)}}{U'_0} = -\phi\left(\frac{\lambda_{u(1)}}{\lambda_u}\right) \qquad (5.2)$$

Note that since $U'_{(1)}$ is of opposite sign to U'_0, the presence of a surfactant reduces the droplet speed. A graphical representation of the dependence of $-U'_{(1)}/(\phi U'_0)$ on a'/b' for κ=0, 0.5, 1 and 2 is given in Fig. 11. (Note that ϕ is not a function of a'/b' or κ). The figure indicates that the relative correction is a decreasing function of κ. This is to be expected since λ_u increases with κ, and $\lambda_{u(1)}$ decreases with κ. Thus $\lambda_{u(1)}/\lambda_u$ must decrease with κ. The figure also shows that $-U'_{(1)}/U'_0$ is an increasing function of a'/b' for $a'/b'<0.5$. After this point as a'/b' increases the curves level-off, and for κ=0, begins to decrease. These results reflect the fact that for $a'/b'<0.5$, $\lambda_{u(1)}$ increases faster with a'/b' than does λ_u, but after 0.5 the reverse begins to be true.

For the gravity driven flow, the first order surfactant distribution ($\Gamma_{(1)}$) may be obtained from (2.42) with $C_{s(1)}$=0. A graph of $\Gamma_{(1)}/Bi^*(1+1/\zeta)$ for κ=0.5 and a'/b'=0.5 is presented in Fig. 12 (dashed line). The graph exhibits the accumulation of surfactant at the downstream pole ($\theta=\pi$) due to the zeroth order flow and is antisymmetric with respect to $\theta=\pi/2$ because of the symmetry in the velocity field (cf. the discussion at the beginning of §3).

The second flow circumstance is the motion of a neutrally-bouyant particle suspended in Poiseuille flow. The zeroeth order velocity is given by Eq. (4.4) as $U'_0=(\lambda_v/\lambda_u)V'$. Since the force on the drop is zero for this case, $F'_{z(1)} = 0$, and Eq. (3.25) may be used to solve for $U'_{(1)}$. The result is

$$\frac{U'_{(1)}}{U'_0} = -\phi \left(\frac{\lambda_{u(1)}}{\lambda_u} - \frac{\lambda_{v(1)}}{\lambda_v} \right) \qquad (5.3)$$

where use has been made of the zeroth order result $U'_0=(\lambda_v/\lambda_u)V'$ to eliminate V'. Graphs of $-U'_{(1)}/(\phi U'_{(0)})$ as a function of a'/b' for κ=0, 0.5, 1 and 2 are given in Fig. 13. The graphs indicate that $-U'_{(1)}/(\phi U'_{(0)})>0$ for the values of a'/b' and κ used, and therefore the droplet speed is once again retarded because of the surfactant adsorption. The dependencies of the correction on a'/b' and κ are similar to that for the gravity driven motion (Fig. 11).

The first order surfactant distribution for the motion of a neutrally bouyant sphere in Poisueille flow is given in Fig. 12 (solid line) for κ and a'/b' equal to 0.5. This figure should be compared with the zeroeth order velocity field as given in Figs. 5a and 5b. Because of the zeroth order flow, surfactant is swept away from the stagnation ring at 23.58° and the downstream pole, and towards the upstream pole and the stagnation ring at 156.42°. This causes the accumulation of surfactant at the upstream pole and the 156.42° ring and a depletion in the other two stagnation areas. Note importantly that even in this first order theory, the minima and maxima do not occur precisely at the stagnation zones but are offset from these. This is because (from (2.42)), extreme behavior in $\Gamma_{(1)}$ occurs when the dilatation is at a minima or maxima, not when the surface velocity is zero.

The last flow is the motion of droplet suspended in Poisueille flow in a vertical tube and acted upon by gravity. The zeroth order

velocity is given by Eq. (4.6). Again from (3.25) with $F'_{z(1)}$ the first order velocity may be obtained. The result is:

$$\frac{U'_{(1)}}{U'_0} = -\phi \left(\frac{\lambda_{u(1)}}{\lambda_u} - \frac{\lambda_{v(1)}}{\lambda_u} \frac{V'}{U'_0} \right) \tag{5.4}$$

for a given value of $\frac{V'}{U'_0}$. This latter ratio, obtained from (4.6) is a function of U'_{H-R} and may take on any value depending on U'_{H-R}. Thus for this case the droplet speed may be accelerated in the presence of surfactant absorption if V'/U'_0 is large enough. This possibility is indicated in Table IV, where it is shown that for $\kappa=a'/b'=0.5$, values of U'_0/V' less than or equal to 0.8 result in acceleration of the particle ($U'_{(1)}/U'_0>0$).

4.6 Discussion and Summary

This study has focused on the determination of the hydrodynamic drag exerted on a spherical fluid particle in a tube for the cases in which the particle interface is clean and covered by surfactant adsorbed from the continuous liquid phase filling the tube. For the case of a clean interface, the converged drag coefficents for uniform and Poiseuille flow past a fixed sphere were found to be within one-tenth of a percent or less of the values obtained by Hyman and Skalak (1969 and 1970) for sphere to tube diameter ratios of 0.1 to 0.8 and particle to continuous phase viscosity ratios of 0 and 1 (Table III). This agreement (as well as the agreement with solid sphere results,

Table II) lends confidence to the surfactant calculations which were undertaken using the same collocation scheme as that for the clean surface. Fully converged velocity fields and values for the location of surface stagnation points - hydrodynamic details not computed by Hyman and Skalak - were also calculated.

With regards to the motion of a surfactant-laden drop, to compute the influence of the adsorbed monolayer on the hydrodynamic drag, the surface surfactant distribution must be determined so as to calculate the interfacial tension gradient or Marangoni force. The calculation of this distribution is a complicated problem because of the involved nature of surfactant transport. The distribution of surfactant on the particle interface is determined by the competing effects of bulk and surface diffusion and convection, and the kinetic exchange of surfactant between the particle surface and the sublayer of fluid underneath the surface. In this study a perturbative approach was adopted which simplifies the determination of the surfactant surface concentration by isolating in a simplified way one nonconvective transport mechanism, kinetic exchange. In this approach, the kinetic exchange of surfactant at the interface by adsorption and desorption is assumed to be much faster than the time for convection of surfactant from one pole of the drop to the other ($Bi=O(\epsilon^{-1})$ and $\zeta=O(1)$, $\epsilon<<1$)). Diffusion of surfactant in the bulk and surface is relegated to higher order effects by the assumption that the bulk and surface Peclet numbers are of order one, and the adsorption depth Peclet number Pe_A is of order $O(\epsilon^2)$. Within this perturbation scheme, to order zero in ϵ, the surface surfactant concentration was shown to be uniform, and the drag was therefore

described by the clean surface drag coefficients λ_u and λ_v. The first order surfactant distribution is determined solely by the zeroth order surface dilatation. The first order drag coefficents were computed from the Marangoni surface force corresponding to the first order surfactant distribution. The solutions obtained for the flow due to the Marangoni surface force may be viewed in a general way since the flow due to any arbitrary surface force may be obtained from the framework by replacing the ϕ term on the left hand side of (3.19) with the arbitrary surface force exerted as a funtion of θ.

The results for uniform flow resembled those for uniform flow past a spherical droplet in an infinite medium: The only stagnation regions along the clean surface are at the poles (Fig. 4); surfactant molecules collect at the downstream stagnation pole (Figs. 12), and the resulting Marangoni stress retards the terminal velocity ($U'_{(1)}/U'_0$ <0, Fig. 11). Recall that in this statement and the ones that follow below, for $U'_0>0$, the upsteam pole is the pole at $\theta=0$ and the downsteam pole is at $\theta=\pi$ and the upstream (downstream) stagnation rings are located at positive (negative) z (refer to Figure 1).

The most interesting surfactant results were obtained for particles placed in Poiseuille flow. For neutrally bouyant particles the zeroth order flow exhibited two stagnation points at the poles and two stagnation rings (Figs. 5a and 5b). The surface flow for this case is such that fluid moves away from the upstream stagnation ring and downstream pole and towards the upstream pole and downstream stagnation ring. It is important to note that the back flow towards the upstream stagnation point and away from the downstream pole is due to the Poiseuille component of the flow at infinity. As the

centerline velocity V' increases relative to U_0', the stagnation rings move towards $\theta=\pi/2$ (Table IV). As a result of the zeroth order surface velocity distribution, surfactant accumulates in the first order state at the upstream pole and downstream stagnation ring and is depleted at the other stagnation zones (Fig. 12). Between the upstream stagnation ring and upstream pole a Marangoni tension in the minus z direction is created. The same is true between the downstream pole and downstream stagnation ring. These Marangoni tractions are balanced by stresses exerted in the positive z direction by the liquid surrounding the fluid particle. Such stresses accelerate the particle, and therefore tend to make $U_{(1)}'/U_0' > 0$. Between the downstream and upstream rings a Marangoni tension in the positive z direction arises, and a balancing continuous fluid drag decelerates the particle as it acts in the minus z direction. These effects are reflected in Eq. (5.4) where the first term on the right hand side accounts for the retarding stress of the region between the rings and the second term represents the accelerating stresses of the ring to pole regions. For the case of the neutrally bouyant particle, the relationship between V' and U_0' is such that the decelerating effects predominate and the velocity is retarded (Fig. 13, Table IV).

If the densities of the particle and continuous phases are not equal, then the particle is subject to a bouyancy force. When the particle is placed at the center of a vertical tube and suspended in Poiseuille flow with fixed centerline velocity V', U_0'/V' is determined by the ratio of the gravitational settling velocity in an infinite medium U_{H-R}' (a measure of the bouyancy force) to V' (Eq. (4.6)). Several cases are possible. If the bouyancy force and the centerline

velocity are in the same direction, then $U'_{H-R}/V'>0$. From Eq. (4.6) it is clear that for this case $U'_0/V'>0$ and is larger than the neutrally bouyant value. From Eq. (5.4), $U'_{(1)}/U'_0<0$ and, in fact, is larger (in absolute value) than the neutrally bouyant value. Thus for this case the drop is retarded even more than for the case of the neutrally bouyant sphere. The reason is clear: As U'_{H-R}/V' increases from zero, U'_0/V increases from the neutrally bouyant value and the stagnation rings approach the poles. The regions on the surface of Marangoni stress which cause acceleration of the drop disappear, and thus retardation is increased.

Consider next the case in which the bouyancy force is in the opposite direction to that of the Poiseuille centerline velocity ($U'_{H-R}/V' <0$) but larger than $-\lambda_v$ (the value which arrests the clean sphere translation). Then U'_0/V' is still larger than zero (Eq. (4.6), but smaller than the neutrally bouyant value of λ_v/λ_u. As U'_{H-R}/V' tends to $-\lambda_v$, U'_0/V' tends to zero (Eq. (4.6)) and Eq.(5.4) indicates that $U'_{(1)}/U'_0$ will become larger than zero. Thus droplet acceleration can be realized in the limit in which U'_{H-R}/V' tends to $-\lambda_v$ and U'_0/V consequently becomes vanishingly small. The reason is as U'_{H-R}/V' approaches $-\lambda_v$, the stagnation rings approach $\pi/2$ and the Marangoni stresses which accelerate the drop increase at the expense of those which retard the translation. Hence the eventual increase in speed with surfactant adsorption.

Finally, for the case in which the bouyancy and the centerline velocity are in opposite directions ($U'_{H-R}/V' <0$) and $U'_{H-R}/V' <-\lambda_v$,

U_0'/V' becomes less than zero (Eq. (4.6)) and the sphere moves opposite to the Poiseuille flow. The surfactant distribution increases monotonically towards the downstream pole (now at θ=0) and Marangoni stresses simply retard the speed ($U_{(1)}'/U_0' < 0$, Eq. (5.4)).

Appendix A

$$\begin{bmatrix} S_n^3 \\ S_n^4 \end{bmatrix} = P_{n-1}(\cos\theta) + \int_0^\infty dk\{k\sin(k\cos\theta)\left[\begin{bmatrix} T_n^1 \\ T_n^2 \end{bmatrix} \sin\theta I_1(k\sin\theta)\right.$$

$$\left. + \begin{bmatrix} T_n^3 \\ T_n^4 \end{bmatrix} \sin^2\theta I_0(k\sin\theta)\right] + \cos(k\cos\theta)\left[\begin{bmatrix} T_n^1 \\ T_n^2 \end{bmatrix} k\cos\theta I_0(k\sin\theta)\right.$$

$$\left. + \begin{bmatrix} T_n^3 \\ T_n^4 \end{bmatrix} (2\cos\theta I_0(k\sin\theta) + k\sin\theta\cos\theta I_1(k\sin\theta))\right]\}$$

$$\begin{bmatrix} S_n^5 \\ S_n^6 \end{bmatrix} = \begin{bmatrix} (1-n) \\ (3-n) \end{bmatrix} \frac{C_n^{-1/2}(\cos\theta)}{\sin\theta} + \int_0^\infty dk\{k\cos\theta\sin(k\cos\theta)$$

$$\left[- \begin{bmatrix} T_n^1 \\ T_n^2 \end{bmatrix} \sin\theta I_1(k\sin\theta) - \begin{bmatrix} T_n^3 \\ T_n^4 \end{bmatrix} \sin\theta I_0(k\sin\theta)\right]$$

$$+ \sin\theta\cos(k\cos\theta)\left[\begin{bmatrix} T_n^1 \\ T_n^2 \end{bmatrix} kI_0(k\sin\theta)\right.$$

$$\left. + \begin{bmatrix} T_n^3 \\ T_n^4 \end{bmatrix} (2I_0(k\sin\theta) + k\sin\theta I_1(k\sin\theta))\right]\}$$

$$\begin{bmatrix} S_n^7 \\ S_n^8 \end{bmatrix} = \begin{bmatrix} S_n^5 \\ S_n^6 \end{bmatrix} - \left(\begin{bmatrix} (n^2-1) \\ (3-n)(1-n) \end{bmatrix} \frac{C_n^{-1/2}(\cos\theta)}{\sin\theta} + \int_0^\infty dk\{\cos(k\cos\theta) \right.$$

$$\left[\begin{bmatrix} T_n^1 \\ T_n^2 \end{bmatrix} k^2(\sin^2 - \cos^2\theta) I_1(k\sin\theta) \right.$$

$$\left. + \begin{bmatrix} T_n^3 \\ T_n^4 \end{bmatrix} \sin\theta (k^2(\sin^2\theta - \cos^2\theta) I_0(k\sin\theta) + 2k\sin\theta I_1(k\sin\theta)) \right]$$

$$- k\cos\theta\sin(k\cos\theta) \left[\begin{bmatrix} T_n^1 \\ T_n^2 \end{bmatrix} (2k\sin\theta I_0(k\sin\theta)\ I_0(k\sin\theta)) \right.$$

$$\left. - I_1(k\sin\theta)) + \begin{bmatrix} T_n^3 \\ T_n^4 \end{bmatrix} (3\sin\theta I_0(k\sin\theta) + 2\sin^2\theta k I_1(k\sin\theta)) \right] \}$$

Table I.

The number of collocation points necessary to achieve the accuracy requirement for the gas bubble (κ=0)

λ	a'/b	0.1	0.2	0.3	0.4	0.5	0.6	0.7	0.8	0.9
λ_u, λ_v	m	4	4	5	7	7	9	10	11	13
$\lambda_{(1)}$	p	4	4	5	7	7	9	10	11	13
	m	3	4	5	5	6	6	6	9	10

Table II.

Comparison of converged values of drag coefficients λ_u and λ_v with the results of Haberman and Sayre (1958) and Wang and Skalak (1969) for a solid particle ($\kappa = 10^8$).

			Haberman and Sayre		Wang and Skalak	
a'/b'	λ_u	λ_v	λ_u	λ_v	λ_u	λ_v
0.0	1.0000	1.0000	1.000	1.000	1.000	1.000
0.1	1.2632	1.2547	1.263	1.255	1.263	1.255
0.2	1.6795	1.6348	1.680	1.635	1.680	1.635
0.3	2.3701	2.2289	2.371	2.231	2.370	2.229
0.4	3.5914	3.2157	3.596	3.218	3.592	3.216
0.5	5.9474	4.9953	5.970	5.004	5.949	4.996
0.6	11.092	8.6130	11.135	8.651	11.10	8.617
0.7	24.676	17.474	24.955	17.671	24.70	17.49
0.8	74.670	47.620	73.555	47.301	74.97	47.81
0.9	469.15	266.37				

Table III.

Comparison of converged values of drag coefficients λ_u and λ_v with the results of Hyman and Skalak's exact solution (1970) for a fluid droplet.

				Hyman and Skalak	
a'/b'	κ	λ_u	λ_v	λ_u	λ_v
0.1	0.0	1.1632	1.1631	1.16	1.16
	1.0	1.2111	1.2063	1.211	1.206
0.2	0.0	1.3900	1.3895	1.39	1.39
	1.0	1.5209	1.4965	1.520	1.496
0.3	0.0	1.7251	1.7211	1.725	1.722
	1.0	1.9951	1.9222	1.995	1.922
0.4	0.0	2.2626	2.2486	2.263	2.241
	1.0	2.7647	2.5820	2.765	2.582
0.5	0.0	3.2224	3.1295	3.222	3.130
	1.0	4.1197	3.6847	4.123	3.685
0.6	0.0	5.2043	4.8453	5.205	4.846
	1.0	6.8070	5.7435	6.808	5.744
0.7	0.0	10.257	8.8356	10.26	8.838
	1.0	13.242	10.321	13.22	10.32
0.8	0.0	28.615	21.704	28.59	21.72
	1.0	34.450	24.231	34.47	24.26
0.9	0.0	173.39	109.89		
	1.0	182.98	111.91		

Table IV.

Angular location of upstream stagnation ring (a'/b'=0.5).

κ	U_0'/V'	θ	$-U'_{(1)}/U'_0\phi$
Neutrally bouyant			
0.0	0.9712	14.84°	0.1335
0.5	0.9169	23.58°	0.0491
1.0	0.8944	26.59°	0.0254
2.0	0.8743	29.10°	0.0104
Suspended droplet acted upon by bouyancy (κ=0.5)			
0.5	0.85	41.10°	0.0076
	0.80	54.16°	-0.0096
	0.75	72.50°	-0.1077

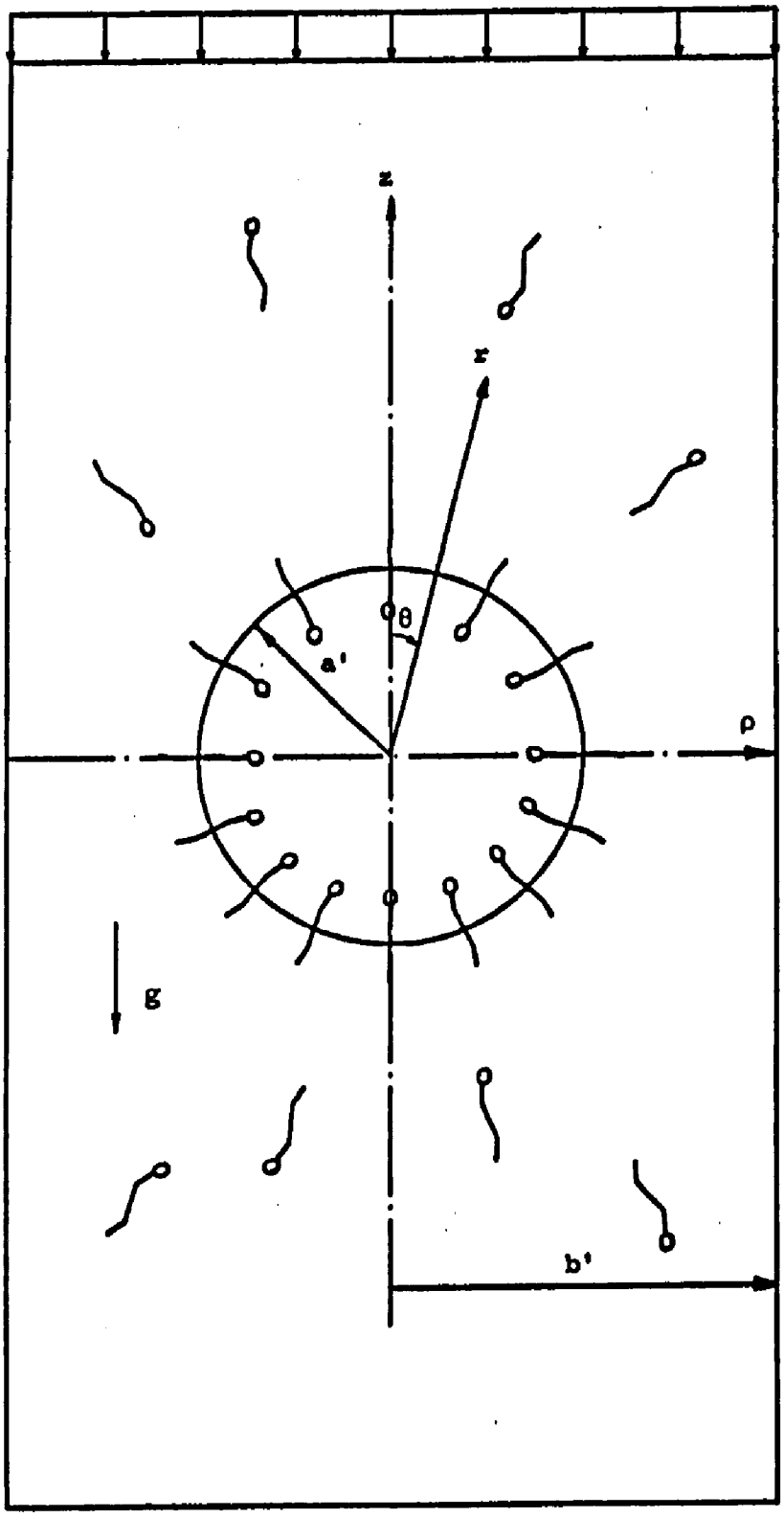

Figure 1

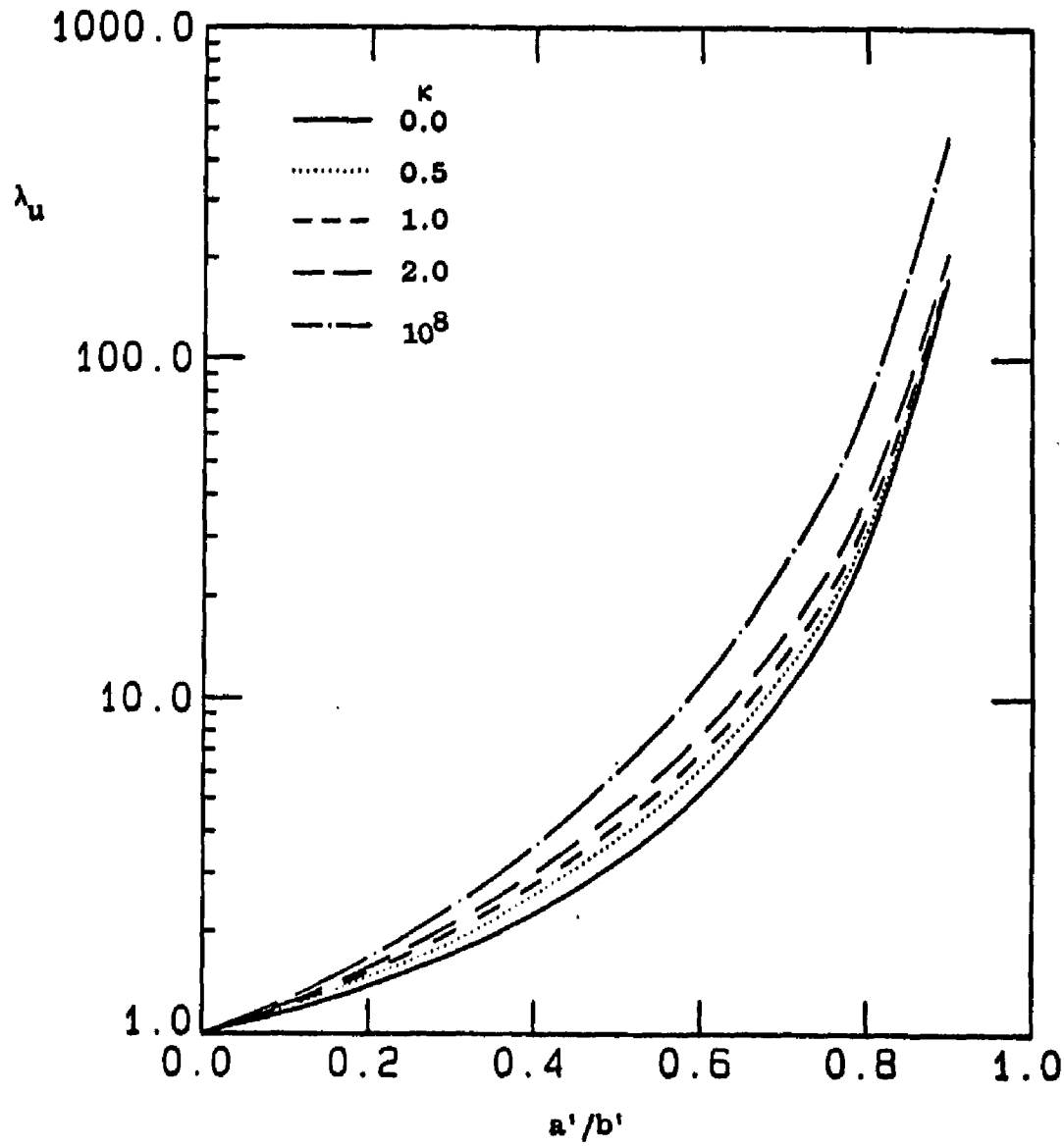

Figure 2

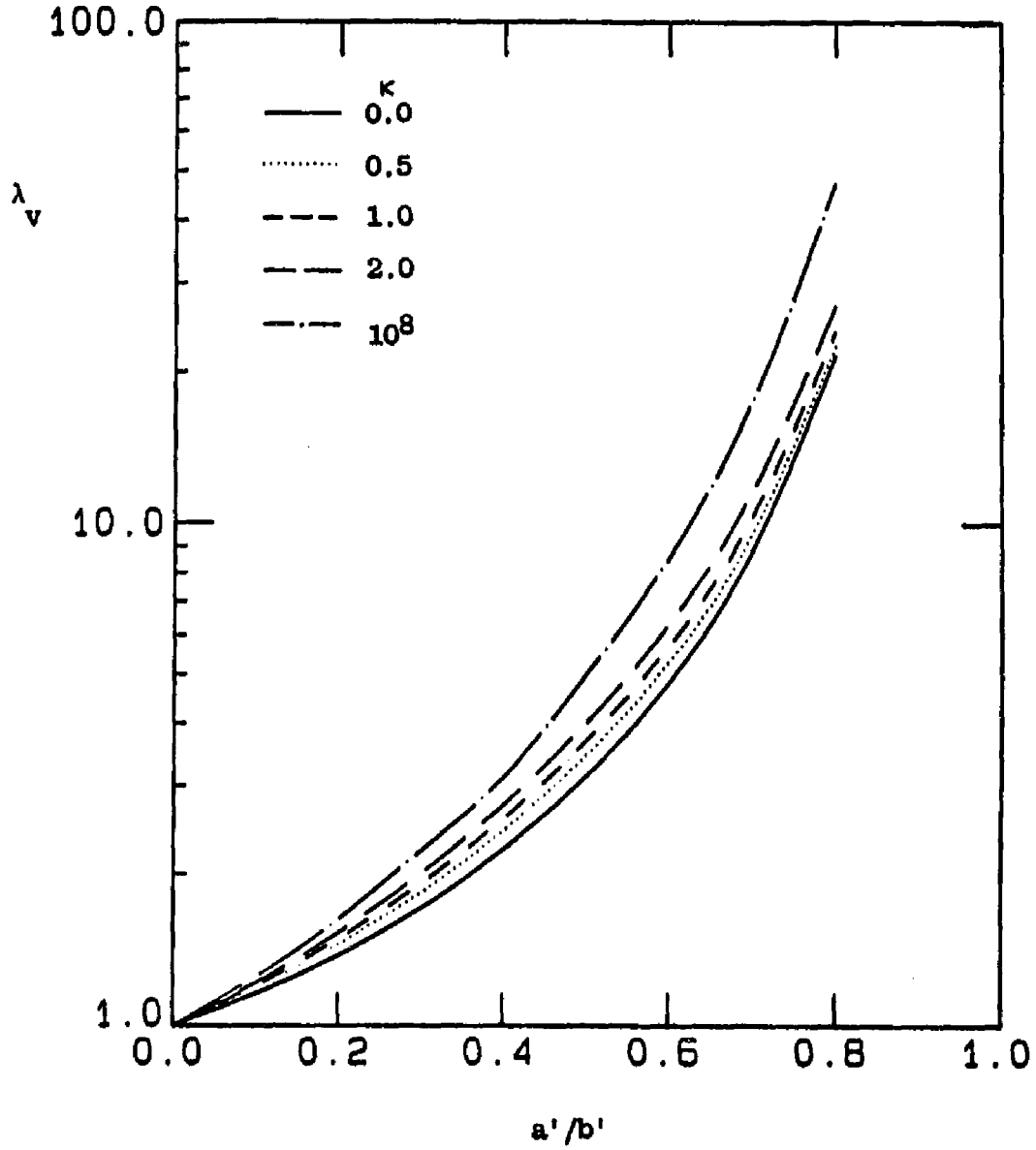

Figure 3

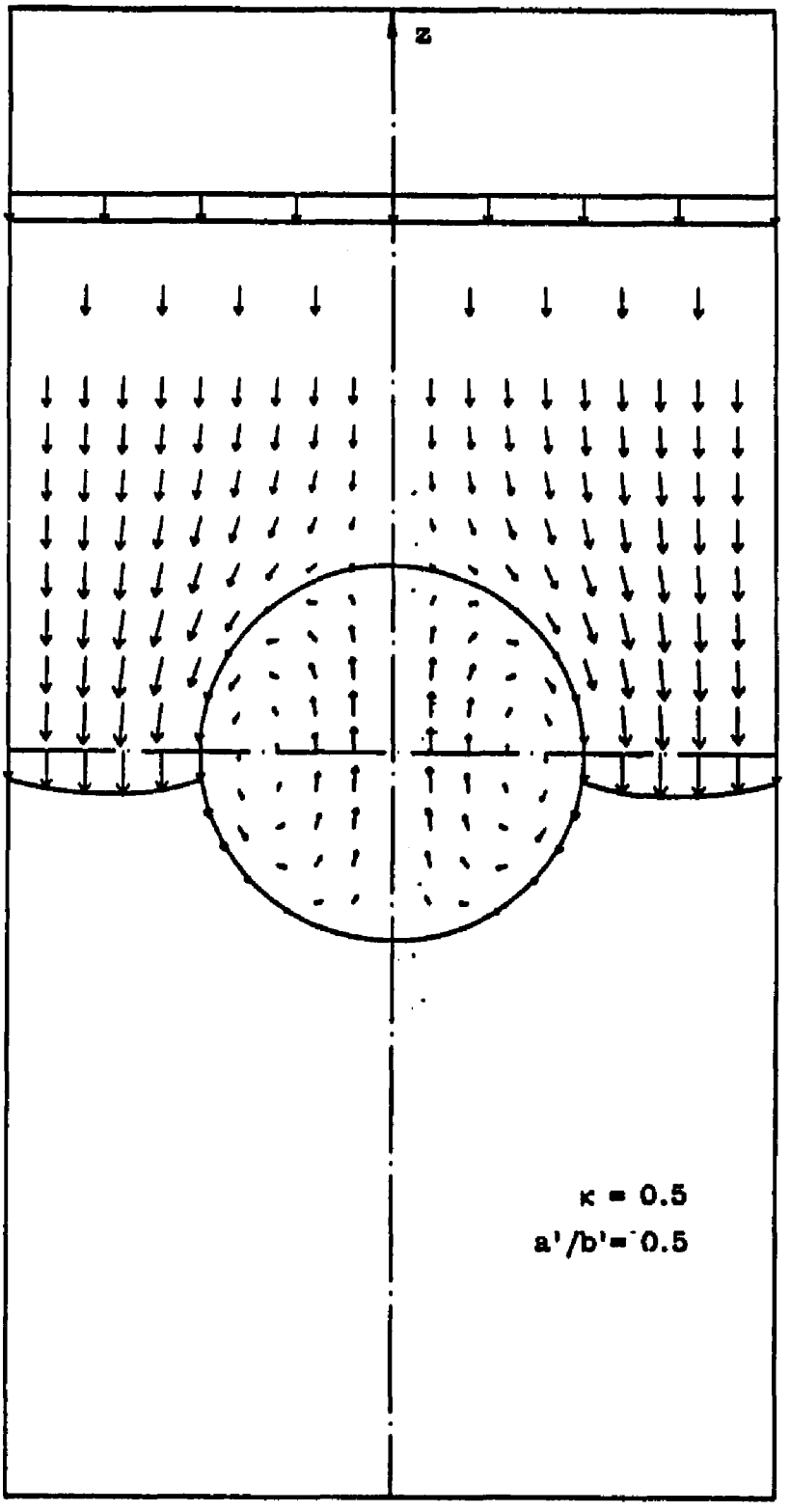

Figure 4

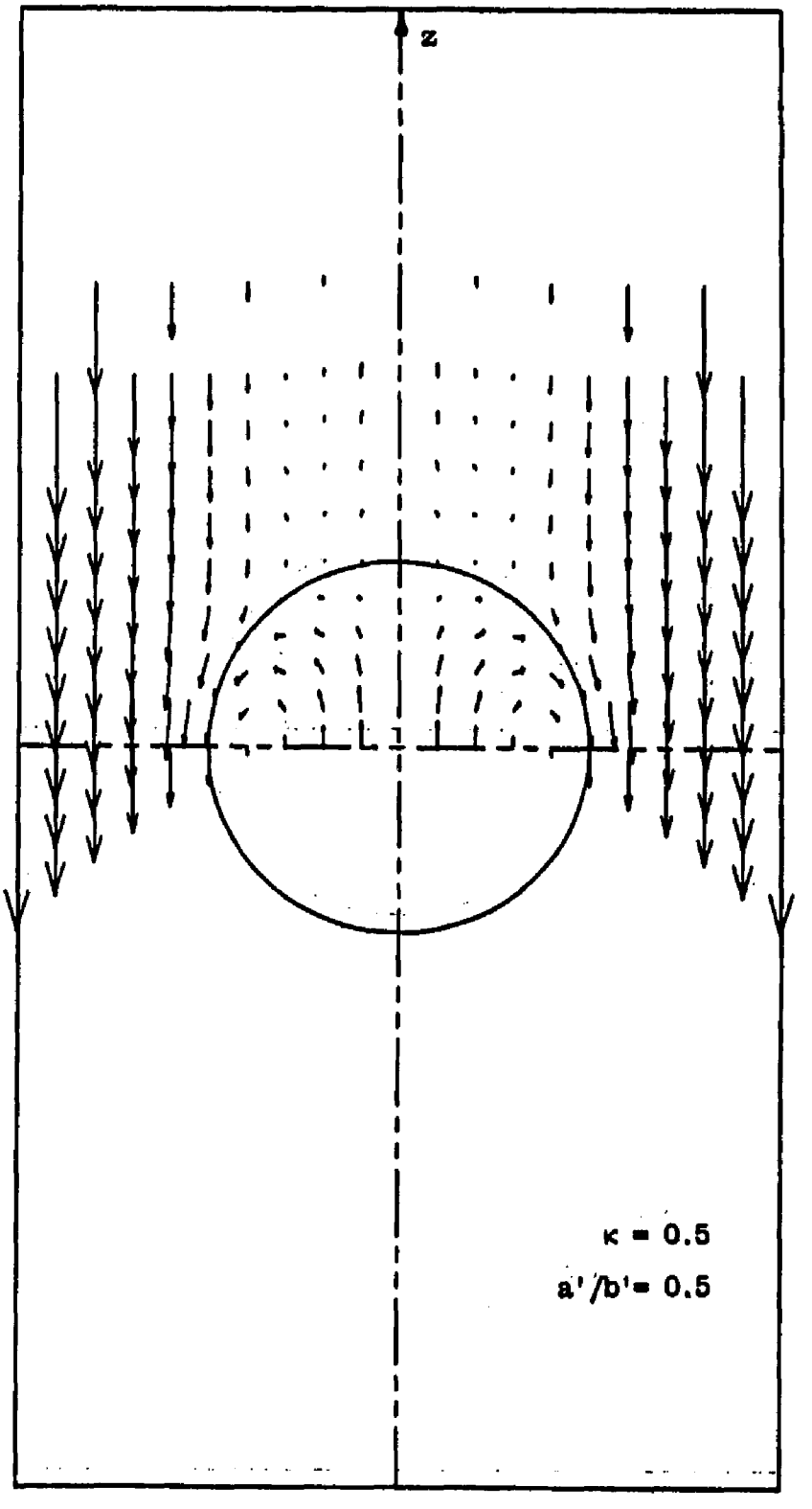

Figure 5a

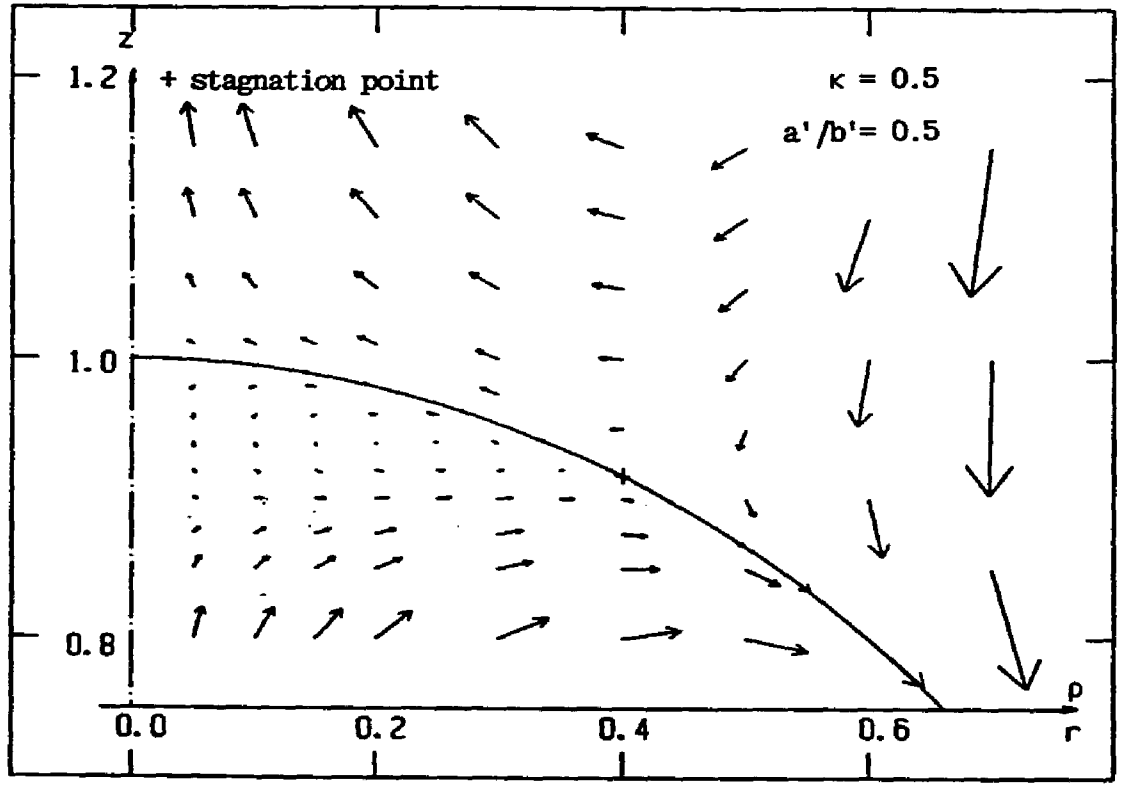

Figure 5b

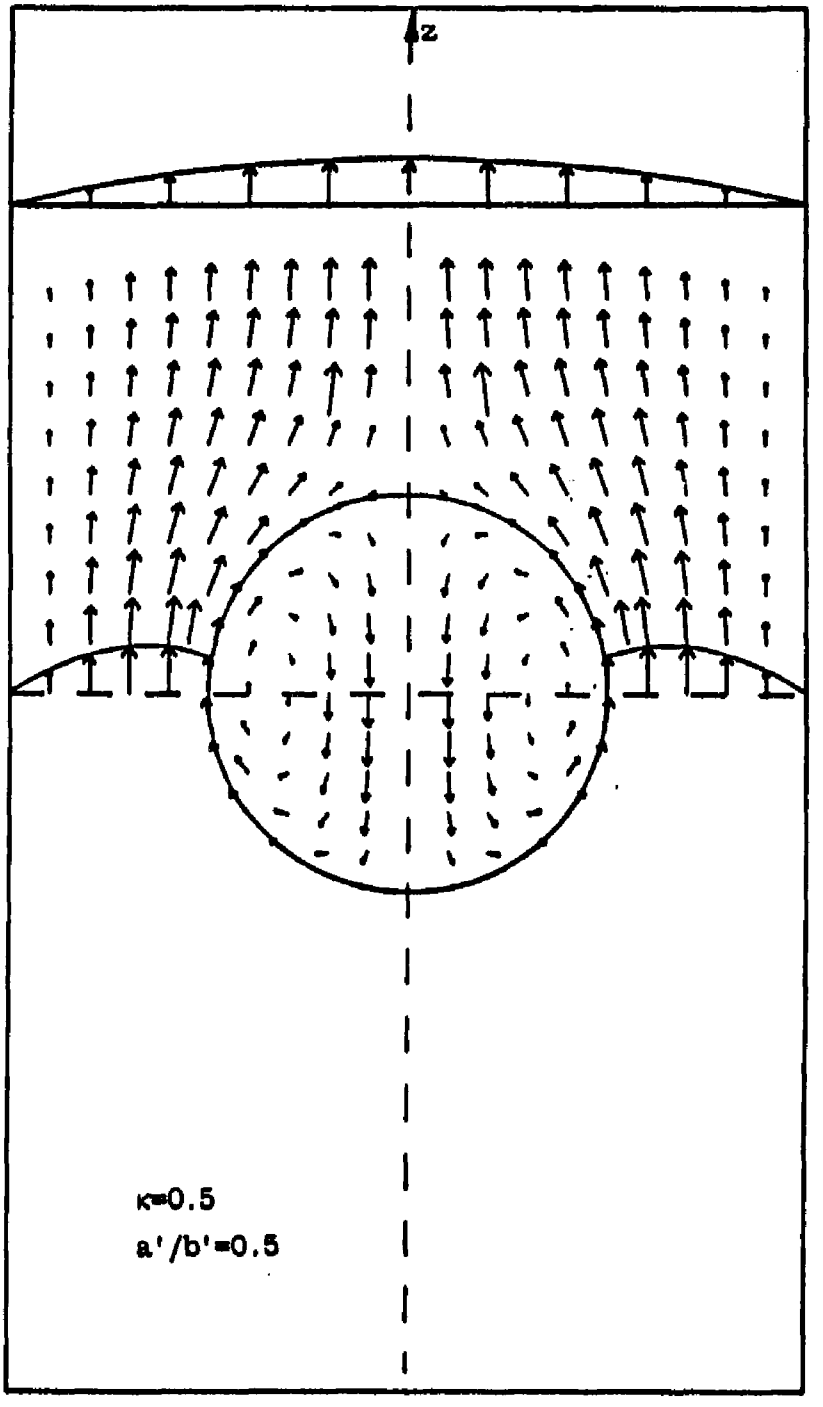

Figure 6

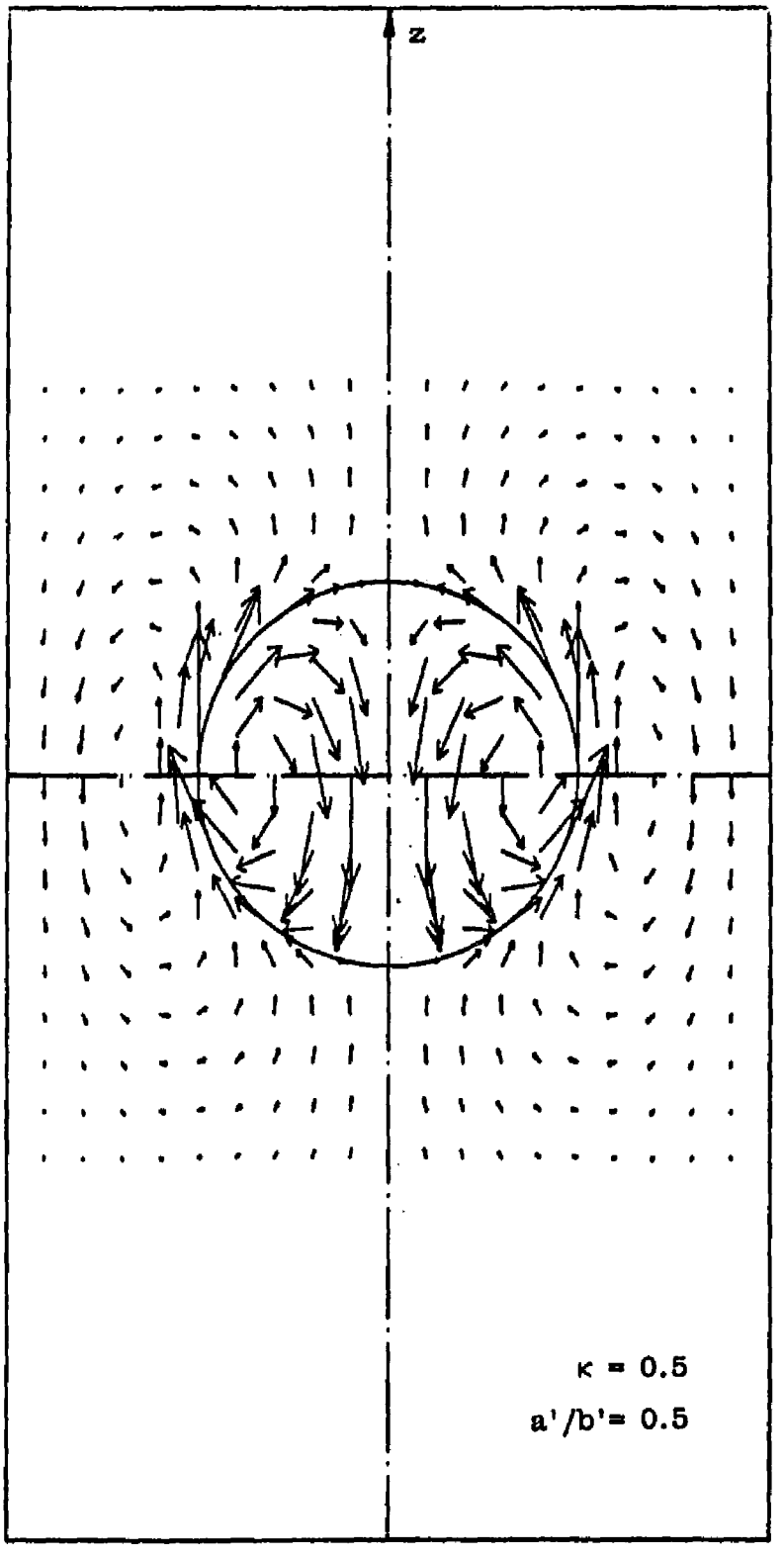

Figure 7

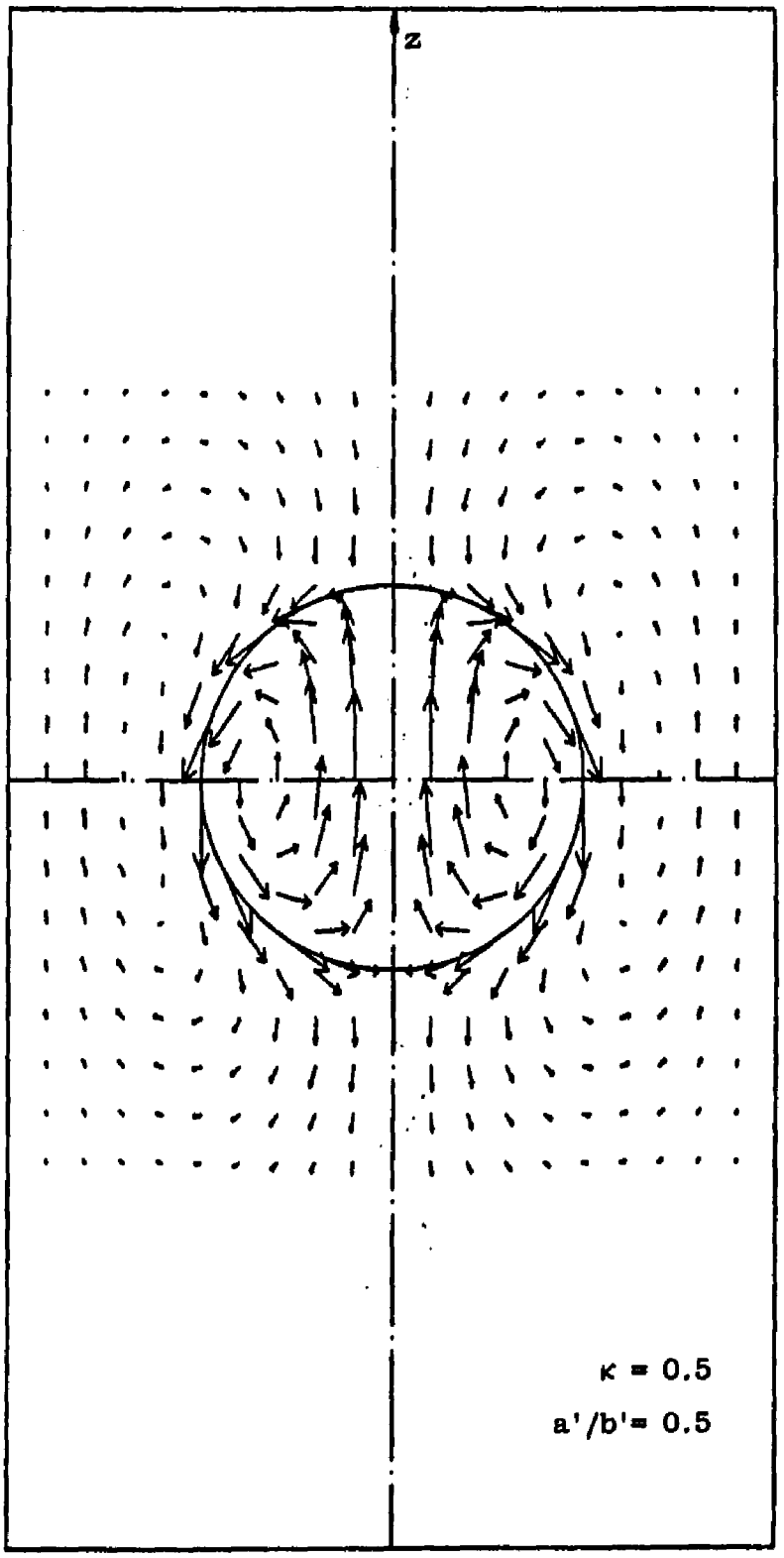

Figure 8

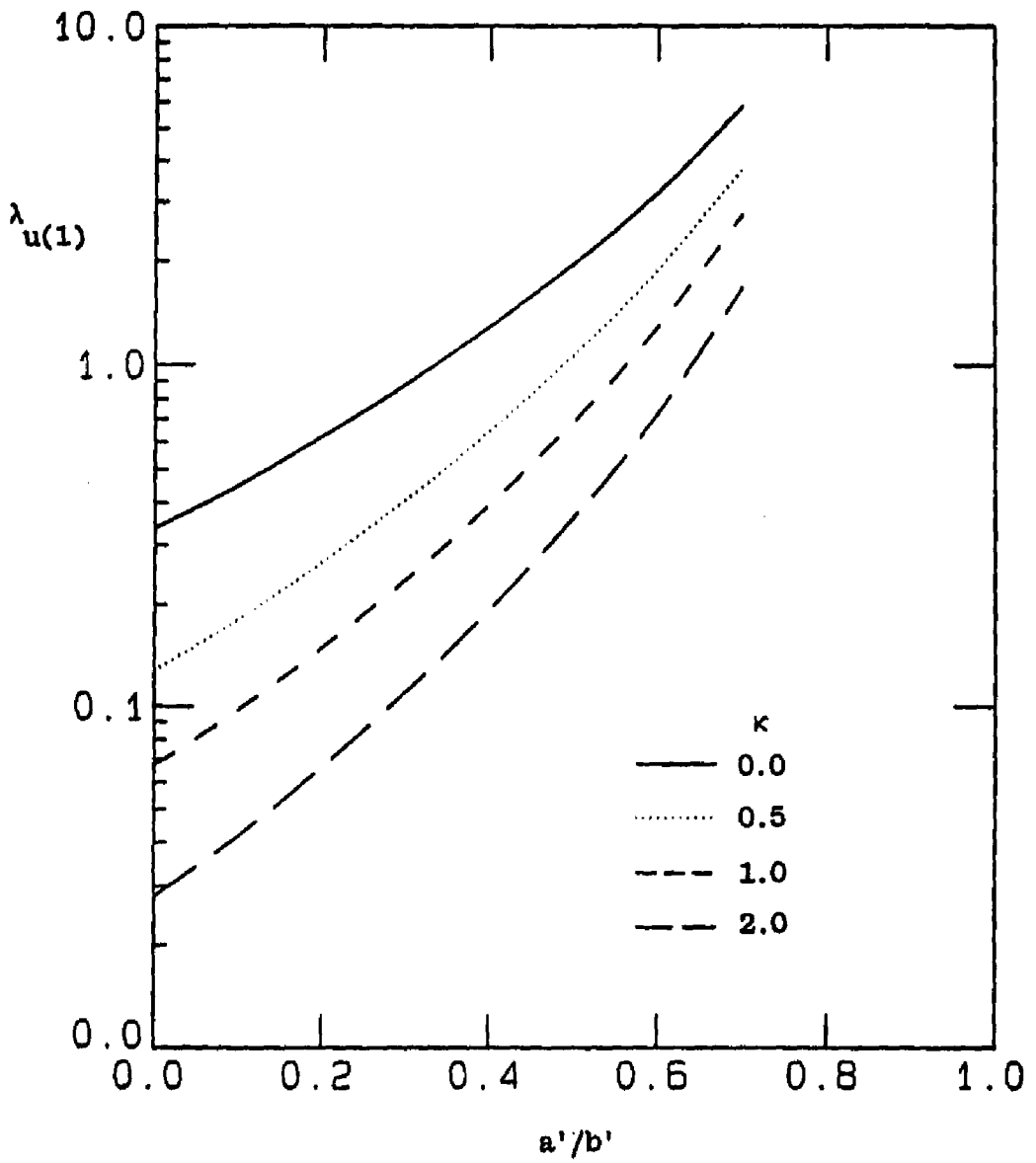

Figure 9

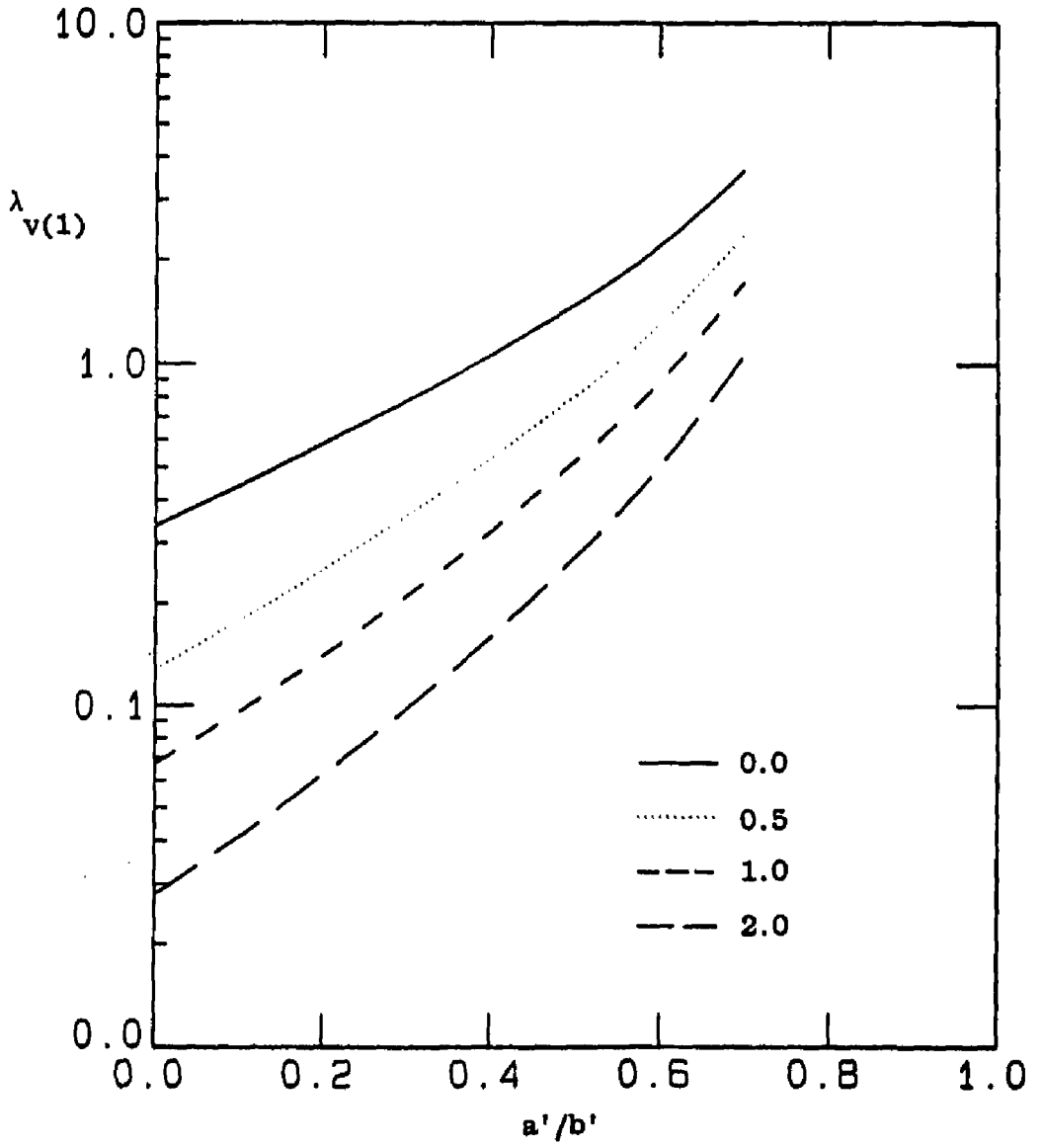

Figure 10

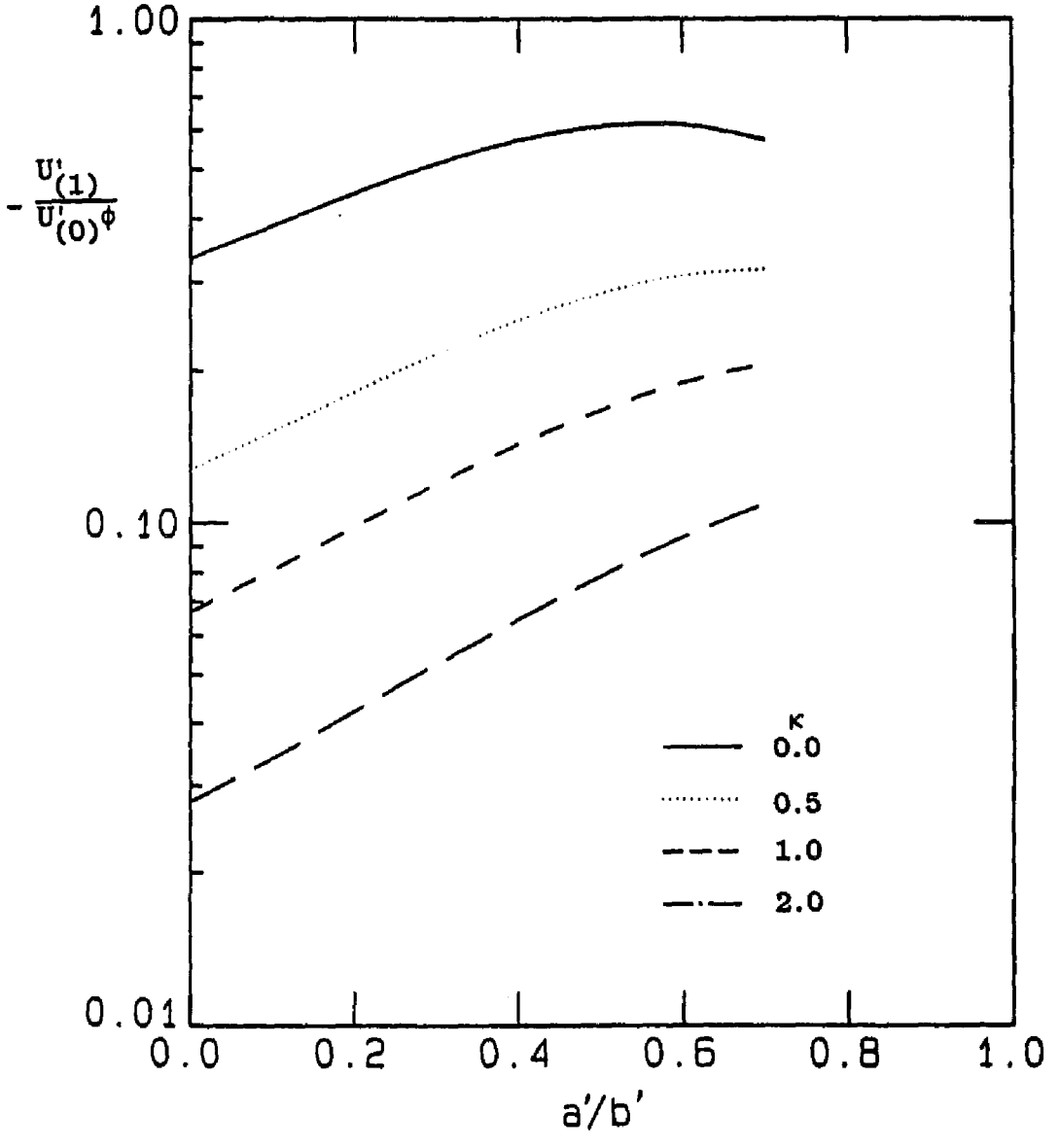

Figure 11

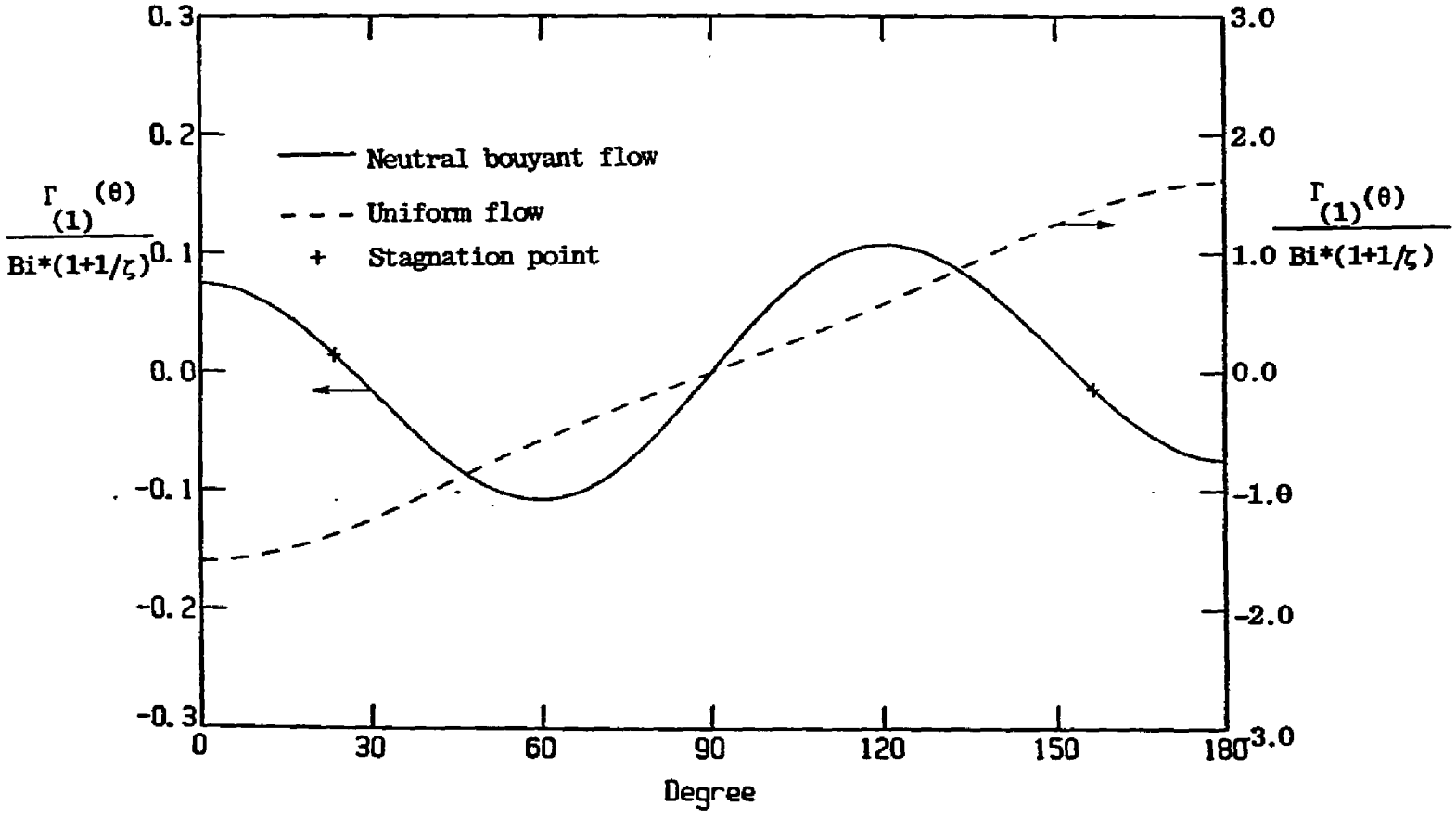
0.3
0.2
0.1
0.0
-0.1
-0.2
-0.3
3.0
2.0
1.0
0.0
-1.0
-2.0
-3.0
0
30
60
90
120
150
180
Degree
Neutral bouyant flow
Uniform flow
Stagnation point
Γ(1)(θ) / Bi*(1+1/ζ)
Γ(1)(θ) / Bi*(1+1/ζ)

Figure 12

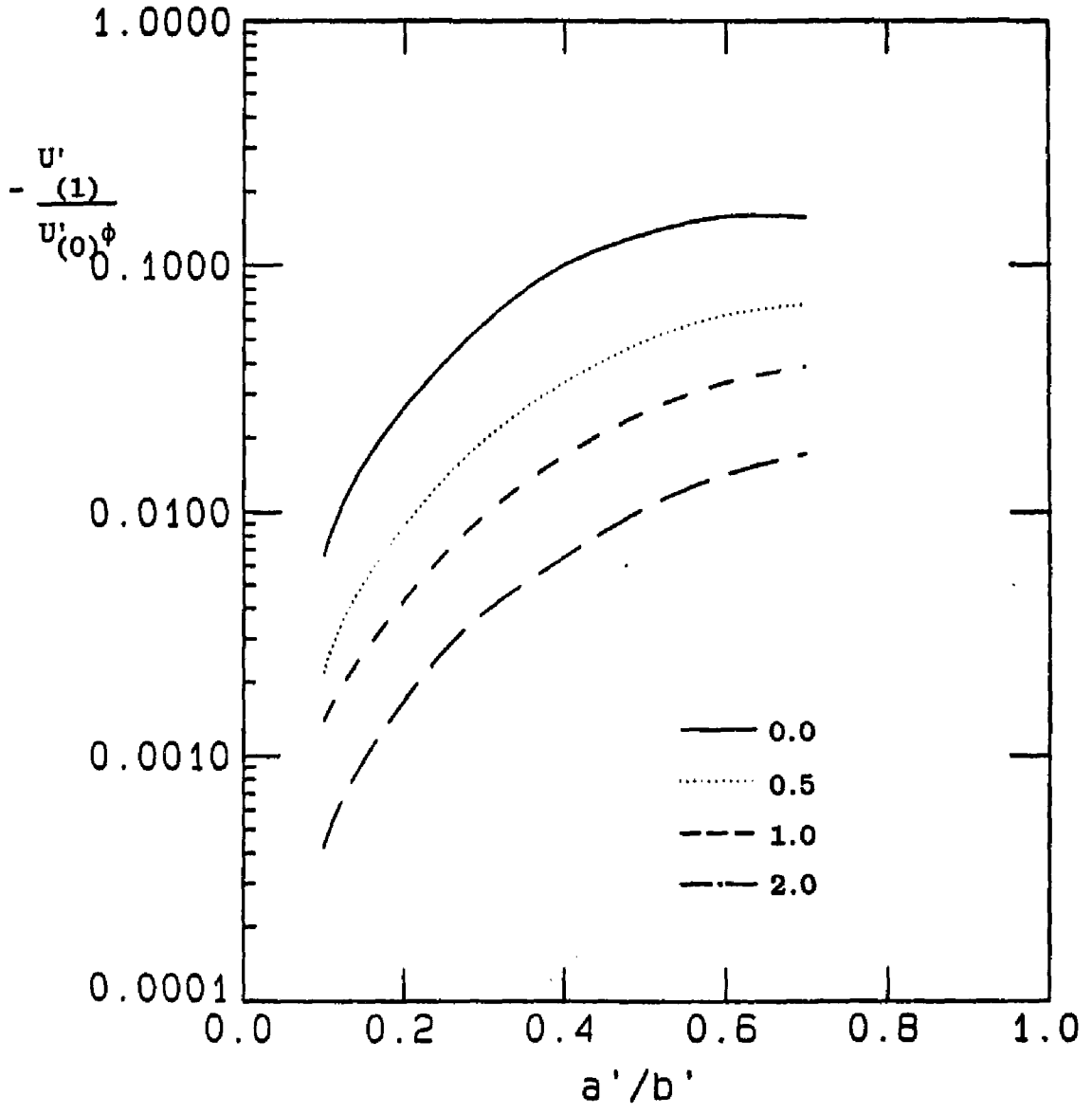

Figure 13

Chapter 5

The Influence of Surfactant on Droplet Motion Inside a Cylindrical Tube: II. Stagnant Cap Regime

5.1 Introduction

This chapter is the second part of a two part study on the influence of surfactants on the creeping translation of a fluid sphere in a cylindrical tube. As is well known, the presence of surfactant molecules in the continuous phase through which a fluid droplet translates reduces the terminal velocity of the droplet. The mechanism for this physicochemical effect was first suggested by Frumkin and Levich (1947). When a fluid droplet moves through a continuous liquid phase that contains a bulk soluble surfactant, the surfactant molecules adsorb onto the interface of the droplet. Once adsorbed, they are convected to the trailing or rear pole of the droplet where they accumulate in the vicinity of that pole. This accumulation eventually causes desorption of the molecules into the sublayer of liquid immediately adjacent to the rear part of the interface. The desorption locally elevates the bulk concentration of surfactant relative to the concentration far from the drop, and the surfactant diffuses away into the bulk. The convection of surfactant to the rear lowers the surface concentration near the leading pole and leads to both a surface diffusive flux from the rear to the leading pole, and additional adsorption from the adjoining liquid sublayer at the droplet front. The sublayer concentration, depleted by this

adsorption, is replenished by diffusion as the concentration of surfactant in this sublayer is lower than that far from the drop.

The accumulation of surfactant at the rear of the drop by convection lowers the interfacial tension in this region relative to the front end because the surfactant molecules which are compressed at the rear by the accumulating action of the convection exert an outward force (the surface pressure). This difference in interfacial tension causes the surface to be tugged towards the front pole and since this action (a Marangoni tension) is opposite to the direction of surface convection, the surface flow is retarded. The reduction in the surface flow increases the drag exerted by the continuous phase on the droplet, causing the droplet to decelerate.

The surfactant gradient which develops at steady state determines the Marangoni tension and hence the magnitude of the terminal velocity reduction. The gradient which evolves is a function of the relative rates with which the surfactant transport processes take place. Two regimes provide bounds on the retardation. If the rate of surface convection is much slower than either the rate of surface diffusion, or the rates of the series mechanisms of adsorption and desorption and bulk diffusion, then the surface concentration is asymptotically close to Γ_0', the value which is realized under equilibrium (zero-flow) conditions. In this case, the concentration at the rear of the drop is only slightly larger than Γ_0', and that at the front end is just less than Γ_0'. This is the regime of uniform retardation, referred to as such because the small deviation of the surface concentration from Γ_0' creates a distributed Marangoni tension which uniformally retards the surface velocity. The regime has been studied theoretically for the

motion of a drop in an infinite medium by Frumkin and Levich (1947), Levich (1962), Newman (1966), Schechter and Farley (1963) and Agrawal and Wasan (1979). In Part I of this series, the uniform retardation regime was studied for fluid spheres in tubes.

If the rate of surface convection is fast both with respect to the rate of surface diffusion and fast when compared to either the rate of bulk diffusion or the rates of adsorption and desorption, then the surfactant is swept into a cap region where the surface velocity is equal to zero. For a given bulk concentration of surfactant, this regime results in the greatest retardation. Obviously, if enough surfactant is present in the continuous phase the stagnant cap angle can stretch across the entire surface of the droplet resulting in a completely immobile interface and a terminal velocity characteristic of a solid particle. The stagnant cap regime has been examined theoretically for the infinite medium case by Savic (1983), Griffith (1962), Davis and Acrivos (1966), Harper (1972, 1973, 1974 and 1982), and Sadhal and Johnson (1982).

In this chapter, we study the stagnant cap regime for a fluid sphere in a tube. We consider the case of a single droplet translating in steady, axisymmetric creeping flow with the interfacial tension large enough so that viscous tractions do not distend the droplet from sphericity. Thus both the Reynolds and capillary numbers are each assumed to be much smaller than one, where the Reynolds number is defined as $\rho' U_0' a'/\mu'^{(2)}$ and the capillary number as $\mu'^{(2)} U_0'/\sigma'$. (Here σ' denotes the interfacial tension and $\mu'^{(2)}$ the viscosity of the continuous phase.) This study is divided into four sections. The first

(Sec. 2) provides the formulation. The solution procedure is described in Sec. 3, and the results and conclusions are presented in Sec. 4.

5.2 Formulation

5.2.1 Governing Equations and Boundary Conditions

The problem under examination is that of a fluid droplet moving steadily and axisymmetrically through a continuous liquid in an infinitely long cylindrical tube. Both the droplet and continuous phases are assumed to be incompressible and Newtonian. Far away from the droplet, the continuous fluid flow is either stationary or Poiseuillian. The Reynolds and capillary numbers are assumed to be small enough so that inertia is negligible and the droplet retains a spherical shape. A bulk soluble surfactant is present in the continuous phase and is adsorbed on the surface of the droplet. Adsorbed surfactants is swept to the rear part of the droplet, where a stagnant cap forms. The concentration of surfactant far from the droplet is assumed to be uniform. In the solution technique which will be used both cylindrical (ρ,ω,z) and spherical coordinates (r,θ,ϕ) are needed. The origin of both systems is located at the center of the moving droplet, and therefore in these systems the tube wall is moving in the axial direction. The angle θ is measured from the front stagnant point and the cap ϕ is counted from the rear stagnation point. The gravitational force is acting in the -z direction (see Fig.1).

In formulating the hydrodynamic equations for the droplet motion, droplet and continuous phase variables are denoted by superscripts

(1) and (2) respectively. Dimensional quantities are marked by a prime, and dimensionless quantities are unprimed throughout the analysis. The tube and the droplet radius are denoted by b' and a' respectively. Coordinates are nondimensionalized by the droplet radius a'. The kinematic variables (of both phases) are scaled as follows: velocities by the steady translational velocity of the droplet in the absence of the surfactant in the tube, U_0', and shear stress tensors τ_{ij}' and pressure P' by $\mu'^{(2)}U_0'$, where $\mu'^{(2)}$ is the viscosity of the exterior fluid. The surface surfactant concentration Γ' is nondimensionalized by Γ_∞' where $1/\Gamma_\infty'$ is the limiting area per mole of the surfactant and κ is the viscosity ratio $\mu'^{(1)}/\mu'^{(2)}$. Since the flow is axisymmetric and incompressible, velocities may be represented by a stream function ψ' which is nondimensionalized by a'^2U_0'.

The Navier-Stokes equation for steady axisymmetric creeping flow can be written in terms of the stream function $\psi^{(i)}$ (Happel and Brenner (1970)) as:

$$E^2(E^2\psi^{(i)}) = 0 \qquad (i = 1, 2) \tag{2.1}$$

where E^2 is the axisymmetric stream function operator. In spherical coordinates, E^2 is denoted by E_s^2 and is

$$E_s^2\psi^{(i)} = \frac{\partial^2\psi^{(i)}}{\partial r^2} + \frac{\sin\theta}{r}\frac{\partial}{\partial\theta}\left(\frac{1}{\sin\theta}\frac{\partial\psi^{(i)}}{\partial\theta}\right) \tag{2.2}$$

while in cylindrical coordinates, it has the form

$$E_c^2\psi^{(i)} = \frac{\partial^2\psi^{(i)}}{\partial z^2} + \frac{\partial^2\psi^{(i)}}{\partial \rho^2} - \frac{1}{\rho}\frac{\partial\psi^{(i)}}{\partial \rho} \tag{2.3}$$

The velocity components can be expressed in terms of the stream function:

$$V_r^{(i)} = -\frac{1}{r^2\sin\theta}\frac{\partial\psi^{(i)}}{\partial\theta}, \qquad V_\theta^{(i)} = \frac{1}{r\sin\theta}\frac{\partial\psi^{(i)}}{\partial r},$$

$$V_z^{(i)} = -\frac{1}{\rho}\frac{\partial\psi^{(i)}}{\partial\rho}, \qquad V_\rho^{(i)} = \frac{1}{\rho}\frac{\partial\psi^{(i)}}{\partial z}. \tag{2.4}$$

The boundary conditions are formulated at the center of the droplet, the tube wall, the droplet surface and far from the droplet. These are:

(1) At the droplet center $\lim_{r\to 0} V_r^{(1)}$ and $\lim_{r\to 0} V_\theta^{(1)}$ exist.

(2) Far from the droplet, the velocity field is either uniform

$$\lim_{|z|\to\infty} V_z^{(2)} = -U \tag{2.5}$$

or of Poiseuille type

$$\lim_{|z|\to\infty} v_z^{(2)} = V\left(1 - \frac{\rho^2}{b^2}\right) - U \qquad (2.6)$$

where U is the velocity of the droplet and V is the center line velocity of the Poiseuille flow at infinity (nondimensionalized by U_0').

(3) At the tube wall, $\rho=b$ $(b=b'/a')$

$$v_z^{(2)} = -U, \qquad v_\rho^{(2)} = 0 \qquad (2.7a,b)$$

(4) At the surface of the droplet, $r=1$ $(r=r'/a'=1)$

$$v_r^{(1)} = v_r^{(2)} = 0 \qquad 0\le\theta\le\pi \qquad (2.8a,b)$$

$$v_\theta^{(1)} = v_\theta^{(2)} \qquad 0\le\theta\le\pi \qquad (2.9)$$

The stress conditions are determined by the following. Due to the assumption that the droplet retains its spherical shape, the normal stress balance on the interface is replaced by an integrated force balance:

$$F_z' = 2\pi\mu'^{(2)}U_0' a^2\int_0^\pi \{(-P^{(2)} + \tau_{rr}^{(2)})\cos\theta - \tau_{r\theta}^{(2)}\sin\theta\}\sin\theta d\theta$$

$$= \frac{4}{3}\pi a'^3(\rho'^{(1)} - \rho'^{(2)})g' \qquad (2.10a)$$

where F'_z is the hydrodynamic drag exerted by the exterior fluid on the drop, $\rho'^{(i)}$ is the density of phase i and g' is the gravitational acceleration. Equation (2.10a) will be used to determine the droplet terminal velocities. Writing the pressure, the normal ($\tau_{rr}^{(2)}$) and shear ($\tau_{r\theta}^{(2)}$) stresses in terms of the stream function in spherical coordinates, (2.10a) may be expressed in the form

$$F'_z = a'U'_0\mu'^{(2)}\pi\int_0^{\pi} r'^3\sin^3\theta \frac{\partial}{\partial r'}\left[\frac{E^2\psi^{(2)}}{r'^2\sin^2\theta}\right]d\theta \qquad (2.10b)$$

The tangential stress condition has to depend on the distribution of the surfactants. This distribution is established from the solution of the equation of surfactant conservation at the interface of the droplet; at steady state this relation is in the form

$$\frac{1}{\sin\theta}\frac{\partial}{\partial\theta}(\sin\theta\Gamma V_s) = \frac{1}{Pe_s\sin\theta}\frac{\partial}{\partial\theta}(\sin\theta\frac{\partial\Gamma}{\partial\theta}) + Q(\Gamma,C_s) \qquad (2.11)$$

where V_s is the surface velocity ($V_s=V_\theta^{(i)}(\theta,r=1)$), and Pe_s is the surface Peclet number ($Pe_s=\frac{a'U'_0}{D'_s}$, D'_s is the surface diffusion coefficient). The function $Q(\Gamma,C_s)$ in (2.11) describes the adsorption-desorption kinetics (C_s is the surfactant sublayer concentration and nondimensionalized by C'_∞, $C_s=C(r=1,\theta)$). Here the

Langmuir formulation for the adsorption kinetics is adopted (Davies and Rideal 1963); thus in dimensional form

$$Q'(\Gamma',C_s') = -\alpha'\Gamma' - \beta'C_s'(\Gamma' - \Gamma_\infty') \tag{2.12}$$

where α' and β' are kinetic constants of desorption and adsorption respectively. From (2.12), the concentration Γ' which is in equilibrium with the sublayer surfactant concentration C_s' can easily be obtained from $Q'(\Gamma',C_s')=0$; thus

$$\frac{\Gamma'}{\Gamma_\infty'} = \frac{kC_s}{1 + kC_s} \tag{2.13}$$

where $k = \beta'C_\infty'/\alpha'$ and is the ratio of adsorption to desorption rates. Nondimensionalization of (2.12) by $U_0'\Gamma_\infty'/a'$ yields after some manipulation and combination with (2.11) the surfactant mass equation

$$\frac{1}{\sin\theta}\frac{\partial}{\partial\theta}(\sin\theta\Gamma V_s) = \frac{1}{Pe_s\sin\theta}\frac{\partial}{\partial\theta}(\sin\theta\frac{\partial\Gamma}{\partial\theta}) - Bi[C_s(\Gamma - 1) + \frac{1}{k}\Gamma]$$

where (2.14)

$$Bi = \frac{\beta'C_\infty'}{(U_0'/a')}$$

and is the nondimensional ratio of the rate of adsorption of surfactant onto the surface to the rate at which surfactant is convected from one end of the droplet to the other.

This study is concerned with conditions for which a stagnant cap forms on the surface of the droplet. Stagnant cap conditions are realized when $Bi \to 0$ and $Pe_s \to 0$ because, in these limits, Eqn.(2.14) becomes

$$\frac{1}{\sin\theta}\frac{\partial}{\partial\theta}(\sin\theta\Gamma V_s) = 0 \qquad (2.15)$$

Integrating this equation, the following simple form can be obtained:

$$\Gamma V_s = \text{constant}/\sin\theta \qquad (2.16)$$

This equation should be satisfied everywhere on the surface of the droplet and therefore the constant must be zero in order to have a bounded solution at $\theta = 0$ and π. Hence on each portion of the droplet surface, either $V_\theta = 0$ or $\Gamma = 0$. Here only the case of a cap at the trailing edge is considered. This surfactant organization is always realized with the uniform flow. It is also realized if the drop is suspended in a Poiseuille flow as long as the sphere velocity is larger than the centerline velocity or on the opposite direction. For a single cap at the trailing edge, the following surface conditions are valid:

$$V_\theta^{(1)} = V_\theta^{(2)} = 0 \qquad \pi-\phi<\theta\leq\pi \qquad (2.17a,b)$$

$$\tau_{r\theta}^{(2)} - \tau_{r\theta}^{(1)} = 0 \qquad 0<\theta\leq\pi-\phi \qquad (2.18a)$$

This completes the hydrodynamic boundary conditions, but note that the cap angle ϕ is as yet undetermined. The cap angle is computed from the physicochemical properties of the surfactant as described below.

On the stagnant cap region, the distribution of the surfactant can also be expressed by the tangential stress balance.

$$\tau_{r\theta}^{(2)} - \tau_{r\theta}^{(1)} = \frac{1}{\mu'^{(2)} U_0'} \frac{\partial \sigma'}{\partial \Gamma'} \frac{\partial \Gamma'}{\partial \theta} \qquad \pi - \phi \leq \theta < \pi \qquad (2.18b)$$

where σ' is the surface tension. With the choice of the Langmuir adsorption isotherm (Eqn.(2.12)), the dependence of the surface tension on the surfactant surface concentration ($\sigma'(\Gamma')$) may be formulated from the Gibbs adsorption equation,

$$\frac{d\sigma'}{d\mu'} = - \Gamma' \qquad (2.19)$$

where μ' is the chemical potential. The bulk concentration is assumed to be dilute enough so as to be ideal, $\mu' = \mu_0'(T', p') + R'T'\ell n(C')$, where T' denotes the temperature, p' is the thermodynamic pressure and R' is the gas constant. Integrating (2.19) gives

$$\sigma' = \sigma_0' - R'T'\Gamma_\infty'\ell n(1/(1 - \Gamma'/\Gamma_\infty')) \qquad (2.20)$$

where the relation between C_s and Γ (Eqn.(2.13)) is used and σ_0' is surface tension of the clean interface. Consequently, from (2.20) $\frac{\partial \sigma'}{\partial \Gamma'}$ is calculated to be

$$\frac{\partial \sigma'}{\partial \Gamma'} = - \frac{R'T'}{(1 - \Gamma'/\Gamma'_\infty)} \tag{2.21}$$

Substituting Eq.(2.21) into Eq.(2.18b) yields the following equation:

$$\tau_{r\theta}^{(2)} - \tau_{r\theta}^{(1)} = - Ma \frac{1}{(1-\Gamma)} \frac{\partial \Gamma}{\partial \theta} \qquad \pi-\phi \leq \theta \leq \pi \tag{2.18c}$$

where

$$Ma = \frac{R'T'\Gamma'_\infty}{\mu'^{(2)}U'_0} \tag{2.22}$$

The dimensionless surfactant concentration profile in the stagnant cap region can be obtained from the integral of the tangential stress condition (Eqn.(2.18c)) as follows:

$$\int_0^\Gamma \frac{d\Gamma}{1-\Gamma} = \frac{1}{Ma} \int_{\pi-\phi}^{\pi} (\tau_{r\theta}^{(2)} - \tau_{r\theta}^{(1)}) d\theta \tag{2.23}$$

where the concentration at the edge of the cap ($\theta=\pi-\phi$) is defined to be equal to zero.

The total amount of surfactant on the droplet surface can now be obtained by substituing the concentration, Γ, from equation (2.23) into Eqn.(2.13). Thus,

$$\frac{kC_s}{1+kC_s} = \frac{1}{2} \int_{\pi-\phi}^{\pi} \{1 - \exp[-\frac{1}{Ma} \int_{\pi-\phi}^{\theta} (\tau_{r\theta}^{(2)} - \tau_{r\theta}^{(1)}) d\theta]\} \sin\theta d\theta \tag{2.24}$$

The problem is not fully determined until C_s, the sublayer concentration, is obtained. Formally, C_s can be obtained by solving the steady convective-diffusion equation in the continuous phase, i.e.

$$Pe\vec{V}\cdot\vec{\nabla}C = \nabla^2 C \tag{2.25}$$

where ∇^2 is the Laplacian operator, $Pe=U_0'a'/D'$, D' is the bulk diffusivity of the surfactant and C is the bulk concentration. the boundary conditions on the bulk concentration are:

$$\frac{1}{Pe_A}\frac{\partial C}{\partial r}\Big|_{r=1} = Bi[C_s(\Gamma - 1) + \frac{1}{k}(\Gamma - C_s)] \tag{2.26}$$

and

$$\lim_{|z|\to\infty} C(z,\rho) = 1 \tag{2.27}$$

$$\frac{\partial C}{\partial \rho}\Big|_{\rho=b} = 0 \tag{2.28}$$

where $Pe_A = Pe\delta'/a'$ and δ' is the adsorption depth of the surfactant, Γ_∞'/C_∞'. As the limit $Bi \to 0$ and Pe_A chose O(1), Eqn.(2.26) is reduced to $\frac{\partial C}{\partial r}\Big|_{r=1} \to 0$, therefore C_s is a constant which is equal to 1. Thus the final equation for the cap angle siza is:

$$\frac{k}{1+k} = \frac{1}{2}\int_{\pi-\phi}^{\pi}\{1 - \exp[-\frac{1}{Ma}\int_{\pi-\phi}^{\theta}(\tau_{r\theta}^{(2)} - \tau_{r\theta}^{(1)})d\theta]\}\sin\theta d\theta \tag{2.29}$$

5.3 Solution Technique

In cylindrical and spherical coordinates, the solution of (2.1) may be obtained by the method of separation of variables. For the droplet interior, only the solution in spherical coordinates is needed. The form for $\psi^{(1)}(r,\theta)$ which admits bounded solutions as $r\to 0$ for $V_r^{(1)}$ and $V_\theta^{(1)}$ (as given by (2.4)) is:

$$\psi^{(1)}(r,\theta) = \sum_{n=2}^{\infty}(E_n^{(1)}r^n + F_n^{(1)}r^{n+2})C_n^{-1/2}(\cos\theta) \tag{3.1}$$

where $C_n^{-1/2}(\cos\theta)$ is the Gegenbauer polynomial of order n and degree -1/2.

For the continuous fluid, the mixed coordinates solution of (2.1) which is bounded as $|z|\to\infty$ is

$$\begin{aligned}\psi^{(2)}(\rho,z,r,\theta) = \psi^{\infty}(\rho) &+ \int_0^{\infty} dk\{A(k)\rho I_1(k\rho) + B(k)\rho^2 I_0(k\rho)\}\cos(kz) \\ &+ \int_0^{\infty} dk\{A''(k)\rho I_1(k\rho) + B''(k)\rho^2 I_0(k\rho)\}\sin(kz) \\ &+ \sum_{n=2}^{\infty}\{E_n^{(2)}r^{-n+1} + F_n^{(2)}r^{-n+3}\}C_n^{-1/2}(\cos\theta)\end{aligned} \tag{3.2}$$

where

$$\psi^{\infty}(\rho) = \begin{cases} \frac{1}{2}\rho^2 & \text{(Uniform)} \\ -Vb^2[\frac{1}{2}(\frac{\rho}{b})^2 - \frac{1}{4}(\frac{\rho}{b})^4] + \frac{1}{2}\rho^2 & \text{(Poisuelle)} \end{cases} \tag{3.3}$$

and I_0 and I_1 are the modified Bessel functions of the first kind. The above form for $\psi^{(2)}(\rho,z,r,\theta)$ replaces the $K_0(k\rho)$ and $K_1(k\rho)$ integrals of the general solution as given by Haberman and Sayre (1958) with equivalent Gegenbauer summations as described by Leichtberg, et al. (1976).

The technique used to obtain the constants and the k functions in Eq.(3.1) and (3.2) is outlined as follows. First, the boundary conditions on the tube wall are satisfied exactly, by using the Fourier inverse cosine and sine integrals to solve for the unknown coefficients A(k), B(k), A"(k) and B"(k) in (3.2). Second, the stream function is rewritten in a compact form in terms of r,θ and the unknown constants $E_n^{(2)}$ and $F_n^{(2)}$. Finally, a collocation technique is used to satisfy the boundary conditions on the surface of the droplet. In the following subsection §3.1, the first two steps are detailed. The satisfaction of the r=1 boundary conditions using a collocation technique is described in §3.2. Finally, in §3.3 the convergence criteria is formulated, and a verification of the method is presented.

5.3.1 Exact Solution of the Wall Boundary Conditions

Using Eq.(3.2), the boundary conditions (2.7a) becomes

$$\int_0^\infty dk\{A(k)kI_0(bk)+B(k)[bkI_1(bk) + 2I_0(bk)]\}\cos(kz) +$$

$$\int_0^\infty dk\{A"(k)kI_0(bk)+B"(k)[bkI_1(bk) + 2I_0(bk)]\}\sin(kz) = \qquad (3.4)$$

$$- \sum_{n=2}^{\infty}[E_n^{(2)}G_n^1(z) + F_n^{(2)}G_n^2(z)]$$

Instead of using $V_\rho^{(2)}(\rho-b)=0$ (2.7b), the equivalent condition $\psi^{(2)}(\rho-b)=\psi^{\infty}(b)$ is applied for convenience. That is

$$\int_0^{\infty} dk\{A(k)bI_1(bk)+B(k)b^2I_0(bk)\}\cos(kz) + \tag{3.5}$$

$$\int_0^{\infty} dk\{A''(k)bI_1(bk)+B''(k)b^2I_0(bk)\}\sin(kz) = - \sum_{n=2}^{\infty}[E_n^{(2)}G_n^3(z) + F_n^{(2)}G_n^4(z)]$$

where, for i=1,2,3,4, $G_n^i(z)$ are of the form as:

$$G_n^1(z) = (b^2 + z^2)^{-(n+1)/2}P_n[\frac{z}{(b^2 + z^2)^{1/2}}]$$

$$G_n^2(z) = (b^2 + z^2)^{-(n-1)/2}\{P_n[\frac{z}{(b^2 + z^2)^{1/2}}] + 2C_n^{-1/2}[\frac{z}{(b^2 + z^2)^{1/2}}]\} \tag{3.6}$$

$$G_n^3(z) = (b^2 + z^2)^{-(n-1)/2}C_n^{-1/2}[\frac{z}{(b^2 + z^2)^{1/2}}]$$

$$G_n^4(z) = (b^2 + z^2)^{-(n-3)/2}C_n^{-1/2}[\frac{z}{(b^2 + z^2)^{1/2}}]$$

In the above, spherical coordinates (r,θ) have been transformed into cylindrical coordinate (ρ,z). The boundary conditions (3.4) and (3.5)

can be inverted by the inverse Fourier cosine and sine transform so as to solve for A(k), B(k), A"(k) and B"(k). These calculations are carried out in the Appendix A. The resulting expression for the stream function can be written as (cf. the Appendix A):

$$\psi^{(2)}(\theta,r) = \psi^{\infty}(r,\theta) + \sum_{n=2}^{\infty}[E_n^{(2)}S_n^1(r,\theta) + F_n^{(2)}S_n^2(r,\theta)] \qquad (3.7)$$

where $S_n^1(r,\theta)$ and $S_n^2(r,\theta)$ are given in Appendix A.

5.3.2 Collocation Solution of Droplet Surface Boundary Condions

The boundary condition $V_r^{(1)}(r=1,\theta)=0$ (2.8a) can be applied directly to (3.1) to eliminate $F_n^{(1)}$. Thus the inner solution becomes

$$\psi^{(1)}(r,\theta) = \sum_{n=2}^{\infty} E_n^{(1)}(r^n - r^{n+2})C_n^{-1/2}(\cos\theta) \qquad (3.8)$$

If the other boundary conditions at r=1 ((2.8b), (2.9), (2.17a) and (2.18a)) are applied to the solution (3.7) and (3.8), three simultaneous equations in the form of infinite series are obtained. In the collocation technique, the three boundary conditions are satisfied at m discrete points along the surface of the sphere, and the series (3.7) and (3.8) is truncated into a finite form which includes a total of 3m terms. A set of 3m homogeneous simultaneous linear algebraic equation is therefore generated and can be solved

using any standard matrix reduction technique to obtain the 3m unknown constants $E_n^{(1)}$, $E_n^{(2)}$ and $F_n^{(2)}$.

When the boundary conditions on the surface of the sphere are applied by the collocation technique described above, the 3m truncated equations are given as:

$$V\cos\theta_i[1 - (\sin\theta_i / b)^2] - \cos\theta_i = \sum_{n=2}^{m+1}[E_n^{(2)}S_n^3(1,\theta_i) + F_n^{(2)}S_n^4(1,\theta_i)] \tag{3.9}$$

$$V\sin\theta_i[1 - (\sin\theta_i / b)^2] - \sin\theta_i = \sum_{n=2}^{m+1}[E_n^{(2)}S_n^5(1,\theta_i) + F_n^{(2)}S_n^6(1,\theta_i) + \frac{2}{\sin\theta_i}E_n^{(1)}C_n^{-1/2}(\cos\theta_i)] \tag{3.10}$$

$$V\sin\theta_i[1 + (\sin\theta_i / b)^2] - \sin\theta_i = \sum_{n=2}^{m+1}[E_n^{(2)}S_n^7(1,\theta_i) + F_n^{(2)}S_n^8(1,\theta_i) - \frac{2(2n-1)\pi}{\sin\theta_i}E_n^{(1)}C_n^{-1/2}(\cos\theta_i)]$$

$$0<\theta\leq\pi-\phi \tag{3.11a}$$

or

$$0 = \frac{2}{\sin\theta_i}\sum_{n=2}^{m+1}E_n^{(1)}C_n^{-1/2}(\cos\theta_i) \qquad \pi-\phi<\theta\leq\pi \tag{3.11b}$$

where i denotes the collocation point (i=1,2,...,m) and the $S_n^q(1,\theta_i)$ are given in Appendix A. The above equations are valid for Poisueille flow at infinity. The equations valid for uniform flow may be obtained from these by letting V=0.

An important question arises as to how to choose the location of discrete points on the surface of the droplet to obtain a prescribed accuracy. The prescription which was found to be the most rapidly convergent located points such that the the ratio of the points located on the contaminated surface to those on the clean surface part were equal to the ratio of the areas. Thus $m_{cap}/m_{clean} = \phi/\pi-\phi$, where m_{cap} and m_{clean} are, respectively, the number of collocation points in the cap and clean regions.

5.3.3 Convergence Criteria and Verification of Method

As explained in the Introduction, the aim of this study is to compute the hydrodynamic drag on the droplet, and therefore convergence criteria are based on the accurate computation of F_z'. Inserting (3.7) into (2.10b) shows that the drag is determined solely by $F_2^{(2)}$.

$$F_z' = - 4\pi a' \mu'^{(2)} U_0' F_2^{(2)}$$

Hydrodynamic drags are usually expressed in terms of drag coefficients λ. For uniform flow, $F_2^{(2)}$ is obtained from the solution of (3.9)-(3.11) with V=0. The drag coefficient for uniform flow is denoted λ_u and is defined as the ratio of F_z' to the force exerted on a droplet moving at U_0' in an infinite medium. The latter is the Hadamard-Rybczynski value $4\pi' a' \mu'^{(2)} U_0' (\frac{1+3\kappa/2}{1+\kappa})$. Thus

$$\lambda_u = F_2^{(2)} \frac{1 + \kappa}{1 + 3\kappa/2} \tag{3.12}$$

For Poiseuille flow, (3.9)-(3.11) indicate that $F_2^{(2)}$ is the sum of two contributions, one $F_{2u}^{(2)}$ from the uniform flow terms (identical to the previous case) and one from the Poiseuille terms ($F_{2v}^{(2)}$) and which is linear in $V=V'/U_0'$. This reflects the fact that the problem for Poiseuille flow could have been decomposed into two problems, one in which the wall in moving and the flow is quiescent at infinity and another in which the wall is stationary and the flow is Poiseuillian at infinity. The contribution due to the Poiseuille terms gives rise to a drag $-4\pi a'\mu'^{(2)} U_0' F_{2v}^{(2)}$. A drag coefficient, λ_v is defined as this contribution divided by the Hadamard-Rybczynski drag for a sphere moving with velocity V'. Thus

$$\lambda_v = F_{2v}^{(2)} \frac{1 + \kappa}{1 + 3\kappa/2} \tag{3.13}$$

and the total drag in terms of drag coefficients is

$$F_z' = - 4\pi a'\mu'^{(2)} \left(\frac{1 + 3\kappa/2}{1 + \kappa}\right) [U_0'\lambda_u - V'\lambda_v] \tag{3.14}$$

Convergence criteria for λ_u and λ_v were formulated as follows. For a given cap angle, the distribution of collocation points is given by $m_{cap}/m_{clean} = \phi/(\pi-\phi)$. An integer number for m_{cap} was selected, and the m_{clean} was computed from the distribution relation. The drag

coefficients λ_u and λ_v are then computed. A next set is chosen with integer values for m_{cap} and m_{clean} which are larger than the previous values but still satisfy the distribution relation. Calculated values of λ_u and λ_v are then compared with the previous values, and the calculations are stopped when the absolute value of the percent change is less than 0.1.

This section concludes with a verification of the method. Previous studies by Sahdal-Johnson (1983) have computed λ_u analytically in an infinite medium. In Table I their results are compared with those obtained by the present technique for $\kappa = 0$ and several values of ϕ. The results show excellent agreement. In Table II and Table III, comparisons are made of the drag coefficients λ_u and λ_v in a tube for clean (cap angle $\phi = 0$, Table II) and completely contaminated or solid ($\phi = 180$, Table III) surface conditions with those of Hyman and Skalak (1970). The latter authors solved for the drag on fluid and solid spheres moving in an infinite chain inside a cylindrical tube, and the results listed in the tables are for sphere separations of 40 radii. Again excellent agreement is obtained.

5.4 Results and Discussions

The results for the coaxial hydrodynamic motion of a spherical droplet in a tube in the presence of a stagnant cap of surfactants are presented in the following sub-sections. Section 4.1 contains the numerical results for the drag correction coefficients for an axially translating droplet, λ_u, and for Poiseuille flow past a stationary

droplet, λ_v. The droplet terminal velocity, at two distinct flow conditions, and the corresponding flow fields are presented in Section 4.2. Finally, in Section 4.3, the stagnant cap angle is determined, from the interfacial stress balance condition, in terms of the physicochemical parameters.

5.4.1 The Drag Correction Coefficients

The hydrodynamic drag, F_z', acting on a droplet moving in a tube, can be expressed as the sum of the following two contributions: the drag due to coaxial translation of the droplet and the drag due to Poiseuille flow past a stationary droplet. The superposition of these flow fields is permissible provided the stagnant cap angle is constant and its location is congruent with the convective field around the droplet. According to equation (3.14), the drag on a droplet in pure translation is $-\xi'\lambda_u U_0'$, where $\xi'=4\pi a'\mu'^{(2)}(1+3\kappa/2)/(1+\kappa)$. The drag due to Poiseuille flow can be expressed as $\xi'\lambda_v V'$, where V' denotes the centerline fluid velocity in the absence of the droplet.

The translating drag correction coefficients, λ_u, is shown in figures 2(a,b,c) for κ=0, 0.5 and 2, respectively, as a function of the sphere-to-tube radii ratio, a'/b', and for six values of the cap angle varying between zero (for a clean droplet) and π (solid sphere). The numerical calculations have been performed for $a'/b' \leq 0.6$ so that the deformation of the droplet can be neglected. The general behaviour of the drag coefficient shown in these figures exhibits monotonic increase in the drag exerted on the fluid droplet for increasing radii ratio, a'/b', and cap angle. In the limit $a'/b'=0$,

the values of the drag coefficients for different cap angles correspond to the case of a droplet moving in unbounded fluid, and coincide with the exact solution of Sadhel and Johnson (1983). The increase in the drag for increasing values of a'/b' is associated with the increase of the shear rates in the diminishing gap between the sphere perimeter and the tube wall. A similar trend is observed with increasing cap angles, although this effect is primarily due to the immobilization of larger interfacial area and, consequently, enhanced shear rates in its vicinity.

The dependence of the drag coefficient on the viscosity ratio, κ, is also shown to increase, for a fixed value of a'/b', with increasing κ. The actual increase in the drag is larger than that of λ_u due to the monotonic growth of ξ' which varies between 1 for κ=0 and 3/2 for $\kappa \to \infty$. This behaviour is compatible with the fact that increasing viscosity ratio results in diminishing droplet interfacial velocity and, concomitantly, increasing shear rates. Furthermore, for large viscosity ratio, the influence of the cap angle on the magnitude of the drag coefficient is reduced because the retardation of the surface velocity due to large κ becomes significant in comparison with the immobilization effect due to the presence of surfactants. Consequently, no significant change is observed in the values of λ_u for large cap angles between 150 and 180°.

The variations of the drag coefficient for Poiseuille flow past a stationary sphere exhibit a similar behaviour (figures 3a,b,c). It is important to note, however, that λ_u is always larger than λ_v, and this difference is more pronounced at larger values of a'/b' and κ. The larger magnitude of λ_u, as compared to λ_v, is due to the fact that its

definition is based on the uniform velocity far from the sphere, while λ_v is defined for a unit centerline velocity of the Poiseuille profile. Hence, the flow rate for the case of uniform flow, is twice that for Poiseuille flow, and, therefore, higher shear rates develop in the gap between the sphere and the tube wall. This effect is enhanced when the ratio a'/b' increases due to the diminishing Poiseuille velocity near the wall.

5.4.2 Droplet Terminal Velocity and Flow Characteristics

The terminal velocity of a surfactant laden sphere along the axis of a tube can now be ascertained for two distinct flow situations: (i) the motion of a droplet in a vertical tube due to gravity, and (ii) the motion of a droplet in a tube due to gravity and Poiseuille flow. The second case is restricted to motions in which the sphere moves in the opposite direction to the Poiseuille flow, or in the same direction with a translation velocity larger than the Poiseuille centerline velocity. The latter can be realized, in general, in the presence of an external force. The need for these restrictions stems from the fact that only flow situations which guarantee cap formation, by persistent convective sweeping of the surfactants along the sphere surface towards the rear stagnation point, are permitted in the present analysis. In the case when the directions of the sphere motion and the Poiseuille flow coincide, and the sphere velocity is smaller than the Poiseuille centerline velocity (as in the case of neutrally buoyant sphere suspended in Poiseuille flow), (cf.Chapter 4) have shown that in addition to the presence of the stagnation points at the sphere poles, two stagnation rings develop due to flow

recirculation. The consequence of such flow organization may result in surfactant accumulation in a form of two additional stagnant belts in the vicinity of the stagnation rings.

Based on the discussion above, the second flow situation, in which both gravitational force and Poiseuille flow are present, can be described by direct superposition of two distinct flows: droplet translation due to an gravity and Poiseuille flow past a stationary sphere. This superposition requires, of course, that the geometries of the two flows be identical and the position and size of the stagnant cap be the same. Thus, the complete description of the combined flows can be obtained from the description of case (i) and Poiseuille flow in a tube past a fixed droplet.

The flow field for each of these motions has been calculated by computing the velocity at discrete points inside the sphere, in the exterior phase and on the interface. The computation has been carried out by using the expressions for the stream function (equations (3.7) and (3.8)) for increasing values of m until a 1% convergence is attained.

The terminal velocity of a sphere in a vertical tube due to gravity can be obtained from the balance between the drag and buoyancy forces. Hence,

$$- U\lambda_u\xi' - \frac{4}{3}\pi a'^3(\rho'^{(1)}-\rho'^{(2)})g' = 0 \qquad (4.1)$$

and the droplet terminal velocity, U, is, therefore

$$\frac{U'}{U'_{H\text{-}R}} = \frac{1}{\lambda_u} \qquad (4.2)$$

where U'_{H-R} denotes the Hadamard-Rybczynski gravitational velocity in unbounded medium and is given by

$$U'_{H-R} = - \frac{a'^2(\rho'^{(1)} - \rho'^{(2)})g'}{3\mu'^{(2)}} \frac{1+\kappa}{(1+3/2\kappa)} \qquad (4.3)$$

The velocity fields associated with the gravitational settling (or rise) of a droplet in a vertical tube are shown in figures 4(a,b,c) for three stagnant cap angles of 30, 90 and 150°, respectively. These velocity fields are presented for $a'/b'=0.5$ and $\kappa=0.5$ in the reference frame in which the sphere is stationary and the tube wall, and the fluid far from the sphere, are moving with the terminal velocity U'. The velocity vector is shown in discrete points, and its magnitude has been scaled by the terminal velocity.

The stagnant cap in figure 4 is located around the downstream pole of the sphere. This immobile interface results in region of lower velocity both inside and outside the sphere. Furthermore, the recirculating flow pattern inside the sphere, which is symmetric in the case of a clean interface, is shifted away from the immobile cap region. The asymetry is more pronounced at larger cap angles (figure 4b). At cap angles close to 180°, the motion inside the drop is practically halted (figure 4c).

In the second case, when the droplet is moving due to gravity and Poiseuille flow, the force balance requirement is

$$(V'\lambda_v - U'\lambda_u)\xi' - \frac{4}{3}\pi a'^3(\rho'^{(1)} - \rho'^{(2)})g' = 0 \qquad (4.4)$$

and, therefore, the terminal velocity, U', can be obtained from the equation:

$$\frac{U'}{V'} = \frac{1}{\lambda_u}\frac{U'_{H-R}}{V'} + \frac{\lambda_v}{\lambda_u} \qquad (4.5)$$

Equation (4.5) is valid only when U'>V' or when these velocities have opposing directions. The sphere velocity can be maintained at zero if $U'_{H-R} = -V'\lambda_v$. For smaller values of U'_{H-R} (faster settling) the motion of the sphere will always be opposite to that of the Poiseuille flow. If, on the other hand, $U'_{H-R} > 0$ (the droplet is rising), the droplet velocity will exceed the Poiseuille centerline velocity only if $U'_{H-R} > V'(\lambda_u - \lambda_v)$.

The velocity fields for Poiseuille flow past a stationary sphere are shown in figures 5(a,b,c), for $a'/b' = 0.5$, $\kappa = 0.5$ and cap angles of 30, 90 and 150°, respectively. The velocity vectors in these figure are scaled by the Poiseuille centerline velocity. The superposition of these fields with the corresponding flows for a sphere moving due to gravity (figure 4) will provide a complete description of the second flow situation. As before, increasing the cap angle reduces the velocity in its vicinity and shifts the recirculation region towards the front stagnation point. In addition, the interfacial velocity is smaller for this flow in comparison with the previous one due to the lower volumetric flow rate.

5.4.3 The Stagnant Cap Angle

The hydrodynamic results presented hitherto have been obtained independently from the surfactant adsorption/desorption kinetics for the general case when the sorption rate is much slower than the interfacial convection rate so that stagnant cap formation is guaranteed. The hydrodynamic solution, therefore, has been obtained for an a priori prescribed cap angle, ϕ. Still, in order to determine the drag force acting on a droplet in the presence of a stagnant cap, it is necessary to establish first the size of this cap. The size of the stagnant cap is influenced not only by the viscous interfacial forces and the Marangoni force, but, in addition, by the physicochemical parameters which control the total amount of surfactants adsorbed onto the interface.

The influence of the viscous and interfacial forces and the sorption kinetics on the size of the stagnant cap is apparent from the tangential stress balance on the immobile interface (equation 2.18c). This condition can be satisfied only by an appropriate surface tension distribution along the immobile surface which, in turn, is related to the surfactant concentration profile according to the non-linear Langmuir adsorption isotherm.

Equation (2.24) provides the implicit expressions for the cap angle, ϕ, in terms of the kinetic rate constant, k, and the Marangoni number, Ma. The velocity scale used in the definition of the Marangoni number (Equation 2.22) has been chosen intentionally as the clean droplet velocity U_0' to eliminate the dependence of Ma on the cap angle, ϕ. The kinetic rate constant ($k=\alpha C_\infty'/\beta$) can be calculated from the known bulk concentration, C_∞', and adsorption and desorption constants (β and α, respectively). The Marangoni number can be also

calculated for a specific surfactant, with a known limiting packing concentration Γ'_∞, and the corresponding velocity of an uncontaminated drop. Finally, the tangential stresses in equation (2.24) can be evaluated from the respective expressions for the exterior and interior stream functions (Equations 3.7-3.8).

Two limiting states are immediately apparent from equation (2.24). For large values of the Marangoni number (Ma>>1), the exponential function can be linearized to yield the Sadhael-Johnson result

$$\frac{k}{1+k}\,Ma = \frac{1}{2}\int_{\pi-\phi}^{\pi}\int_{\pi-\phi}^{\pi}(\tau_{r\theta}^{(2)} - \tau_{r\theta}^{(1)})d\theta\,\sin\theta\,d\theta \qquad (4.6)$$

which is also valid for the linear Gibbs monolayer. The opposite limit (Ma→0) yields explicit relation between the kinetic rate constant and the cap angle, independent of the Marangoni number, in the form:

$$\frac{k}{k+1} = \frac{1}{2}\,(1 - \cos\phi) \qquad (4.7)$$

Furthermore, equation (4.7) indicates that the formation of a stagnant cap in the limit Ma→0 is independent of the geometric configuration and the hydrodynamic forces, and that it is uniquely determined by the kinetic rate constant. Still, according to the stress balance condition (equation (2.18c), the cap can be realized only when $\Gamma\to 1$ so that the ratio $M_a/(1-\Gamma)$ is finite. If, on the other hand, the right hand side of equation (2.18c) vanishes as Ma→0, the interfacial

mobility is restored and the droplet motion is not hindered by the presence of surfactants. This situation is predicted by the linear kinetic equation which was used by Sadhal and Johnson (1983) and is reducible to the form of equation (4.6). Their conclusion is that in the limit of vanishing Marangoni number the cap angle approaches zero so that all of the adsobed surfactant molecules are concentrated in the downstream stagnation point. The non-linear kinetic expressions prohibits excessive compression of the surfactant layer such that a finite stagnant cap can be established with a uniform concentration distribution. It is important to note, however, that at elevated surface concentrations ($\Gamma \to 1$) the surface tension may become prohibitively low (large capillary number; see equation 2.18c), and consequently the droplet spherical shape will not be maintained.

The numerical calculations undertaken to evaluate the cap angle from equation (2.24) were performed by evaluating the tangential stresses at the collocation points and using the Euler integration method. A test for the accuracy of the computations is presented in figure 6. This figure compares the exact results of Sadhal and Johnson (1983), for a capped gas bubble translating in unbounded fluid, with the present collocation solution in the limit of large Ma (equation 4.6). From the figure, it is clear that the present calculations are in excellent agreement with the exact solution, and the deviation does not exceed 5%.

The cap angle results, for a gas bubble rising coaxially in a tube, are presented in figure 7 for different values of a'/b' (including $a'/b'=0$, which describes the motion of a bubble in unbounded fluid) and a constant Marangoni number. The Marangoni number, in this figure, is scaled by the Hadamard-Rybczynski velocity

$U_{H-R'}$ which differs from the actual droplet velocity in the tube. For a constant sphere radius, a', the droplet velocity decreases with increasing value of a'/b' (or decreasing tube radius) and cap angle. The total amount of surfactants on a sphere of radius a' is constant when k is constant (as shown by equation 2.13). The cap angle, on the other hand, may vary with a'/b' and the sphere velocity. At large values of a'/b', the increased shear rate in the vicinity of the sphere interface results in a stronger compression of the surfactant molecules on the interface so that an equal amount of surfactants forms smaller cap angles. The behaviour is monotonic with decreasing values of the rate constant. In the limit k=0, no surfactant is adsorbed onto the interface (ϕ=0), and the interface mobility is recovered. At sufficiently large values of k (e.g. large bulk concentration), the cap angle reaches π and the bubble behaves as a solid sphere. Any additional increase in the value of k (corresponding to increased bulk concentration) cannot influence the cap geometry although the interfacial tension is further reduced due to increased surface concentration.

In order to determine the cap angle and, subsequently, the sphere velocity, the results are presented in an alternative way in figure 8 for a'/b'=0.2, 0.4 and 0.6 and a wide range of Marangoni numbers. (The results for a sphere moving in unbounded fluid are given in Chapter 2. In these figures, the Marangoni number is scaled by the velocity of the sphere in the absence of surfactants, U_0'. These graphs can be used to determine the cap angle for known sphere and tube radii (a' and b'), rate constant (k) and Marangoni number (with U_0' given in). Once the cap angle is known, the drag coefficient can be obtained from

figures 2 and 3 for the appropriate configuration, and the sphere velocity can then be computed from equations (4.2) or (4.5), depending on the flow conditions. Conversely, if the actual sphere velocity is measured experimentally, one can use the present results to determine the rate constant, k.

Figure 8 also demonstrates consistently the fact that the cap angle increases with increasing Ma (for a fixed value of k) which represents larger restoring interfacial forces. The results for large Marangoni numbers ($Ma \geq 100$) have been calculated from the asymptotic equation (4.6) without loss of accuracy. Similarly, at small values of Ma the stagnant cap solution approaches the limiting expression given by equation (4.7) although the behaviour exhibits a significant departure from the equation (4.7) when the cap angle is close to π. This deviation is explained by the fact that a solid sphere behaviour, at Ma=0, can only be realized when the bulk concentration is infinite ($k \to \infty$) and, thus, the sphere is completely covered by surfactants at the maximum surface pressure ($\Gamma=1$).

Appendix A

I. Solution for A(k), A"(k), B(k) and B"(k)

Integrating the inverse Fourier cosine and sine integrals from Eqn.(3.4) and Eqn.(3.5) yields:

$$A(k)kI_0(bk) + B(k)[bkI_1(bk) + 2I_0(bk)] = -\sum_{n=2}^{\infty}[E_n^{(2)}H_{nc}^1(k) + F_n^{(2)}H_{nc}^2(k)]$$

$$A"(k)kI_0(bk) + B"(k)[bkI_1(bk)+2I_0(bk)] = -\sum_{n=2}^{\infty}[E_n^{(2)}H_{ns}^1(k) + F_n^{(2)}H_{ns}^2(k)]$$

$$A(k)bI_1(bk) + B(k)b^2I_0(bk) = -\sum_{n=2}^{\infty}[E_n^{(2)}H_{nc}^3(k) + F_n^{(2)}H_{nc}^4(k)]$$

$$A"(k)bI_1(bk) + B"(k)b^2I_0(bk) = -\sum_{n=2}^{\infty}[E_n^{(2)}H_{ns}^3(k) + F_n^{(2)}H_{ns}^4(k)]$$

where, $H_{nc}^i(k)$ and $H_{ns}^i(k)$ are:

$$H_{nc}^i(k) = \frac{2}{\pi}\int_0^{\infty}G_n^i(z)\cos(kz)dz \qquad H_{ns}^i(k) = \frac{2}{\pi}\int_0^{\infty}G_n^i(z)\sin(kz)dz$$

For i=1,2,3,4, $H_{nc(s)}^i(k)$ are given as (Leichtberg et al.,(1976)):

$$H_{nc(s)}^1(k) = b_{nc(s)}\frac{2}{\pi n!}k^nK_0(bk)$$

$$H^2_{nc(s)}(k) = - b_{nc(s)} \frac{2}{\pi n!} k^{n-2}[n(n-1)K_0(bk) - (2n-3)bkK_1(bk)]$$

$$H^3_{nc(s)}(k) = -b_{nc(s)} \frac{2}{\pi n!} bk^{n-1}K_1(bk)$$

$$H^4_{nc(s)}(k) = b_{nc(s)} \frac{2}{\pi n!} bk^{n-3}[(2n-3)bkK_0(bk) - (n-2)(n-3)K_1(bk)]$$

where

$$b_{nc} = (-1)^{n/2} \quad \text{n=even} \qquad b_{ns} = (-1)^{(n-1)/2} \quad \text{n=odd}$$

A(k), B(k), A"(k) and B"(k) can be solved in terms of the unknown constants $E_n^{(2)}$ and $F_n^{(2)}$. That is:

$$A(A")(k) = \sum_{n=2}^{\infty}[E_n T^1_{nc(s)}(k) + F_n T^2_{nc(s)}(k)]$$

$$B(B")(k) = \sum_{n=2}^{\infty}[E_n T^3_{nc(s)}(k) + F_n T^4_{nc(s)}(k)]$$

where the $T^i_n(k)$'s (i=1,2,3,4) functions appearing above are defined as

$$T^1_{nc(s)}(k) = [(2 + bk\Omega)H^3_{nc(s)}(k) - b^2H^1_{nc(s)}(k)]/\Delta$$

$$T^2_{nc(s)}(k) = [(2 + bk\Omega)H^4_{nc(s)}(k) - b^2H^2_{nc(s)}(k)]/\Delta$$

$$T^3_{nc(s)}(k) = [b\Omega H^1_{nc(s)}(k) - kH^3_{nc(s)}(k)]/\Delta$$

$$T^4_{nc(s)}(k) = [b\Omega H^2_{nc(s)}(k) - kH^4_{nc(s)}(k)]/\Delta$$

where Ω and Δ are defined below

$$\Omega = \frac{I_1(kb)}{I_0(kb)} \qquad \text{and} \qquad \Delta = b^2kI_0(bk) - 2bI_1(bk) - b^2kI_1(bk)\Omega$$

Thus, the stream function $\psi^{(2)}$ is written in an compact form interms of E_n and F_n:

$$\psi^{(2)}(r,\theta) = \psi^{\infty}(r,\theta) + \sum_{n=2}^{\infty}[E_n^{(2)}S_n^1(r,\theta) + F_n^{(2)}S_n^2(r,\theta)]$$

where S_n^1 and S_n^2 are given in the following secion.

II. Expressions for S_n^q's. (q=1,000 8)

$$S_n^1(r,\theta) = r^{-n+1}C_n^{-1/2}(\cos\theta) +$$

$$\int_0^\infty dk\ \cos(kr\cos\theta)\{T_{nc}^1(k)r\sin\theta I_1(kr\sin\theta) + T_{nc}^3(k)(r\sin\theta)^2 I_0(kr\sin\theta)\} +$$

$$\int_0^\infty dk\ \sin(kr\cos\theta)\{T_{ns}^1(k)r\sin\theta I_1(kr\sin\theta) + T_{ns}^3(k)(r\sin\theta)^2 I_0(kr\sin\theta)\}$$

$$S_n^2(r,\theta) = r^{-n+3}C_n^{-1/2}(\cos\theta) +$$

$$\int_0^\infty dk\ \cos(kr\cos\theta)\{T_{nc}^2(k)r\sin\theta I_1(kr\sin\theta) + T_{nc}^4(k)(r\sin\theta)^2 I_0(kr\sin\theta)\} +$$

$$\int_0^\infty dk\ \sin(kr\cos\theta)\{T_{ns}^2(k)r\sin\theta I_1(kr\sin\theta) + T_{ns}^4(k)(r\sin\theta)^2 I_0(kr\sin\theta)\}$$

$$\begin{bmatrix} S_n^3 \\ S_n^4 \end{bmatrix} = P_{n-1}(\cos\theta) + \int_0^\infty dk(k\sin\theta\sin(k\cos\theta)\left[\begin{bmatrix} T_{nc}^1 \\ T_{nc}^2 \end{bmatrix} I_1(k\sin\theta)\right.$$

$$\left. + \begin{bmatrix} T_{nc}^3 \\ T_{nc}^4 \end{bmatrix} \sin\theta I_0(k\sin\theta)\right] + \cos\theta\cos(k\cos\theta)\left[\begin{bmatrix} T_{nc}^1 \\ T_{nc}^2 \end{bmatrix} kI_0(k\sin\theta)\right.$$

$$\left. + \begin{bmatrix} T_{nc}^3 \\ T_{nc}^4 \end{bmatrix} (2I_0(k\sin\theta) + k\sin\theta I_1(k\sin\theta))\right]$$

$$-k\sin\theta\cos(k\cos\theta)\left[\begin{bmatrix} T_{ns}^1 \\ T_{ns}^2 \end{bmatrix} I_1(k\sin\theta) + \begin{bmatrix} T_{ns}^3 \\ T_{ns}^4 \end{bmatrix} \sin\theta I_0(k\sin\theta)\right])$$

$$+ \cos\theta\sin(k\cos\theta)\left[\begin{bmatrix} T_{ns}^1 \\ T_{ns}^2 \end{bmatrix} kI_0(k\sin\theta)\right.$$

$$\left. + \begin{bmatrix} T_{ns}^3 \\ T_{ns}^4 \end{bmatrix} (2I_0(k\sin\theta) + k\sin\theta I_1(k\sin\theta))\right]$$

$$\begin{bmatrix} S_n^5 \\ S_n^6 \end{bmatrix} = \left[\begin{bmatrix} (1-n) \\ (3-n) \end{bmatrix} \frac{C_n^{-1/2}(\cos\theta)}{\sin\theta} + \int_0^\infty dk \{ k\cos\theta \sin(k\cos\theta) \left[- \begin{bmatrix} T_{nc}^1 \\ T_{nc}^2 \end{bmatrix} I_1(k\sin\theta) \right.\right.$$

$$\left. - \begin{bmatrix} T_{nc}^3 \\ T_{nc}^4 \end{bmatrix} \sin\theta I_0(k\sin\theta) \right] + \sin\theta\cos(k\cos\theta) \left[\begin{bmatrix} T_{nc}^1 \\ T_{nc}^2 \end{bmatrix} k I_0(k\sin\theta) \right.$$

$$\left. + \begin{bmatrix} T_{nc}^3 \\ T_{nc}^4 \end{bmatrix} (2I_0(k\sin\theta) + k\sin\theta I_1(k\sin\theta)) \right]$$

$$+ k\cos\theta\cos(k\cos\theta) \left[\begin{bmatrix} T_{ns}^1 \\ T_{ns}^2 \end{bmatrix} I_1(k\sin\theta) \right.$$

$$\left. + \begin{bmatrix} T_{ns}^3 \\ T_{ns}^4 \end{bmatrix} \sin\theta I_0(k\sin\theta) \right] + \sin\theta\sin(k\cos\theta) \left[\begin{bmatrix} T_{ns}^1 \\ T_{ns}^2 \end{bmatrix} k I_0(k\sin\theta) \right.$$

$$\left. \left. + \begin{bmatrix} T_{ns}^3 \\ T_{ns}^4 \end{bmatrix} (2I_0(k\sin\theta) + k\sin\theta I_1(k\sin\theta)) \right] \right\}$$

$$\begin{bmatrix} S_n^7 \\ S_n^8 \end{bmatrix} = \begin{bmatrix} S_n^5 \\ S_n^6 \end{bmatrix} - \left(\begin{bmatrix} (n^2-1) \\ (3-n)(1-n) \end{bmatrix} \frac{C_n^{-1/2}(\cos\theta)}{\sin\theta} \right.$$

$$+ \int_0^\infty dk\{\cos(k\cos\theta)\left[\begin{bmatrix} T_{nc}^1 \\ T_{nc}^2 \end{bmatrix} k^2(\sin^2\theta - \cos^2\theta)I_1(k\sin\theta) \right.$$

$$\left. + \begin{bmatrix} T_{nc}^3 \\ T_{nc}^4 \end{bmatrix} \sin\theta(k^2(\sin^2\theta - \cos^2\theta)I_0(k\sin\theta) + 2k\sin\theta I_1(k\sin\theta))\right]$$

$$- k\cos\theta\sin(k\cos\theta)\left[\begin{bmatrix} T_{nc}^1 \\ T_{nc}^2 \end{bmatrix} (2k\sin\theta I_0(k\sin\theta) - I_1(k\sin\theta)) \right.$$

$$\left. + \begin{bmatrix} T_{nc}^3 \\ T_{nc}^4 \end{bmatrix} \sin\theta(3I_0(k\sin\theta) + 2k\sin\theta I_1(k\sin\theta))\right]$$

$$+ \sin(k\cos\theta)\left[\begin{bmatrix} T_{ns}^1 \\ T_{ns}^2 \end{bmatrix} k^2(\sin^2\theta - \cos^2\theta)I_1(k\sin\theta) \right.$$

$$\left. + \begin{bmatrix} T_{ns}^3 \\ T_{ns}^4 \end{bmatrix} \sin\theta(k^2(\sin^2\theta - \cos^2\theta)I_0(k\sin\theta) + 2k\sin\theta I_1(k\sin\theta))\right]$$

$$+ k\cos\theta\cos(k\cos\theta)\left[\begin{bmatrix} T^1_{ns} \\ T^2_{ns} \end{bmatrix} (2k\sin\theta I_0(k\sin\theta) - I_1(k\sin\theta))\right.$$

$$\left. + \begin{bmatrix} T^3_{ns} \\ T^4_{ns} \end{bmatrix} \sin\theta(3I_0(k\sin\theta) + 2k\sin\theta I_1(k\sin\theta))\right]\}$$

The above integrals must be evaluated numerically.

Table I

A comparison of λ_u for a gas bubble (κ=0)
in the infinity medium
with the results from Sahdal-Johnson (1983)

cap angle ϕ	λ_u	λ (Sahdal-Johnson)
0	1.0	1.0
30	1.025	1.028
60	1.166	1.167
90	1.355	1.356
120	1.469	1.471
150	1.499	1.499
180	1.500	1.500

Table II

A comparison of λ_u and λ_v for a clean gas bubble (ϕ=0, κ=0)
with the results from Hyman-Skalak (1970)

			Hyman-Skalak(1970)	
a'/b'	λ_u	λ_v	λ_u	λ_v
0.1	1.1632	1.1631	1.16	1.16
0.2	1.3900	1.3895	1.39	1.39
0.3	1.7251	1.7211	1.725	1.722
0.4	2.2626	2.2409	2.263	2.241
0.5	3.2224	3.1295	3.222	3.130
0.6	5.2043	4.8453	5.205	4.846

Table III

A comparison of λ_u and λ_v for a solid sphere (ϕ=180) with the results from Hyman-Skalak (1970)

a'/b'	λ_u	λ_v	Hyman-Skalak(1970) λ_u	Hyman-Skalak(1970) λ_v
0.1	1.2633	1.2548	1.263	1.255
0.2	1.6793	1.6348	1.680	1.635
0.3	2.3701	2.2289	2.371	2.231
0.4	3.5914	3.2157	3.596	3.218
0.5	5.9473	4.9953	5.970	5.004
0.6	11.093	8.6130	11.135	8.651

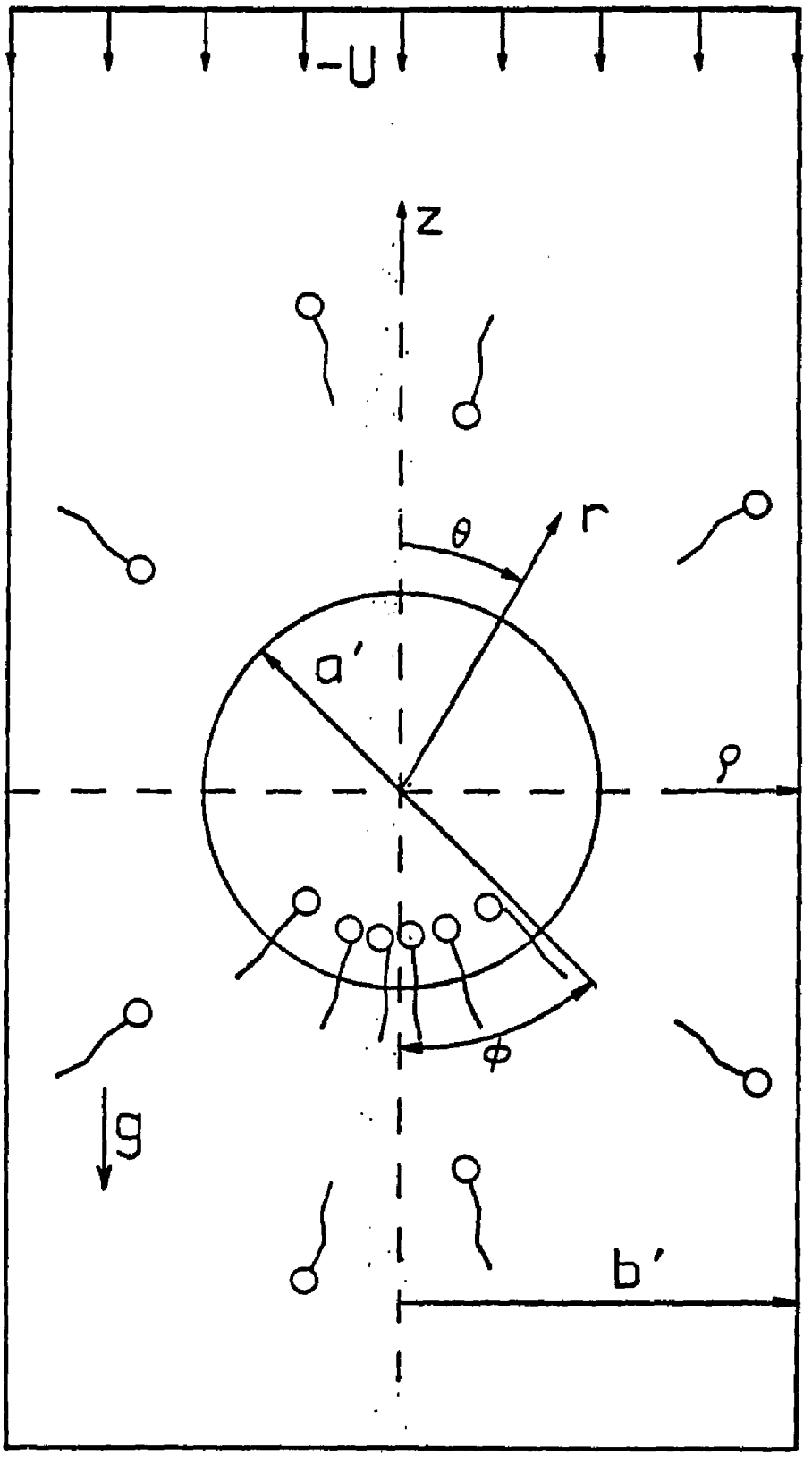

Figure 1

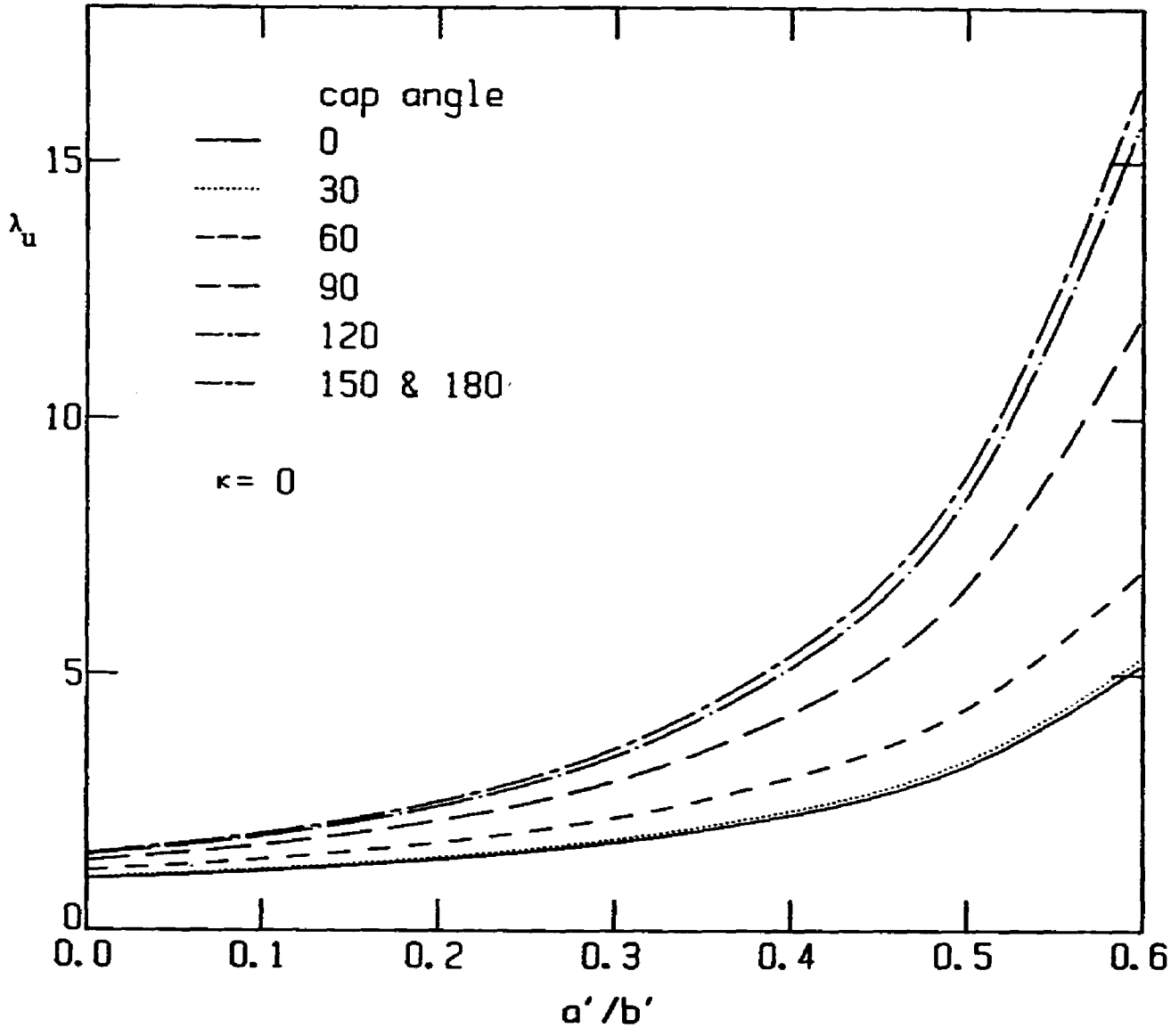
cap angle
0
30
60
90
120
150 & 180
κ= 0
λu
15
10
5
0
0.0
0.1
0.2
0.3
0.4
0.5
0.6
a'/b'

Figure 2a

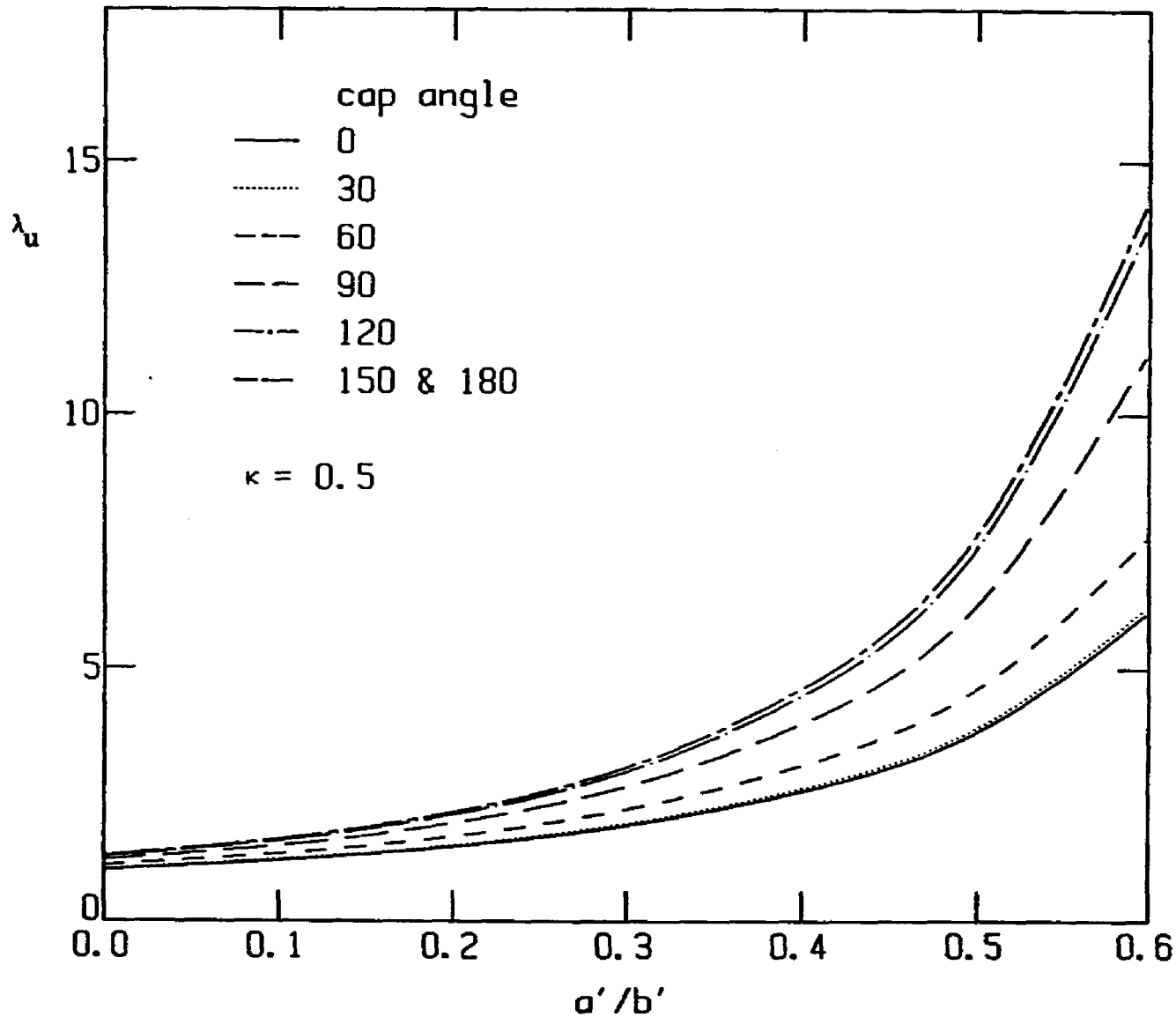
cap angle
0
30
60
90
120
150 & 180
κ = 0.5
λ_u
15
10
5
0
0.0
0.1
0.2
0.3
0.4
0.5
0.6
a'/b'

Figure 2b

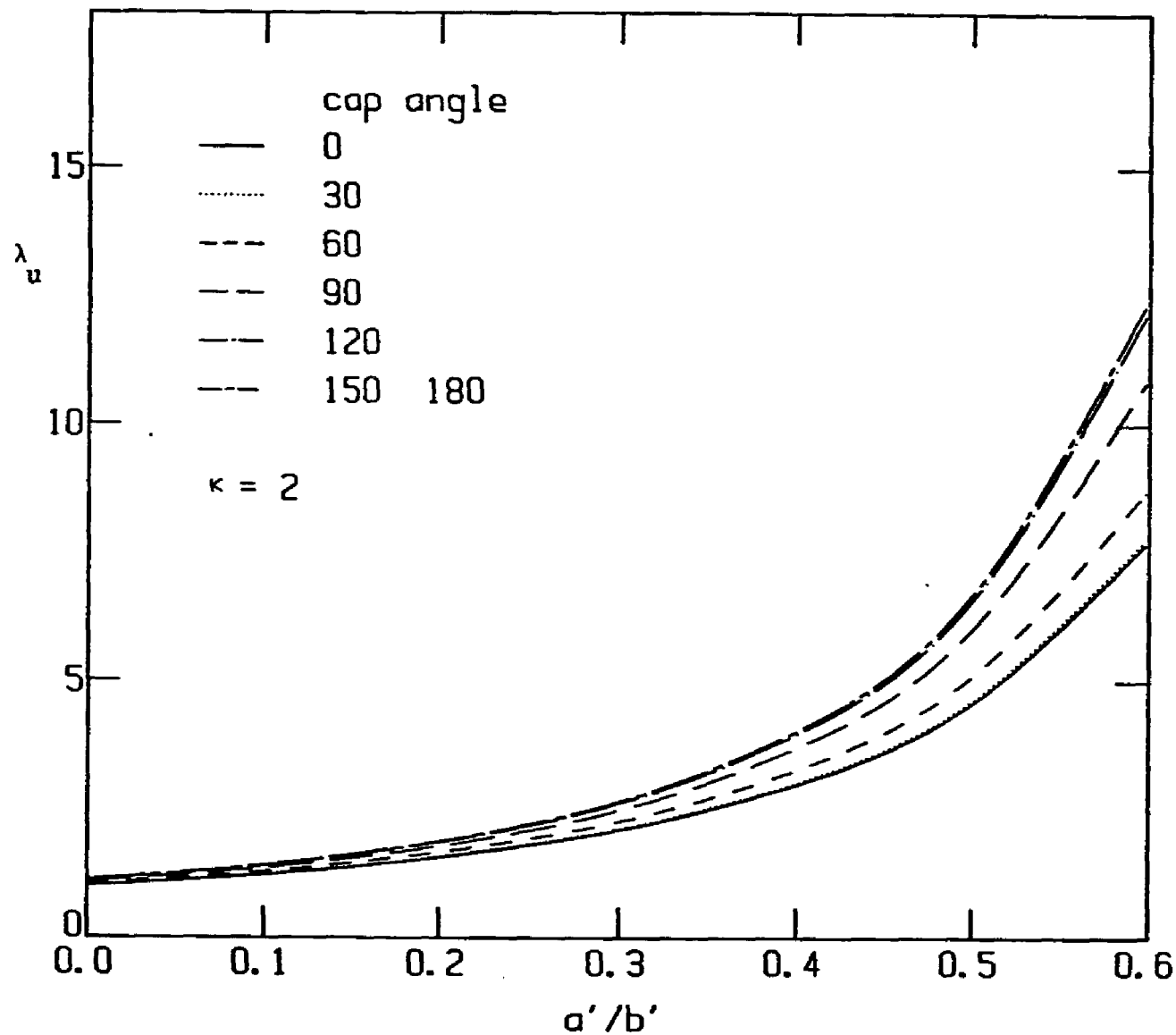
cap angle
0
30
60
90
120
150 180
κ = 2
λ_u
15
10
5
0
0.0
0.1
0.2
0.3
0.4
0.5
0.6
a'/b'

Figure 2c

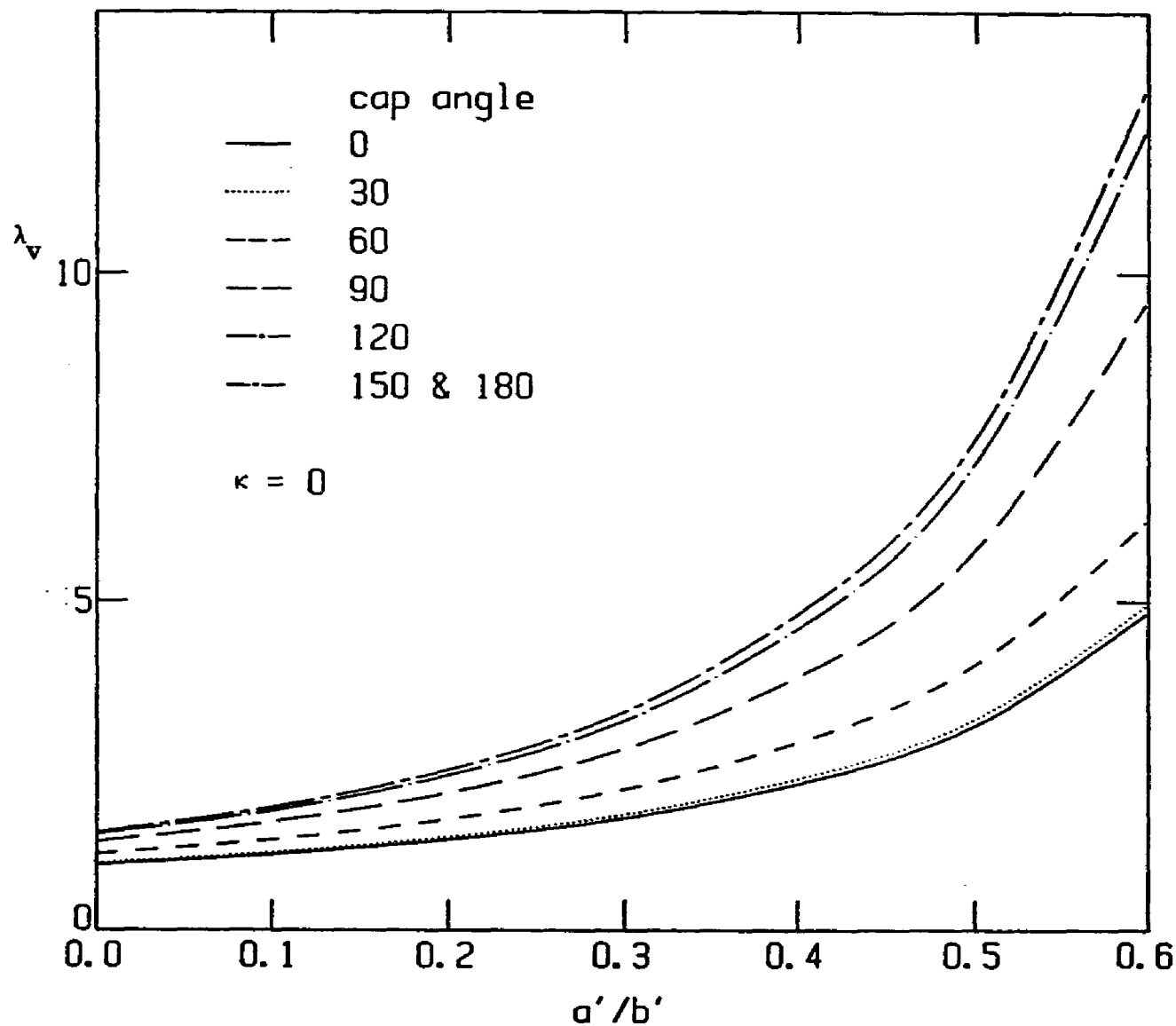

Figure 3a

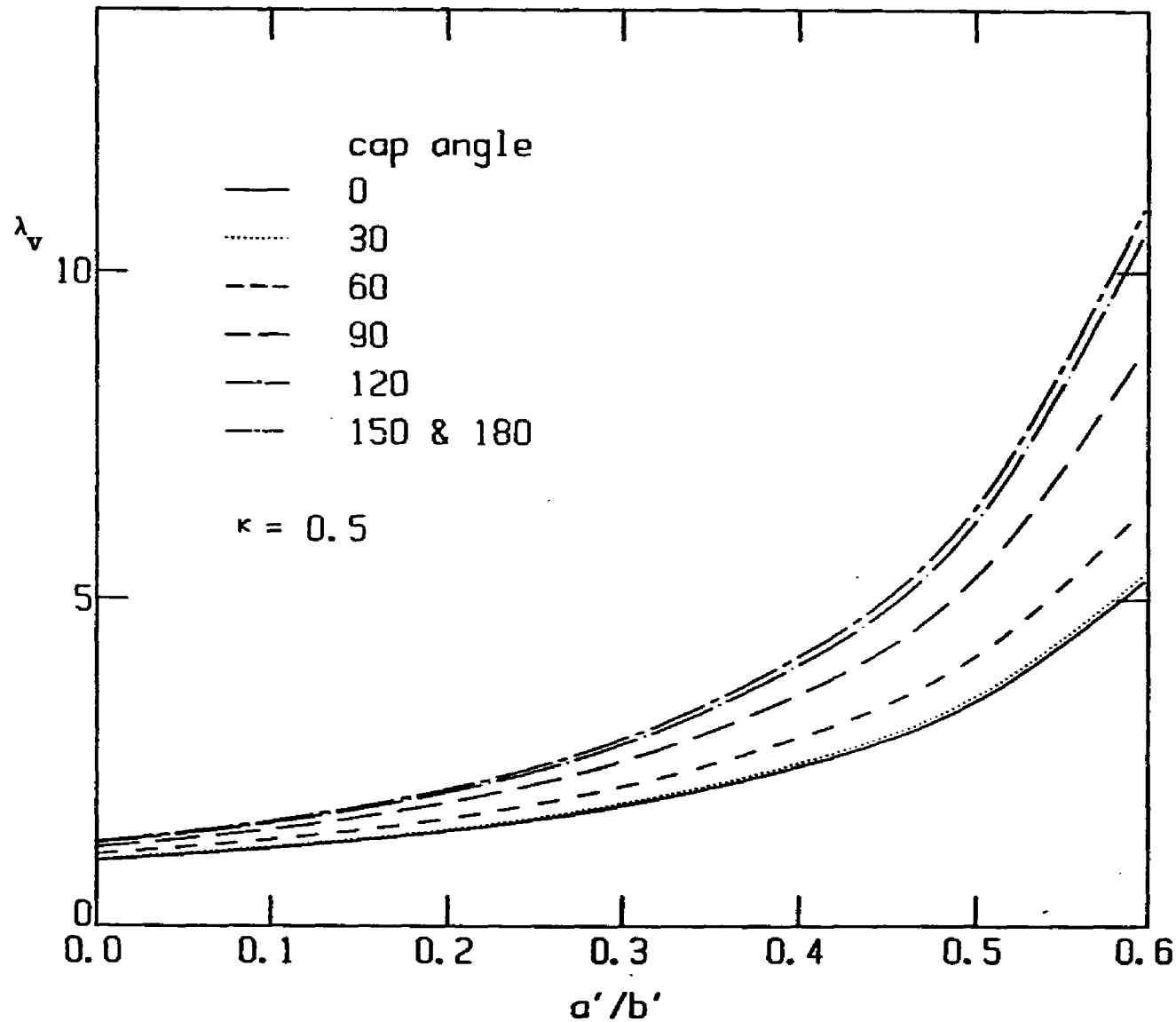
cap angle
0
30
60
90
120
150 & 180
κ = 0.5
λ_v
10
5
0
0.0
0.1
0.2
0.3
0.4
0.5
0.6
a'/b'

Figure 3b

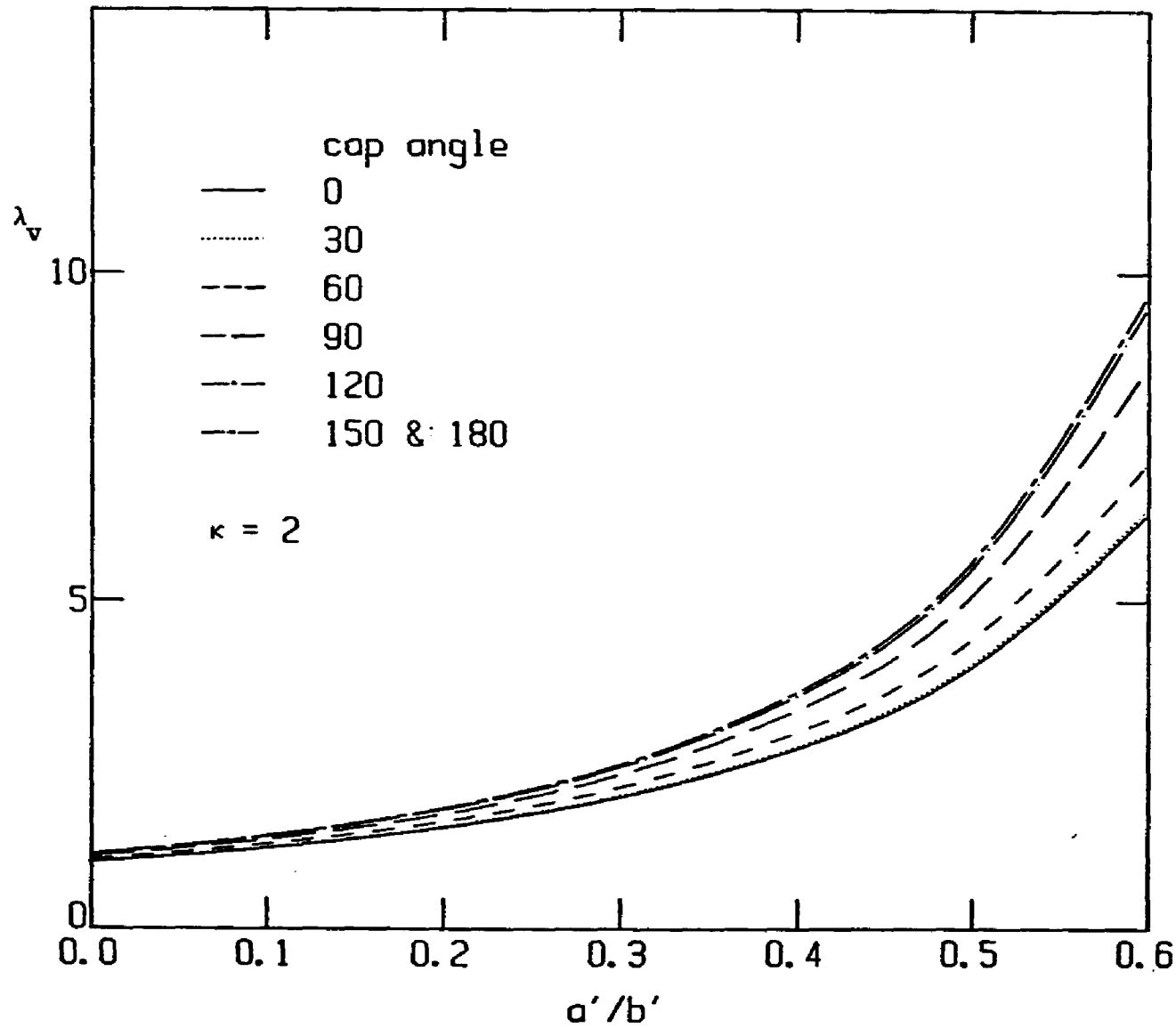

Figure 3c

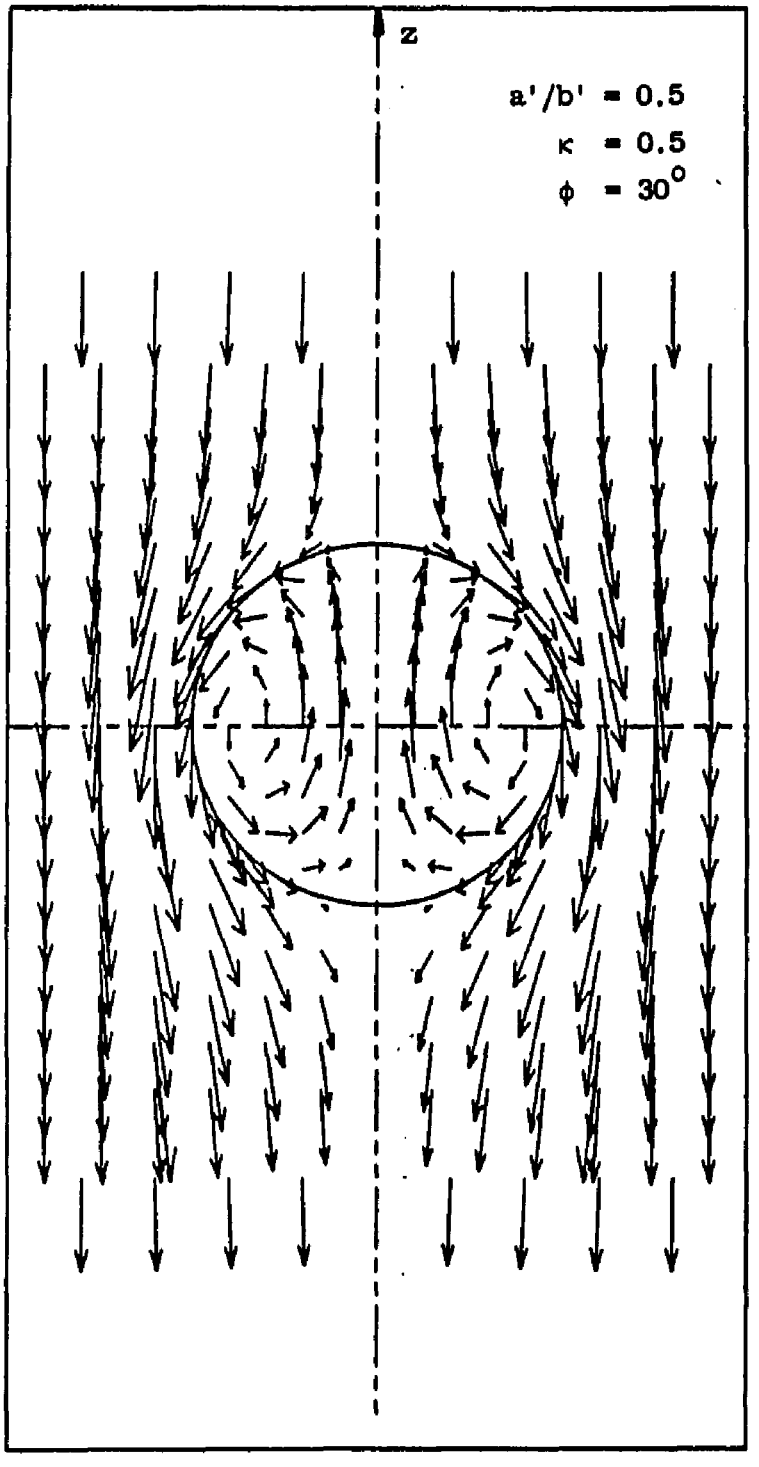

Figure 4a

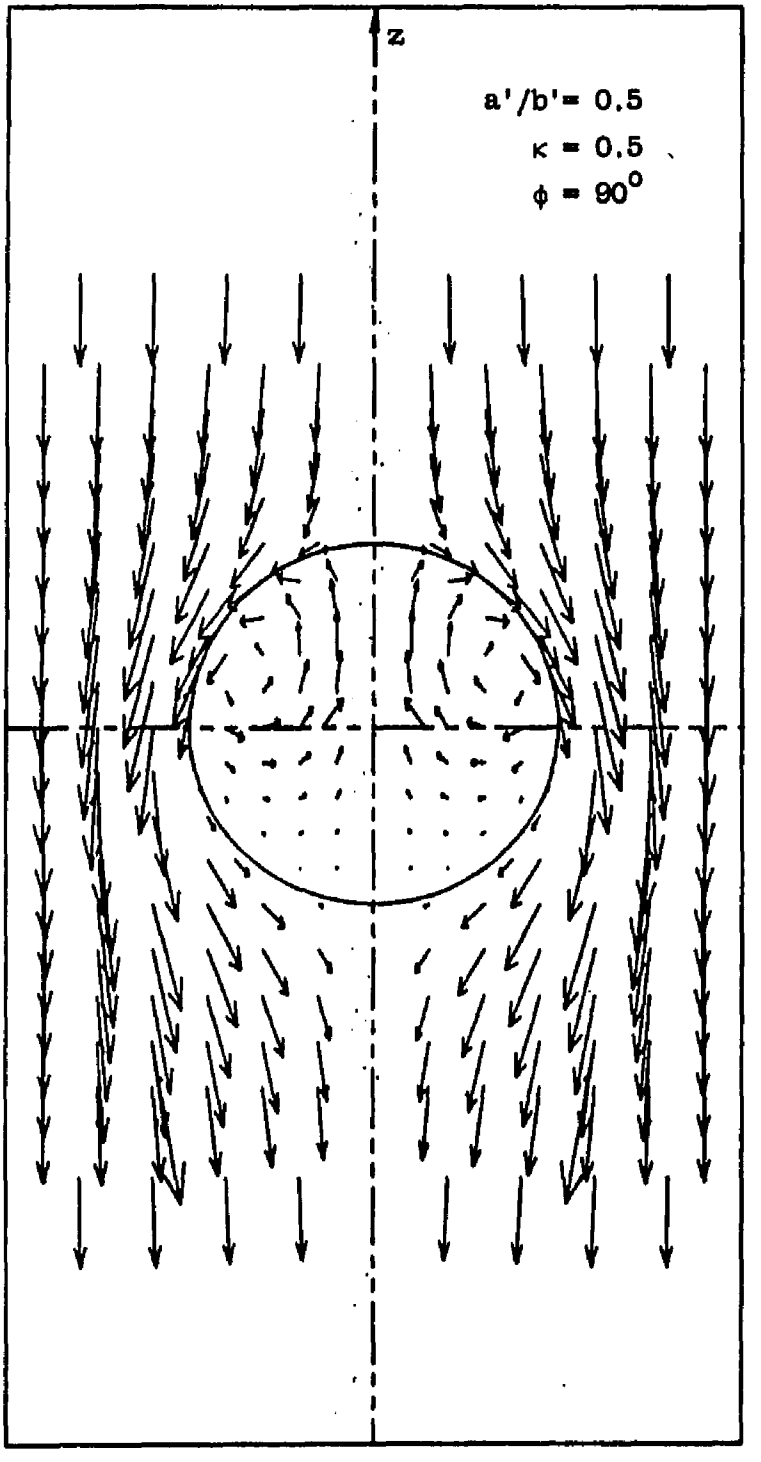

Figure 4b

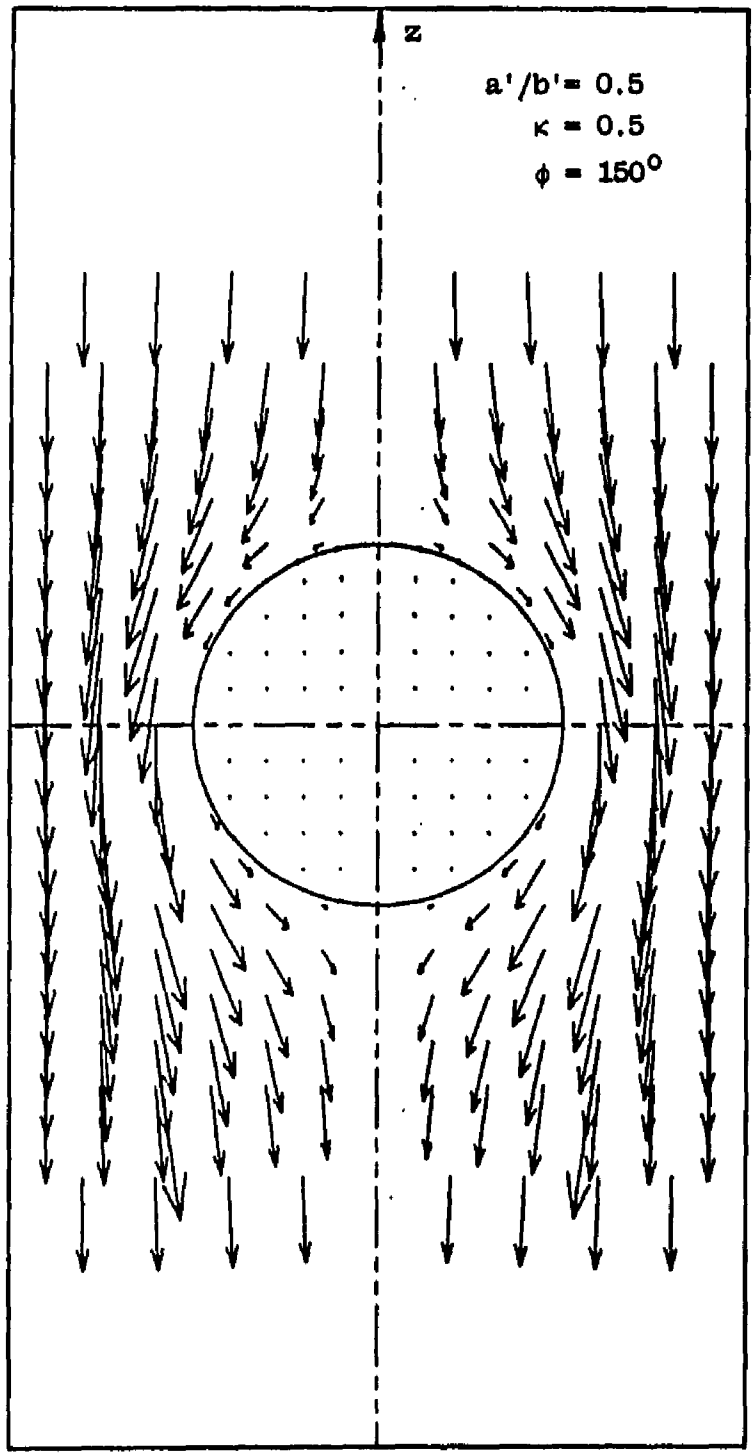

Figure 4c

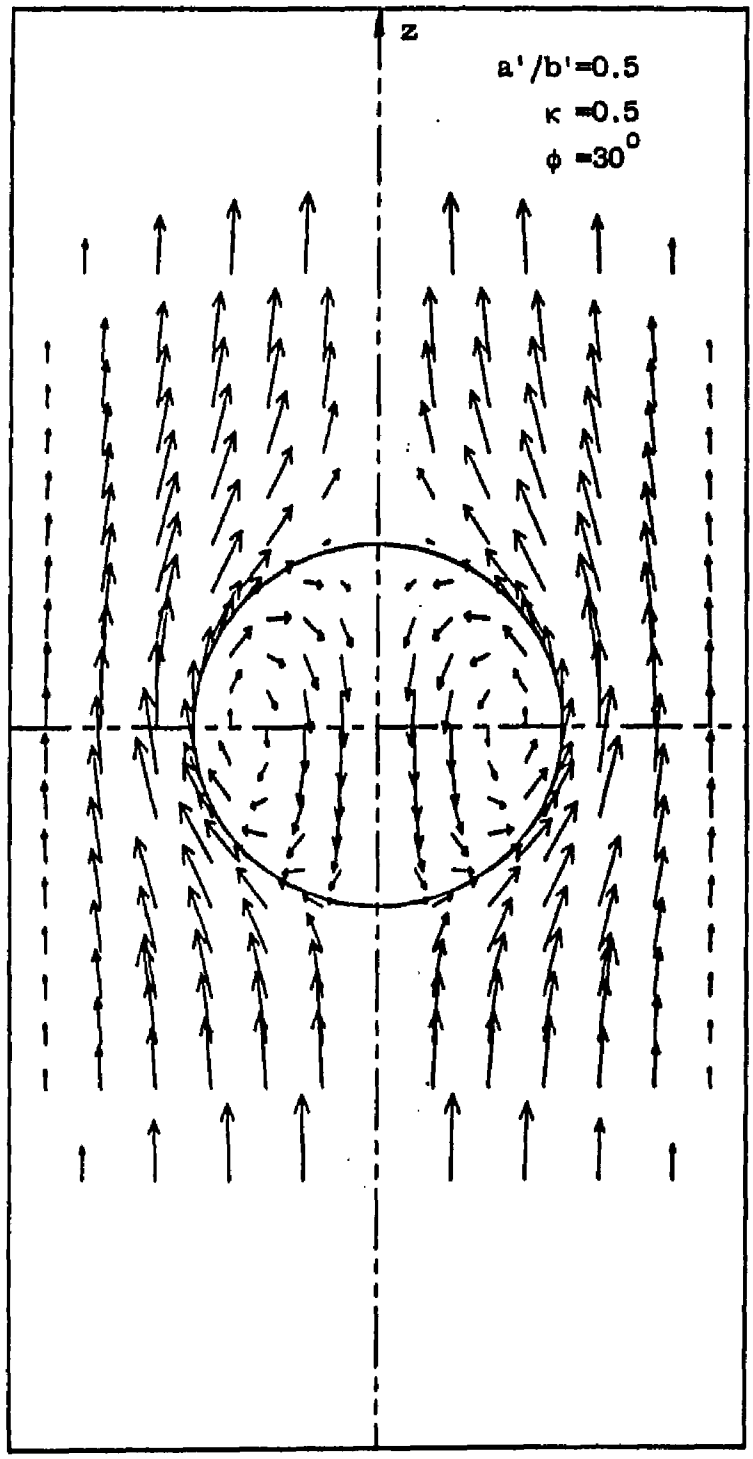

Figure 5a

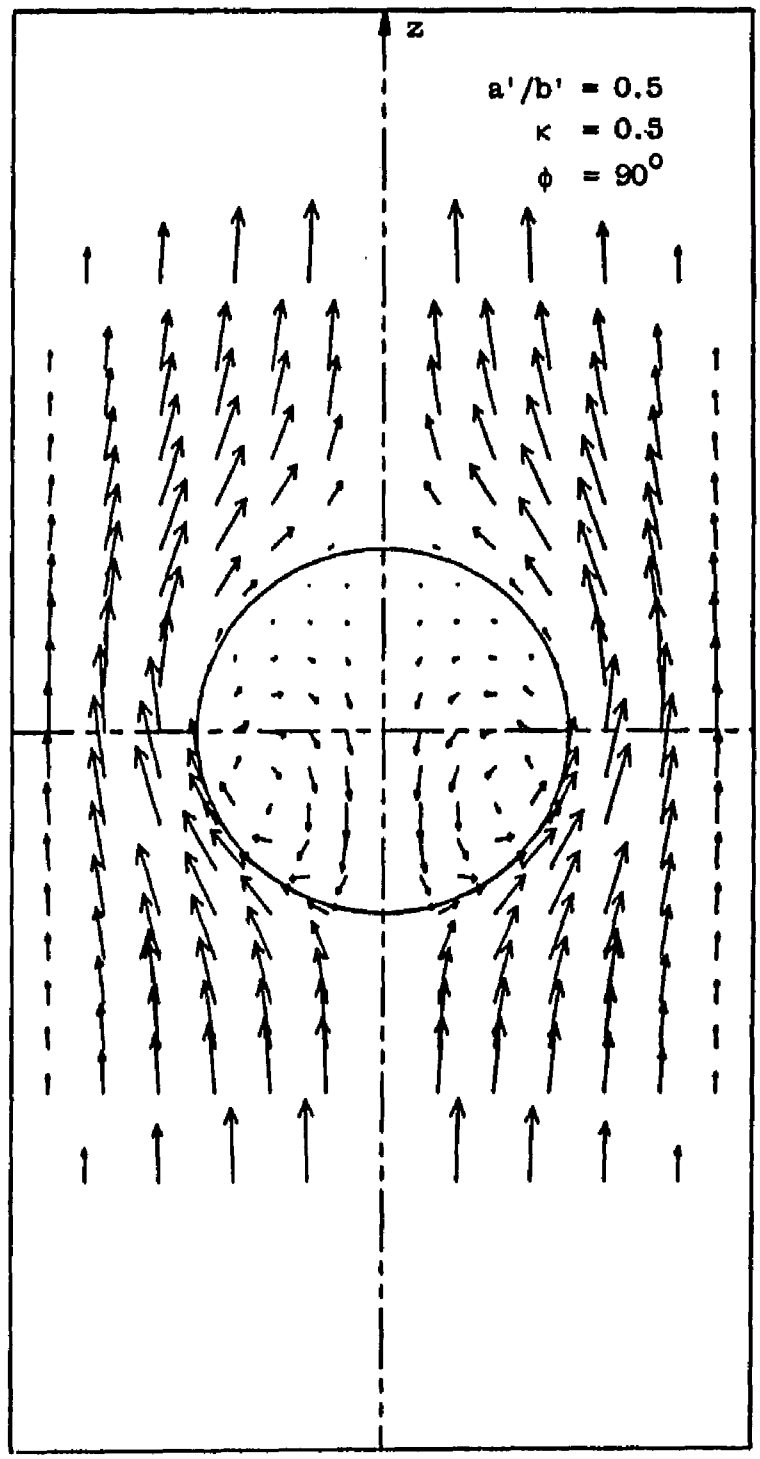

Figure 5b

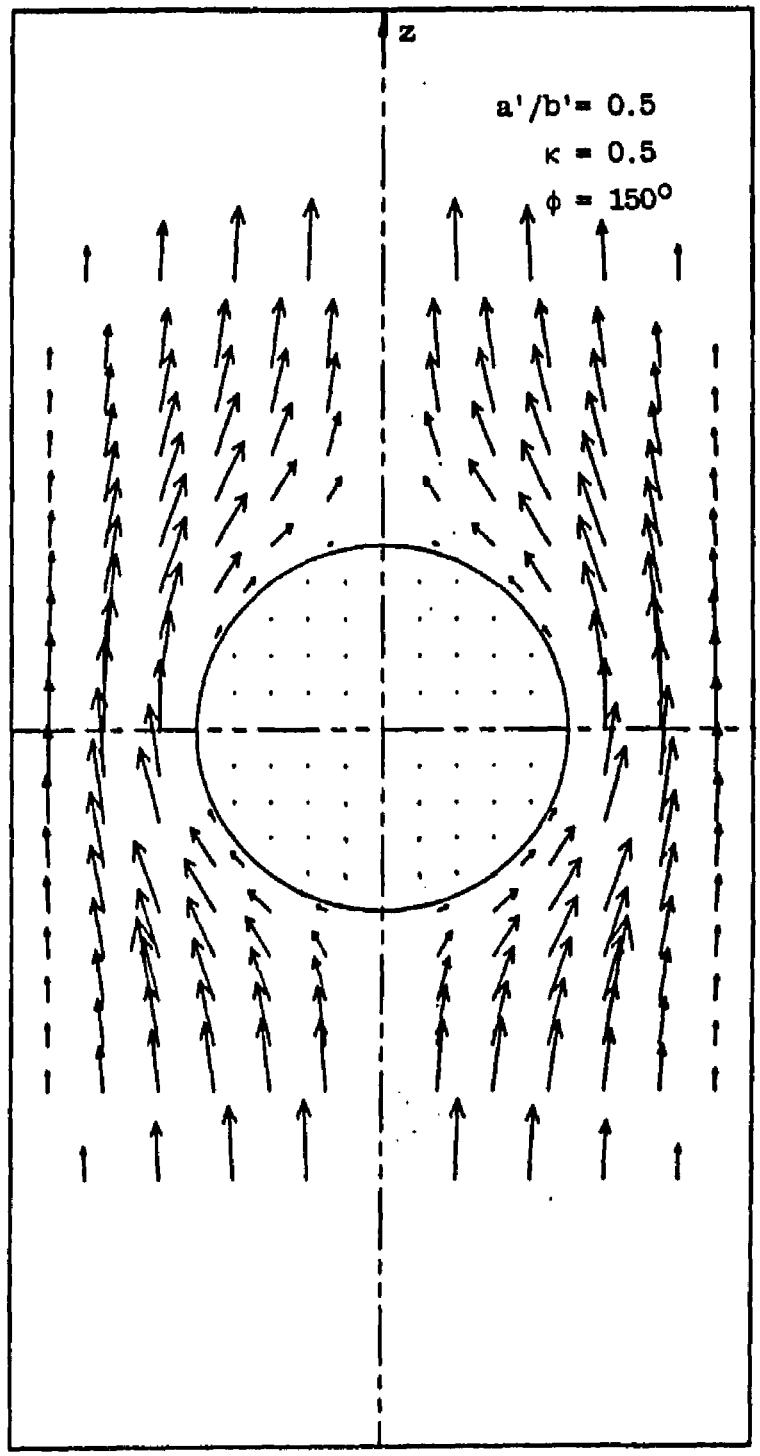

Figure 5c

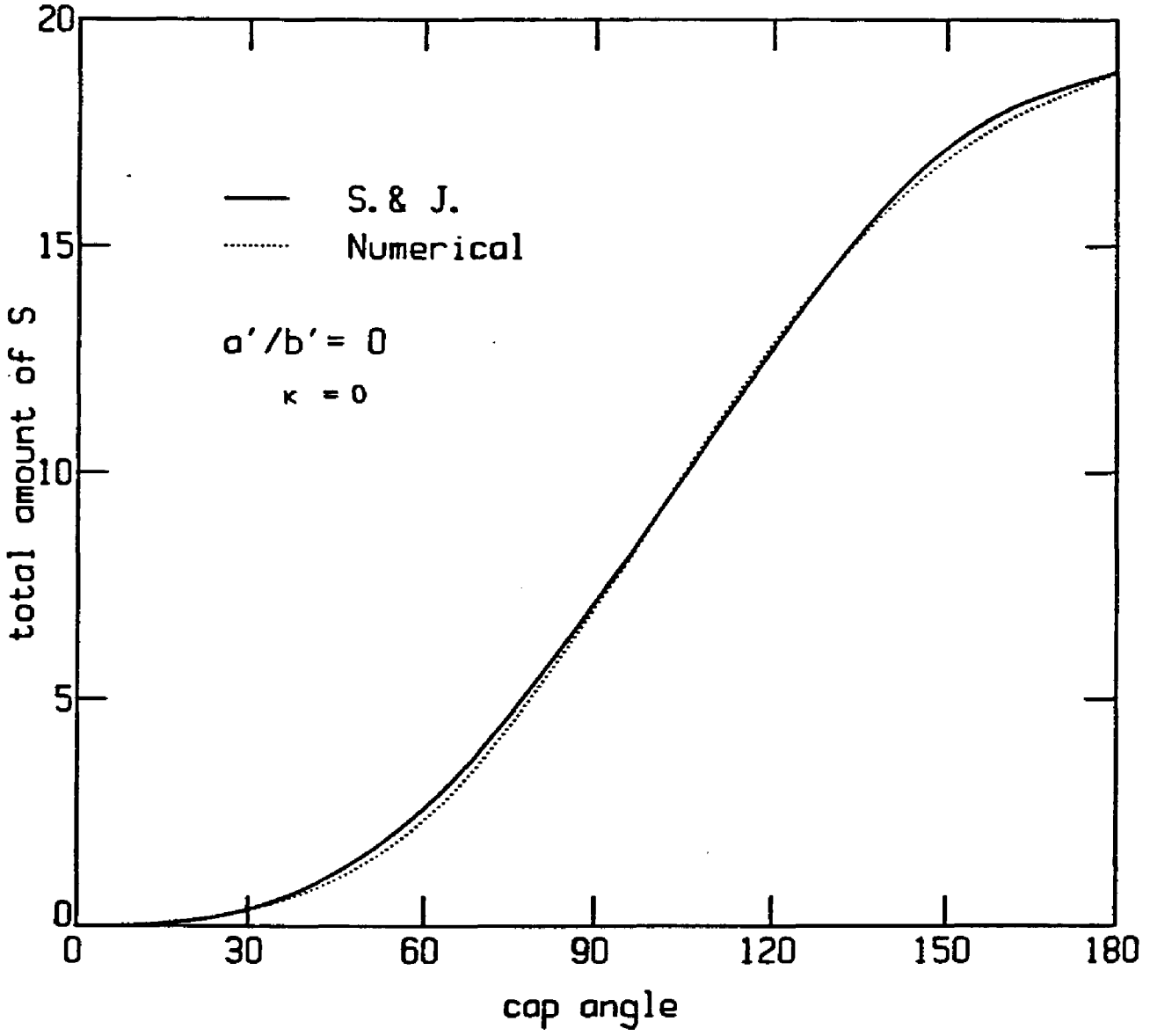
20
15
10
5
0
0
30
60
90
120
150
180
total amount of S
cap angle
S. & J.
Numerical
a'/b' = 0
κ = 0

Figure 6

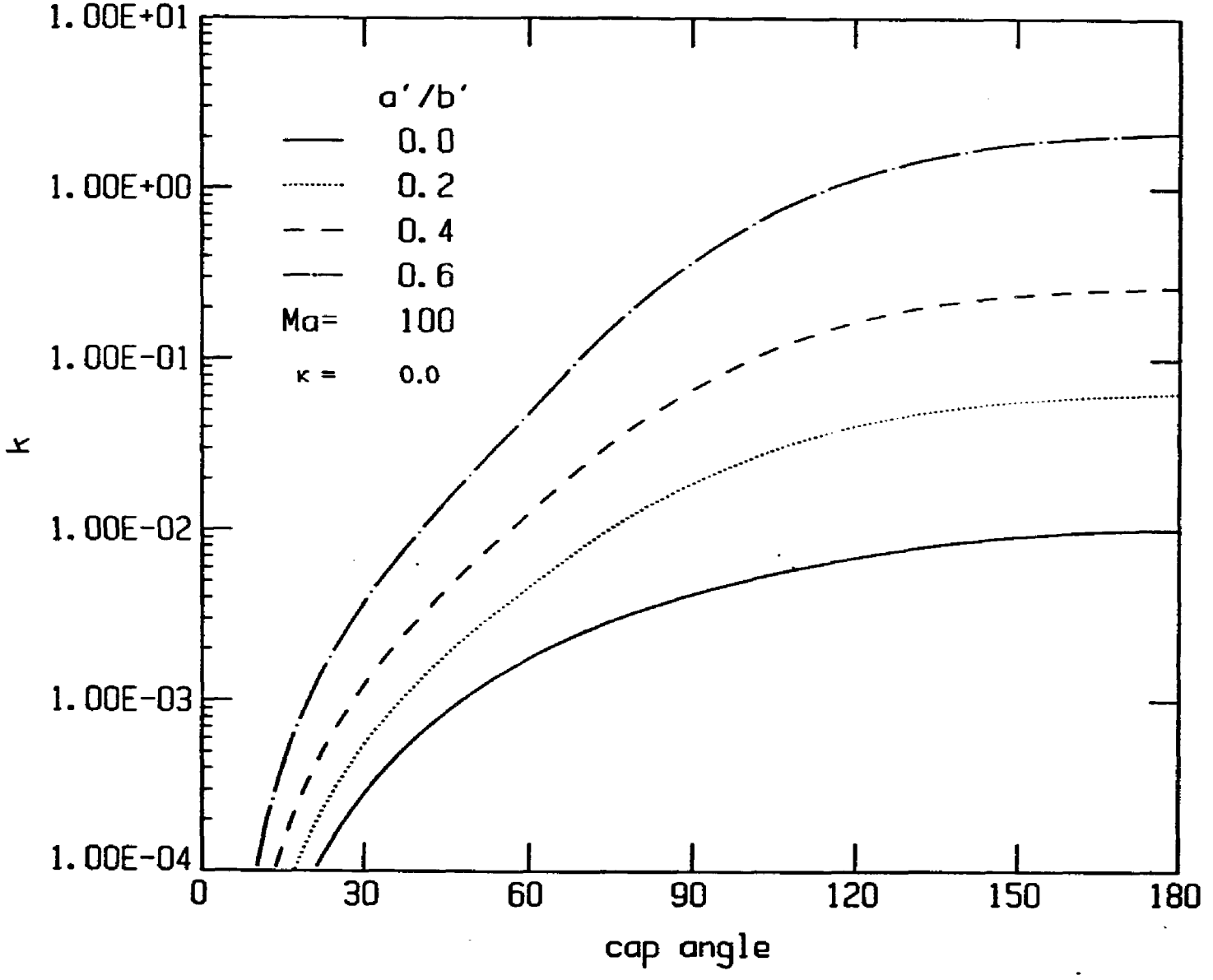
1.00E+01
1.00E+00
1.00E-01
1.00E-02
1.00E-03
1.00E-04
K
a'/b'
0.0
0.2
0.4
0.6
Ma= 100
κ = 0.0
0
30
60
90
120
150
180
cap angle

Figure 7

k
1.00E-05
1.00E-04
1.00E-03
1.00E-02
1.00E-01
1.00E+00
1.00E+01
1.00E+02
0
30
60
90
120
150
180
cap angle
M_a
0
0.1
1.0
10
100
1000
a'/b' = 0.2
κ = 0

Figure 8a

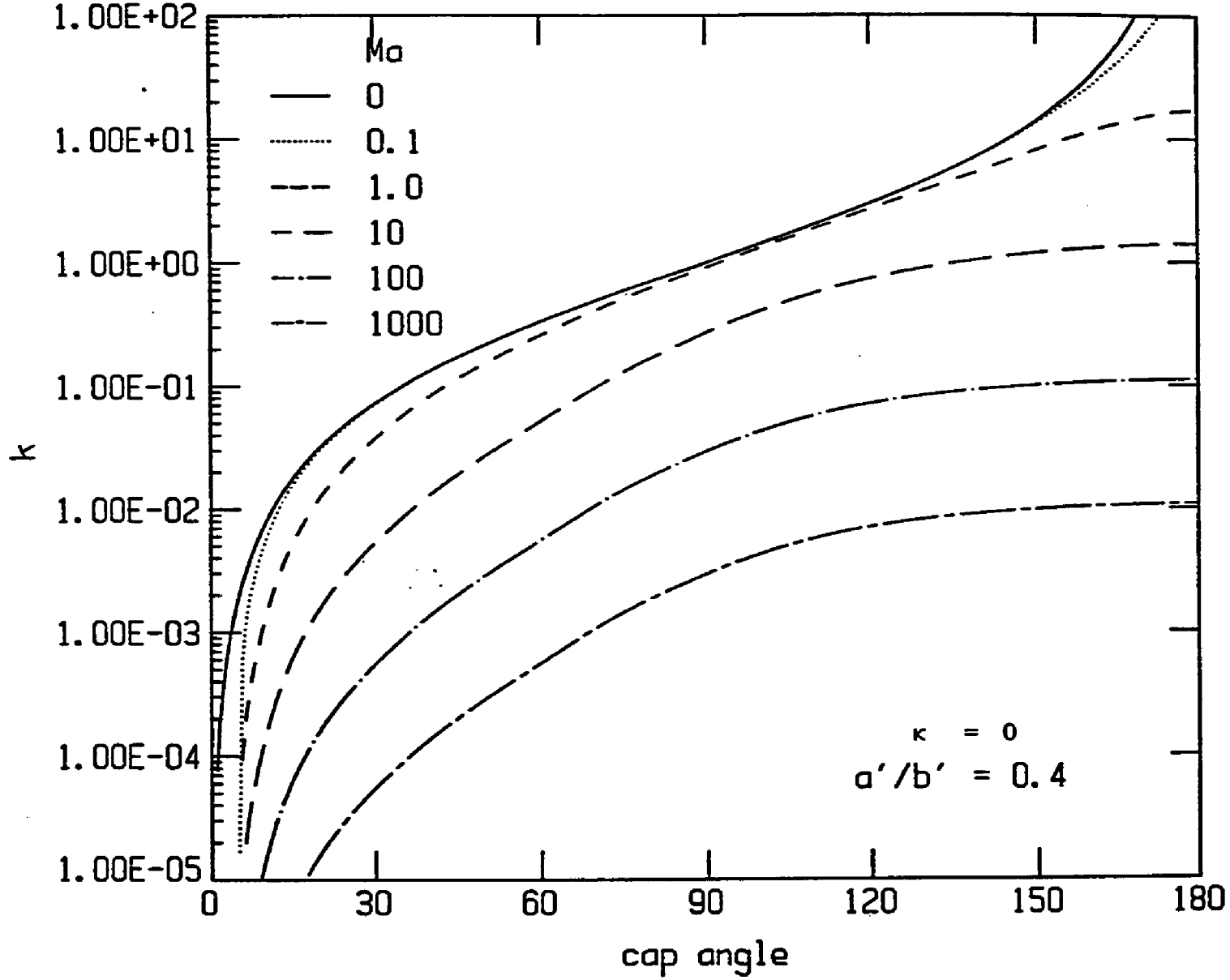
1.00E+02
1.00E+01
1.00E+00
1.00E-01
1.00E-02
1.00E-03
1.00E-04
1.00E-05
K
Ma
0
0.1
1.0
10
100
1000
κ = 0
a'/b' = 0.4
0
30
60
90
120
150
180
cap angle

Figure 8b

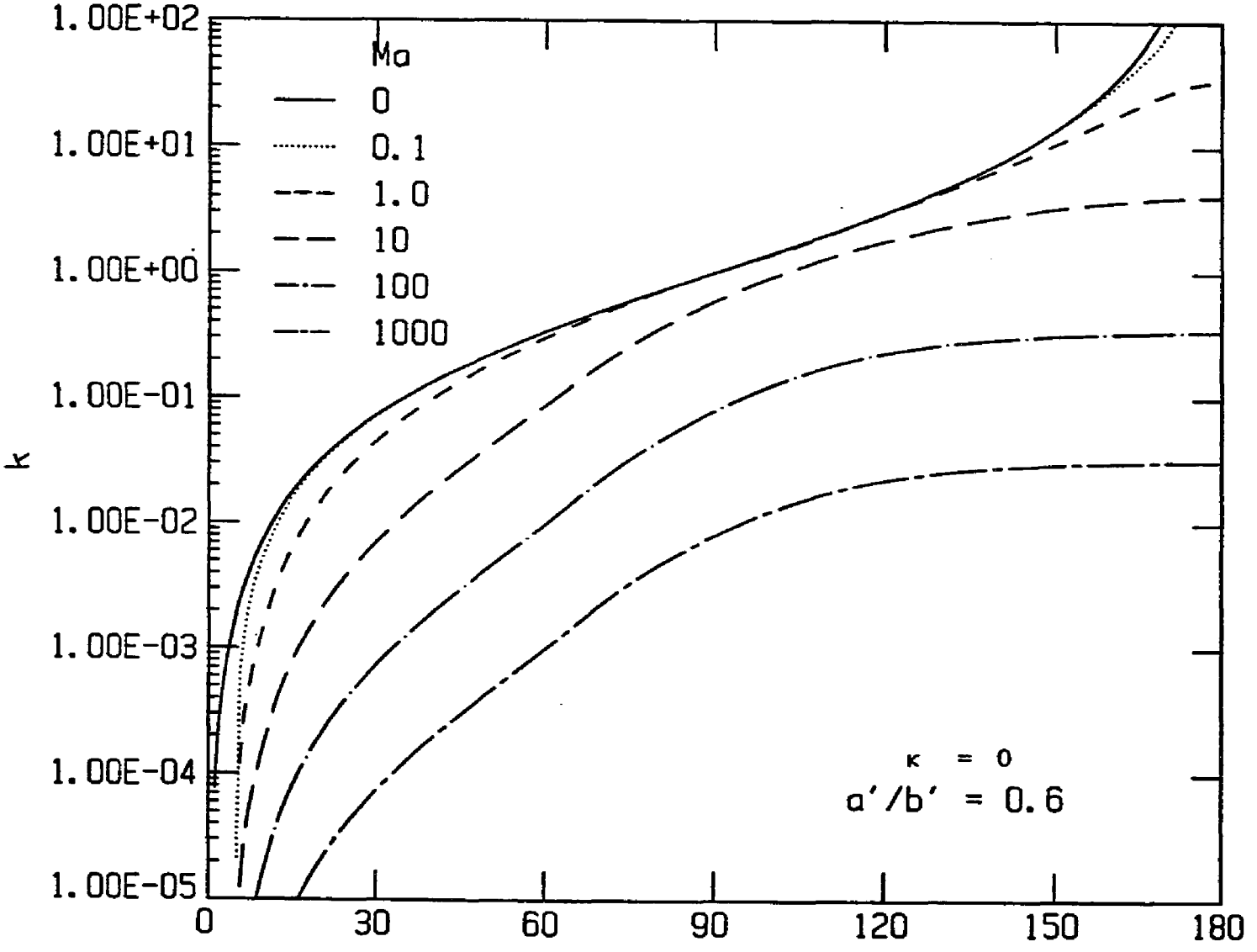
1.00E+02
1.00E+01
1.00E+00
1.00E-01
1.00E-02
1.00E-03
1.00E-04
1.00E-05
κ
Ma
0
0.1
1.0
10
100
1000
κ = 0
a'/b' = 0.6
0
30
60
90
120
150
180
cap angle

Figure 8c

Chapter 6

Concluding Remarks

The influence of bulk soluble surfactants on the creeping motion of spherical fluid droplets in an infinite medium or in a tube has been investigated analytically in order to predict the axisymmetric translational velocities. The surfactant distribution was determined by the competition between sorption kinetics and surface convection, with bulk diffusion assumed to be faster than the kinetic exchange. Four problems were investigated, two concerned with the motion in an infinite medium, and two in the constrained geometry of a tube. The infinite medium problems computed the steady translational velocity for the case of slow sorption kinetics (the stagnant cap regime) and the unsteady motion due to the transient adsorption of a monolayer for arbitrary rate of kinetic exchange. The tube problems calculated the steady translational velocities for arbitrary sphere to diameter ratios for the cases of uniform retardation (fast sorption kinetics) and the stagnant cap regime.

The major results obtained from this study are as follows. In an infinite medium for the stagnant cap regime (Chapter 2), a nonlinear surface equation of state (the Frumkin relation) was used to compute the relationship between the cap angle and the bulk concentration and physicochemical properties of the surfactant. The results allow for the realistic prediction of the bulk concentration necessary to completely stagnate the surface, and the compression of the cap angle with increased sphere velocity. The results also indicate that the linear isotherm is only valid for either large

Marangoni number or small cap angle (cf. Chapter 2). For the case of small Marangoni number, as is usually the case in polymer rheology, the linear isotherm can underpredict the cap angle as the surface pressure in the cap region is underestimated.

The equation that describes the unsteady hydrodynamics of gradual droplet retardation with the adsorption of surfactant (Chapter 3) was solved for arbitrary values of the ratio of the kinetic exchange to the surface convection (the Biot number). Unsteady profiles of the translational velocities and the surface surfactant distribution were obtained. The simulations showed the expected trend: As the Biot number is successively decreased, the time necessary for the steady velocity to be achieved is increased. It was also shown that this time will diminish as the Marangoni number is increased.

In a cylindrical tube, the influence of surfactant on the hydrodynamics was first solved perturbatively (Chapter 4) in the limit of sorption controlled uniform retardation. In this perturbation procedure an ordering parameter ϵ was constructed as the ratio of the convective rate of surfactant transport to the rate of adsorption and desorption from the bulk to the surface, that is $\epsilon=1/Bi$. The limit ϵ equal to zero yields equations identical to the case of a clean droplet, and the first order equations describe corrections to the hydrodynamic drag. First order drag coefficients were obtained; it was shown that the presence of an adsorbed surfactant layer can accelerate the droplet when the droplet is suspended in Poiseuille flow and bouyancy is directed opposite to the direction of the Poiseuille flow.

The results of the study of a spherical fluid droplet in a cylindrical tube in the case of small Biot number, i.e. when sorption kinetics are slow relative to convection allowing stagnant caps to form, were given in Chapter 5. The exact equations governing the hydrodynamics and mass transfer were solved numerically. The drag coefficient was a strong function of the cap angle ϕ for the ratio of the drop to tube diameters a'/b' larger than 0.4. The cap angle as a function of the surfactant physicochemical parameters was also calculated, and it was found that for large Marangoni numbers, very little surfactant is necessary to completely stagnate the interface.

The two solution techniques used for solving the problems addressed in this study are the Galerkin technique and the boundary collocation method. For the unsteady problem, the Galerkin residual method was adopted to solve the nonlinear transient mass conservation equation and obtain the translational velocity. It was found that for a Biot number larger than 0.05, a sufficiently converged solution can be obtained without the expense of extended computer time. For the tube problems, the boundary colllocation method was used. This method was quite powerful in its ability to obtain satisfactorally converged results. This was especially true in solving the mixed boundary problem of zero velocity in the cap and continuity of tangential stress in the surfactant free region. Of key importance, however, was the location of the collocation points. Convergence of better than .1% were obtained with only 36 points on the semiarc surface of the droplet. This is especially remarkable comsidering the difficulties encountered by other investigators.

Areas of interest for future research arise from the results and discussions in the above four chapters. Some of them are detailed

below. First, in this study, the bulk diffusion of surfactant was not included due to the assumption $BiPe_A \to 0$. The effects of concentration gradients within the bulk can be included by solving the bulk continuity equation for the surfactant.

Recall the solution procedure used in Chapters 4 and 5. This method can be used to solve the problem of more than one droplet moving in a tube retarded by surfactant (cf. Leichtberg, et al 1976). This is a second area of research suggested by this study.

Thirdly, in Chapters 4 and 5, the solutions for the drag coefficients for the surface force caused by the distribution of surfactant can apply to other surface forces. An example is the motion of a droplet caused by Marangoni forces derived from an imposed temperature gradient, which is of interest in the area of microgravity thermophoretics.

The fourth problem which is suggested is the effect of more than one stagnation zone on the surface of the droplet. According to Chapter 4, when the centerline velocity of the Poiseuille flow is larger than the terminal velocity (as, for example, in the motion of a neutrally bouyant sphere), there are two stagnation rings which form on the clean surface of the droplet aside from the two stagnation points. The surfactant adsorbed on the surface of the droplet under the above flow circumstance will form one surfactant stagnant cap and one surfactant stagnation ring for the case of slow adsorption kinetics.

Finally, an experimental study based on this research could be formulated in order to measure the sorption kinetic constants.

REFERENCES

1. Agrawal,S.K.and Wasan,D.T. 1979 The effect of interfacial viscosities on the motion of drop and bubbles. The Chem. Engng. J. **18**, 215-223.

2. Ambari,A.,Gauthier-Manuel,B. and Guyon,E. 1985 Direct measurement of tube wall effect on the Stokes force. Phys. Fluids **28**, 5.

3. Beitel,A. and Heideger,W.J. 1971 Surfactant effects on mass transfer from drops subject to interfacial instability. Chem. Engng. Sci. **26**, 711-717.

4. Bikerman,J.J. 1973 Foams, Springer-Verlag: New York.

5. Bohlin,T. 1960 On the drag of a rigid sphere moving in a viscous liquid inside a cylindrical tube. K, tek. Hogsk. Handl. No. 155.

6. Boussinesq,M.J. 1913 J., Ann. Chim. Phys. **29** (8) 349, 357, 364.

7. Brenner,H. 1970 Pressure drop due to the motion of neutrally buoyant particles in duct flows. J. Fluid Mech. **43**, 641-660.

8. Brenner,H. 1971 Pressure drop due to the motion of neutrally buoyant particles in duct flows: II. Spherical droplets and bubbles. I/EC Fundamentals **10**, 537-543.

9. Burgers,J.M. 1940 Proc. K. ned.Akad. Wet.**43**,425,646.

10. Coutanceau, 1971 These d'Etat, Universite de Poitiers.

11. Davis,R.E. and Acrivos,A. 1966 The influence of surfactants on the creeping motion of bubbles. Chem. Engng Sci. **21**, 681-685.

12. Davies,J.T. and Rideal,E.K. 1963 Interfacial Phenomena. Second Edition Academic Press.

13. Deryagin,B.,Dukhin,S.and Lisichenko,B. 1960 The Russian J. of Physical chemistry physical Physical **33** 389-.

14. Edge,R.M. and Grant,C.D. 1972 The motion of drops in water contaiminated with a surface active agent. Chem. Engng Sci. **27**, 1709-1721.

15. Elzinga,E.R. and Banchero,J.T. 1961 Some Observation on the Mechanics of Drops in Liquid-Liquid System. AIChE J.,**7**, 394.

16. Evans,E.A.and Skalak,R. 1980 Mechanics and Thermodynamics of Biomembranes. CRC Press, Inc. Boca Raton,Florida.

17. Faxen,H. 1922 Die Geschwindigkeit zwen Kugeln, die unter Ein winung der Schwere in einen zahen Flussigkeit fallen. Ann. Phys. **68**, 89.

18. Faxen,H. 1923 Die Bewegung either starren Kugel langs der Achse eines mit zaher Flussigkeit gefullten Rohres. Ark.Mat.Astr.Fys.**17**, 1-28.

19.Frumkin,A. and Levich,V.G. 1947 Zh. Fiz. Khim. **21**, 1183.

20.Garner,F.H. and Skelland, A.H.P. 1956 Effects of Surface active Agents on Extraction from Droplets. Engng., Design, and Equipment **48**, No.1 51-58.

21.Ginley,G.M. and Radke,C.J. 1988 The influence of solution surfactants on the flow of long bubble through a cylindrical capillary. ACS Symposium Series, Toronto,Canada June 5-11, 1988.

22.Greenstein,T. and Happel,J. 1970 The slow motion of two particles symmetrically placed about the axis of a circular cylinder in a direction perpendicular to their line of centers. Appl. Scient. Res. **22**,345-359.

23.Griffith,R.M. 1962 The effect of surfactants on the terminal velocity of drops and bubbles. Chem. Engng Sci. **17**, 1057-1070.

24.Haberman,W.L. and Sayre,R.M. 1958 Motion of rigid and fluid spheres in stationary and moving liquids inside cylindrical tubes. David W. Taylor Model Basin Report No. 1143, U.S. Navy Dept.

25.Hadamard,J. 1911 Mouvement permanent lent d' une sphere liqide et visqueuse dans un liquide visqueux. J.,C. R. Acad. Sci., Paris, **152**, 1735.

26.Happel,J. and Byrne,B.J. 1954 Motion of a sphere and fluid in a cylindrical tube. Ind. Engng. Chem. **46**, 1181-1186; corrections 195 Ind. Engng. Chem.**49**, 1029.

27.Happel, J. and Brenner,H. 1973 Low Reynolds Number Hydrodynamics. Second Edition. NoorDhoff International Publishing, Leyden.

28.Harper,J.F.1973 On bubbles with small immobile adsorbed films rising in liquids at low Reynolds numbers. J. Fluid Mech. **58**, 539-545.

29.Harper,J.F. 1974 On Spherical bubbles Rising Steadily in Dilute Surfactant Solutions. [Q.J.] Mech.appl.Math.,**xxvii**,Pt.1 87-100.

30.Harper,J.F. 1982 Surface activity and bubble motion. (Review Paper presented) Appl. Sci. Res. **38**, 343-351.

31.He,Z.,Quintana,G.,Dagan,Z. and Maldarelli,C. 1988 The unsteady translation of a fluid droplet owing to the adsorption of a surfactant monolayer. Int. J. Multiphase Flow (submitted).

32.He,Z., Dagan,Z. and Maldarelli,C. 1988 The influence of surfactant on droplet motion inside a cylindrical tube: I. Uniform retardation controlled by sorption kinetics. J. Fluid Mechanics (accepted).

33.Hirasaki,G.J.and Lawson,J.B. SPEJ 1985,**25**, 176-190.

34.Holbrook,J.A. and Levan,M.D. 1983 Retardation of droplet motion by surfactant: Part 1. Theoretical development and asymptotic solutions. Chem. Engng. Commun. **20**, 191-207.

35.Holbrook,J.A. and Levan,M.D. 1983 Retardation of droplet motion by surfactant: Part 2. Numerical solutions for exterior diffusion, surface diffusion, and adsorption kinetics. Chem. Engng. Commun. **20**, 273-290.

36.Horton,Y.J.,Fritsch,T.R. and Kintner,R.C. 1965 Experimental determination of circulation velocities inside drops. The Canadian J. Chem. Engng. June, 143-146.

37.Hsu,H.Y. 1938 Certain integrals and infinite series involving ultra-spherical polynomials and Bessel functions.(CCNY Engineering Library).

38.Huang,W.S. and Kintner,R.C. 1969 Effects of Surfactants on Mass Transfer Inside Drops. AIChE J.,**15**, Sept. 735-744.

39.Hyman,W.A. and Skalak,R. 1969 Tech. Rept. No.3, Proj. No. NR 062-393, Dept. Civil Eng. and Eng. Mech., Columbia Univ.

40.Hyman,W.A. and Skalak,R. 1970 Tech. Rept. No.5, Proj. No. NR 062-393, Dept. Civil Eng. and Eng. Mech., Columbia Univ.

41.Kynch,G.J. 1959 The slow motion of two or more spheres falling in a viscous fluid. J. Fluid. Mech. 193-208.

42.Ladenburg,R. 1907 Uber den Einfluss von Wanden Auf die Bewegung einer Kugel in either reibenden Flussigkeit. Ann. Phys. **23**,447-458.

43.Leichtberg,S.,Pfeffer,R. and Weinbaum,S. 1976 Stokes flow past finite coaxial clusters of spheres in a circular cylinder. Int. J. Multiphase Flow.**3**,147-169.

44.Levan,D.M. and Newman,J. 1976 The Effect of Surfactant on the Terminal and Interfacial Velocities of a Bubble or Drop. AIChE J. **22**, 4, 695-701.

45.Levan,D.M. 1981 Motion of a droplet with a Newtonian interface. J. Colloid & Interface Sci. **83** (1), 11-17.

46.Levich,V.G. 1962 Physicochemical Hydrodynamics. Prentice-Hall, Englewood Cliffs, N.J.

47.Mast,R.F. 1972 SPE 3997, presented at the Annual Fall Meeting of SPE, New Orleans,LA, October 4-6.

48.Moulai-Mostefa,N.,Meister,E. and Barthes-Biesel,D. 1986 Effect of surfactant on the flow of large gas bubbles in capillary tubes. Physicochemical Hydrodynamics: Interfacial Phenomena. NATO conference, LaRabida, Espagne, July 11-15, 1986.

49.Newman,J. 1966 Retardation of falling drops. Chem. Engng Sci. **22**, 83-85.

50.Paine,P.L. and Sherr,P. 1975 Biophys. J. **15**, 1087.

51.Rybczynsky,N. 1911 On the translatory motion of a fluid sphere in a viscous medium. Bull. Int. Acad. Pol. Sci. Lett. Cracovie (Series A) 40.

52.Sadhal,S.S. and Johnson,R.E. 1983 Stokes flow past bubbles and drops partially coated with thin films. Part 1. Stagnant cap of surfactant film - exaxt solution. J. Fluid Mech. **126**, 237-250.

53.Savic,P. 1953 Circulation and distoration of liquid drops falling through a viscous medium. Nat. Res. Counc. Can., Div. Mech. Engng. Rept. **MT**-22.

54.Saville,D.A. 1973 The effects of interfacial tension gradients and droplet behavior. Chem. Eng. J., **5**, 251.

55.Schechter,R.S. and Farley,R.W. 1963 Interfacial Tension Gradients and Droplet Behavior. Can.J.Chem.Eng. June 103-107.

56.Skalak,R.,Chen,P.H. and Chien,S. 1972 Effect of hematocrit and rouleaux on apparent viscousity in capillaries. Biorheology **9**, 67-89.

57.Tozeren,H. 1983 Drag on eccentrically positioned spheres translating and rotating in tubes. J. Fluid Mech. **129**, 77-90.

58.Wakiya,S. 1953 A spherical obstacle in the flow of a viscous fluid through a tube. J. Phys. Soc. Japan **8**,254-257.

59.Wang,H. and Skalak,R. 1969 Viscous flow in a cylindrical tube containing a line of spherical particles. J.Fluid Mech. **38**,75-96.

60.Wasserman,M.L. and Slattery,J.C. 1969 Creeping flow past a fluid globule when a trace of surfactant is present. AICHE J. **15** (4), 533-548.